SI-Traceable Space-based Climate Observing System:
a CEOS and GSICS Workshop
National Physical Laboratory, London, UK,
9-11 Sept. 2019

SITSCOS Workshop Report

Editors: Nigel Fox, Tim Hewison, Greg Kopp, Bruce Wielicki

Table of Contents

Lead Authors

Hartmut Boesch, NASA/JPL
Helen Brindley, Imperial College, London
Fabien Carminati, Met Office, UK
Nigel Fox, NPL
Dennis Helder, Univ. of S. Dakota
Tim Hewison, EUMETSAT
Derek Houtz, Swiss Federal Institute for Forest, Snow and Landscape Research (WSL)
Sam Hunt, NPL
Greg Kopp, Univ. of Colorado / LASP
Marty Mlynczak, NASA/LaRC
Thomas S. Pagano, NASA/JPL
Hank Revercomb, University of Wisconsin-Madison / Space Science
Erik Richard, Univ. of Colorado/LASP
Philip Rosenkranz, Massachusetts Institute of Technology (retired)
Yolanda Shea, NASA/LaRC
Stefan Simis, Plymouth Marine Laboratory, Plymouth, UK
Dave Smith, Science and Technologies Facilities Council / RAL Space
Thomas C. Stone, USGS
Wenbo Sun, Science Systems and Applications Inc.
Jack Xiong, NASA/GSFC
Bruce Wielicki, NASA/LaRC
Hu Yang, Cooperative Institute for Satellite Earth System Studies, Univ. of Maryland
Xin Ye, Changchun Institute of Optics, Chinese Academy of Sciences

Contributing Authors

Douglas Adler, Univ. of Wisconsin-Madison / Space Science
Hartmut Aumann, NASA/JPL
Rosemary R. Baize, NASA /LaRC
R. Bantges, Imperial College London
Fred Best, Univ. of Wisconsin-Madison / Space Science
William Blackwell, MIT Lincoln Laboratory
Hartmut Boesch, Univ. of Leicester
H. Brindley, Imperial College London
Steven E. Broberg, NASA/JPL
S. Buehler, Univ. Hamburg, Meteorological Institute
Martin Burgdorf, Univ. Hamburg, Meteorological Institute
Jim Butler, NASA / GSFC
Fabien Carminati, Met Office, UK
Odele Coddington, Univ. of Colorado / LASP
R. Cooke, Delft Univ.
Dorothée Coppens, EUMETSAT
C. Currey, NASA-LARC
Sean Devlin, NPL
B. M. Dinelli, CNR, Bologna
Dave Doelling, NASA / LaRC
Eric Fetzer, NASA/JPL
Gary A. Fleming, NASA /LaRC
Jon Gero, Univ. Wisconsin-Madison / Space Science
D. Goldin, SSAI
Paul Green, NPL
Chawn Harlow, Met Office, UK
Robert Holz, Univ. of Wisconsin-Madison / Space Science
Xiuqing Hu, CMA-NSMC
Thomas Jackson, Plymouth Marine Laboratory, Plymouth, UK
Viju John, EUMETSAT
Edward Kim, NASA Goddard Space Flight Center
Robert Knuteson, Univ. Wisconsin-Madison / Space Science
L. Labonnote, Univ. Lille
Robert Vincent Leslie, MIT Lincoln Laboratory
Q. Libois, CNRM, Université de Toulouse, Météo-France, CNRS, Toulouse
Chao Lin, Changchun Institute of Optics, Chinese Academy of Sciences
Constantine Lukashin, NASA / LaRC
Evan M. Manning, NASA/JPL
C. Merchant, Univ. Reading
J. Mittaz, NPL, Univ. Reading
Mark Mulligan, Univ. Wisconsin-Madison / Space Science
Fred Nagle, Univ. Wisconsin-Madison / Space Science
Tim Nightingale, Science and Technologies Facilities Council / RAL Space
H. Oetjen, ESA-ESTEC
L. Palchetti, CNR, Florence
Jonathan Pearce, NPL

Dan Peters, Science and Technologies Facilities Council / RAL Space
Claire Pettersen, Univ. Wisconsin-Madison / Space Science
Peter Pilewskie, Univ. Colorado / LASP
Sharon Ray, NASA/JPL
M. Ridolfi, CNR, Florence
M. Riese, IEK- Forschungszentrum Jülich
C.M. Roithmayr, NASA-LARC
R. Saunders, Met Office, UK
Paul Smith, Univ. of Colorado / LASP
Larrabee Strow, Univ. of Maryland under contract to NASA
Joe Taylor, Univ. of Wisconsin-Madison / Space Science
Joao Teixeira, NASA/JPL
K. Thome, NASA-GSFC
David Tobin, Univ. of Wisconsin-Madison / Space Science
Tim Trent, Univ. of Leicester
Kevin Turpie, NASA / GSFC
Radka Veltcheva, NPL
Likun Wang, Riverside Technology Inc. at NOAA
Long Wang, Changchun Institute of Optics, Chinese Academy of Sciences
E. Woolliams, NPL
A. Wu, SSAI
Xiaolong Yi, Changchun Institute of Optics, Chinese Academy of Sciences
Xuejun Zhang, Changchun Institute of Optics, Chinese Academy of Sciences
Giuseppe Zibordi, Joint Research Centre of European Commission, Ispra, Italy

1   Summary Report

1.1   Workshop Purpose – Defining Space-Based Climate Observation Requirements

The SI-Traceable Space-based Climate Observing System Workshop (hereafter denoted *SITSCOS*) was hosted by the National Physical Laboratory in London, UK, 9-11 September 2019 and sponsored by the UK Space Agency. The workshop was organized under the auspices of the Global Space-based Inter-Calibration System (GSICS) and the Committee on Earth Observation Satellites - Working Group on Calibration and Validation (CEOS-WGCV). The goal of the workshop was to quantify the benefits and resulting requirements of a space-based climate observing system and produce this *Workshop Report* summarizing current measurement capabilities, climate-based needs, and future plans for implementation. The international workshop included about 100 attendees and spanned users, satellite instrument designer/builders, metrologists, and space agencies with expertise across a wide range of applications and technologies.

1.1.1   Historical Background

The requirements and calibrations of satellite instruments for climate observations have been addressed in two earlier U.S.-led workshops. The first was held in 2002 [1] and the second in 2006 (Achieving Satellite Instrument Calibration for Climate Change, or ASIC[3], 2007 [2]). Both reports considered SI traceability as well as stability requirements. At the time, most of the requirements relied on stability and overlap given the lack of demonstrated SI-traceable satellite instruments at the accuracy required for climate change observations, where decadal climate signals are typically a few tenths of 1 percent in magnitude.

In the decade following those initial workshops, extensive advances have been made in spaceborne instrument development, ground and in-orbit calibration systems, and analysis of climate change accuracy requirements. In 2007, the U.S. Earth Science *Decadal Survey* [3] called for the flight of new SI-traceable high-accuracy infrared and reflected-solar spectrometers to serve as climate benchmarks as well as in-orbit intercalibration references for other sensors. The baselined CLARREO (Climate Absolute Radiance and Refractivity Observatory) mission built on early work on infrared high-accuracy spectrometers [4], [5], extending the concept to both infrared and reflected-solar spectrometers [6] (Wielicki et al. 2013; *Workshop Report* §8.4, 11.1). Over 100 journal papers on CLARREO requirements analyses, intercalibration methods, and instrument SI traceability in orbit (see *https://clarreo.larc.nasa.gov/docs-references-A-F.html*) have helped solidify this Tier 1 NASA mission.

Meanwhile, similar efforts in the UK, Italy, and China began to design reference spectrometers for the complete reflected solar spectrum, with the UK-led TRUTHS ([7], [8], *Workshop Report* §11.2) and China-led CSRB (*Workshop Report* §11.3*)* as well as the complete infrared spectrum with the Italy-led FORUM (*Workshop Report* §11.4*)*. The international CEOS, WMO (World Meteorological Organization) and CGMS (Coordination Group for Meteorological Satellites) developed a "Strategy Towards an Architecture for Climate Monitoring from Space" that also called for reference space-based spectrometers to serve as anchors for the climate change monitoring system [9]. In 2015, a U.S. Academy of Science report on continuity of climate observations [10] recommended that NASA use quantified climate science objectives and quantitative quality of observations including calibration accuracy to determine requirements for long-term climate observations. In 2016, NASA began implementation of the CLARREO Pathfinder mission, which includes a nearly full-spectrum reflected-solar spectrometer (but lacks the infrared spectrometer which was baselined for the full CLARREO

mission's instrument suite) and is scheduled for launch on the International Space Station beginning in 2023 (*Workshop Report* §8.4, 11.1). In 2016, the WMO released its latest GCOS (Global Climate Observing System) *Implementation Report*. That report reviews the status of Essential Climate Variable observations and provides recommendations for action by the international community. The 2016 GCOS report confirms the need to implement Satellite Calibration Missions such as CLARREO and TRUTHS (Action A16, WMO-GCOS, 2016 [11]). In 2017, the second U.S. Earth Science *Decadal Survey* report [12] set quantified climate science objectives as well as accuracy requirements, including the critical need for SI-traceable reference spectrometers (both reflected solar and infrared) to support climate science objectives, with requirements documented in the *Decadal Survey's* Science and Applications Traceability Matrix (SATM). NASA followed through with continued support for the CLARREO Pathfinder demonstration mission in the early 2020s.

A recent paper "Designing the Climate Observing System of the Future" summarizes the need for designing a dedicated international climate observing system; methods used to design such a system; and a summary of its economic benefits, costs, and return on investment [13]. In late 2019, ESA approved development of the TRUTHS reflected-solar spectrometer mission as well as the FORUM mission for improved calibration and new observations of the far-infrared spectrum. China continues to develop a series of reference spectrometers, with the first versions planned for flight in the early 2020s at accuracies within a factor of 2 or 3 of those planned for CLARREO Pathfinder, TRUTHS, and FORUM. Later versions will improve calibration accuracy to reach the original CLARREO and TRUTHS mission accuracy goals as designated in the two *Decadal Survey* reports [3], [12] as well as the mission summary papers [6], [8], [14].

1.1.2   Current Status of Requirements and Measurement Capabilities

The workshop attendees strongly supported the need for higher accuracy observations for climate change as well as other applications, and that a key mechanism to achieving these was through rigorous inter-calibration against SI-traceable references. The hope is that the workshop, this resulting *Workshop Report*, and a dedicated special issue in the *Journal of Remote Sensing* can help move toward those goals in both the short and long term.

This *Workshop Report* integrates information from the last decade of progress on laboratory metrology, SI traceability of satellite instruments, GISCS and CEOS inter-calibration, climate science accuracy requirements, and analysis of the economic value of more accurate climate change observations. The report addresses not only climate observations but also the advantages of improved SI traceability for other space-based applications such as weather prediction/analysis/re-analysis, land & ocean surface imaging, microwave imaging and sounding observations, presenting a summary of 13 years of research progress following the 2002 and 2006 climate calibration workshops mentioned earlier. While the report covers a wide range of relevant topics, there are some areas that it does not cover, including equivalent SI-traceable requirements for active sensors, such as atmospheric cloud aerosol and wind lidar, cloud radar, surface wind scatterometers, and ocean and ice-sheet altimeters. A future workshop should address these newer space-based instrument technologies.

1.2   Workshop Report

> **This report summarizes advances in SI-traceable calibration accuracy and requirements for satellite-based instruments relevant to climate change**

The purpose of this *Workshop Report* is to summarize the results of the workshop in a written form that can be easily understood and used by the research community as well as space agency program managers and other related organizations. The report is broken into several sections for easy access. This

Summary Report, authored by the workshop's Science Organizing Committee, provides a single high-level overview of the workshop and its conclusions and can be read as a standalone document. In the full report following the summary are sections contributed by workshop participants to provide further detail on topics covered in the workshop. These sections are organized by application, remote sensing spectral region, and type of measurement. The summary references these sections where appropriate but is not intended to be comprehensive. The workshop presentations and discussion sections were recorded and are available online for viewing at http://calvalportal.ceos.org/. Many of the topics of this *Workshop Report* are covered in more depth in existing literature references or in the Special Issue of the *Journal of Remote Sensing* devoted to the topic of the workshop. The entire *Workshop Report* can be found online at http://calvalportal.ceos.org/. Researchers are encouraged to build on this document as well as the methods shown in the 2015 *Continuity Report* [10]. Ultimately, independent analyses of climate observation and SI traceability requirements by multiple groups should be developed. In addition, a follow-on workshop for active remote sensing instruments should be encouraged within the next several years.

The primary need for improved SI traceability is for measuring climate change in order to quantify its many causes and, eventually, to monitor successes of mitigation strategies. A system designed for climate will inevitably provide many benefits for additional applications, but climate studies tend to drive the key requirements, particularly in terms of accuracy. The SITSCOS workshop described the urgent need for designing and building a dedicated international climate observing system, in particular one that is more accurate than the current observations used for climate change [9], [12], [13], [15], [16]. Two issues need to be addressed to achieve such a system:

1) Most current observing systems used for climate change were designed for other purposes, such as weather, land resources, or Earth-science process studies. In general, climate change requires an order of magnitude more accuracy of those observations over an order of magnitude more temporal duration and for ten times as many geophysical variables [10], [13].

2) The current measurements used for climate observing lack completeness. An examination of the 2017 *Decadal Survey* SATM tables shows that roughly 2/3 of all climate science objectives lack critical observations by NASA or the international operational and research communities.

In 2015, the U.S. Academy of Sciences "Continuity Report" provided a framework of principles for the design of a long-term monitoring climate change observing system [10]. Two of the key design principles included Quantified Science Objectives and Quality of the observations. Quality of the observations includes calibration uncertainty, sampling uncertainty, and algorithm uncertainty. The calibration uncertainty required is in turn determined from the Quantified Science Objective. These concepts have been used wherever possible in this *Workshop Report*, and many of them can be found in the 2015 *Continuity Report* or the 2017 *Decadal Survey* Science and Application Traceability Matrix tables [10], [12].

While climate change drives many key requirements, there are several additional applications that benefit from improved SI traceability of in-orbit sensors. These include initializing, constraining, and improved testing of Numerical Weather Prediction (§10.1.1), consistency of data products for large constellations of land remote sensing imagers (§10.3), and improved accuracy of ocean color sensors used to study ocean biological processes including carbon sinks and ocean productivity (§10.4). In the case of weather prediction, SI traceability can provide improved bias corrections for satellite radiances used to improve weather prediction as well to improve assimilation data products. Ocean color has traditionally faced extreme accuracy and stability requirements due to the small signal levels of spectral reflectance changes from ocean biology that provide the foundation of the ocean food chain and strongly

impact ocean carbon uptake in the Earth System and is one of the 54 essential climate variables (ECVs). For land resource satellites, large constellations of CubeSats and SmallSats are re-inventing land imaging but are stressing the ability to achieve consistent calibration and consistent data products. These are just a few key examples of non-climate satellite observations that have major benefits from the improved SI traceability discussed in this report.

1.3   Economic Value of a More Accurate and Complete Climate Observing System

Recent studies estimate that an improved and more accurate climate observing system could provide needed climate-change uncertainties 15 to 30 years sooner than current observations [6], [17]–[19]. Using recent economic models, the total value to the world of such a system is estimated at between $5 and $20 trillion dollars as a result of earlier implementation of policy based on more rigorous evidence. The cost of providing such a system might require tripling current investments, meaning an additional $8 billion U.S. dollars per year in global climate research investment ([17], §0) spread among the international community. The estimated return on investment lies between 25:1 and 100:1, which is expected to exceed even that for weather observations.

Inflation-adjusted U.S. investments in climate research have stagnated over the last 25 years, despite the large remaining uncertainties and their large potential economic impacts. Even an additional factor of 5 uncertainty in economic value, in which case the return on investment would range from 10:1 to 250:1, would not change the conclusion of the system's importance. The cost of delaying such a system beyond 2020 has been estimated at $250B to $500 billion/yr [17]. An examination of sensitivity to the economic analysis to underlying assumptions about societal decision-making showed the results to be surprisingly insensitive, being at the level of less than 50% of economic value [17]. A more complete discussion of this topic can be found in section 2 of the *Workshop Report*, including methods and references for the analysis. *The analyses all conclude that a more rigorous and complete international climate observing system would be one of the most cost-effective investments society could make.* In the light of recent post-event mitigation investments resulting from COVID-19, it is perhaps timely for the worlds' governments to consider a more comprehensively planned strategy for arguably the most severe and likely existential risk facing humanity.

1.4   Climate Requirements from Workshop

While the 2002 and 2006 climate calibration workshops primarily focused on the use of stability and overlap requirements, more recent efforts, such as this workshop, have extended that work to SI-traceable accuracy requirements as a much more robust and rigorous method to observe climate change trends over the temporal durations needed. Two major advantages of SI-traceable observations are that they can better withstand measurement-data gaps and can greatly reduce uncertainties in long-term instrument calibration drifts while in orbit [3], [5], [10], [12], [20]. By contrast, strategies reliant on overlap add significant cost to guarantee continuity and also suffer from the prospect of anomalies caused by natural variations such as ENSO and volcanoes etc. The space-borne solar-irradiance measurement record shown in Figure 1.4 gives a striking visual example of the importance of SI-traceable accuracy in long-term data, which help give improved consistency by reducing offsets between instruments and thereby mitigate potential data gaps in measurement continuity.

The effort to focus on SI-traceable accuracy began with early papers by Goody and Anderson [5] for measurements of the infrared spectrum. The 2007 *Decadal Survey* [3] extended the need to include the reflected solar spectrum. Quantification of the requirements of SI-traceable accuracy for climate change trends improved significantly with the analysis methods introduced in Leroy et al. 2008 [20], which

introduced the concept of measuring climate change trends against the background of natural variability. This new perspective encourages a more cost-effective and realistic determination of "How good is good enough?" In particular, it allows the determination of the time required to quantify climate change trends as a function of actual instrument accuracy relative to that of a perfectly calibrated observation. As the actual measurement uncertainty degrades, longer times (usually measured in decades) are needed to achieve the same level of certainty in detecting climate change trends. This type of analysis is widely applicable and greatly improves the ability to determine SI-traceable accuracy requirements for a wide range of climate change variables. Examples of the analyses of calibration accuracy requirements can be found in Wielicki et al. 2013 for the infrared and reflected-solar CLARREO mission [6], in the NASEM *Continuity Report* as the method to quantify the quality of climate change observations [10], and in more recent extensions to cloud properties [21] and temperature/water vapor profiles [22]. The analysis can be applied to any uncertainty in satellite observation (calibration, sampling, retrieval algorithm), but for decadal-change trends, calibration uncertainty tends to dominate the overall measurement uncertainty [6], [10].

Table **1.1** summarizes climate-variable measurement requirements from a range of published studies, many of which are summarized in the different papers of this *Workshop Report* and drive the SI-traceable accuracies for the infrared and reflected-solar

Accuracy requirements have been developed for a wide range of climate change observations from space

spectrometers discussed in those papers. While further analyses are needed for additional climate variables, this table contains results for several of the highest priority Quantified Science Objectives from the 2017 *Decadal Survey*. References are provided for further details on the analysis methods.

Table 1.1: Summary of Climate Variable Measurement Requirements

Climate Variable	Climate Science Quantified Objective (NASEM, 2013, 2017)	Sensor Type	Spectral Region (micron)	SI-Traceable Accuracy Requirement	Reference for Requirement
Shortwave Cloud Radiative Forcing	Cloud Feedback, Climate Sensitivity	Broadband Radiometer	0.3-5.0	0.3% (k=2)	Wielicki et al. 2013, NASEM 2015; 2017 [6], [10], [12]
Longwave Cloud Radiative Forcing	Cloud Feedback, Climate Sensitivity	Broadband Radiometer	5-100	0.6% (k=2)	NASEM, 2017 [12]
Cloud Optical Depth	Cloud Feedback, Climate Sensitivity	Cloud Imager	0.65	0.3% (k=2)	Shea et al. 2017 [21]
Cloud Temperature	Cloud Feedback, Climate Sensitivity	Cloud Imager	11-12	0.06K-0.08K (k=2)	Shea et al. 2017, NASEM, 2017 [12], [21]
Cloud Fraction	Cloud Feedback, Climate Sensitivity	Cloud Imager	11-12	0.4K (k=2)	Shea et al. 2017 [21]
Temperature (Surface)	Climate Sensitivity	IR Sounder	8.5-13	0.06K (k=2)	Leroy et al. 2008, NASEM 2007, 2017 [3], [12], [20]
Temperature (Troposphere)	Climate Sensitivity Lapse Rate Feedback	IR/μWave Sounder	13-14 or μWave	0.06K (k=2)	Liu et al. 2017, NASEM 2017 [12], [23]
Water Vapor (Troposphere)	Water Vapor Feedback	IR/μWave Sounder	6.7 or μWave	0.06K-0.12K (k=2)	Liu et al. 2017, NASEM 2017 [12], [23]
Surface Albedo	Snow and Ice Albedo Feedback	Broadband Radiometer & Cloud Imager	0.3-5.0, 0.65, 1.6, 2.1	1% (k=1)	NASEM, 2017 [12]
Water Leaving Radiance/ Ocean Colour	Ocean productivity carbon cycle	Multi-channel imaging spectrometer	0.38-1	5% at surface equivalent to 0.5% at ToA	GCOS, Simis et al §10.4.1
Total Solar Irradiance	Earth Energy Balance, Solar Forcing	Broadband Radiometer	0.2-5.0	0.01% (k=1)	NASEM, 2013, Kopp 2014 [16], [24]
Spectral Solar Irradiance	Solar Forcing	Solar Spectrometer	0.2-2.4	0.2% (k=1)	Richard et al. 2020 [25]

A critical part of considering the requirements in Table **1.1** is to compare the requirements to current satellite calibration capabilities. Table **1.2** compares current capabilities versus the requirements from Table **1.1**. With the exception of the reference spectrometers planned for flight this decade, almost all satellite instruments have SI-traceable uncertainties that are a factor of 2 to 30 worse than climate requirements, with typical shortcomings of a factor of 5 to 10. A few, such as TSIS-1 TIM and CERES LW, are within a factor of 2 or 3 of the requirements. The upcoming reference spectrometers to be

flown between 2023 and 2030, such as TRUTHS, CLARREO Pathfinder, EMIS, and FORUM, achieve SI traceability that meets or is within about a factor of 2 of climate requirements. Fortunately, reference spectrometers can be used in the future to dramatically improve the SI traceability of the other solar and infrared spectrum space observations as discussed in this *Workshop Report*.

Table 1.2: Current Satellite Instrument Capabilities versus Climate Requirements.

Instrument	SI Traceability in Orbit (*k*=2)	Climate SI Traceable Requirement (k=2) Table 1.1	Current Estimated Stability (k=2)	Spectral Region (μm)	Traceability/Stability References
SOLAR	**SPECTRUM**				
CERES: SW	2%	**0.3%**	0.3%/decade	0.3-5.0	Priestley et al. 2011 [26] Loeb et al. 2016 [27]
MODIS/VIIRS	4%	**0.3%**	0.5 - 1.5%/decade	0.4-2.3	Xiong et al. 2018 [28] Xiong et al. 2017 [29]
2014 Geo Imagers	8-16%	**0.3%**	6%/decade	0.6-1.8	Meirink et al. 2013 [30] EUMETSAT, 2019 [31]
2020 Geo Imagers	6-10%	**0.3%**	TBD	0.4-2.2	Yu et al. 2019 [32]
Ocean Colour sensor* e.g. Sentinel 3- OLCI VIIRS, PACE	3-4%	**0.5%**	0.1%/decade SeaWiFS lunar	0.4-1.1	Simis and Zibordi, 2020 §10.4
Landsat	6-10%	**TBD**	TBD	0.43-2.3	Markham et al. 2014 [33]
Sentinel-2	6-10%	**TBD**	TBD	0.44-2.2	Bouzinac et al. 2018 [34]
TSIS TIM	0.07%	**0.02%**	0.01%/decade	0.2-5.0	Kopp and Lean 2011 [35]
TSIS SIM	0.5%	**0.4%**	< 0.4%/decade	0.2-2.4	Richard et al. 2020 [25]
ROLO Lunar Irradiance Model	5-10%	**0.3%**	< 0.01%/decade	0.35-2.45	Kieffer and Stone, 2005 [36] Stone et al., 2020 [37]
CLARREO Pathfinder (2023)	0.6%	**0.3%**	< 0.3%/decade	0.35-2.35	Kopp et al. 2017 [38]
TRUTHS (2026)	0.3%	**0.3%**	< 0.3%/decade	0.32-2.45	Fox et al. 2011 [8] Fox and Green 2020 [14]
EMIS (2025)	1%	**0.3%**	< 0.3%/decade	0.38-2.35	Zhang et al. 2020 [39]

INFRARED	SPECTRUM				
CERES: LW	1%	**0.6%**	< 0.1%/decade	5-100	Priestley et al. 2011 [26] Loeb et al. 2016 [27]
MODIS/VIIRS**	0.4-1.5% p	**0.06K-0.08K**	0.05-0.5 K/decade	3-15	Xiong et al. 2018 [28] Xie et al. 2010 [40]
Sentinel 3- SLSTR	0.2K	**0.06K-0.08K**	0.2K/decade	3-12	Smith et al. §8
2014 Geo Imagers	2K	**0.06K-0.08K**	~0.7K/decade	3-15	EUMETSAT, 2019 [31]
2020 Geo Imagers	0.4K	**0.06K-0.08K**	TBD	3-15	Yu et al. 2019 [32]
AIRS	0.1-0.25K	**0.06K-0.08K**	0.03-0.06K/decade	3-15	Pagano et al. 2018 [41] Strow and DeSouza-Machado, 2020 [42]
CrIS	0.13-0.2K	**0.06K-0.08K**	0.03K/decade	3-15	Tobin et al. 2013 [43]
IASI	< 0.15K	**0.06K-0.08K**	0.03K/decade	3-15	Pierangelo et al 2020 [44]
FORUM	0.06 - 0.15K	**0.06K-0.08K**	TBD	15-100	Brindley et al. 2020 [45]
IRS	0.15K	**0.06K-0.08K**	TBD	3-16	Zhang et al. 2020 [39]
MICROWAVE	SPECTRUM			GHz	
MSU-Type Temperature Sounders	0.2K ***	**0.06K-0.08K**	0.02K/decade$^{1/2}$ using GPS/RO	54-58	Rosenkranz et al. 2020 [46]
MHS-Type Humidity Sounders	0.4K ***	**1.0K**	TBD	160-190	Burgdorf et al. 2020 [47] Buehler and John 2005 [48]
Microwave Imager Window Channels Tb	0.5K ***	**0.2-0.4K**	0.6K/decade	10-86	Wentz and Draper, 2016 [49] Chen et al. 2014 [50]

*   Indicative ocean colour sensors

** Accuracy quoted as percentage of spectral radiance

*** All passive microwave absolute accuracies are based on assessment by inter-comparisons and do not include rigorous SI-traceability

Figures 1.1 and 1.2 provide a comparison of the current capabilities from Table **1.2** with the climate requirements from Tables 1.1 and 1.2. Figure 1.1 shows reflected solar spectrum capabilities while Figure 1.2 shows the thermal infrared capabilities.

> **Most current satellite calibration capabilities are factors of 5 to 10 less accurate than climate requirements**
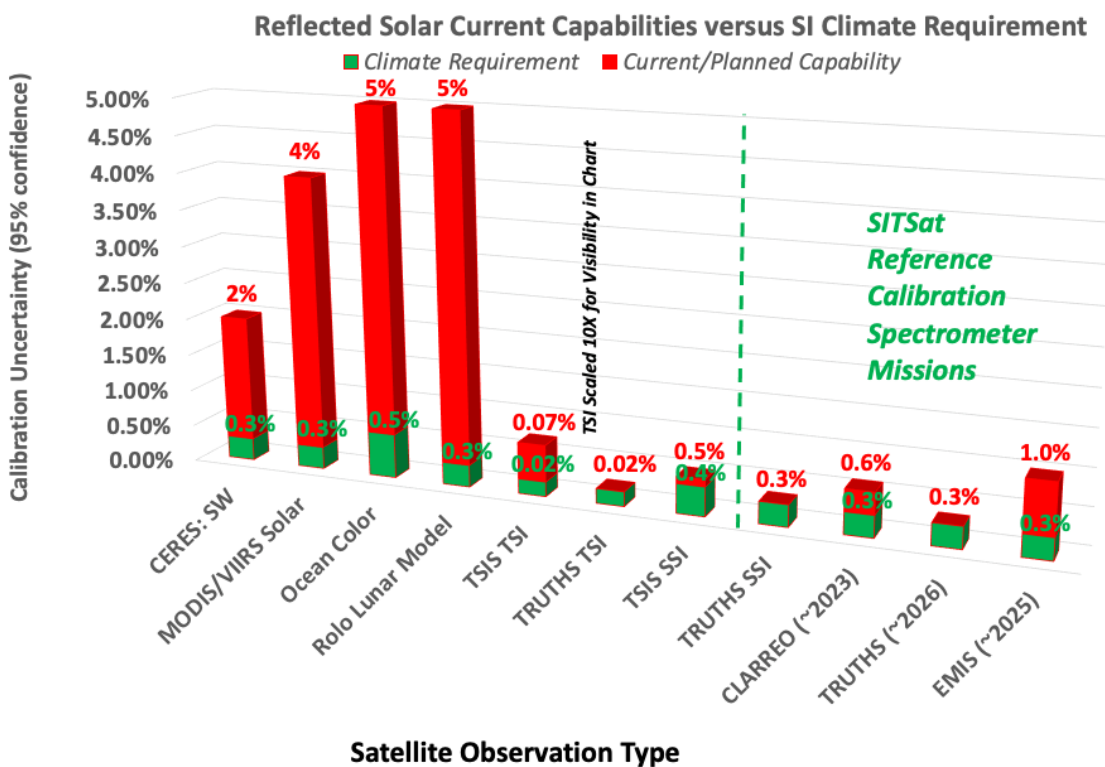
Figure 1.1: Current satellite instrument capabilities versus climate requirements for the reflected-solar spectral region. In the stacked bar chart format, the lower bar is the climate requirement, and the upper bar is the current capability (or near-future capability in the case of the reference spectrometers discussed in this report).

Infrared Current Capabilities versus SI Climate Requirement
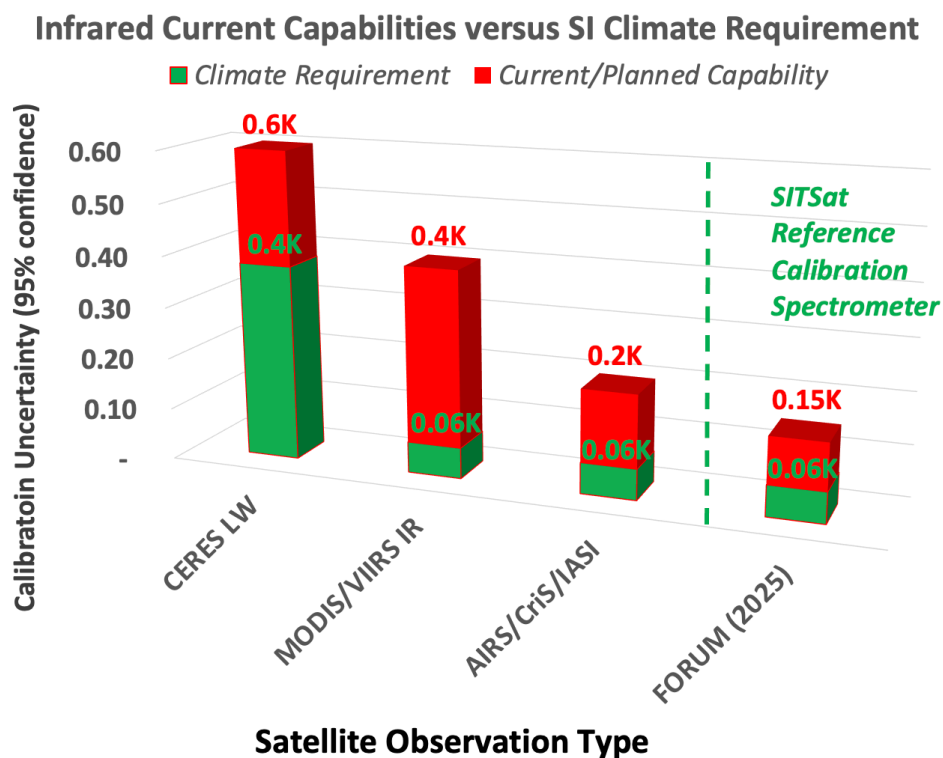
Figure 1.2: Current satellite instrument capabilities versus climate requirements for the thermal-infrared spectral region.

The figures and tables clearly show that there is a very large discrepancy between the SI-traceable calibration uncertainty of current satellite sensors and climate change observation requirements for essential climate variables derived from those sensors. The new reference spectrometers, when used for in-orbit intercalibration, should be capable of major improvements in these critical requirements.

It is also appropriate to ask what happens if the climate requirements above are not reached. In simplest terms, less accuracy will greatly delay the time needed to rigorously detect climate change trends. The requirements are typically set to limit delays to ~ 5 years. Current accuracies can often limit trend detection by several decades. See Section 10.2.2 for examples of trend detection times as a function of instrument accuracy. Further discussion can be found in the 2015 NASEM *Continuity Report* [10] and the 2017 Decadal Survey report [12].

1.5   Definition of Calibration Stability

Because many past efforts for climate requirements have focused on stability more than absolute accuracy, we also include a definition of stability relevant to climate calibration as discussed in this report. Calibration stability refers to the ability of an instrument to maintain its calibration with respect to an invariant reference (https://jcgm.bipm.org/vim/en/4.19.html) over some defined period of time. Instrument calibration uncertainty varies on a continuum of timescales from seconds to decades, and the most rigorous characterizations of instrument stability require power-spectral analyses of the instrument response. For the quantification purposes of this *Workshop Report*, we consider simpler, discrete timescales. Very short timescales (those of individual measurements) are commonly called "instrument noise" and often arise from detector and electronics variability. Intermediate timescales (hours to months) are commonly caused by changing instrument thermal environments (e.g. sunlit vs dark portions of an orbit, changing solar illumination beta angle, or changes in stray light). Instrument variability on these intermediate timescales has been characterised as "structured random" by the

FIDUCEO project. Variations over much longer timescales of years to decades are usually caused by changes in the physical properties of the instrument (optical contamination; source, detector, or thermal property degradation; radiation damage). As a result, "stability" covers a wide range of timescales, and practical applications define the timescales that tend to be considered "noise" vs "stability". For the climate observations relevant for this report, we define instrument *stability* as changes in calibration over timescales longer than a month, while instrument *noise* is considered to be timescales less than a month. With this definition, most instrument noise will vary in sign and magnitude, while stability will tend to manifest as long-term drifts typically of consistent direction.

Most efforts to characterize and thus correct long-term stability relevant for climate observations from spaceborne instruments primarily rely on stability relative to onboard sources (lamps, diffusers, blackbodies) or to other orbiting instruments (e.g. intercomparisons, such as of IASI, AIRS, and CrIS). Unfortunately, most of these characterizations fall short of using "invariant references," as called for in SI-traceable metrology. There are methods that can be used with higher rigour, such as lunar views acquired at the same libration and phase angles, use of the Sun as an SI-traceable source, or by bringing to orbit methods to maintain SI traceability using phase-change cells and methods to monitor blackbody emissivity. Users are cautioned that most current estimates of in-orbit instrument stability are best efforts using intercomparisons and are not yet based on SI-traceable invariant references. One of the purposes of this report is to encourage increased rigour and future understanding of instrument calibration accuracy as well as stability.

1.6   Metrology and Climate Data

At the heart of this workshop and reflecting the community's long-term goals, is the ambition and necessity to mimic the traditions and practices of the international metrology community transitioned into the space environment. Since 1875 with the founding of the metre convention and signing of inter-governmental agreement to adopt the International System of units (SI) as a universal coherent measurement system we have had the means to scientifically communicate and trade in a relatively unfettered and transparent manner. The SI system, through its seven base units, recently all tied to invariant constants of nature [51], provides the mechanism for measurements to be made against references with century scale stability and international uniformity, a pre-requisite for long-time base studies such as climate.

Underpinning the SI are three key metrological principles:

- **Traceability** – documenting and evidencing the link of any measurement to its primary reference
- **Uncertainty** – establishing a rigorous and detailed budget of sources and contributing nature (random/systematic) of uncertainties of any measurement in relation to a defined reference
- **Comparison** – the means to unequivocally demonstrate declared uncertainties are robust and repeatable

Earth observation and Climate science have recognised the need to adopt these principles not only for the direct observations but also through any processing chain to the information product used to inform the policy maker or intermediate user. One of the main challenges that this workshop is seeking to address is how to ensure that the very small uncertainties needed for climate trend detection can be met, are trustworthy, and can stand the test of time so that future researchers can use them as their benchmark reference point.

To achieve these goals not only requires good instrument design and measurement procedures but also rigorous uncertainty analysis and clear documentation to facilitate as full an understanding of any

observation as possible. This is particularly important as it is likely that the building block of this analysis will be relied upon for many years after any calibration and characterisation has taken place and also following the shock of satellite launch and the harshness of space. Strategies and methods to help provide a unified approach to both uncertainty evaluation and its documentation have been established in a number of projects. A good example that is becoming widely adopted, is described in Section 3. This so called Fiduceo approach addresses not only the observation but the means to harmonise together different satellite observations to create multi-decadal climate data records.

1.7   Reflected-Solar Laboratory Methods

Over the last three decades there has been dramatic improvement in the accuracy of laboratory-based optical radiometric measurements, not only for the Earth Observation community but radiometry in general. This primarily stems from the move to detector-based reference standards and the use of lasers as a calibration medium rather than incandescent lamp-based sources often linked to temperature-based scales derived from the use of Planck's law. In the early 1980s, NPL pioneered the development of the cryogenic radiometer [52], [53], an instrument that compares the heating effect of electrical power with that of optical. Through operation at temperatures close to absolute zero (typically < -250 °C), a step change of nearly a factor of 100 in the uncertainty of the radiometric primary scale was achieved [54]. Cryogenic radiometers based on this concept now form the basis of most of the world's optical radiometric scales at NMIs and are formally designated as a primary radiometric reference by the international metrology community [55].

Cryogenic radiometers together with lasers and high quantum-efficiency solid-state detectors revolutionised optical radiation measurements. The intrinsic properties of some solid-state silicon detectors allowed the construction of so-called trap detectors [56], [57], which, based on calibrations at only a few wavelengths allowed prediction at all others, lead to convenient transportable and relatively low-cost transfer standards. When coupled with spectrally-defining filters (multiple glass elements, interference) or indeed spectrometers and appropriate geometry-defining apertures, together with spectrally-tuneable lasers to determine their spectral response to a trap detector, spectral radiance meters could be established enabling very high measurement accuracies of <0.03% [58]. Such radiance meters could then be used to measure broadband sources such as lamps or blackbodies to establish spectrally continuous scales of spectral radiance and irradiance [59], [60] and also thermodynamic temperature [61], which in turn were used to provide improved traceability to the EO community.

However, as the demand for reduced uncertainty for climate observations increased, the intermediate step of calibrating either a radiance meter or indeed a secondary lamp illuminated source was removed. In essence, an optical EO sensor is essentially an imaging radiance meter, albeit usually larger and more costly than its terrestrial counterpart and requiring calibration under operational vacuum conditions. NIST (SIRCUS), NPL (NLRF), and PTB (TULIP) all built laboratory, and in some cases transportable, facilities to directly calibrate the spectral radiance response of imaging spectrometers using integrating spheres illuminated by tuneable laser radiation [58], [62], [63] with radiance determined by a silicon trap detector radiance meter traceable to a cryogenic radiometer. Laser technologies have subsequently improved over the years and such systems have extended out of NMI laboratories to other institutes such as NASA with the GLAMR [64] facility, which will be used to provide an independent secondary characterisation of the HySICS radiometer of the CLARREO Pathfinder.

NPL recently completed the build and test of its new transportable facility called the Spectroscopically Tuneable Absolute Radiometric (STAR) calibration and characterisation (cc) Optical Ground Support Equipment (OGSE). The STAR-cc-OGSE makes use of a novel, fully automated CW laser that is spectrally tuneable continuously from 260 to 2600 nm and illuminates a half-meter diameter integrating

sphere with variable exit port. The STAR system also incorporates conventional lamps into the sphere to allow more rapid linearity testing and also a second combined system with a collimator to allow image quality and other parameters to be assessed. Currently delivering radiometric uncertainties of <0.5% in SWIR spectral region (although capable of <0.1%), it can simultaneously determine spectral response functions of spectroscopic sensors while also providing radiometric gain and assessments of spectral stray light. The facility is currently being used to calibrate the GHG monitoring sensor MicroCARB due for launch in 2022.

1.8   Extending GSICS to an Absolute Scale

The Global Space-based Inter-Calibration System (GSICS) is an international collaborative effort, which aims at ensuring consistent measurement accuracy among space-based observations worldwide for climate monitoring, weather forecasting, and environmental applications [65] [1].

The GSICS routinely monitors the calibration of various channels of Earth-observing satellite instruments and generates GSICS Corrections, which are time-dependent functions that can be applied to tie individual instruments' radiometric calibration to that of community-defined reference instruments. Currently, GSICS algorithms are based on comparisons of collocated observations with hyperspectral reference instruments for the infrared channels of geostationary imagers, and pseudo invariant calibration targets (PICTs) are used to compare the counterpart channels in the reflected solar band to multispectral reference sensors. PICTs currently used by GSICS include deep convective clouds and the Moon – but these could also include classic pseudo invariant calibration sites (PICS), such as Libya-4 and other deserts.

Section 5 of the full workshop report discusses how GSICS products derived from both approaches could be tied to an absolute scale using specialized satellite reference instruments with SI-traceable calibration on orbit, referred to as a SITSats. In principle it would be possible to use a SITSat as a direct replacement for current GSICS reference instrument. The CLARREO Pathfinder mission is designed to enable this approach. Depending on the SITSat orbit and instrument sampling design, however, this approach may not yield a sufficient amount of data to reduce the random uncertainty components of the inter-calibration. In this case, the transfer to an absolute scale could also be achieved either by direct comparisons of observations from the current reference instruments with those from a SITSat – or indirectly, by using the SITSat to characterize the PICTs, as illustrated in Figure 1.3.

Tying GSICS products to an absolute scale would provide resilience against gaps between reference instruments and drifts in their calibrations outside their overlap periods and allow construction of robust and harmonized data records from multiple satellite sources to build Fundamental Climate Data Records, as well as more uniform environmental retrievals in both space and time, thus improving inter-operability.
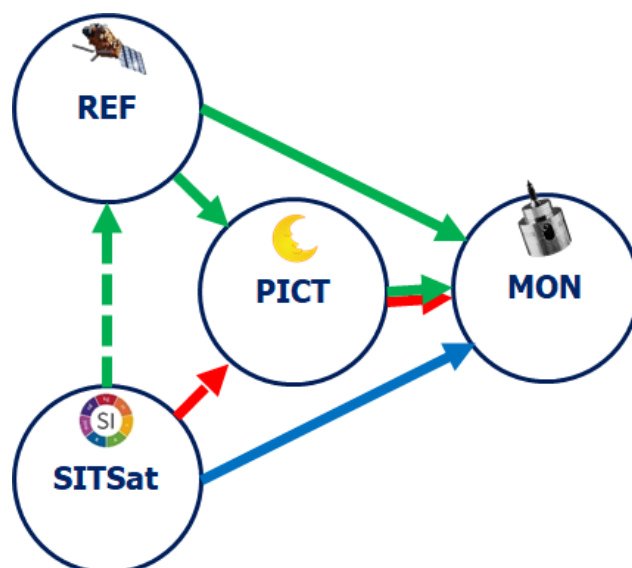
Figure 1.3: The calibration of a monitored instrument (MON) can be tied to an absolute scale using observations from an SI-Traceable Satellite instrument (SITSAT) by various methods: a) Direct comparisons of collocated observations (blue arrow); b) By inter-calibrating GSICS Reference Instruments (REF) (dashed green arrow), which is transferred to the monitored instrument directly or via a Pseudo Invariant Calibration Target (PICT) (green arrows); c) By characterizing the PICT (red arrow).

1.9 Earth Energy Balance – Total Solar Irradiance and Spectral Solar Irradiance

Nearly all the energy powering the Earth-climate system comes from the Sun in the form of radiation spanning the x-ray through the mid- and far-infrared spectral regions with energy peaking in the visible. Since this energy is 3000 times the total of all other Earth-input energy sources combined [66], even small variations in the solar irradiance over long periods of time can have significant impacts on climate, as described by [67].

Global climate change is due to an imbalance in the amount of total incoming vs. outgoing energy. Effects due to the distribution of this energy via ocean and atmospheric phenomena can cause regionally localized variations that can be much greater than – and, occasionally, even in the opposing direction of – the global changes. Atmospheric composition can cause absorption and localized heating or scattering and localized cooling, and those effects can lead to changes in convection, cloud formation, ocean-atmospheric coupling, and winds, all of which, in turn, can influence regional and global climate.

In climate equilibrium, the net incident solar radiation, or the "total solar irradiance" (TSI), is equal to the total outgoing radiation, which is the combination of the reflected solar radiation and the thermal emission from the Earth's surface and atmosphere. Any long-duration imbalance results in global heating or cooling. It is important to measure both incoming and outgoing energies with the climate-driven accuracies given in Table 1.1. A summary by Loeb et al (2009) [68] as well as Mlynczak (*Workshop Report* §6.3) describe measurements of the Earth's net outgoing radiation while Kopp (*Workshop Report* §6.1) and Richard et al. (*Workshop Report* §6.2) respectively describe measurements of the incoming total and spectral solar irradiance.

While the TSI defines the net energy powering the Earth's climate system, giving the input side of the Earth Radiation Budget (ERB), the processes by which this solar energy affects climate are spectrally dependent, as detailed by Gray et al. (2010) [69]. Thus, knowing the spectral distribution of the solar

irradiance is critical for understanding the atmospheric processes involved and for modelling the Earth's climate. The spectral solar irradiance (SSI) is therefore also needed and provides a critical input to Earth-climate models, particularly those involving high-altitude atmospheric absorption, lower-level mixing, and coupled ocean-atmospheric effects.

Variations in the solar irradiance, fortunately, are small, as described by Kopp (2014) [24]. On timescales of days, the TSI can vary by up to ~0.3 % at times of high solar activity due to the evolution and passage of large, dark, cool sunspots on the solar surface. The Earth's climate system cannot re-equilibrate to these short-duration variations. Over the 11-year solar cycle, however, the TSI varies by ~0.1 % and the SSI shows much greater relative variability at ultraviolet and x-ray wavelengths. These are timescales that do permit climate and atmospheric responses, and indeed, there are clear global and regional signatures due to the solar cycle [67]. On multi-decadal to century timescales, solar variability is believed to be at similar levels to those over the solar cycle, which can cause even more pronounced climate effects since the system has longer to equilibrate. Monitoring the solar irradiance for such small variations over multi-decadal timescales is therefore critical to any climate-observing system; but acquiring stable measurements over these timescales drives the need for extremely accurate and stable instruments. Note in Table 1.1 that the radiometric accuracies, particularly of the TSI, are far more demanding than any other measurement accuracy requirement.

Because of the Earth's atmosphere, which transmits, absorbs, or scatters incident sunlight, climate-quality solar-irradiance measurements must be acquired from space. Measurements of the TSI commenced in 1978 and have been uninterrupted since, thanks to a series of nearly twenty NASA, ESA, and NOAA TSI instruments that have overlapped temporally (see Figure 1.4). Improvements in accuracy during this four-decade duration have established that the mean solar irradiance incident at the top of the Earth's atmosphere and normalized to a distance of 1 astronomical unit from the Sun is 1361 W m^2 [35]. While ultraviolet measurements began at about the same time, it was not until 2003 when a continual record spanning nearly the entire solar spectrum was measured with spectral resolution from spaceborne instruments. These latter SSI measurements are summarized by Richard et al. (*Workshop Report* §6.2).

Measurement records from individual instruments overlapping in time are pieced together to produce a composite time series by various means, with one of the most sophisticated and least biased being the statistical-based method described by Dudok de Wit et al. (2017) [70]. The four-decade long measurement-based composite can then be compared to longer-duration proxies that are indicative of the solar activity causing irradiance variability. These proxy records can extend the irradiance measurement record back in time, as described by Lean (2017) [71] as well as Kopp (*Workshop Report* §6.1). Comparisons between the historically extended solar-irradiance record and similar-duration Earth-climate records, such as air and ocean temperatures, sea levels, ice and glacier extents, and vegetation growth, provide a means of estimating the Earth-climate sensitivity to solar forcing.

Improving our understanding of climate sensitivity due to natural forcings such as the Sun requires continued, high-accuracy, stable, long-term solar-irradiance measurements from space in order to correctly attribute the causes of climate variability. These solar-irradiance measurements and their needed SI-traceable accuracies are described in *Workshop Report* §6.1 and §6.2.
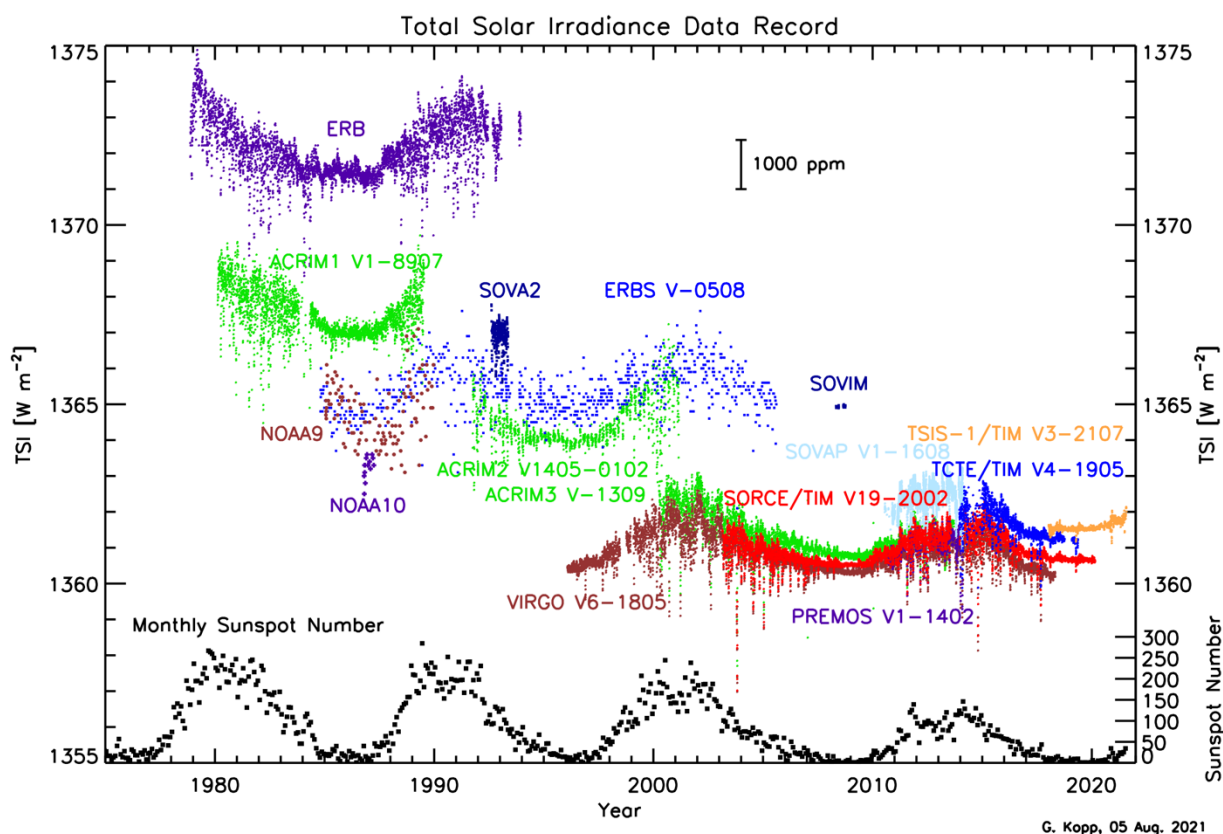
Figure 1.4: The 4-decade long space-based total solar irradiance record has been uninterrupted thanks to the many NASA, NOAA, and ESA instruments contributing to its continuity, which allows construction of a composite time series by accounting for the offsets between the many different instruments. Improved SI-traceable accuracies bring the more recent measurements into better agreement and make the data record more robust against potential future data gaps.

1.10 Earth Energy Balance – Shortwave and Longwave Broadband Outgoing Radiation

Space-borne measurements of broadband reflected solar (shortwave) and thermal infrared (longwave) outgoing top-of-atmosphere radiation from the Earth began in the 1960s [72]. The radiation budget climate record is primarily used to verify climate model performance, study cloud feedback (the largest uncertainty in climate sensitivity), and determine changes in the global heat balance of the planet [10], [73]–[75]. While their primary use has been to support climate research, these measurements have also been used to improve observations of surface solar insolation, benefitting the design of solar panel energy systems.

Current state of the art in broadband outgoing instrumentation is provided by the CERES (Clouds and the Earth's Radiant Energy System) instruments since 2000 on the Terra, Aqua, Soumi-NPP, and JPSS-1 Sun-synchronous spacecraft [76]. CERES total and longwave broadband channels have an SI-traceable uncertainty of 0.5% (k=1), while the shortwave broadband channel is 1.0% (k=1). Stability of the Edition 4 CERES radiative fluxes are estimated at 0.3%/decade for shortwave and 0.2%/decade for longwave [27] Geostationary Earth Radiation Budget (GERB) instruments have been flown on the Meteosat satellite series to improve understanding the diurnal cycle of radiative energy [77] since 2003.

This climate record currently relies on instrument stability and overlap when studying climate change over decades [78]. These authors showed that a gap of even one year in the broadband climate record

leads to critical degradation of the observations of cloud feedback. The paper also showed that a 1-year overlap is required to inter-calibrate successive instruments.

The SI-traceable instrument shortwave channel accuracy required to survive gaps in the climate record were determined to be 0.3% (k=1) by Loeb et al. 2009, and more recently as 0.3% (k=2) [6], [12], [16]. Longwave channel accuracy for cloud feedback was estimated at 0.1% (k=1) [68]. These accuracies for gap survival and to eliminate calibration drift over time are a factor of 5 improvement over current instruments. Meeting these requirements requires new broadband instruments or intercalibration against more accurate full-spectrum reference spectrometers such as those planned for launch by the CLARREO Pathfinder (2023), TRUTHS (~2026) and CSRB (mid 2020s). Simulations of such inter-calibrations have been carried out in the reflected solar spectral region [79], [80] and in the thermal infrared region [81]. CLARREO Pathfinder expects to demonstrate an 0.3% (k=1) or better intercalibration capability and TRUTHS is intended to achieve 0.3% *(k=2)*.

In early 2020, NASA selected a follow-on to CERES named "Libera" (in mythology the daughter of the goddess Ceres), which is planned to fly on the NOAA JPSS-3 spacecraft in 2026 and intends to achieve similar instrument accuracy to CERES. Using current instrument and spacecraft reliability designs in orbit, along with limited fuel remaining for the Terra and Aqua spacecraft, gap risk by the 2026 launch of Libera has been estimated to be ~ 40%. The CLARREO Pathfinder on ISS is currently only planned for a 1-year demonstration mission, but NASA is considering a longer 3- or 5-year deployment, which would allow mitigation of impact on this critical climate record should a gap occur between the CERES and Libera instruments. Further information and references can be found in §6.3 of this report.

1.11   Reflected-Solar Narrowband Imagers

There have been a wide range of reflected-solar narrowband imagers flown on Earth remote sensing satellites since the 1970s. They have been used primarily for meteorological imaging, land resource imaging, ocean biosphere imaging, and atmospheric chemistry. Both SI-traceable ground calibration and changing calibration in orbit have been a major challenge for these sensors since the 1970s [1]–[3], [12] . Recent improvements in both ground and on-orbit calibration have greatly improved the situation but have not advanced to the climate-observing system requirements (see Table 1.2). For land imaging applications, a wide variety of commercial SmallSats and larger research instruments with varying spectral bandpasses and calibration references greatly complicates the use and consistency of data products (§2.3).

The Advanced Very High-Resolution Radiometer (AVHRR) has been widely used on meteorological LEO satellites (NOAA, Metop) from 1978 to the present, but did not include on-board calibration sources [1] and exhibited significant variances in its calibration prior to post-launch harmonization efforts using Earth deserts as a common reference. The Moderate Resolution Imaging Spectroradiometer (MODIS) on the NASA Terra and Aqua spacecraft (2000 to present) represented a major advance over AVHRR, especially in calibration accuracy, and now routinely produces almost 40 Earth remote-sensing data products. SI-traceable accuracy of MODIS spectral bands on orbit is estimated to be ~ 2% *k=1* [28]. MODIS uses on-board solar diffusers with diffuser monitors along with lunar observations at a constant phase angle to monitor on-orbit calibration changes over time. MODIS also included on-board monitoring of band spectral response as well as spatial response, neither of which changed significantly in orbit. The MODIS Terra experienced changes of several percent in polarization sensitivity over time, while the MODIS Aqua did not. As a result of this experience with in-orbit calibration, the MODIS Aqua has been used by GSICS as its reference SI-traceable instrument for intercalibration of reflected solar imagers [65].

More recently, the Visible Infrared Imaging Radiometer Suite (VIIRS), a direct descendant of the MODIS instrument with similar calibration accuracy, has been used on NOAA weather satellites. Both MODIS and VIIRS have been tied to SI standards in their ground calibrations. In-orbit calibrations are primarily to detect changing calibrations over time by using solar diffuser and lunar observations. Because the VIIRS solar diffusers lack a door to protect them from solar exposure when not being used (unlike MODIS), the VIIRS solar diffuser shows much larger degradation than the MODIS diffuser. VIIRS diffuser reflectivity degradation is largest for short wavelength channels (410 nm) and smallest for longer wavelength channels (940 nm), ranging from over 35% to as little as 1% over the first 7 years on orbit for the VIIRS, although some of this degradation is thought to be as a result of some residual hydrocarbon contamination before launch. As a result, the VIIRS uses lunar observations for its stability determination to maintain its 2% calibration accuracy in orbit. Section 7.2.2 of this report (Xiong and Butler) provide a more detailed discussion of MODIS and VIIRS ground and in-orbit calibration uncertainty.

Geostationary meteorological imagers currently have calibration accuracies estimated to range between 3 and 5% k=1 (Section 6 of this report: Table 6.1). While traditional geostationary imagers lacked any on-board calibration for solar-reflectance channels, recent geostationary imagers such as Himawari-8 and the GOES ABI include solar diffusers to improve calibration stability monitoring. They do not, however, achieve the in-orbit accuracy of the MODIS or VIIRS, which remain the GSICS reference instruments for solar inter-calibration.

Landsat imagers have steadily improved their in-orbit calibration over time, especially from Landsat 5 to the more current Landsat 8. While Landsat 5 included only a single onboard lamp calibration source, the currently operating Landsat 8 includes 3 lamps, 2 diffusers, and the ability to view the lunar irradiance at a constant phase angle [82]. The Landsat 9 will be a copy of the Landsat 8 with planned launch in 2021. Landsat 8 has demonstrated less than 0.5%/year degradation of channel sensitivity in orbit comparing on-board sources and PICS (Pseudo-Invariant Calibration Sites) [82]. SI-traceable uncertainty of the Landsat 8 sensors is estimated to be 3 to 5% (k=1) [33]. More recently, the Sentinel 2A and 2B land imagers were launched with an SI-traceable accuracy goal of 3% and a requirement of 5% (k=1) [34], [83]. Intercomparisons between Landsat 8, Sentinel 2A and 2B, MERIS, and MODIS showed agreement within 3% for most channels and within 5% for all channels using desert PICS and deep convective clouds [84]. See §3 for further detail and references.

Ocean colour imagers require highly stable calibrations due to the very small changes in ocean reflectance caused by biological sources and the small size of this signal compared to that of the atmosphere. SeaWiFS ground calibrations obtained 5% SI traceability while system vicarious calibration to the MOBY in-situ ocean site is considered to be within 3% (k=1) for most channels [85]. Stability for SeaWiFS was determined using monthly orbital manoeuvres to view lunar irradiance at constant lunar phase angle. Stability is estimated at better than 0.1% over the mission life [86].

While atmospheric chemistry was not represented at the workshop, these instruments are often high spectral resolution reflected solar instruments with SI-traceable calibration accuracy of 3 to 5%. Examples include TOMS, SCHIAMACY, GOME, OMI, and the SAGE solar occultation instruments [87]. The occultation instruments can achieve high relative accuracy between spectral channels by directly viewing the Sun during solar sunset and sunrise events. Perhaps some of the most important atmospheric sensors in the climate context over the next decades will be those addressing greenhouse gases (GHG). Although we have the OCO series and GOSAT, there are tens more planned for the next decade with the aim that these are linked together as a constellation. Although much of the uncertainty requirements for GHG retrievals is placed on spectroscopy, there is a need for radiance uncertainties of <1% to remove the impact of aerosols and surface albedo and to facilitate an integrated harmonious observing system from the constellation. See Section 10.5

Most optical satellites use post-launch calibration and/or validation using vicarious methods, which use references independent of, and external to, the satellite platform. These include the Moon, clouds, and physical phenomena, such as calculated radiance based on Rayleigh scattering of the atmosphere. However, the most common and widely-used are surface reflectance from bright, spatially-uniform targets – primarily Saharan deserts but also salt flats and snow fields. They rely on either surface-based characterizations using field instruments, the inherent stability of a site used to monitor change, or a calibrated reference through a previous observation by another sensor. Surface-characterized sites use spectrometers usually measuring the surface reflectance compared to a reference reflectance standard (although it can be a radiance measurement) either in campaign mode by teams at the time of a satellite overpass or using autonomous deployed spectrometers (e.g. CEOS RadCalNet [88]). In both cases, the atmosphere needs to be simultaneously characterised to parameterise a radiation transfer code to allow measurements to be propagated to the top of the atmosphere. Section 7.4 indicates that the typical uncertainty of ~ 3-5% k=1 associated with both these methods is dominated by the determination of the absolute reflectance or radiance value and in particular the calibration and use of the field instrument.

For the stable PICS, a similar uncertainty is currently achieved, but here the limitation is primarily due to the accuracy of the radiometric calibration of the site by the reference sensor and its representativeness when used to calibrate another sensor. For current Sun-synchronous sensors there is usually some time delay between observations, and so care has to be taken to account or correct for changes in illumination/view angles and changes in atmospheric conditions [89]. Some improvements can be made by taking results from ensembles of sites where some of the non-uniformity and or surface BRDF uncertainties can be somewhat randomized.

In the last few years formal recognition of the importance of clear evidence of SI-Traceability for these post-launch calibration and validation methods has led to creation of the term 'Fiducial Reference Measurements' (FRM). FRM's distinguish themselves from other post-launch cal/val or in-situ observation by virtue of rigorous documented evidence of traceability usually including some form of comparison but always with transparent accessible methods and uncertainty budgets. It should be noted that the FRM concept in relation to validation of the satellite product applies not only to the direct measurement of the specific 'in-situ' parameter but also the adequacy of its sampling to correlate with the satellite and of course any method or algorithm or auxiliary data need to account for the atmospheric path or viewing angle differences etc. Although being an FRM does not imply high or even adequate accuracy it is an encouragement of the need for robust traceability across the whole Earth observing system [90].

However, with the prospect of non-Sun-synchronous orbits and consequently near simultaneous observations together with agile sensors (pointing capability), the uncertainty achievable from such sites (and indeed the accumulated mean of others) can be reduced significantly towards that needed for climate [79], [91], [92]. The inherent stability of the PICS with suitable characterisation from a SITSat can transform vicarious calibrations into a component element of any future SI-traceable climate observing system.

1.12 Reflected-Solar Spectrometers

One area much in need of improved calibrations is passive reflected-solar studies. These include studies of Earth's radiative energy balance, clouds, aerosols, atmospheric chemistry, land resources/land biosphere, snow cover, and ocean color/ocean biosphere. Reflected-solar instruments commonly degrade by several percent to more than 10% over their lifetime on orbit, often driven by degradation of optical components exposed to high-energy solar UV radiation and/or atomic oxygen in addition to potential step changes from pre-flight calibration to orbit as a function of launch. Given critical climate-

change next-generation observation requirements reaching 0.3% (*k=2*), these current instruments lack the absolute accuracy and SI traceability needed to survive measurement gaps or eliminate uncertainty in calibration drifts over decadal time periods [3], [9], [10], [12], [13]. Sections 4 and 5.3 of the report summarize the state of calibration advances in metrology labs as well as space instrumentation that can achieve these levels of SI traceability. §11 summarizes how high-accuracy SI-traceable orbiting reference spectrometers can be used to transfer their superior calibrations to other orbiting instruments used for climate change observations. In essence, such spectrometers become orbiting metrology laboratories used to calibrate hundreds of sensors using the reflected-solar spectrum to observe global change.

The CLARREO (Climate Absolute Radiance and Refractivity Observatory) Pathfinder mission to the International Space Station planned for launch in 2023 will be the first reflected-solar spectrometer to demonstrate dramatically improved SI traceability in orbit (0.3% *k*=1) as well as the ability to use the spectrometer to match cross-track scanning sensors in time, location, look angle, and spectral wavelengths to

> New high accuracy SI-traceable reference spectrometers (SITSats) will enable 5 to 10x higher accuracy for most satellite climate observations using matched intercalibrations

verify reference intercalibration at the same 0.3% (*k*=1) uncertainty level [6], [21], [38], [79] (https://clarreo-pathfinder.larc.nasa.gov). CLARREO Pathfinder uses a two-axis pointing system to match look angle with other sensors during orbital crossings (under- or over-flights) which will geographically sample tropical to mid-latitude regions of the globe. The ISS orbital plane and precession through the diurnal cycle roughly every month allow matched intercalibrations with nearly all Sun-synchronous and geostationary sensors, with roughly 1000 intercalibrations per year expected for the CERES and VIIRS alone. Each intercalibration orbital crossing from low Earth orbit (LEO) is typically about 3 minutes in duration and results in thousands of matches covering a broad range of viewing geometries and scene types (ocean, land, desert, cloud, dynamic range). Polarization dependence is determined by comparing intercalibrations in highly polarized scenes (cloud-free ocean) with low polarized scenes (thick clouds). Intercalibration is expected to ascertain instrument offset, gain, nonlinearity, polarization dependence, and spectral response shifts. The CLARREO Pathfinder spectrometer will use the Sun as its on-orbit calibration source for relative reflectance observations and will combine this with SI-traceable spectral solar irradiance measurements to provide calibrated radiances. Further detail on instrument design, calibration uncertainty analysis, and intercalibration uncertainty analysis can be found in Sections 8.4 and 11.1.

The TRUTHS (Traceable Radiometry Underpinning Terrestrial- and Helio- Studies) is a UK-led mission recently selected by ESA as part of the Earth Watch program. Similar to CLARREO, TRUTHS has calibration accuracy goals of 0.3% (*k*=2) over the reflected-solar spectrum [8], [14], but uses a very different approach to achieve this level of accuracy. Instead of using the Sun as an on-orbit reference source, TRUTHS uses a cryogenically-cooled (~ 60K) active cavity detector as its reference SI-traceable standard [8], [14], effectively mimicking the traceability chains used on the ground at national metrology institutes. TRUTHS can also acquire direct SI-traceable spectral solar irradiance (0.3% *k*=2) and total solar irradiance (0.02% *k*=2) observations, which CLARREO cannot. The mission is currently intended as a long-term monitoring mission and plans to fly in a 90-degree inclination orbit, allowing it to achieve orbital crossings with all LEO and geostationary sensors, similar to the CLARREO Pathfinder (CPF). While the CPF will obtain observations from 50°S to 50°N in latitude (restricted by the ISS orbit plane), TRUTHS will obtain full global observations as well as intercalibration orbit crossings from the tropics to the polar regions. Estimated launch date is 2026-28. A summary of the TRUTHS mission can be found in Section 11.2.

The China National Space Administration (CNSA) is developing the CSRB (China Space Based Radiometric Benchmark), a TRUTHS-like reference solar spectrometer for flight in the early 2020s. CSRB, like TRUTHS, uses a cryogenically cooled active cavity detector called SCAR to achieve SI traceability in orbit (Zhang et al. 2020, Ye et al 2020). The accuracy goal is 1% ($k=2$) for Earth viewing, 2% (k=2) for lunar viewing, 0.02% for total solar irradiance ($k=2$). The CSRB will also provide an Earth-Moon Imaging Spectrometer (EMIS) for SI-traceable lunar spectral irradiance as well as intercalibration of other orbiting sensors. CNSA plans for a series of such missions with successively increasing accuracy by incorporating lessons learned from prior ones. A summary of the CSRB mission can be found in Section 11.3

Why are three different reference spectrometers in formulation? First, all high-accuracy standards require independent verification by multiple methods, analyses, and research groups. This is the standard process developed for the international metrology laboratories used to determine SI standards and their uncertainty characteristics [93]. A similar process is needed in orbit to achieve SI-traceable verified accuracy at climate change levels that are a factor of 5 to 10 improvement over the best current space-borne instruments. Climate change surprises will have large economic impacts and require high confidence in accuracy over decades of satellite measurements. Multiple independent international and open-access reference spectrometers can provide that confidence, and multiple instruments from different international research organizations can reduce the risk of measurement gaps.

Table **1.3** summarizes the Earth observation characteristics and accuracies of the three reflected-solar reference spectrometer missions mentioned. The CPF is currently within a factor of 2 of the most stringent SI-traceable requirements, and TRUTHS, as planned, will meet the requirements. The CSRB is planned to approach CLARREO and TRUTHS accuracy levels over successive missions in the 2020s. For further information on these three spectrometers, see §11 of this report.

Table 1.3: Reflected-Solar Reference Spectrometers

Mission	Spectral Coverage (nm)	Spectral Sampling (nm)	Spatial Resolution (km)	Spatial Swath (km)	Orbit Inclination (deg)	SI-Traceable Accuracy	Launch Year
CLARREO	350-2300	3	0.5	70	51.6	0.3% *(k=1)*	2023
TRUTHS	320-2450	1-8	0.05-0.1	100	90	0.3% *(k=2)*	~2028
CSRB	380-2350	10	0.1	50	90	0.5% *(k=1)*	2025

1.13 Lunar Spectral Irradiance

Space-borne instruments often include on-board calibration references to provide sensitivity and spectral calibrations. These, however, are subject to degradation with time and use in the space environment, and they cannot achieve the accuracies or stabilities needed across multi-decadal timescales from multi-instrument platforms.

The Moon can provide a needed long-term on-orbit calibration source for these different platforms. The lunar surface, which is a natural solar diffuser, has a reflectance that is effectively time-invariant, so benchmarking the Moon as a high-accuracy on-orbit absolute radiometric reference enables broad inter-calibration capability even between non-overlapping instruments. Since the lunar radiance is comparable in magnitude to Earth-scene radiances, Earth-viewing instruments with lunar-pointing capabilities can safely observe the Moon for on-orbit calibrations. Knowledge of the spectral lunar irradiance at the time of those calibrations enables corrections for intrinsic instrument degradation, gain variations, spectral-sensitivity changes, and optical throughput over the duration of the instrument's

lifetime. Data from temporally non-overlapping instruments can even be directly compared via their disparate measurements of the Moon by knowing the lunar irradiance at the times of each observation.

The empirical Robotic Lunar Observatory (ROLO) model, created using ground-based measurements over many lunar phases and libration angles, provides spectral lunar irradiance as a function of time. This model is described in detail by Stone et al. (*Workshop Report* §7.3). The current ROLO capabilities are at the 5 – 10 % level on an absolute scale and the ~2 % level for relative variations. Improving this model by a factor of 10 would enable broader use for space-based Earth-climate sensors by helping other instruments achieve the accuracy and stability levels given in Table 1.1. Some efforts to achieve this from new ground-based observations are planned by the ROLO team and underway in Europe with a goal to improve uncertainties to <2% [94].

Several future missions, including the three reflected-solar radiometers listed in Table **1.3**, are intended to provide new lunar measurements to enable these desired ROLO model improvements. The CLARREO Pathfinder's HyperSpectral Imager for Climate Science (HySICS) (see description by Kopp et al., *Workshop Report* §11.1) will have improved absolute accuracies based on direct solar-irradiance measurements and will acquire lunar measurements intended to greatly improve the lunar-irradiance model. A high-altitude balloon flight of a prototype HySICS acquired such proof-of-concept measurements in 2014 [38]. The TRUTHS mission (Fox et al., *Workshop Report* §11.2) similarly will acquire direct, high-accuracy lunar measurements using its on-board cryogenic radiometer and spectrometer. Ye et al. (*Workshop Report* §11.3) describe a similar planned Chinese mission, CSRB, that intends to supplement this lunar dataset as well. These three large missions are spaced in time, which will benefit the lunar-irradiance model by providing several lunar phase and libration-angle measurements. Finally, the ARCSTONE, a CubeSat mission currently in the development phase, is specifically dedicated to the issue of acquiring spectral lunar-irradiance measurements. Its mission goals are to measure lunar irradiances to an accuracy of < 0.5 % (k=1) across the 350 to 2300 nm spectral range from low Earth orbit [95].

The improved lunar reference model resulting from these planned space-based assets will enable high-accuracy absolute calibrations and inter-calibrations of past, current, and future Earth-observing sensors, meteorological imagers, and long-term climate-monitoring satellite systems, such as needed for the SITSCOS.

1.14   Infrared Spectrometers

Infrared spectrometers have become a major data source for global weather prediction models and re-analysis data products [96], [97]. Typically flown in low Earth orbit, their global-sampling designs have focused on weather applications, with typical SI-traceable uncertainty in orbit estimated at ~ 0.1K to 0.2K (k=1) (e.g., AIRS, IASI, and CrIS) [43], [98]. These instruments have also demonstrated good stability on orbit, varying from 0.03K to 0.2K per decade depending on instrument, spectral band or channel, and signal level (Smith et al., 2015, Strow and De-Souza Machado, 2020). Stability estimates are made primarily using instrument intercomparisons as opposed to SI traceable uncertainty estimates. Improved bias corrections for weather prediction applications are aiming for SI-traceable uncertainties less than 0.06K (k=1) (§5.1). However, climate science applications, as shown in Table **1.1**, require even more stringent uncertainties of 0.03K (k=1) [10], [12], [21], [22]. As a result, while current weather application infrared spectrometers are excellent instruments, further improvements of a factor of 3 to 5 in SI-traceable calibration uncertainty are needed for future improvement of weather and climate science applications.

Advances in infrared metrology and space-borne instrument design over the last 20 years have enabled designs capable of reaching the desired 0.03 (k=1) SI-traceable uncertainty level ([5], Revercomb et al.

§8.4, and Brindley et al., §11.4). These advances include very high-emissivity blackbodies (emissivity > 0.998) that can be temperature controlled over a very wide range of Earth-viewing temperatures. The large temperature control range requires on-orbit verification of detector nonlinearities. The use of three phase-change cells (gallium at 30°C, water at 0°C, mercury at -39°C) promises on-orbit calibration of all three terms in the equation for blackbody thermistors to less than 0.016K (Revercomb et al. §8.4). These authors demonstrate that the use of a heated halo or quantum laser can monitor blackbody emissivity to achieve an uncertainty contribution of less than 0.02K. These interferometer designs also allow control of polarization sensitivity to similar uncertainty levels. The next step is to demonstrate these types of advances in orbit.

There are two international efforts underway to fly much higher-accuracy infrared spectrometers capable of serving as reference SI-traceable calibration sources for inter-calibration in orbit. The ESA FORUM mission, described by Brindley et al. (§11.4), is planned for flight in 2026 and includes an infrared interferometer designed to observe the wavelength range of 100 to 1600 cm^{-1}, including the first spectrally-resolved observation of the entire far-Infrared spectral region that dominates water vapor greenhouse emissions to space. The SI-traceable accuracy goal for FORUM is 0.03K (k=1) for the spectral region from 300 to 1100 cm^{-1}, which includes most of the far-Infrared critical water vapor absorption spectrum at 300 to 600 cm^{-1}, as well as the temperature profile sensing CO_2 spectrum near 650 cm^{-1}. Spectral resolution is 0.36 cm^{-1}, similar to weather spectrometers. FORUM is designed to fly in close formation (~ 1 minute) with the EUMETSAT IASI-Next Generation instrument on the METOP-SG-A1 satellite. This will allow overlapping coverage of the entire thermal infrared spectrum for calibration of broadband sensors such as CERES. It will also enable improved intercalibration of IASI-NG and NOAA CrIS instruments from 1100 to 645 cm^{-1} for temperature sounding calibration relevant to weather and climate change observations. FORUM, however, will not cover the spectral bands that IASI and CrIS observe above 1600 cm^{-1}.

A second international effort underway is the Chinese space agency CSRB (Chinese Space based Radiometric Benchmark) planned for launch in the early to mid-2020s [39], [99]. The instrument design achieves its accuracy by following the concepts developed by the University of Wisconsin prototype described in Revercomb et al (§8.4). CSRB provides a 17-km nadir field of view (similar to FORUM, AIRS, IASI, and CrIS) and covers the contiguous 600 to 2700 cm^{-1} wavelength region with spectral resolution of 0.5 cm^{-1}. The first CSRB instrument's SI-traceable accuracy goal is less than 0.07 K (k=1), or about a factor of 2 worse than that of FORUM, although later flights of CSRB are planned to reach the 0.03K (k=1) climate goal.

1.15   Infrared Narrowband Imagers

Current-generation infrared narrowband imagers such as MODIS and VIIRS have calibration SI traceability that is typically much more accurate than reflected solar narrowband imagers (§7.2) but usually not as accurate as the infrared spectrometers summarized in §11.

The greatest experience with SI traceability of thermal infrared imagers on orbit is from the MODIS Terra and Aqua instruments, which are now reaching 20 years on orbit ([28]; Xiong et al. §7.2). Pre-launch calibration is traced to NIST temperature standards using a high-emissivity (0.998) variable-temperature blackbody and cooled NIST transfer detectors. On-orbit calibration is traced to an on-orbit blackbody with varying temperature control (270 to 315K) in addition to scans of deep space.

For typical radiance levels at nadir view, the Aqua MODIS instrument has an uncertainty that ranges from 0.2% to 0.8% (k=1) with window channels in general providing higher accuracy than infrared sounding channels for atmospheric temperature, water vapor, and ozone [28]. Terra MODIS typical radiance uncertainty varies from 0.1% to 2.3%, again with higher uncertainty for sounding channels.

For 30% of typical radiance levels (e.g., cold cloud images), accuracies of the sounding channels can be lower by a factor of 3 to 5 than for typical radiance levels, with several of the channels reaching uncertainties of 2 to 3% on Terra and Aqua MODIS. The most accurate channels are the atmospheric window channels at 3.7-μm and 8 to 12 μm wavelengths which range from 0.2 to 0.7% at low radiance levels and 0.15 to 0.5% at typical radiance levels. Gain corrections over time for the imager thermal infrared channels are much lower (typically < 1%) than those of the reflected solar channels.

There is much less experience with calibration of the NOAA VIIRS imager, but early results indicate similar performance to MODIS [29], [100]. Direct inter-comparisons of MODIS and VIIRS show that their thermal channels are within about 0.1K for most channels at typical radiance levels [100].

A detailed comparison of the multiple methods used to determine on-orbit calibration of reflected solar and thermal band spectral channels for MODIS, VIIRS, the GOES imager, and GOES-ABI can be found in Datla et al. 2016 [101].

Overall, like the infrared sounder spectrometers, the infrared imagers are not yet able to meet climate-science needed SI-traceable accuracies of 0.03 to 0.06K (k=1). Note that for a typical 10 μm window channel, 0.03K uncertainty is approximately 0.05%. Combining the summary in this section with the requirements in Table **1.1**, a factor of 3 to 20 improvement in uncertainties (depending on wavelength) for infrared imagers is needed for climate-change science applications. Achieving this level of uncertainty will likely require infrared reference spectrometers in orbit as described in §8.4, 11.3.3, and 11.4 of this *Workshop Report*. Intercalibration methods at the required 0.03 (k=1) uncertainty level have been demonstrated in Tobin et al. (2016, 2006) [81], [102] as well as in Revercomb et al. (§8.4).

1.16   Thermal-Infrared Laboratory Methods

In §8 the current state of the art in pre-flight calibration methods for the thermal infrared (TIR) are discussed using examples such as NASA MODIS and ESA SLSTR. In this spectral region the underpinning methods and route to SI-traceability have not changed significantly for many decades. Although in the last decade, with the drive for further improvements in accuracy some evolutionary advances have started to be introduced which whilst not necessarily making a major difference to pre-flight calibration uncertainty may help to reproduce this performance in-flight

The primary calibration reference for the TIR spectral range is the predictable radiance from a 'Planckian' black body radiator at a given temperature. For this spectral region the black body operates near ambient temperature allowing relatively large aperture sources to be created. With good design and spectrally flat black coating, emissivity's of >0.999 can be achieved and contact thermometers can readily measure temperatures with uncertainties <1 mK.

Of course, in practice, ensuring uniform temperature over a large emitting surface is not trivial nor is the management of stray radiation, noting that most of the surrounding measurement environment including the instrument under test are self-emitting radiation in the same spectral range. However, achieving the pre-flight uncertainties needed for most TIR missions, even at climate quality is not really a current issue. This is not necessarily the case for some upcoming missions such as ESA FORUM (§11.4), where the wavelength region of interest is extended into the far infrared ~ 100 um. This spectral extension requires improvements to the measurements of emissivity of black coatings in this region.

Although also of benefit for pre-flight, the availability of new Carbon nanotube black coatings provide lower spectral reflectance than most current black coatings and thus can improve the emissivity of the black bodies, allowing simpler designs which can enable greater thermal uniformity. These are particularly useful for spaceflight, where mass and volume are at a premium. Additionally, for spaceflight, metal and other freezing-point reference black bodies have now been designed and tested

to allow the temperature defining contact thermometers to be absolutely calibrated in space, removing uncertainties associated with drift. These recent developments will more readily facilitate the transfer of pre-flight calibration performance onto the spacecraft.

1.17 Passive Microwave Imagers and Sounders

The designs of microwave sounders on current satellites are optimized for weather applications, where they continue to provide some of the highest impact observations when assimilated into numerical weather prediction models. However, their data could also provide valuable climate insights – but challenges exist as improvements in radiometric calibration are needed to achieve the desired accuracy and stability of satellite-based microwave-radiometer observations intended for the production of climate data records.

In §9, Houtz et al. emphasize the importance of linearity, stability, low antenna sidelobes, and high-frequency stability in establishing traceability of measurements to an SI-traceable standard [46]. Data from such an instrument could be used for climate studies and also to transfer its calibration to weather-satellite instruments. With the selection of a suitable orbit, a climatology of the diurnal variation in the measured parameters could be compiled and used to understand and refine trends from earlier microwave radiometers over past decades, as these terms tend to dominate these instruments' uncertainties. Furthermore, multi-year stability would be verified by comparison to radio-occultation measurements, which can also provide a valuable link to these SI-traceable observations.

§9.2.3 goes on to introduce the potential application of lunar calibration to microwave radiometers, as its radiance is highly predictable and could be accurately modelled. As the Moon is observed by many satellite microwave sensors, lunar observations could be used to fit such a model. This would need to account for full microwave spectral coverage and the observed phase lag due to microwaves' penetration deep into the lunar surface and the associated thermal cycle. Initial applications of this newly developing microwave lunar calibration method focus on calibration trending, which could then be extended to perform inter-calibration between microwave sensors. However, the long-term aim of tying microwave lunar calibration models to SI requires the development of SI-traceable microwave observations of the Moon.

1.18 Relation to Global Stocktake Activities

High accuracy reference SITSats from the U.S., Europe, and China are planned for launch in the mid 2020s

This workshop was primarily focussed on the measurement needs for climate with a particular emphasis on those directly impacting the Earths' radiation imbalance and consequently uncertainty in the predictions of climate models. The emergence of SITSats designed to support this goal also provides the opportunity to upgrade the performance of the earth observing system as a whole, enabling improved observations for many other applications critical to understanding the Earth's cycles and the specific impacts of climate change together with the necessity and progress of climate action.

Attracting significant international attention at present is the global stocktake resulting from the Paris agreement of 2015 and ambitions of many nations to implement net zero targets to seek to keep global warming to < 2 °C above pre-industrial levels. To monitor progress towards achieving this goal, governments have agreed to undertake 5 yearly stocktakes of net equivalent carbon emissions. In the near term this stocktake is based on nationally declared inventories which are primarily derived from 'bottom up' audits and have little if any contribution from space-based observations. The nationally

declared net values should account for the effect of emissions (direct from fossil fuels and as a result of land use including biological methane and thawing of permafrost etc) and sinks (natural and manmade). In addition to accounting for nationally controllable sinks it is also important, from a global perspective, to monitor major non-national sinks such as those of the ocean which accounts for sequestration of half of all CO2 emissions. Measurements of water leaving radiance and from it ECVs such as Ocean Colour and the biology responsible are critical for this overall global assessment.

Remote sensing of the Earth will increasingly play an important role in this Stocktake and understanding of the various earth cycles which contribute. For the oceans, this is already the case and §10.4 presents a discussion on the importance of SI-traceability and the need for increased uncertainty, GCOS equivalent to a requirement of ToA radiance uncertainties of, 0.5% are needed. Although, the current space-based observing system is far from meeting this directly, strategies to use well-calibrated in-situ sites on the Ocean e.g., the buoys MOBY and Boussole support calibrations of the system (sensor and retrieval algorithm) as a pragmatic workaround. However, with SITSats, direct ToA calibrations of Ocean colour missions over different parts of the ocean including coastal zones, where the current strategy has significant issues, at the uncertainties needed for climate and the stocktake become possible.

Similarly, measurements of surface vegetation (biomass e.g., forests) and land use on a global scale can only realistically be carried out from space. Whilst not necessarily requiring the very high accuracies of some applications such as radiation budget and even ocean colour, improvements will lead to better quantification of carbon stocks and land classification for emissions/sinks inventories. It will also support efforts for sustainable food supplies with improved crop yield estimates and automated farming. In some cases, SITSats may contribute directly to these observations but in the main it is through the upgrade of performance of imagers like Sentinel 2 and Landsat adding additional confidence and rigour through ensuring SI-traceability and unequivocal trust in the data and resultant information.

In terms of emissions, SITSats are unlikely to make a significant direct contribution to the measurement of GHGs, lacking the spectroscopic resolution needed for accurate retrievals. However, in some cases their hyperspectral resolution may still be enough to detect large emitters of methane, carbon dioxide and also total column water vapour (§10.5). However, the world has already set-about the design and build of a dedicated constellation of GHGs satellites to facilitate the necessary audits that will likely be needed in the future. To enable the timelines and geographical coverage needed requires a significant number of satellites operated in complimentary orbits. An international cooperative partnership of space agencies is required not only to provide the necessary resources but also to ensure the necessary trust in the observations.

SITSats can play a key role in supporting this constellation. They can, not only provide the means to ensure the <1% uncertainty in in-flight radiometric calibration is achieved, but also help address sensitivities in the retrieval algorithms due to effects of surface albedo and aerosols (§10.5). The SITSats will fundamentally be able to provide the unambiguous mechanism to enable interoperability across the different observing platforms and delivery of a trusted data set to support the global stocktake from a coherent constellation of satellites viewing the Earth in an unbiased diurnally representative manner.

1.19   Active Lidar and Radar Sensors

A follow-on workshop should be planned for SI traceability of active satellite sensors in 2026

While passive sensors dominated satellite remote sensing over the first 7 decades of space-based observation of the Earth, in the last 20 years active sensing using lidar, radar, and GPS signals have become an increasingly critical part of Earth observations.

Examples include radar altimeters for sea level (JASON) and polar ice elevation (CryoSat), scatterometers for ocean surface wind speed (QuikSCAT), lidar for aerosols and clouds (CALIPSO), lidar for ice sheet altimetry (ICESAT), lidar for atmospheric winds (Aeolus), radar for clouds and precipitation (CloudSat, GPM), and GPS Radio Occultation for temperature and water vapor profiles (COSMIC). Radar and lidar have also been used to measure gravitational anomalies (GRACE).

Many of these active sensing systems have now developed climate records exceeding a decade in length. As these active sensor observations are used for key climate change observations, a deeper understanding of the SI traceability of their instrument accuracy will become more and more important to evaluate the uncertainty of their climate change records.

Some of the active sensors have begun to consider the requirements for climate change records. Several analyses have been carried out for GPS radio occultation atmospheric temperature climate records [103], [104]. Another example is the climate change record for cloud height and cloud fraction from satellite lidar [105], [106]. The GRACE mission is currently working to understand the uncertainty of the gap in observations between the GRACE and GRACE FO and provided a summary of that progress at the workshop.

While most of the active sensing research communities were not ready to contribute to the 2019 SITSCOS workshop, a future workshop should endeavour to include more studies of the SI-traceable calibration of active sensors, their impact on climate change observations, and the relevant accuracy requirements for future sensors.

1.20 Reflected-Solar Polarimeters

Polarimeters, like active sensors are a relatively new satellite measurement and have been pioneered by recent POLDER observations of aerosols and cloud properties. Polarization observations are useful for both direct retrievals of atmosphere and surface properties as well as for correction of polarization effects in reflected solar imagers and spectrometers. New missions such as PACE expect to achieve major advances in earth observation of aerosols and ocean colour through the combination of polarimeters with other active and passive reflected solar instruments. As for active spaceborne sensors, there is a need for further development of climate quality instrument requirements including SI traceability of polarimeter observations.

1.21 Conclusion

There is an increasing urgency to reduce uncertainties in climate observations and climate change predictions. Such improvements are key to advancing our understanding of the economic, political, and societal impacts of climate change mitigation and adaptation investments, approaches, costs, and benefits. This leads to an urgent call to implement and maintain improved SI traceability of satellite remote sensing observations used in support of climate science and in providing rigorous observations of climate change. The technologies such as orbiting SI reference spectrometers to provide these advances have been demonstrated in the laboratory, on the ground, and in high-altitude balloon experiments and will be demonstrated in space in a few years.

The workshop developed a set of recommendations consistent with the new requirements, capabilities, and opportunities

While the currently planned SITSat reflected-solar and infrared spectrometers represent a great advance, further work is needed across the climate observing system to achieve the required accuracy and increased confidence in climate change observations in a sustainable manner:

- The reflected-solar SITSat teams should consider use of the Moon as a stability verification over long time periods independently of their existing SI-traceability approaches. This may allow reaching stability verification at the < 0.1%/decade level at relatively low cost. Further improvements in the accuracy of lunar irradiance models are also required.

- Current NASA plans for the CLARREO Pathfinder mission include demonstration of intercalibration for VIIRS and CERES instruments on JPSS, but should be extended to include Geostationary imagers and chemistry sensors, PACE ocean color, Landsat, Sentinel 2, SmallSat land imaging constellations, and international surface calibration sites. These plans should also extend the mission operations plan from the current one year to five years to enable overlap with the TRUTHS and CSRB SITSats.

- The U.S. should be encouraged to add the developed infrared SITSat CLARREO-like spectrometer to complement the reflected solar spectrometer to reach the required SI traceability goals from independent sensors through the entire thermal infrared spectrum (at least 200 to 2000 cm^{-1}). FORUM whilst complimentary will not meet the necessary accuracy through the entire infrared spectrum, and its accuracy goals are still in development. The LIBRA Chinese mission is meant to achieve those goals but only through improvement of multiple missions.

The world's space agencies should initiate plans to strategically sustain on an operational basis an SI traceable climate observing system into the long-term in readiness to continue and reap full benefit from the current planned SITSats. Whilst one of the benefits of high accuracy SI traceability means that gaps in observations between missions can exist without necessarily compromising the longer-term data record, overlapping continuity reduces sensitivities in monitoring climate change resulting from natural events like ENSO and volcanoes.

- Passive microwave instruments require further work on laboratory calibration references, SI traceability at climate change accuracies and flight of demonstration reference calibration sensors in orbit.

- Active sensing by radar, lidar, and gravity missions are newer satellite capabilities and have recently begun to consider climate change requirements and SI-traceability requirements on orbit. These sensors were not considered in the current report. Extensive additional research on SI traceability is needed in the area of active sensors as well as polarimeters.

- Continued efforts to increase the number and nature of FRM quality surface measurements to provide complementarity to the SITSats and the need to build confidence in the complete network of EO observations in-situ and space and their integration to further improve models and understanding of processes and Earth cycles.

- A follow-on SITSCOS workshop should be planned for 2026 to consider early results and status of the SITSat missions, as well as to extend the scope of the next workshop to include progress and plans for SI traceability of microwave, polarimeter, and active satellite sensors including lidar, radar, gravity, and radio occultation sensors, which are an increasingly critical part of climate observing system monitoring as well as studies of climate processes.

The SITSCOS workshop was a valuable international effort toward defining more rigorous climate observing system requirements. The workshop also demonstrated that these improvements in SI traceability of satellite remote sensors would also benefit applications varying in weather prediction, ocean biology, and land surface remote sensing. Given the new missions in the 2020s relevant to improving on-orbit calibration (CLARREO Pathfinder, TRUTHS, FORUM, and two Chinese missions), a follow-on workshop in ~ 2026 could provide a major update on the topic of SI traceability

of spaceborne Earth observations. At that time, similar calibration-improvement efforts in passive microwave, gravity, active radar, and active lidar should be included. The future of all aspects of climate-observing measurements is encouraging, and we look forward to dramatic improvements in resulting research in the next decade.

We thank the workshop participants for their work on presentations, contributions to this workshop report, and special issue papers. More detail than in this *Workshop Report* can be found in the *Remote Sensing* journal special issue based on this workshop, as well as references in the workshop report.

§1 Authors: **B. A. Wielicki[1], T. Hewison[2], N. Fox[3], G. Kopp[4]**, [1]NASA / LaRC, [2]EUMETSAT, [3]NPL, [4]Univ. of Colorado / LASP

2 Societal Need

2.1 Introduction

Climate change drives a wide range of current and future societal impacts that cross the spectrum of human activities. Unfortunately, large uncertainty remains in key climate science questions that in turn drive uncertainty in

> **How much should society invest in climate-change research?**

cost/benefit analyses of societal mitigation and adaptation strategies. One of the largest of these factors is the uncertainty in climate sensitivity, which remains a factor of four at 90% confidence level [107]. These levels of uncertainties in climate sensitivity make recognizing the imminent importance of and funding for necessary international climate-mitigation policies difficult.

Climate sensitivity can be thought of as the volume dial on the climate system: It determines the amount of long-term warming that will occur for a given level of forcing. The amount of warming in turn drives a host of global and regional climate system changes including sea level rise, temperature and precipitation extremes, water resources, and ecosystems. Those climate system changes then drive economic impacts. While economic impacts of climate change including costs of mitigation and adaptation strategies have been studied extensively (e.g., IPCC Working Group II and III reports), little attention has been placed on the economic value of improved climate science. For science, 'business as usual' means doing the best science for the usual societal investment in scientific research for a particular discipline. In the U.S., federal government investment in climate science is ~ $2 billion dollars/year and has remained constant for the last 25 years when adjusted for inflation (see USGCRP annual reports). Yet the proper economic question to ask is "How much should society invest in climate research?" Such a question falls under the umbrella of research called "Value of Information," or VOI. We will summarize in this article the need for an improved climate observing system, as well as recently documented estimates of such an observing system's economic value and return on investment.

2.2 Need for an Advanced Climate Observing System

There are many observations that are used by climate scientists to determine climate change over decades and even centuries. Unfortunately, very few of them were designed with climate change observations in mind. A good example is our weather observing system, which has typical temperature absolute accuracies of 0.3K compared to the desired 0.03K for decadal climate change [10]. For many if not most observations, climate change observations would typically require a factor of 5 to 10 more accuracy than weather or process observations with the evidential rigour that the accuracy is tied traceably to international standards [e.g., SI standards maintained by the world's national metrology institutes (NMIs)]. A second challenge is that there are roughly 50 essential climate variables (ECVs) in the climate system [11] compared to 5 for weather prediction. This large difference is driven by the many complex systems that interact in determining the Earth's climate system and its impact on society. These include measures of the global atmosphere, ocean, cryosphere, biosphere (land and ocean), land use, land hydrology, chemistry, solar variability, and geology, including volcanism. Third, weather can be thought of as one small part of the climate system at a subset of climate timescales: those out to a few days as opposed to those including seasonal, annual, decadal, and even century timescales. As a result, climate system observations must deal with much greater complexity, at much higher accuracy, over much longer timescales than weather. The observations must maintain their accuracy and traceability to international standards over decades: times longer than the life of in-situ or even satellite-based instrumentation, indeed longer than the length of a scientist's or engineer's career.

The challenge of such an observing system far exceeds typical scientific observing systems including those of weather, large particle physics experiments, or astronomy, which are some of the largest current scientific endeavours. It is perhaps not surprising that we currently lack such a rigorously detailed and designed climate observing system. Instead, we have a collage of weather, resources, and research observing systems that are cobbled together in a heroic effort to study climate change. In some cases, like surface air temperature, there are 7 different weather observing systems (surface sites, weather balloons, ocean buoys, ocean ships, aircraft, infrared satellite sounders, and microwave satellite sounders) allowing sufficient independence to verify, improve, and eliminate most artifacts that might confound climate change observations, although still resulting in accuracies requiring decades to confidently quantify long-term change. But for most of the 50 essential climate variables, there are at most two (and often none), leading to major challenges in detecting calibration drifts, changes in instrument design or sampling, or accurately bridging gaps in observations that may last several years, leading to increased uncertainty and unreliability in the merged long-term data records.

There are many national and international documents that discuss the shortcomings in our current climate observations [9]–[13], [15]. But the bottom line remains that we lack a rigorously designed and maintained 'trustworthy' climate observing system. In the most recent U.S. National Academy Earth Science Decadal Survey [12], an examination of over 30 quantified and prioritized climate science objectives shows that critical observations are missing for 80% of the "Most Important" climate science objectives, 71% of "Very Important" objectives, and 47% of "Important" objectives. Critical observations are missing for roughly 2/3 of all climate science objectives. See Chapter 9 and Appendix B and C of the report for details [12].

2.3 Designing an Advanced Climate Observing System

How would one design a rigorous international climate observing system? Discussion of this topic can be found in recent Academy of Science reports: the "Continuity Report" [10], and the Earth Science Decadal Survey [12]. An overview of the topic is also discussed in a recent journal article in AGU Earth's Future [13]. We give a summary of key points in the list below.

> **Improved accuracy, SI traceability, and documented transparency of methods and analysis are key elements of a future 'advanced climate observing system'**

- Use of quantified climate science objectives based on major national and international reviews and reports such as the IPCC and USGCRP reports. Examples would be to narrow the uncertainty in long term climate sensitivity or aerosol radiative forcing by a factor of 2. Or to reach a specific level of accuracy in the rate of global and regional sea level rise. See a wide range of examples in the 2018 Decadal Survey (chapter 9 and Appendix B of [12].
- Rigorous quantitative requirements for instrument accuracy, sampling accuracy, and remote sensing retrieval accuracy sufficient to eliminate large delays in quantifying climate change trends. Observing system lack of accuracy increases trend uncertainty beyond the minimum caused by climate system internal natural variability. This increase typically extends the time to detect climate change trends by decades. [6], [10], [15], [20].
- Improved use of Observation System Simulation Experiments (OSSEs) to quantify the utility of a given observation to reduce scientific uncertainty in past and future climate change [12], [13], [108].
- Traceability of instrument observations to international (SI) standards to enable removal of calibration drifts and the ability to rigorously deal with data gaps. This is especially critical for space-based observations which provide many of the global climate change data sets. [3], [12].

- Provision of a much more complete set of climate system observations based on quantified climate science objectives, which currently suggest that critical observations are missing for 2/3 of all climate science objectives in the recent 2018 Decadal Survey report. GCOS implementation plans provide definition of the 54 essential climate variables [11].
- Follow existing GCOS observing principles [11].
- Provide independent observations of all essential climate variables (instruments, techniques, systems) to allow verification of climate system surprises after they occur.
- Provide independent analysis (methods, research groups) of all essential climate variables. Almost all computer code has errors, but independent development of analysis systems will have different errors, thereby allowing comparisons to discover and correct issues.

2.4   Cost and Economic Value of an Advanced Climate Observing System

The above list indicates that major improvements are needed in climate system observations: both long term climate change and climate process observations. Some of the advances would simply require more rigorous processes than currently employed (independent analysis) while others would require improved global sampling, or design of instrumentation with more accurate traceability to international standards. In many cases, more complete observations would require application of new technologies such as space-based advanced lidar (wind profiles, aerosols, clouds, ocean phytoplankton), radar (rain, snowfall, convective vertical velocities), and radio occultation temperature profiles. New technologies for in-situ observations would also be key, such as adding chemistry measurements to deep ocean floats, and increasing the depths the floats reach as well as lower-cost instruments to facilitate increased geographically representative sampling.

How much would such an observing system cost? Adding independent observations, independent analyses, higher accuracy, and more complete observations might triple the cost of current global investments in climate research (observations, analysis, modelling, data storage/archive/distribution). Building a global climate observing system will also require increased investment in the data analysis, climate modelling, and data stewardship needed to benefit from such a system. The total of global climate research investments is currently estimated at $4 billion/yr, so that an additional $8 billion/yr might be required. The investment would be required for many decades (at least 30 years) because of the intrinsic long-term nature of climate change itself. Once built, however, efficiencies of reproduction and scale might decrease costs over time for the basic instrumentation, which is one of the largest costs.

Given that $8 billion/yr is a significant global investment, how could we estimate what the return on that investment might be? Four recent research papers [17]–[19], [109] have estimated that economic value and concluded that through 2100 it ranges from $5 to $20 trillion U.S. dollars. The cost of tripling the global investment in climate research (including development of the more rigorous climate observing system above) was estimated to provide a return on investment of roughly $50 per dollar invested [17]. All economic values are given in net present value using a discount rate of 3% (the nominal value from [110]).

As scientists, how do we understand such large economic value and return on investment estimates? We first need to consider some basic economic concepts. We begin by scaling the magnitude of global gross domestic product or "global economy" as roughly $85 trillion U.S. dollars. Second, "business as usual" carbon dioxide emissions are predicted to cause climate damages in 2050 to 2100 that range from 0.5% to 5% of GDP annually [110]. Such damages would range from 400 billion to $4 trillion per year. The large range is, to first order, because the uncertainty in climate sensitivity remains a factor of 4 at 90% confidence level [107], [110]. Climate sensitivity measures the amount of global temperature change per unit change in atmospheric carbon dioxide. A range of economic impact studies conclude

that impacts rise roughly as the square of the amount of global temperature change [110]. The economic value of narrowing the uncertainty in critical issues like climate sensitivity as a result are very large.

Relating the economic value of benefits that return in the future to alternative investments that could be made requires the use of a concept called Discount Rate. All future benefits are discounted by a selected percentage per year to account for the fact that most people would prefer to have money now vs the future, and to allow comparison of how the same funds could be invested in alternative investments, including those with short term goals. The nominal discount rate used for long term climate change is 3% ([110]) but arguments have been made for both lower values at 1.5% [111], or higher values at 5%. Using the nominal 3% discount rate, an investment that pays back in 10 years is discounted by 1.03^10 or a factor of 1.3, 25 years by a factor of 2.1, 50 years by a factor of 4.4, and 100 years by a factor of 21. This makes it obvious that discount rate is very important to such calculations, and that paybacks 100 years in the future are negligible. For climate change returns on investment, discount rate is then used to derive the Net Present value by discounting any return by the number of years into the future that it will be realized. There is another way to think about discount rate and why 3% might be a reasonable value for global issues such as climate change. The growth rate of global GDP averages about 3% and has so for a long period of time. Therefore, discounting at 3% per year also provides a reference to returns that are above those expected for global average GDP increase.

Now that we have a few basic concepts in mind, Figure 1 provides a schematic for the economic value of information (VOI) estimates in the Cooke et al. papers [17]–[19]. This figure shows the methodology for converting improved climate science knowledge into economic value. The blue boxes on the left give the baseline condition with business-as-usual greenhouse gas emissions, which, through climate sensitivity, leads to the baseline amount of climate change, which in turn leads to the baseline amount of economic impact. This is the state with no or modest societal action on climate change. Meanwhile society (and scientists) are looking through 3 fuzzy lenses at climate change: the first fuzzy lens is that of natural variability of the climate system such as swings between warm and cold phases of the ENSO cycle or the Arctic Oscillation or the Pacific Decadal Oscillation. These are examples of internal variability of the climate system itself and represent noise that we must detect human climate signals against. Even a perfect observing system cannot eliminate this fuzzy lens. The second fuzzy lens is the fact that our climate observations are themselves inaccurate whether through calibration, sampling, or through weak relationships to the climate variable desired (e.g., indirect proxy observations). When added to the fuzzy lens of natural variability, these observing system uncertainties can delay the time to detect climate trends by 5 to 50 years [6], [10], [20].
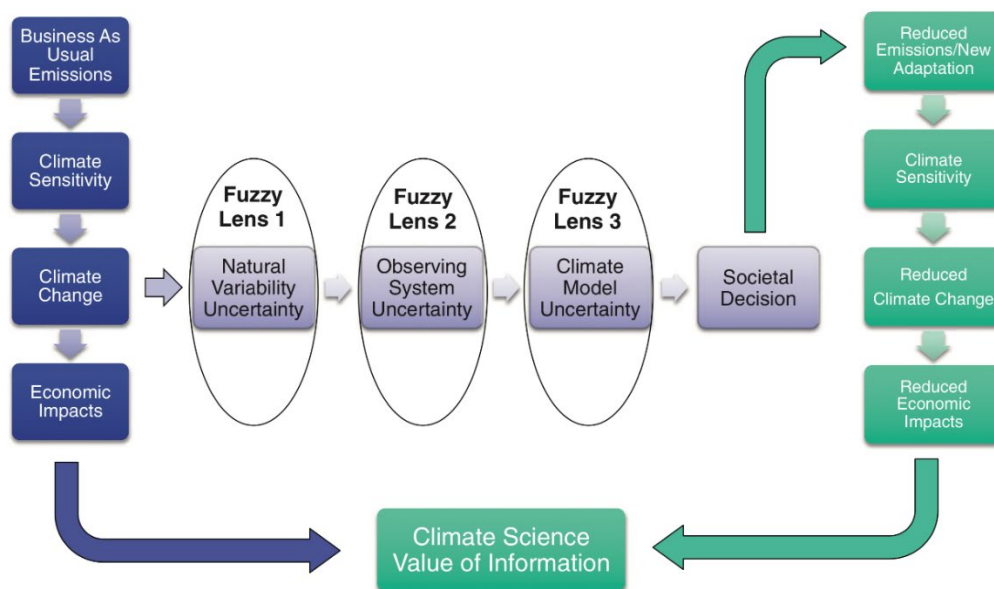
Value of Information Estimation Method

Figure 2.1 Schematic for estimating the economic value of improved climate change information (from Weatherhead et al. 2017).

This large information time delay is the factor in societal decisions that improved accuracy in our climate observations can directly impact. The third fuzzy lens is that of climate model uncertainty. Climate models are used to predict the change that will occur under a range of proposed emissions scenarios (e.g., weak, moderate, or strong greenhouse gas emissions policies). But those

> **Improved accuracy in observations significantly reduces time for evidence (scientific and economic) to be sufficiently trustworthy to oblige action from policy makers**

models are imperfect and currently show a range of a factor of 4 uncertainty in climate sensitivity [107]. Improving the models requires both improved climate process observations for driving model uncertainties (e.g., aerosol forcings, cloud feedbacks, glacier melt) as well as improved long-term decadal observations of climate change to verify model performance and uncertainties. As a result, this fuzzy lens can also be improved through a more rigorous climate observing system.

The key concept used in Figure 2.1 is that better observations, analysis, and modelling can shorten the time to reduce critical climate science uncertainties like climate sensitivity that are holding back improved societal decisions on balancing emissions reduction vs. later climate change adaptation. The shortened time to reach a given level of confidence can be related to the amount of improvement in accuracy and quality of the observations of climate change for key elements such as cloud feedback [6], [10], [12]. This shortened time to narrow uncertainty can, in turn, be used to relate changes in society decision points to change in emissions strategies. Once emission strategies are changed, then economic estimates of reduced economic impacts and costs of emissions reductions can be used to determine the Net Present Value of improved observations [17]–[19].

> **Cost of delay in establishing an adequate climate observing system is 50x that of the investment**

While such studies cannot predict when society will make such decisions, they can compare the sensitivity of change in economic value if society requires more or less confidence in scientific predictions (e.g., 80% vs 90% vs 95%), requires lower or higher climate change signals to occur, changes which emissions reduction strategy is used (moderate or strong), which discount rate is used (2.5%, 3%, 5%), or even how soon such improved climate observations become available (5, 10, or 20 years). Sensitivity to how society makes the decision (moderate or high confidence, amount of signal, emissions reduction strategies) only varies the economic value by about 30% [17]. Discount rate variations can vary the economic value from $3 trillion to $18 trillion [17]. Changing when the more rigorous climate observations become available suggest that every year of delay costs society ~ $500 billion in lost investment opportunity, a figure 50 times the estimated cost of such observation improvements.

What are additional caveats on such an economic analysis in addition to those mentioned? There are uncertainties in the cost of climate change impacts from factors that were not included in the SCCM2010 analysis and would therefore increase the economic value: ocean acidification, international conflicts over resources and refugees, species loss, unexpected climate change accelerations (e.g., tipping points) such as arctic or sea bottom methane release, and larger-than-IPCC-estimated amounts of sea level rise. Uncertainties that could reduce the economic value would include unexpected rapid shift to greenhouse gas emissions well beyond the current Paris agreement (factor of 2 to 4 faster) or unexpected early technological breakthroughs in cost reduction of renewable energy and battery technologies (e.g., a sudden factor of four reduction in 2025). Such technology breakthroughs would be in excess of the existing rapid reductions underway in solar, wind, and battery technologies with learning rates of 15 to 25% cost reduction for every doubling of cumulative production.

How do such economic value estimates compare to weather prediction economic value? An estimate for the U.S. alone was given as $33 billion/year and ROI of 6:1 [112]. The global climate change observing system value discussed above provides an ROI that is roughly 10 times as large as the U.S. current weather prediction ROI.

2.5   Conclusions

In summary, we lack a designed, rigorous, and complete global climate observing system. The cost of providing such a system might be an additional $8 billion U.S. dollars per year in global climate research investment (tripling current levels). A new improved climate observing system could reduce trend-detection uncertainties 15 to 30 years sooner than current observations. The total value to the world of such a system is estimated at between $5 and $20 trillion dollars. Return on investment is estimated as 25 to 100:1. The return on investment is expected to exceed that for weather observations. Inflation adjusted U.S. investments in climate research have stagnated over the last 25 years, despite the large remaining uncertainties and their large potential economic impacts. Even very large uncertainty of a factor of 5 in economic value would not change the conclusion: ROI would in that case range from 10:1 to 250:1. The cost of delaying such a system is estimated at roughly $500 billion/yr. A new global international climate observing system would be one of the most cost-effective investments that society could make.

§2   Authors: **B. Wielicki[1]** and **R. Cooke[2]**, [1]NASA / LaRC, [2]Delft Univ.

§2   Editor: **Greg Kopp**, Univ. of Colorado / LASP

3 Earth-Observation Metrology for Climate Data Records

3.1 Metrology and Climate Data Records

The international metrology community, through the establishment of the international system of units (SI), has achieved measurement stability and consistency over a century-long period. This has been accomplished on the basis of several key principles – namely traceability, uncertainty analysis, and comparison – which demand an evidence-based approach to ensure unequivocal credibility and confidence in measurement results [93].

Climate observations from space have similar measurement goals. Long-term records of satellite-sensor observations (Fundamental Climate Data Records, or FCDRs) and derived environmental parameters (Climate Data Records, or CDRs) must have irrefutable credibility and stability at a level that

> **For observations of the Earth and climate to be trustworthy, they must be tied to SI, as with other commerce and science disciplines**

justifiably permits the evaluation of climatic trends [20]. To achieve this, satellite Earth observations should ideally follow the same approach as the wider metrology community. Indeed, this need has been acknowledged by (F)CDR generators in recent years (e.g., ESA CCI [113]), which has led to a number of initiatives to develop the science of Earth Observation (EO) metrology – beginning with the development of the CEOS QA4EO (Quality Assurance for Earth Observation) principle and associated guideline framework [114].

A key reason the adoption of metrological best practice in the Earth Observation community remains a developing area is the relative complexity of the problem compared to the traditional domain of metrology, which is often based on laboratory measurements. Firstly, current satellite observations often do not have robust measurement traceability to SI at the necessary uncertainty levels – often due to the launch of the satellite potentially degrading the direct traceability chain and lack of methods of sufficiently low uncertainty to SI. Furthermore, uncertainty analysis is challenging due the large data volume, the often-complex data processing chains together with complex error-covariance structure present in the derived spectral imagery, and the fact that satellite observations are generally not repeatable. In recent years, however, methodologies have been developed by the EO metrology community to make the problem more tractable, for example the H2020 FIDUCEO project [115].

A key contribution from the FIDUCEO project was the development of a framework to describe the error-covariance structure of EO datasets. Error effects in satellite imagery may be correlated between pixels and bands to varying degrees, which, following the FIDUCEO definitions, may be categorised as follows:

- Random (or independent) effects – "those causing errors that cannot be corrected for in a single measured value, even in principle, because the effect is stochastic. Random effects for a particular measurement process vary unpredictably from (one set of) measurement(s) to (another set of) measurement(s). These produce random errors which are entirely uncorrelated between measurements (or sets of measurements) and generally are reduced by averaging."
- Structured random effects – "where across many observations there is a deterministic pattern of errors whose amplitude is stochastically drawn from an underlying probability distribution; "structured random" therefore implies "unpredictable" and "correlated across measurements""
- Systematic (or common) effects – "those for a particular measurement process that do not vary (or vary coherently) from (one set of) measurement(s) to (another set of) measurement(s) and therefore produce systematic errors that cannot be reduced by averaging."

Each of these categories of error-correlation can dominate at different scales of analysis. For example, for a given pixel at a given instant, measurement noise may cause the dominant uncertainty and so the random effects are the most significant. When considering somewhat larger-scale analyses, such as with monthly gridded products, completely random errors will tend to cancel out, leaving structured random effects to dominate. Finally, in decadal-scale or global analyses, these structured random effects will also cancel out, leaving seemingly small systematic and inter-sensor harmonisation (if the record is of multiple sensors) effects to dominate. This is illustrated for a simulated Sea Surface Temperature CDR in Figure 3.1.
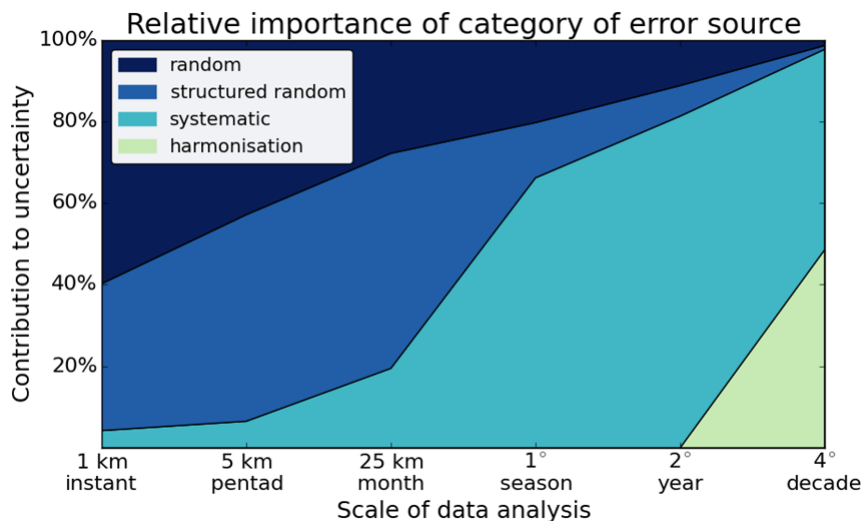

Figure 3.1 - An illustration of the dominant sources of uncertainty by error-correlation scale at different scales for analysis for a simulated Sea Surface Temperature record

Analyses of CDRs are performed across the full range of temporal and spatial scales, so scientists must be provided with the full range of error-covariance information so they may each understand the validity of their results and form credible conclusions. This is of particular importance for climate science given the large-scale analysis of long-term datasets where systematic and harmonisation effects dominate. The characterisation of these effects has, however, either been poorly communicated or not even fully understood and may have been at a lower priority than effects dominating at the per-pixel scale (e.g. noise). In reality, for any climate-focussed satellite mission, a clear description of the total error-covariance structure should be core to the delivered product.

3.2   EO Metrology Methods

As indicated above, performing uncertainty analysis of FCDRs and CDRs and disseminating the derived covariance information is a challenging problem. In recent years, methodologies have been developed to simplify this analysis, while remaining metrologically rigorous (i.e., respecting the metrology community's *Guide to the Evaluation and Expression of Uncertainty* [93]. Key progress towards this was made within the FIDUCEO project, which developed a step-by-step process to characterise, evaluate, and disseminate (F)CDR uncertainty information. A summary of their approach [6] is provided here.

These methodologies are increasingly being adopted in the EO metrology community, through initiatives such as the ESA FDR4Atmos and FDR4Alt projects, which are looking to develop FCDR and CDRs for historic ESA atmospheric monitoring and altimetry missions, respectively.

3.2.1 Measurement Function Centred Analysis of Error Sources

As with all uncertainty analysis, the first step towards deriving measurement uncertainty is understanding the system's measurement equation. Generally, this may be written as,

$$y = f(x, \dots, x_N)$$
<div align="right">*Equation 1*</div>

where y is the measurand (e.g., radiance) and x_i are the input quantities (e.g., detector counts, calibration coefficients etc.). Uncertainty analysis is then performed by considering in turn each of these different input quantities to the measurement function. Each input quantity may be influenced by one or more error effects, which are described by an uncertainty distribution.

Within the FIDUCEO project, a schematic representation of the sensor measurement function, called the *uncertainty tree diagram*, formed the starting point of the analysis. Such diagrammatic representations can be extremely useful tools when attempting to understand the measurement function.

An example of such a diagram is shown in Figure 3.2. At the centre of this diagram is the measurement function for the sensor. From this function, branches spread from each input quantity, which may themselves be determined by their own measurement functions (for example here x_2 is determined with quantities χ_a and χ_b), to their uncertainty. This uncertainty can be traced back through to its impact on the measurand by the sensitivity coefficients on each branch. Finally, the physical effects which cause each respective uncertainty are connected to the end of each branch. Note that we should also consider the extent to which the measurement function describes the true physical state of the instrument – this is accounted for by including the term $+0$ at the end of the measurement function. This explicitly represents effects, expected to have zero mean, that are not captured by the measurement function (i.e., there is an uncertainty associated with the form of the measurement equation itself).
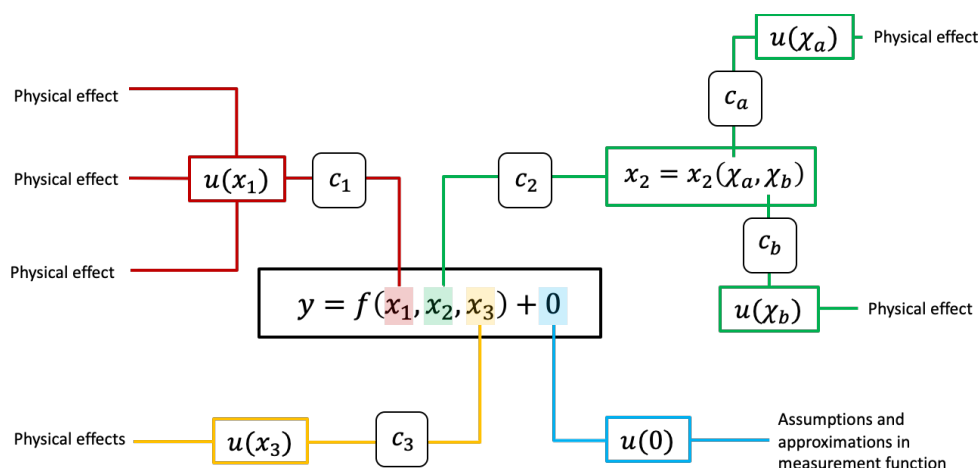
Figure 3.2 - Example uncertainty tree diagram

3.2.2 Characterisation of Error Sources

Each of the effects identified at the end of each of the *uncertainty tree diagram* branches should then be understood, quantified and reported. The FIDUCEO project developed a template *Effects Table* to ensure all the relevant information is captured. This includes:

- the uncertainty associated with the given effect
- the sensitivity coefficient required to propagate uncertainties associated with that effect to the uncertainty associated with the measurand

- the correlation structure over spatial, temporal and spectral scales

Table 3.1 shows an example *Effects Table* with a description of how it should be populated.

Table 3.1 - Example Effects Table with description of required content

Name of effect		A unique name for each source of uncertainty in a term of the measurement function
Affected term in measurement function		Name and standard symbol of affected term
Correlation type and form	Between columns	Error-correlation form over relevant spatial and temporal scales
	Between rows	
	Over time	
Correlation scale	Between columns	Parameterisation of error-correlation forms, defining length scale of correlation
	Between rows	
	Over time	
Channels/bands	List of channels / bands affected	Channel names
	Error correlation coefficient matrix	Cross-channel error-correlation matrix
Uncertainty	PDF shape	Functional form of estimated error distribution for the term
	units	Units in which PDF shape is expressed
	magnitude	Value(s) or parameterisation estimating width of PDF, i.e. standard uncertainty
Sensitivity coefficient		Value, equation or parameterisation of sensitivity of measurand to term

3.2.3   Propagation of Uncertainties to Derived Product and Dissemination

With the information provided in the *Effects Table* for each of the measurement error effects, it is then possible to evaluate its contribution to the total uncertainty of the measurand using the law of propagation of uncertainty [113]. This potentially provides very many uncertainty contributions, and so it is convenient for the data user to combine these values in categories based on their error-correlation form. The FIDUCEO project provided users with per-pixel uncertainties separated into the previously described *random*, *structured*, and *common* forms leading to the creation of so-called EasyFCDR products. This simpler product balances the need to preserve the necessary covariance information while providing the user with a comprehensible and more manageable data product.

3.3   Conclusions

The application of rigorous metrology in the development of FCDRs and CDRs is crucial to ensure datasets produced are of irrefutable credibility and are stable at a level that justifiably permits the evaluation of climatic trends. In the growing field of EO metrology, methodologies have been developed to enable (F)CDR uncertainty analyses which are being increasingly adopted in the EO community; their use is recommended more widely to ensure the development of robust climate datasets going forward.

One open issue remaining in EO metrology is the question of traceability. Currently, for Earth observations from space, this is only achievable to an agreed reference but not unequivocally to the SI. For the visible and near-infrared, this problem will be solved in the near future, however, with the planned launch of SI-traceable reference satellites including the CLARREO Pathfinder, TRUTHS, and CSRB (see §12).

§3   Authors: **S. Hunt[1], E. Woolliams[1], J. Mittaz[1,2]** and **C. Merchant[2]**, [1]NPL, [2]Univ. of Reading

§3   Editor: **Greg Kopp**, Univ. of Colorado / LASP

4   Establishing Traceability to SI: Pre-flight

4.1   Introduction to SI Traceability

Since 1875, with the signing of the metre convention, international trade and consistency in scientific and engineering endeavours has been facilitated through the use of a common internationally harmonised measurement system, System International (SI). A measurement framework consisting of well-defined quantities underpinned by seven base units defined with the intention of century-scale stability, reproducibility, and universality. Of course, prior to this time, there was still trade and scientific consistency, but these required conversions between measurement units of different countries and/or trading blocs. The base units were redefined in 2020 so that all seven were tied to an invariant constant of nature, removing the last remaining artefact-based definition, the kilogram, from the system [https://www.bipm.org/en/measurement-units]. See Figure 4.1.

The seven defining constants of the SI and the seven corresponding units they define:

Defining constant	Symbol	Numerical value	Unit
hyperfine transition frequency of Cs	Δv_{Cs}	9 192 631 770	Hz
speed of light in vacuum	c	299 792 458	m s^{-1}
Planck constant	h	6.626 070 15 x 10^{-34}	J s
elementary charge	e	1.602 176 634 x 10^{-19}	C
Boltzmann constant	k	1.380 649 x 10^{-23}	J K^{-1}
Avogadro constant	N_A	6.022 140 76 x 10^{23}	mol^{-1}
luminous efficacy	K_{cd}	683	lm W^{-1}

Figure 4.1: The defining invariant constants of nature underpinning the SI

In establishing the SI, the world's member governments created in parallel the international metrological framework needed to maintain and ensure global consistency, i.e., a central independent laboratory, the Bureau International des Poids et Mesures (BIPM), coordinating the National Metrology Institutes (NMI) of member nations under the auspices of the intergovernmental General Conference on Weights and Measures (GCPM). The scientific direction and strategy are supported by technical experts drawn from – but not representing – member states in the form of a Comitè International des Poids et mesures (CIPM) and associated consultative committees (CC) for each unit. The latter are comprised of technical experts formally representing member states with the necessary capabilities in the specific SI quantity/specialism. The framework extends further into a few geographically regional groupings of NMIs (RMOs) to ensure that all NMIs are linked, e.g., Europe, Asia-pacific, and the Americas. This hierarchical metrological framework guarantees international consistency and 'degrees of equivalence' (effective uncertainties) of measurements disseminated by individual NMIs and consequently traceability to SI.

> Traceability to the International System of Units (SI) ensures unambiguous consistency, trust, and stability of measurements through time by linkage to fundamental constants of nature and has been embedded in intergovernmental agreements since 1875

At the highest level, NMI experts agree not only on primary definitions for quantities but also practical means of realising and disseminating measurement scales and quantities and undertake formal comparisons and peer reviews of their 'deliverable uncertainties' amongst themselves. The comparisons and peer review process are extended throughout the RMOs to ensure all NMIs and their calibration services are linked with results and associated evidence made transparent and visible through an open

data base https://www.bipm.org/kcdb/. It should be noted that some NMIs may have measurement capabilities and the means to realise the SI-quantity with lower uncertainties than can be readily evidenced by formal comparison with peers, as was the case with the first cryogenic radiometers for optical radiometric quantities, which were nearly a factor of 10^2 lower in uncertainty than previous methods. For these situations, detailed uncertainty budgets and consistency within combined uncertainties need to be demonstrated, but the NMI declared value is acceptable.

Secondary calibration laboratories, including instrument manufacturers, can then establish SI-traceability through accessing a calibration or comparison with an NMI and evidencing their capability by some form of independent review. Note that for this to be considered SI-traceable requires independent unequivocal evidence that the uncertainty budget derived at the end of the calibration chain is robust and repeatable, i.e., there is documented evidence (ideally the result of a comparison of some form). For SI-traceability, it is not sufficient to simply obtain a calibration, transfer standard, or even primary standard from an NMI – the method used needs to be documented and an uncertainty budget of its use in any subsequent measurement needs to be derived and evidenced. This calculated uncertainty subsequently needs to be added to that of the NMI/primary standard as well as the linkage to that standard.

In summary, there needs to be a full documented review of the measurement process and associated environment leading to the identification of all potential sources of uncertainty. For each, there then needs to be an assessment of any corrections that might need to be applied for potential systematic/bias effects, with any correlations and any resultant uncertainty assessed. Finally, sufficient repetitions, in number and nature, to enable the random effects to be both assessed and reduced to a level commensurate with the uncertainty demands and practicalities of the measurement are needed.

Metrology best practise can be summarised as achieving and demonstrating the following:

- **Traceability** (to SI or other community agreed **reference**)
- **Uncertainty analysis** (full breakdown, including correlation related to the **reference**)
- **Comparison** (to independently demonstrate consistency and validation of uncertainty in making the measurement)

4.2 SI Traceability for Earth Observing and Climate

In common with all applications, quantitative measurements of physical measurands, including of biochemical systems, should be performed and reported in units with an uncertainty traceable to the SI. Observation of the Earth from space for other than pure imagery-related applications is no exception. For any temporal application, particularly long time-base observational series, as needed for climate, it is not only imperative but also needs to be carried out with very high

> Traceability to SI requires evidence of traceability to a reference through some form of comparison and a documented assessment of uncertainty to the reference at the time of the measurement

accuracies, often very close to those currently realisable by NMIs at the primary standard level, as indicated in Section 1. This is because the size of any potential 'signal' (change from a point in time) is so small that it can take decades to be larger than that of possible background natural variability. Therefore, any observation and the sensor that is used to make it must be reliable and tied to an invariant reference with uncertainty small enough to allow reliable detection as early as possible, meaning close to that of the SI-primary standard for each individual time/space measurement and with an instrument sufficiently stable that relatively short-term noise can also be removed by averaging.

For space-based observations, this provides many additional challenges compared to a laboratory or even terrestrially based observations. Not only is the measurement instrument subjected to violent launch forces between final ground calibrations and first use on orbit, but also the in-orbit operational environment can lead to unpredictable degradation, particularly for optical sensors, which cannot easily be recalibrated/characterised through a normal 'back to the lab' SI-traceable calibration. This weakened traceability chain has severely limited the resultant uncertainties that have been achieved to-date and the confidence that can be assigned to them. Strategies to assess degradation of pre-flight calibration both from on-board systems and vicarious methods have been implemented over the years and many are discussed in various sections throughout this document. All seek to either validate or assign an updated calibration to the in-flight sensor together with an uncertainty. However, these are rarely achieved at the uncertainty levels needed for climate and often suffer from the inability to fully recharacterize or assess some of the critical sources of uncertainty/degradations in space. For example, the on-board calibration systems themselves can be subject to degradation. The new SITSats, described in §11, provide the opportunity for a paradigm shift in the levels of uncertainty and consequential strength and confidence in the SI-traceability chain that can be achieved. However, even these cannot readily perform a full SI-traceable re-calibration of all sub-systems on-orbit. Fortunately, by design and pre-flight characterisation/calibration, they can at least reduce their potential contribution of the overall measurement uncertainty to manageable levels.

4.3 Pre-flight SI Traceability

Even though some critical characteristics of a sensor may change on launch with the prospect of continued degradation thereafter, the need for rigorous, comprehensive, SI-traceable characterisation and calibration remains paramount. Firstly, it is essential to know that any model of sensor performance is consistent with pre-flight evaluation to ensure unexpected errors haven't occurred, either through design or build. Secondly, the detailed parameterisation of this model and an evaluation of interdependencies and sensitivities of the design to different stimuli and environmental conditions provides essential insight to evaluate and correct potential unpredictable changes in flight performance.

Some characterisations can be considered relative, and thus the need for SI-traceability is limited. Most, however, particularly those that are critical to determining measurement performance in terms of physical units, must be tied to SI at uncertainty levels commensurate with the application needs. This means that any calibration facility and associated reference standards should ideally have a significantly lower uncertainty than that intended in-flight. The demanding requirements now being sought for climate make this increasingly challenging, as the uncertainties required in space are themselves close to those normally delivered in the laboratory.

In planning a pre-flight calibration and characterisation plan, it is important to have as thorough of an understanding of the sensor measurement equation from input to signal to delivered product. This measurement equation should consider all the contributing sub-systems and components of the sensor, their physics and environmental dependencies, e.g., their temperature coefficients, interactions, and potential degradation mechanisms. These should be presented and summarised in a clear manner and ideally translated into a software simulation model to allow performance evaluation. This summary should include evidence to support any corrections and uncertainty evaluations, in particular, the route to SI-traceability. Graphical methods developed as part of the EU FIDUCEO project illustrated in §3 of this report provide a good basis.

A comprehensive evaluation of the measurement equation makes it clear where the most critical sources of error and uncertainty lie and thus where to focus attention in a calibration and characterisation plan, particularly in terms of SI-traceability. The exact operational nature of the sensor and, to some extent,

the intended application and prospective applications drive the specific requirements and ultimately the route to SI-traceability and the specific SI base unit. In some cases, there may be more than one route. However, the SI has been constructed to ensure complete coherence between the units and, providing the appropriate metrological practises are followed, there will be no anomalies caused by this choice.

4.4 Pre-flight SI Traceability for Optical Sensors

In the context of this document, 'the prospect of a high-accuracy SI-traceable climate observing system', the focus is on passive optical sensors, i.e., the spectral range from around 200 nm to 100 μm. This is where effects relating to the radiation balance of the Earth and associated carbon cycle, together with the majority of space-observed ECVs, are primarily observed. In addition, microwave sensors are important for atmospheric water vapour and temperature and lidar and SAR for biomass (carbon) and altimeters for ice thickness, sea height,

> **Even though there is often change of pre-flight calibration coefficients of satellites due to the harshness of launch, it is imperative that rigorous pre-flight calibration and characterisation of all critical sensor parameters is undertaken to facilitate change detection and correction in orbit**

etc. All require pre-flight SI-traceability which should follow the same principles as in the passive optical domain. However, with the possible exception of microwave sounders, many of the detailed traceability chains are quite different in nature.

Passive optical sensors measure either emitted thermal optical radiation or solar radiation (directly incident or following an interaction (reflection, transmission) of some form. In both cases, the principal measurement can be a broad spectral integral or spectrally resolved to various resolutions. Because of the relationship between optical radiation and thermodynamic temperature, as a result of Planck's law, traceability chains for the principal measurement quantity (radiance/irradiance/'brightness temperature') can be established to both the Temperature and Radiometric scales, i.e., the Kelvin and the (radiometric) Watt. For the solar domain, the trend is towards radiometric scales whilst for thermal infrared measurements, blackbody radiators tied to the Kelvin are used. The need for some level of spectral characterisation to account for imperfect emissivities and atmospheric absorptions means that there is often a hybrid approach. For example, radiometrically-calibrated spectral radiometers are now being used to at least validate the performance of blackbody reference standards used in pre-flight calibration e.g., NIST TXR [116] and NPL AMBER [117].

Simplistically, pre-flight calibration of the 'gain' of a sensor (the conversion of digital counts to SI units) is the result of presenting a known stimulus, similar in characteristics to that of the intended measurand, whilst the sensor is operated across its range of expected environmental conditions, i.e., overfilling the entrance aperture with the sensor operating in a thermally variable vacuum chamber. However, even though this process provides many challenges at the uncertainty levels being sought for climate, it is also important that many other characteristics of the sensor are evaluated under the same conditions (although not all are necessarily applicable to the same extent for each sensor). Although it may be possible to assess the resultant impact of some of these characteristics as part of an integrated and/or end-to-end calibration, assessing them independently allows the overall uncertainty budget to be built up in a transparent manner allowing proper treatment of any correlations and the contributory nature (random/systematic) of the error sources. Such thorough pre-flight calibrations can also aid evaluation of unexpected anomalies both pre-flight and post-launch.

Some of the below characteristics/parameters can be determined in a relative manner and do not necessarily require SI-traceability to a reference. However, they should still be evaluated in a metrologically robust manner, i.e., with a documented method and an associated uncertainty budget.

- Spectral stray light (out of band, scattering …)
- Spatial stray light (out of field/MTF/PSF/diffraction...)
- Spectral response function (shape, wavelength, end-to-end and sub-systems…)
- Non-linearity
- Noise (dark, photon, detector, electronics …)
- Geometry (FoV, limiting aperture area)
- Degree/nature of polarisation

For thermal infrared sensors, spectral stray light can be particularly challenging, as the sensors' self-emission (near ambient temperature) is of a similar spectral characteristic to that of the signal from the desired observation. Spectral response is similarly more demanding for spectroscopy missions where quantitative values are of particular importance, for example GHG missions. In these cases, it is only the availability of spectrally tuneable lasers that allows the characterisation uncertainties (< 1 % for bandwidths in the required tenths of nm scale) to be achieved.

In recent years, the availability of laser radiation spanning the optical spectrum UV-TIR has also made possible step-change reductions in uncertainties for many radiometric calibrations and characterisations, not least that of the radiometric gain calibration itself. This is explored in §4.4.3.

4.4.1   Thermal-Infrared Measurement Sensors

As indicated above, SI-traceability for the thermal infrared is primarily to the temperature scale through the calculable emission of radiation from a blackbody determined by Planck's law. This requires a spectrally flat (or nearly so) high-emissivity surface (entity) of known and ideally uniform temperature. The formal link to SI is generally achieved through a thermometer (typically, one or more platinum resistance sensors) embedded into the substrate supporting the emitting surface (black coating). Operating at near-ambient temperatures, such blackbody targets can be made with large apertures and high emissivity to overfill satellite sensors and have been successfully used for many years. Efforts to reduce uncertainty have focussed on the use of new black coatings for higher emissivity, for example carbon nanotubes [118], and improving confidence in thermometry. Improved coatings allow new designs, which can also improve temperature uniformity and modelling. To meet the needs of forthcoming missions like the ESA FORUM [119] , improvements to extend the spectral range of primary SI facilities for diffuse reflectance have also been required.

Similar standards to these blackbodies can and are typically flown on-board the spacecraft. For these, on-going research is also evaluating how to use phase-change cells, such as the melting point of mercury and gallium and the triple point of water, to provide a means for checking the calibration of thermometers in orbit through direct linkage to an SI primary standard. Gero et al. [120] have also devised methods to evaluate the emissivity of the blackbody in space.

For spectral calibration, the sensor spectral response function is generally determined by an independent calibration using a monochromatic source and reference detector, in either a relative or absolute manner, traceable to radiometric quantities.

4.4.2   Solar-Reflective Measurement Sensors

To provide Lambertian radiation to overfill the entrance aperture of a solar-reflective measuring sensor, an incandescent-lamp-illuminated integrating sphere (see Figure 4.2) or flat diffuser plate, such as Spectralon [121], is usually used instead of a blackbody, as typically used for the thermal infrared. For the solar-reflective spectral range, the needed temperature of any blackbody radiator would need to be >>1000 K (and ideally ~6000 K) to have a spectral profile similar to that of the Sun (i.e., similar to that being measured) and of sufficient intensity to calibrate the spectral bands of the sensor. Although high-temperature blackbodies are readily available, they often cannot provide the necessary aperture size.
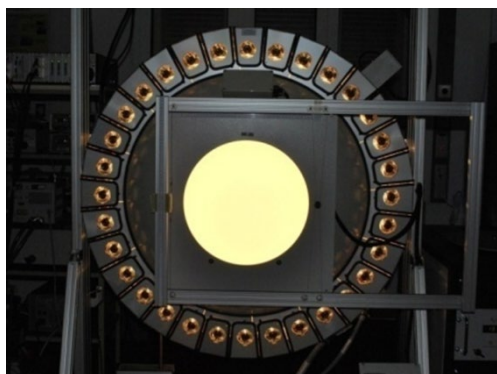

Figure 4.2: An example lamp illuminated integrating sphere for the radiance calibration of large aperture sensors such as satellite cameras

In considering choice of practical sources that can be used to generate the necessary radiance for solar-reflected sensors, it is important to consider the spectral range of use. Some can achieve spectral shapes equivalent to a colour temperature of 10,000 K or more, but this is usually only achievable as a continuum for a limited part of the spectrum. The illumination source of choice is generally an incandescent Tungsten halogen lamp (an approximation to a 3000 K blackbody). However, increasingly, lasers are being used (see Section 5.4.3).

The most common route to SI-traceability for solar-reflective band sensors is through the radiometric watt (see Figure 4.3). In some cases, Planck's law is still used with the lamp-illuminated calibration source traced to the spectral radiance of a blackbody operating at > 2500 K in a relative manner through some intermediate spectrally defining transfer standard, e.g., a spectrometer or filter radiometer. To maintain good emissivity and achieve high operating temperatures, this type of blackbody can only have relatively small exit apertures of a few mm (<~15 mm in diameter). In most cases, the link to SI thermodynamic temperature is now traced back to the radiometric watt through a calibrated spectral radiance meter [59]. As in the thermal infrared, where specific spectral information is needed at some point in the calibration chain, some form of spectral-defining element, e.g., a filter or spectrometer, which may be part of the calibration system/source or instrument to be calibrated, must be spectrally characterised.
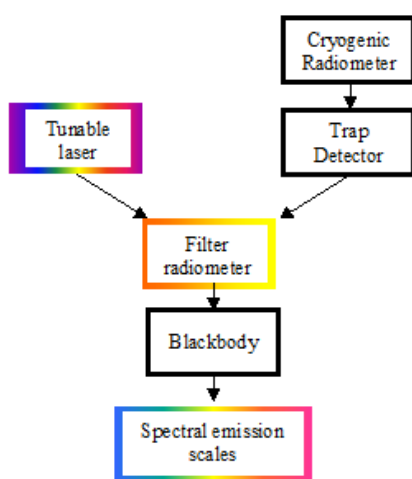

Figure 4.3: A typical traceability chain of an NMI- linking scales of spectral radiance and irradiance through a Planckian blackbody whose thermodynamic temperature has been measured with a spectrally defined filter radiometer calibrated against a primary standard cryogenic radiometer

As an alternative to the blackbody, synchrotron radiation can be used, utilising the Schwinger theory as opposed to Planck. These are primarily used for high-energy radiation <400 nm [122].

The most common primary radiometric standard in use at the world's NMIs is the cryogenic radiometer. Recommended by CIPM consultative committees [123], it provides the most accurate link to SI. It has

been in widespread use for the last 30+ years following its first successful implementation at NPL in the 1980s [53]. Alternate methods using the predictable quantum efficiency of solid-state silicon photodiodes, initially proposed in the late 1970s [124], can achieve similar levels of uncertainty but only over much more limited spectral ranges than the cryogenic radiometer [54], [57].
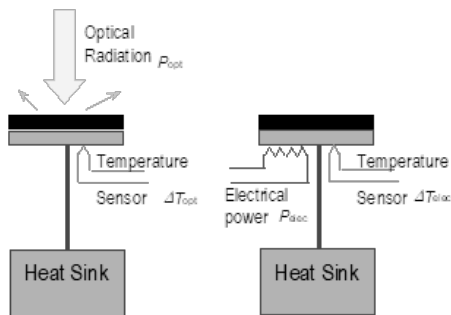

Figure 4.4: Schematic representation of the Electrical substitution principle

. If $\Delta T_{opt} = \Delta T_{elec}$, then $P_{opt} = P_{elec}$

The operating principal of the cryogenic radiometer is quite simple and has some similarities to that of a blackbody in as much as it consists of a blackened surface of high emissivity to absorb incident radiation, typically a cavity, although shown as a flat plate for simplicity in Figure 4.4. In this case, the cavity is designed to have a relatively low mass and some degree of thermal isolation so that the absorbed radiation causes a temperature rise over a nominally stable thermal reference. By replicating the temperature rise via applying a current through an electric heater attached to the cavity in the absence of optical power, the power of the optical radiation can be determined as equivalent to that of the applied electrical power, which can be measured extremely accurately. In principle, this places the end of the SI-traceability chain on electrical

quantities, however,[123] makes clear that this should be considered as the primary standard of choice for optical radiation measurements.

The 'electrical substitution' principal described above has been in use for more than 120 years, but cooling to cryogenic temperatures (<~20 K) at NPL in the early 1980s [52], [53] led to a reduction in uncertainty of nearly two orders of magnitude. In general, cryogenic radiometers measure radiant power (with entering light underfilling an aperture) of a monochromatic (usually a laser) beam of radiation. This beam of now-calibrated power is then used to calibrate the response of a detector. Through use of a range of wavelengths, the response characteristics of a detector can be determined and interpolated for any wavelength. If an aperture of known area is placed in front of the cavity and overfilled by a beam of known spatial uniformity, the irradiance of the beam can also be determined; for example, the Cryogenic Solar Absolute Radiometer (CSAR) on the solar platform at PMOD in Davos, Switzerland is used to measure total solar irradiance as part of the WMO primary observation system [125], [126].

Following determination of a primary spectral responsivity scale, spectral irradiance and radiance can be established (see Figure 4.3). For monochromatic scales, only a geometric defining system is required in front of a calibrated detector to establish a radiance or irradiance meter. For the measurement of non-monochromatic sources, e.g., a lamp, the Sun, or the solar-illuminated Earth, an additional spectrally-
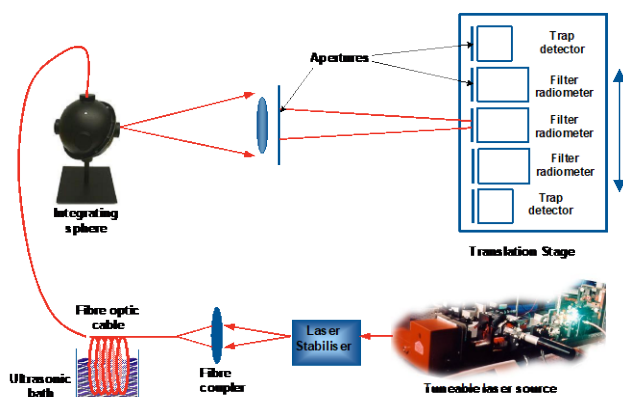

Figure 4.5: Schematic representation of a laser based facility to calibrate the spectral response of a filter radiometer against a reference silicon trap detector , a transfer standar to the cryogenic radiometer. Fibre optic cable is use to transport laser from the laser to a small integrating sphere but is vibrated by an ultrasonic bath to remove the effects of speckle.

defining element needs to be included in the measuring system. The throughput of this element can be measured independently or, more conveniently, as the combined response with its detector using a spectrally-tuneable monochromatic light source e.g., a Ti:Sapphire laser in comparison to a calibrated detector (see Figure 4.5) [58]. The calibrated (ir)radiance meter (filter radiometer) can then be used to measure the (ir)radiance of any source, including a lamp-illuminated integrating sphere or reference high-temperature blackbody [127] with uncertainties < 0.06 % (k=2). At present, such lamp-illuminated sources are commonly used to calibrate Earth-viewing satellite instruments. However, it is clear that the laser could be used directly, i.e., the laser can directly illuminate the satellite sensor or via an intermediate diffusing element, such as a large integrating sphere, removing steps in the traceability chain and reducing uncertainty.

4.4.3   Laser-based EO Calibration Facilities

The use of tuneable lasers for calibrations can, of course, add significant time to the calibration process for radiometric gain of multi-spectral or hyperspectral sensors compared to the use of a broadband source, as they only provide discrete spectral inputs. However, if the spectral response function is also required, particularly where the requirements may be demanding, for example in an atmospheric composition monitoring spectrometer, the two measurements can be combined.

> **Availability of tuneable lasers and cryogenic radiometers now allow pre-flight calibration and characterisation of optical sensors in the solar reflective domain with uncertainties commensurate with the needs of climate**

In addition, the same measurement can be reanalysed and used to simultaneously assess and correct for spectral stray light [128]. Although non-linearity can also be assessed using such a facility, the likely spectral nature of stray light may require too much additional time, as each wavelength (or at least a significant number of them) would need to be assessed independently compared to when using a broadband spectrally continuous source. However, if this assessment requires the establishment and alignment of two different facilities, the extra time may be compensated for.

NASA's Goddard facility has built and is using a tuneable laser-illuminated integrating sphere for the calibration and characterisation of many of its optical EO sensors. This Goddard Laser for Absolute Measurement of Radiance (GLAMR) [64] facility (Figure 4.7 and Figure 4.6) is derived from an evolution of the NIST SIRCUS facility [62]. Similar facilities to SIRCUS exist at NPL and other NMIs.
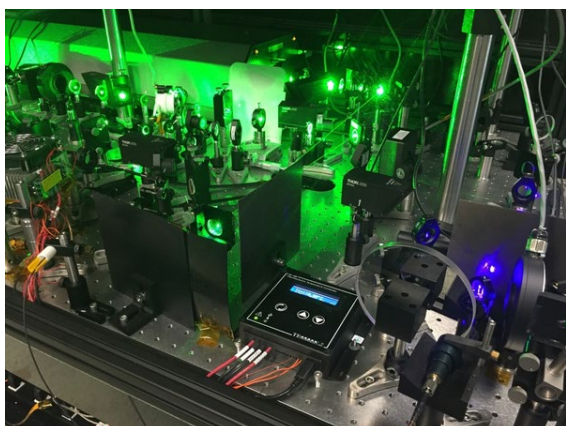

Figure 4.7: Tuneable laser suite used as part of the NASA GLAMR satellite calibration facility
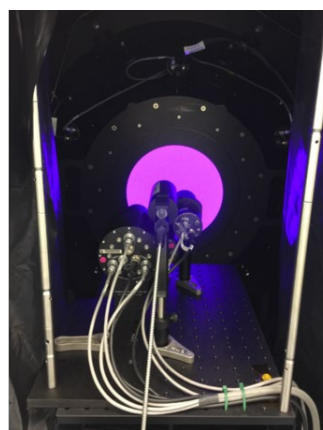

Figure 4.6: Laser illuminated Integrating sphere of the NASA GLAMR.

In late 2020, NPL completed the testing of a new satellite calibration facility called the Spectroscopically Tuneable Absolute Radiometric (STAR) calibration and characterisation (c & c) Optical Ground Support Equipment (OGSE) (see Figure 4.8) [129]. This STAR-cc-OGSE has been built as a transportable and modular facility that can travel to the cleanroom environments of organisations where satellite sensors are being calibrated as opposed to the sensors coming to it. This flexibility primarily stems from a new automated tuneable laser capability. This novel laser has capacity to deliver continuously tuneable continuous wave (CW) laser radiation of relatively high power $>\sim10$ mW from 260 to 2600 nm in a 'select and go' manner. The modular laser system has automated self-realignment/optimisation of mirrors of various frequency doubling and mixing cavities so that when different wavelengths are selected, the system optimises performance at the chosen wavelength using an integrated wavemeter.
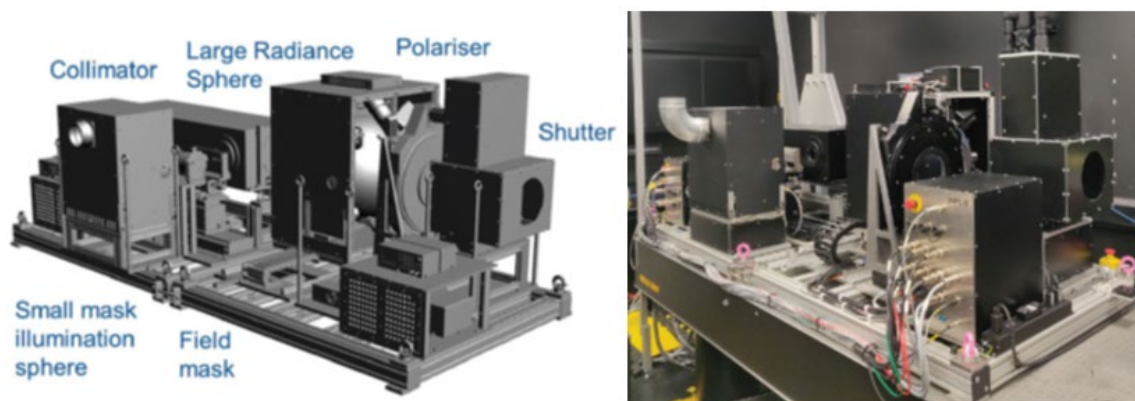

Figure 4.8; Schematic (left) and photo (right) of the NPL STAR-cc-OGSE

The CW nature means the facility can achieve very high spectral resolution and wavelength accuracy compared to a pulsed laser system typical of more commonly used OPO systems. The modular build of the laser allows it to be configured in different ways to suit the spectral range of the application. To ensure maximum flexibility and efficiency of the STAR-cc-OGSE, not only is laser radiation coupled into a large (variable exit aperture of up to 200 mm diameter) integrating sphere for absolute radiometric calibration, but it can also be fed, via a smaller sphere, into a collimator to facilitate image quality and other non-radiometric characterisations. In both optical configurations, a rotating polariser can also be inserted to enable the polarimetric properties of the sensor to be determined.

In addition to the monochromatic laser radiation, each integrating sphere is also equipped with a variety of broadband incandescent 'white light' sources with intensity adjustment to allow multiple light levels without changing spectral content. In this way, relatively rapid linearity testing can be carried out as well as other radiometric calibrations and characterisations where the extra accuracy attainable by the lasers is not justified compared to other constraints such as time.

Some care has to be taken when using coherent laser radiation, particularly with very high spectral resolution sensors where the entrance slit of the spectrometer can be very small, due to potential interference effects with any parallel optical interfaces/windows and also the effects of 'speckle'. Without active intervention, the radiation will be non-uniform and the size of speckles can be commensurate with those of slits in high-resolution spectrometers. Although the coherence of lasers will mean speckle always exists, its effects can be minimised by changing and randomising the speckle pattern through movement or vibration of some form of the radiation onto or off of the speckle-producing surface. This vibration needs to be done at a frequency large enough that it is not seen by the time integral of any detector element under test. As shown in Figure 4.5, a high-frequency vibration of

a fibre by an ultrasonic bath is effective, as can be the rotation of a diffuser or even the vibration of a loudspeaker.

Although facilities like STAR and GLAMR can produce uniform sources of radiance, these have to be coupled into a vacuum tank, often through a window, and the absolute value of radiance determined. For STAR, this final element, the link to SI-traceability, is a photodiode with beam-defining apertures positioned inside the vacuum tank next to the sensor under test viewing the STAR source. When measuring monochromatic radiance, only the spectral responsivity and view-defining optics of this detector impact the uncertainty, and these can be < 0.02 % in the visible region of the spectrum. However, for a large aperture sensor, residual non-uniformity in the beam will reduce the achievable uncertainties to a few tenths of a percent depending on aperture size. In stepping through wavelengths (picometer size steps are achievable), any spectral response function (high and low resolution) of the sensor under test can be determined as well as spectral stray light. In this latter case, measurements of the spectrometer as a whole will only see radiation at the monochromatic input value, which should only be seen in the spectral band of the sensor corresponding to it. As the system is fully automated, although it can take a few seconds to change from one wavelength to another, the process can be run continuously and not overly constrain measurement time within thermal vacuum facilities.

4.5　Summary

SI-traceability is mandatory for climate measurements and is increasingly so for many other applications. Although post-launch degradation from pre-flight calibration coefficients is commonplace, it is essential that comprehensive, rigorous, and well-documented calibration and characterisation are performed. Without such pre-flight knowledge, it can be highly challenging to distinguish causes of anomalies in-flight. Methods have now evolved in pre-flight calibration that closely mimic those previously only performed in NMIs, providing opportunities for a step change in performance. Not only is it essential that those performing pre-flight calibrations make optimum use of such capabilities, but they must also ensure that they document and make transparent to the scientific user community all the evidence and calibration coefficients they derive. They and the satellite builders should also make clear the route to SI-traceability, their uncertainty budget, and the underpinning comparison to peer evidence that supports it.

§4　　Authors: **Nigel Fox**, **Paul Green, Sean Devlin**, NPL
§4　　Editor: **Greg Kopp**, Univ. of Colorado / LASP

5 Extending GSICS to Inter-Calibrate Satellite Radiances to an Absolute Scale

This section introduces products of the Global Space-based Inter-Calibration System (GSICS) and addresses how they could be tied to an absolute scale using comparisons with SI-Traceable Satellite instruments, with short, well-documented traceability chains that are verifiable on-orbit.

5.1 Introduction to GSICS and Its Products

The Global Space-based Inter-Calibration System (GSICS) is an international collaborative effort established under the auspices of the World Meteorological Organisation (WMO) and the Coordination Group for Meteorological Satellites (CGMS). GSICS aims at ensuring consistent measurement accuracy among space-based observations worldwide for operational focussed organisations addressing climate monitoring, weather forecasting, and environmental applications [65]. This is achieved through a comprehensive calibration strategy, which involves routine monitoring of instrument performances, operational inter-calibration of satellite instruments, tying the measurements to designated absolute references and standards, and recalibration of archived data.

One goal of GSICS is to produce sensor-specific calibration datasets for enabling long-term, consistent GEO and LEO cloud, aerosol, land use, and other environmental retrievals. It is important to understand the specific capabilities of GSICS in this overall effort. In an ideal scenario, consistent retrievals would be achieved by having multiple exact copies of a sensor that has perfect onboard calibration systems. Given the reality of the current constellation of sensors, however, there are many considerations that must be weighed, which are summarized in Figure 5.1. These largely involve transferring the most accurate calibrations from designated "reference" (REF) sensors or SI-Traceable Satellites (SITSats) to less accurate "monitor" (MON) sensors.

Instrument Calibration
- Count to radiance response
- Sensor Gain degradation
- Detector response equalization
- Scan angle dependence
- Polarization
- Straylight
- Properly characterized spectral response functions
- Out of band response
- Geolocation

Inter-calibration
- Radiometric scaling to a reference SITSAT
- as if the SITSAT onboard calibration system was installed on the target sensor.
- is scene independent

Spectral Band Adjustment
- Spectral band scaling between target and reference sensor
- is scene dependent
- as if the global mosaic is composed of exact sensor copies
- usually considered in the sensor retrievals

Sensor Retrievals
- Cloud/aerosol/land use/ocean color retrievals are consistent in both space and time
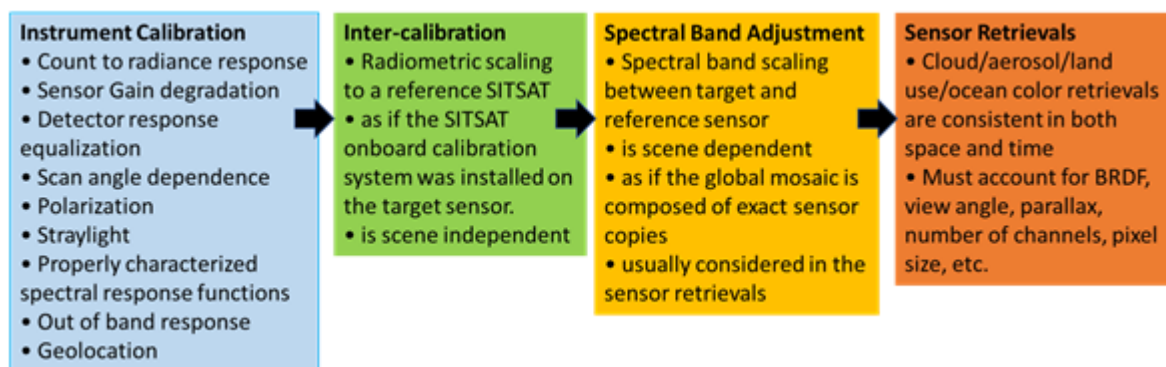- Must account for BRDF, view angle, parallax, number of channels, pixel size, etc.

Figure 5.1: The calibration and retrieval sequence needed to radiometrically scale an instrument's signal to a designated SI-traceable reference to achieve consistent cross-platform retrievals.

The dedicated agency instrument calibration teams are best suited to resolve the sensor dependencies as described in the blue box in Figure 5.1. Ideally, the onboard calibration issues are resolved by the calibration teams, with corrections made available (or applied) in the Level-1 (L1) product. Next in the sequence is the 'Inter-calibration' step (green box), in which a radiometric scaling is applied to the L1 dataset. GSICS calibration products specifically tie the sensor's L1 data to a reference instrument's calibration. If a narrowband sensor, such as VIIRS, is used as the designated absolute reference, then the radiometric transfer is based on the monitored instrument's spectral response function (SRF). It must be noted that the scaling does not yield equal radiance/reflectance values between the monitored

and reference instruments if their SRFs differ, because Earth-viewing spectra are dependent on scene type (surface classification, cloud properties, and atmospheric column).

Inter-calibration of L1 data key to inter-operability in L2 product generation

Consistent calibration among sensors is only one of the many factors in Figure 5.1 (yellow and orange boxes) that need to be considered in order to provide uniform sensor retrievals. For example, cloud masking requires confident pixel-level determination of clear-sky or overcast conditions, and therefore pixel resolution can significantly influence the cloud properties perceived by different sensors. In this case, the spectral band adjustments need to be scene dependent, which requires proper scene identification as best determined in the retrieval process. SITSat spectra can be used to validate the scene type at-sensor signal estimated by the retrieval process to ensure the spectral response differences were properly taken into account. These same Spectral Band Adjustment Factors (SBAFs) are used to remove dependencies due to spectral band differences when characterizing invariant ground sites in order to transfer the calibration from the reference to monitoring sensor.

One part of GSICS' strategy involves direct comparisons of collocated observations from pairs of satellite instruments, which are used to systematically generate calibration functions to compare and correct the biases of *monitored instruments* to community-

GSICS corrections inter-calibrate Monitored Instruments to Reference Instruments

defined *references*. This is currently applied to inter-calibrate the infrared (IR) channels of geostationary (GEO) imagers to hyperspectral sounders on low-Earth orbit (LEO) satellites, which are used as references to generate GEO-LEO IR GSICS Corrections. These are derived by various satellite operating agencies from a commonly-agreed algorithm [130], similar to the simultaneous nadir overpass (SNO) method originally developed for LEO-LEO comparisons [131], but extended to include a range of view angles.
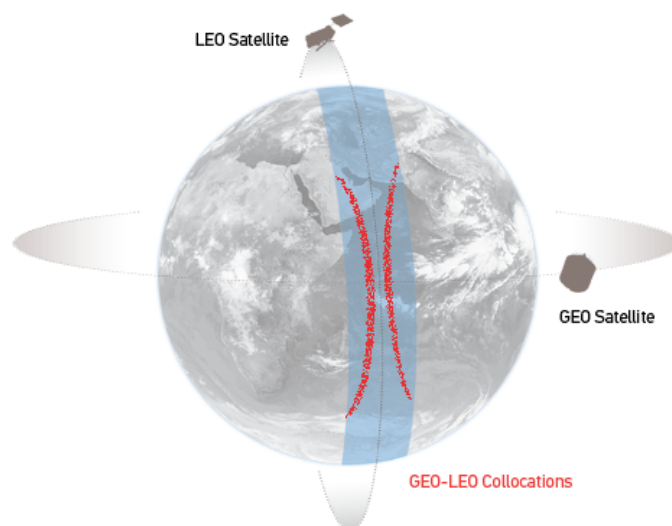

Figure 5.2: Schematic illustration of the geostationary orbit (GEO) and polar low Earth orbit (LEO) satellites and distribution of their collocated observations.

This algorithm is based on the comparison of collocated simultaneous observations from pairs of satellite instruments with similar viewing geometries. Because a hyperspectral instrument is used as a calibration reference for contemporary satellites, it is possible to accurately synthesise the equivalent radiance of the multispectral monitored instrument by convolving its spectral response function with the observed scene radiance spectra. However, some reference instruments, such as CrIS and AIRS, do not provide complete or contiguous spectral coverage of all monitored instruments' IR channels. Algorithms have thus been developed to compensate for spectral gaps [132], which introduce additional, but quantifiable, uncertainties into the GSICS products.

An extension of the SNO approach, sometimes known as ray-matching, could be applied to inter-calibrate counterpart channels in the reflected solar band (VIS/NIR). However, GSICS currently applies a complementary, indirect approach whereby the observations of Pseudo Invariant Calibration Targets

> **GSICS GEO-LEO VIS/NIR corrections use Pseudo Invariant Calibration Targets with multispectral satellites as references**

(PICTs) such as the Moon or deep convective clouds (DCCs) [133] are used to transfer the calibration of the reference instrument to the monitored instrument. [The classical Pseudo Invariant Calibration Sites (PICS) traditionally used for vicarious calibration could also be considered as a subset of PICTs.] These observations need not be simultaneous but do need to be made under directly comparable conditions - for example, viewing and solar geometry and, in the case of PICTs, be able to account for any potential changes in atmospheric conditions. However, it is also possible to use a lunar irradiance model to account for changes due to the Moon's phase and libration [134]. There is, however, currently no hyperspectral satellite instrument covering the full spectral band of GEO imagers' visible and near-infrared channels that would make a suitable reference. So instead, GSICS have selected S-NPP/VIIRS as a multispectral reference instrument due to its spectral characteristics, calibration stability, and quality of its characterisation [29]. This necessitates the use of SBAFs [135] to account for the radiance differences introduced by the monitored and reference instruments' equivalent channels having non-identical spectral response functions. Similar approaches have also been proposed for thermal infrared and microwave - e.g., using the Moon as a reference [136].

These methods are used to derive effective calibration corrections (or, equivalently, new calibration coefficients) which are distributed as GSICS products to facilitate interoperability and allow for accurately integrating data from multiple observing systems into operational near real-time processing, as well as for re-analysis applications.

5.2   Applying the Concept of Traceability to GSICS Products

While the concept of traceability can mean different things to different communities, when applied to GSICS products, it is used in its formal metrological definition and refers to the ability to relate the corrected radiance of the monitored satellite instrument to the community-defined reference instruments through an unbroken chain of comparisons, with stated uncertainties. Naturally, the different levels of uncertainty associated with each comparison will affect the overall quality with which the end product is traceable back to the reference and the ideal is that the reference should ultimately be that of SI.

5.2.1   Traceability Concept Applied to Direct Inter-Calibration

For GSICS products derived by direct inter-comparison of a monitored instrument to a single reference instrument, the traceability chain is established by combining the uncertainty budget of the inter-comparisons with that of the reference instrument itself. For example, [137] considers all processes contributing to the uncertainty on the comparisons and propagates these through a model of the comparison in a Type-B uncertainty analysis, following the BIPM Guide to the Expression of

Uncertainty in Measurement (GUM) [93]. The GSICS GEO-LEO IR inter-calibration algorithm includes provision of the estimated random uncertainty for each correction by propagating noise and scene variability through the weighted regression used to generate them. These estimates can be validated using a Type-A analysis of their time series.

However, in the absence of a robust operationally-deployed SI-traceable reference instrument, it is often desirable to use comparisons with multiple instruments – for example, to provide greater reliability, to improve diurnal coverage by using platforms with different equator crossing times, and to extend the period over which inter-calibration is possible beyond the lifetime of a single instrument. This allows us to ensure the full range of the monitored instrument's operating conditions are covered. In these cases, it is still possible to establish a traceability chain by selecting one instrument as a community-defined Anchor Reference. Results derived from other instruments are then adjusted to be consistent with those from the anchor by constructing a series of double differences between them and using these to define relative delta corrections, which are applied to each time series before they are combined. Uncertainties provided with each component correction and its delta correction are used as a weighting in the composite product, which is referred to as a Prime GSICS Correction [138].

> **Prime GSICS corrections combine multiple references using double-differences**

It is important to test the relative stability of the products derived from comparisons with each instrument before they are combined, as the delta correction is defined over the whole overlap period between each pair of reference instruments. Continuous monitoring of their double differences is therefore critical. However, any drift in the relative difference between instruments before or after the overlap cannot be accounted for.

The Prime GSICS Correction approach has been applied to combine results from historical references used for Fundamental Climate Data Records (FCDRs), as illustrated by [139], who applied the concept to recalibrate the water vapour and infrared channels of Japanese geostationary imagers using Infrared Atmospheric Sounding Interferometer (IASI), Atmospheric Infrared Sounder (AIRS), and High-resolution Infrared Radiation Sounder/2 (HIRS/2) as reference instruments.

5.2.2   Traceability Concept Applied to Indirect Inter-Calibration

The chief advantage to the use of PICTs, including the Moon, is that this approach does not require simultaneous observations from the monitored and reference instruments; a single reference instrument can be applied to any point in time. Although it is assumed that the PICT itself is stable, its long-term variability needs to be considered as one of the uncertainty sources of the comparison – along with other terms, such as atmospheric contributions and sampling errors, as for other vicarious calibration techniques described in Section 7.4.

In this case, the reference instrument's observations of the PICT are used to characterise its reflectance over the full range of conditions for which it is to be applied - e.g., solar and viewing geometries, seasonal, or lunar variations. Typically, this is performed over a period of several years, usually starting soon after launch, when the reference instrument's calibration is believed to be most reliable, and this period defines the reference itself. Application to other periods would require an uncertainty to be prescribed associated with the assumed long-term stability of the PICT.

Traceability of these GSICS products could be established by propagating their inputs' variability and uncertainty through a measurement model representing the inter-calibration algorithm (including SBAFs), and simplified uncertainties are provided with the products. This can be especially challenging where radiative transfer models are used, as, although it is possible to propagate uncertainties in the model's inputs, it is much more difficult to quantify the uncertainties in the model itself and there are

known differences between different models. Currently, VIS/NIR GSICS products are provided with uncertainty estimates based on a Type-A analysis of their time series.

5.3　Tying GSICS Products to an Absolute Scale – SITSats

Most satellite missions attempt to calibrate their instruments against SI standards before launch (see §4). GSICS, working together with CEOS, aims to define best practices to characterise satellite instruments pre-launch using SI-traceable references to tie them to an absolute radiance scale. However, this traceability chain may be compromised during launch due to uncontrolled changes to the instrument as a result of launch and its on-orbit operating environment, potentially leaving some uncertainty in the actual measurement accuracy. For this reason, GSICS endorses the establishment of an observing system with calibration directly traceable to SI-standards on-orbit to act as an inter-calibration reference, which could be used to anchor inter-calibration products to an absolute scale – a long-term aim of GSICS.

A satellite mission such as CLARREO Pathfinder with the HyperSpectral Imager for Climate Science (HySICS) [38], TRUTHS, or the Chinese Radiometric Benchmark (see §11), in which an instrument whose SI-traceability is verifiable in orbit, could be used as a reference to achieve this goal. These are referred to as SI-Traceable Satellite instruments (SITSats).

In the simplest case, shown by the green arrow in Figure 5.3a, such a SITSat can be used as a reference in direct inter-calibration of the MON instrument(s) by SNO/Ray-matching (generally done for the IR) or the PICT (in the VIS/NIR case) instead of the current REF instrument. However, depending on the design of the SITSat and choice of its orbit, this approach may not yield a sufficient amount of data to reduce the random uncertainty components of the inter-calibration. Furthermore, the duration of such inter-calibration products is limited to SITSat's operating lifetime. In this case, the transfer to an absolute scale could also be achieved either by direct comparisons of observations from the REF with those from a SITSat – or indirectly, by using the SITSat to characterize the PICTs, as shown in Figure 5.3b and described in Section 7.4.Figure 5.3b and described in §5.4.

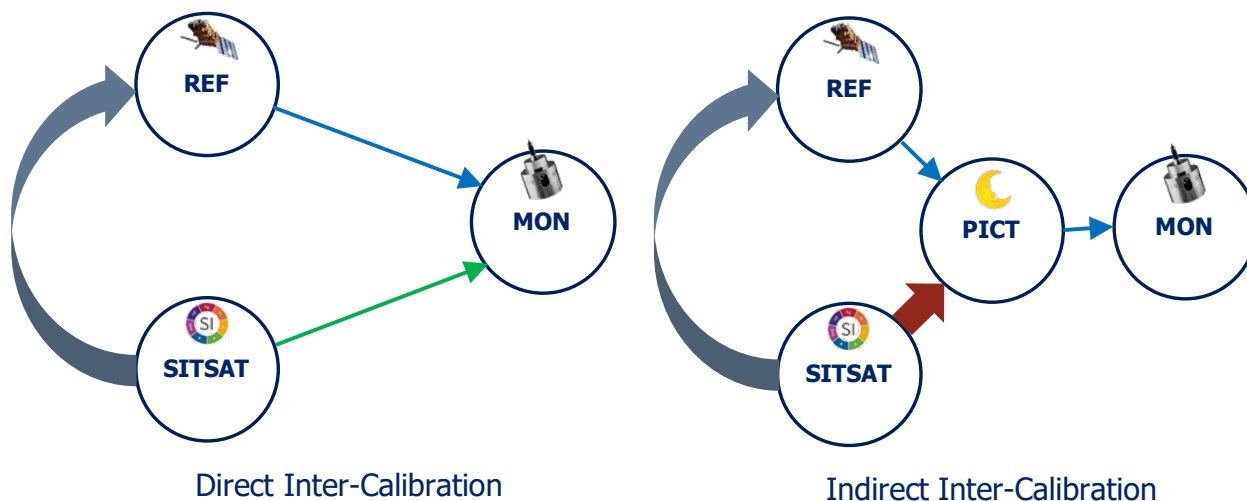
Direct Inter-Calibration　　　　Indirect Inter-Calibration

Figure 5.3: Different approaches to provide traceability of inter-calibration products for a Monitored instrument (MON) to an SI-Traceable Satellite instrument (SITSat); Left (a): Direct Inter-Calibration: Using Ray-matching/SNO-like approach to transfer the calibration of Reference Instrument (REF) or SITSat to MON (blue/green arrows); Right (b): Indirect Inter-Calibration: Using a Pseudo Invariant Calibration Target (PICT) to transfer calibration of REF or SITSat to MON (blue/red arrows).

Alternatively, the SITSat calibration can be transferred to MON by first recalibrating the REF – either directly or indirectly, as shown by the curled grey arrows in (a) and (b).

Currently, GSICS products take the reference instrument as the truth - no uncertainty is associated with their calibration. To compare the radiances after applying the GSICS correction to an absolute scale requires the reference instruments' uncertainty to SI to be included – and this typically dominates their overall uncertainty budget. This situation would change if it were possible to tie the inter-calibration to an absolute scale through the use of a SITSat. SITSat designs typically have a better calibration accuracy than the current reference instruments used in GSICS, so their introduction could reduce the overall uncertainty with which inter-calibration can be applied to an absolute scale, as shown in Table 5.1.

Table 5.1 Example Standard Uncertainties (k=1) in the calibration for Geostationary Imagers in different spectral bands – before and after calibration correction, shown as required and typical calibration accuracy in each spectral band and typical uncertainty associated with the GSICS Calibration/Correction algorithm, the current inter-calibration reference and those a SI-Traceable Satellite instrument used as a reference. Systematic uncertainty of reference instrument's calibration needs to be added to that of the GSICS Correction to obtain the combined uncertainty.

	VIS (0.4-0.75µm)	NIR (0.75-1.3µm)	SWIR (1.3-3.0µm)	TIR (3-15µm)
2014 GEO Imagers Typ. Cal. Acc.	~7% [30], [141] ~4% [31], [142]	~ 7% [30] ~4% [65]	⪅ 5% [30] ~5% [65]	⪅1K [31], [143]
2020 GEO imagers Typ. Cal. Acc.	~3% [[144] <5% [32]	~3% [144] <3% [32]	~3% [144] ⪅5% [32]	⪅0.2K [144] ⪅0.2K [32]
2022 GEO imagers Req. Cal. Acc.	<5% [145] <3% [146]	<5% [145] <3% [146]	<5% [145] <4% [146]	<0.7K [145] <1.0K [146]
GSICS Correction Method (excl. Reference contr.)	<1% [133]	~1% [147]	~3% [147]	⪅0.1K cold Tb [137]
GSICS Reference Calibration Acc.	⪅2% [148]			⪅ 0.1K [140]
GSICS Correction with SITSat	0.15% [80]			0.02K [81]
SITSat Reference Calibration Acc.	0.3% [149]			0.03K [81]

Two uncertainties are generally involved in transferring a SITSat or REF calibration to a MON instrument to obtain SI traceability and associated uncertainties:

a) *GSICS Correction Method* uncertainty is an estimate of the uncertainty on the corrected radiances introduced by the inter-calibration algorithm – e.g. [137]. It assumes a single reference instrument as the truth and does not associate an uncertainty with it. This provides a means of assessing and maintaining consistency.

b) *GSICS Reference Calibration* uncertainty represents the calibration accuracy of the REF (or SITSat).

In the case of the Prime GSICS Correction, a) would include the uncertainty introduced by the delta corrections, propagated through the blending process, and b) would be the calibration accuracy (SI traceability) of the Anchor reference.

Table 5.1 also includes some typical values for the required calibration accuracy for current and near-future geostationary imagers where the uncertainty is mainly driven by the needs of weather. Ideally, these requirements should be technology-free, but will vary by application. In case an instrument's actual performance is outside the requirements, GSICS Corrections could be applied to bring it within desired limits.

Presenting the capabilities (for the current observing system and using SITSats) allows users of different applications to judge whether they are useful now or potentially useful in future.

5.3.1   Methods to Tie GSICS Infrared Products to an Absolute Scale

For direct inter-calibration methods, as used in current GSICS GEO-LEO IR products, the hyperspectral reference instrument itself can be inter-calibrated with a SITSat (curled arrow in Figure 1a). For example, the SNO method can be applied to compare it with a Sun-synchronous reference instrument's calibration with a $k=3$ uncertainty <0.1K within 2 months of collocations, which would span a range of latitudes [81]. A correction would then be derived to transfer the reference instrument to the on-orbit SI-standard, which would be applied in addition to the current GSICS product.

This approach can be combined with the Prime GSICS Correction to extend support to FCDR generation, based on a series of double-differences to tie the whole time series to the SITSat reference at one point in time, following the principle demonstrated by Tabata et al. [139], and also by John et al. [150].

> A SITSat could tie GSICS reference instruments to an absolute scale using SNOs

5.3.2   Methods to Tie GSICS Reflected-Solar Band Products to an Absolute Scale

The same approach can be applied to inter-calibrate reference sensors used for indirect inter-calibration methods, such as used in the current GSICS GEO-LEO VIS/NIR products using a SITSat with hyperspectral VIS/NIR bands. Its calibration would then be transferred to GSICS products derived either from PICTs or direct comparisons with current reference instruments. However, because of the additional constraints needed to align solar as well as viewing geometries, the number of comparisons is more limited. Roithmayr et al. [80] showed a steerable SITSat would be able to meet requirements for on-orbit direct inter-calibration of VIIRS' reflected solar band channels with a $k=2$ uncertainty of 0.3% within 1 year. However, this capability depends on the polarisation sensitivity of the monitored instrument, which would require additional constraints on the inter-calibration sampling [79]. Shorter time intervals and fewer matchups are, of course, needed where uncertainty demands are not as high as those for long-term climate monitoring.

> SITSat observations tie Pseudo Invariant Calibration Targets to an absolute scale

Another approach can be considered for indirect inter-calibration methods, in which the PICTs themselves are characterised by the SITSat. If these observations covered the full range of viewing conditions, it would be possible to transfer the SITSat calibration to the PICT as shown by the red arrow in Figure 5.3b. The particular challenges for terrestrial targets include consistent PICT identification to ensure that the atmospheric, aerosol, and residual cloud column is observed in a standard way, such that their contributions to the comparison's uncertainty do not compromise its traceability [78]. A final option would be to use the SITSat as a reference to directly inter-calibrate the GEO or LEO imagers (green arrow in Figure 5.3a) - although that is obviously only applicable to the operational lifetime of the SITSat.

However, any of these approaches to tie GSICS products for VIS/NIR channels to a SITSat would benefit from careful coordination with its operators to ensure its observing strategy provides sufficient sampling to achieve the required uncertainty in the inter-calibration product. In practice, GSICS will investigate a multi-method approach, combining the direct inter-calibration of the reference instrument, and the characterisation of multiple PICTs. The balance between these approaches will depend on specific needs for each PICT and the capabilities of the SITSat and will evolve as different SITSats become available.

5.4 Benefits of SITSats to GSICS

The benefits of being able to inter-calibrate satellite instruments to an absolute scale include the resilience against gaps between reference instruments and drifts in their calibration outside their overlap period. This

> Inter-calibration to an absolute scale protects FCDRs from gaps and drifts

would allow construction of robust and harmonized data records from multiple satellite sources to build FCDRs as well as more uniform environmental retrievals in both space and time, thus improving inter-operability.

Additional benefits may be realised depending on the design of the SI-traceable reference instrument and its operating platform. In particular, hyperspectral instruments covering the full spectral band of popular channels in the visible, near-infrared, and thermal infrared could accurately simulate radiances of multi-spectral monitored instruments, making an ideal reference instrument. Such hyperspectral instruments could also be used to validate any SBAFs or similar algorithms to compensate for spectral gaps in other reference instruments, as well as characterise the spectral characteristics of various PICTs. Furthermore, by covering the full dynamic range, it could be possible to resolve other instruments' nonlinearities. Also, by operating such an instrument on a non-Sun-synchronous platform, any diurnal variations in the monitored instrument's calibration could be accounted for, multiple reference instruments could be inter-calibrated, and terrestrial PICTS could be characterised over the full range of solar geometries. Finally, SITSat designs typically have better calibration accuracy than the current reference instruments used in GSICS, which could reduce the overall uncertainty with which inter-calibration can be applied to an absolute scale, as shown in Table 5.1.

However, a number of challenges remain for GSICS. The approaches described above need to be refined and applied to other inter-calibration methods. Careful consideration needs to be made to how different SITSat observing strategies could be exploited to monitor the degradation of sensor optical components not resolved by onboard calibration systems. For example, scan angle dependence of the scanning mirrors and polarization could be fully characterised with sufficient varying observing parameters in the inter-calibration of other satellite instruments. This also requires that GSICS prioritise PICT targets to characterise. To optimise the benefits of such a SI-traceable reference would benefit from cooperation between GSICS and its operators to ensure sufficient acquisitions are available.

Ultimately, the ability to inter-calibrate a satellite instrument to an SI-standard provides irrefutability of scientific observations. A priority for the satellite calibration community should be to establish suitable reference satellite instruments with SI-traceable calibrations on-orbit. While there would still be a need for continuous monitoring to validate the instruments' calibration and ensure consistency, multiple SITSats may eventually provide sufficient spectral, geometric, and temporal coverage and long-term continuity to replace the role of current REF instruments used in GSICS inter-calibration products.

§5   Authors: **Tim Hewison[1], Dave Doelling[2], Constantine Lukashin[2], Dave Tobin[3], Viju John[1], Xiuqing Hu[4], Likun Wang[5], Dorothée Coppens[1]**, [1]EUMETSAT, [2]NASA / LaRC, [3]UWISC-SSEC, [4]CMA-NSMC, [5]Riverside Technology Inc. at NOAA

§5   Editor: **Greg Kopp**, Univ. of Colorado / LASP

6   Earth Energy Budget

At the most fundamental level, Earth's climate is determined by the planet's incoming vs. outgoing energy. 99.96 % of that incoming energy is the radiant energy from the Sun [66] and is monitored from space via instruments measuring the total solar irradiance (TSI). How that energy interacts with the Earth's atmosphere and surface depend on the spectral composition of that energy, or the spectral solar irradiance (SSI). In addition to scattering some of this incident radiation back into space, the energy that is absorbed heats portions of the Earth's system, which then thermally emits at mid- and far-infrared wavelengths. This outgoing energy, some being solar reflected and some being thermal emission, must also be measured to determine, via measurements, the net Earth energy balance (or "imbalance," as is the more realistic case if the climate system is not in equilibrium).

6.1   The Total Solar Irradiance (TSI)

6.1.1   Introduction

Total solar irradiance (TSI) measurements provide the most accurate and most stable measurements of the radiant energy input from the Sun to the Earth's climate system [66]. Long-

> **The Sun provides nearly all of the energy powering the Earth's climate system**

term changes in the TSI can thus directly affect climate via solar forcing. Indirect solar-forcing mechanisms, such as due to aerosol feedbacks, cloud radiative forcing, ice melt, and sea-surface evaporation, can amplify or suppress the solar-variability forcings. These feedbacks, which may be indirect and/or nonlinear, can be hard to quantify but are critically important in understanding climate variability.

6.1.2   Timescales of Solar Variability

Fortunately, the TSI, being the dominant driver of the Earth's climate, is very stable, having variabilities on different timescales described by Kopp [152], [153]. On multi-million-year

> **Variations in the Sun's radiant energy directly and indirectly affect climate**

timescales, the Sun's output increases at a rate of a mere 10^{-10} yr^{-1}. On timescales of 19 000 to 420 000 years, although not caused by intrinsic solar variability, Earth-orbital variations known as the Milankovitch cycles can directly cause changes in the energy incident on the Earth and thus affect climate. These long-term effects are well known and relatively straightforward to estimate.

Shorter-term solar variations have higher uncertainties, being due to lesser-known physical processes in the Sun and the solar dynamo. On century to multi-century timescales, which are of the most interest to present-day climate researchers, solar-variability changes are thought to be ~ 0.1 %. Changes on these timescales have the highest uncertainties, being longer than direct measurements provide. Variabilities on 11-year solar-cycle timescales are better known, having been directly observed by space-based instruments for the last four decades, and are ~0.1 % peak-to-peak. Both these and the multi-century variabilities have discernable effects on climate, as detailed in the extensive review by Gray *et al.* [69] and a shorter synopsis by Lean [67] (as well as those from many other authors). Changes on 27-day solar-rotational as well as shorter, multi-day timescales can be as large as 0.3 %, although the Earth-climate system cannot respond fully to variations at these shorter periods.

6.1.3   TSI Measurement Requirements

To understand the influences of solar variability on climate, stable long-term TSI records are needed. With the Sun being very stable over exceedingly long timescales, instrument measurements must be

even more stable than the expected (and very small) solar variability to be discerned. This drives the need for extremely accurate and stable instruments.

Two approaches to achieving the desired solar-variability measurements desired for a TSI climate data record are described by Kopp [152]. The *stability-and-continuity* approach is more appropriate for measurements over a relatively short time range, while the *absolute-accuracy* approach has benefits for discerning changes over longer times. Currently the measurement record relies on measurement stability and continuity, whereby possible solar variations are detected by acquiring TSI measurements from an uninterrupted series of instruments having good stability (aka "long-term precision"). Overlap between successive instruments can correct for calibration differences on an absolute scale that cause the offsets shown in the space-borne TSI measurement record in Figure 6.1. As the uncertainties in overlapping measurements increase monotonically forward or backward in time from any starting point, eventually the uncertainties from this stability-and-continuity approach will exceed the actual solar variations across that time span, driving the need for better accuracies on an absolute scale.

> **Total solar irradiance measurements require high accuracy and long-term stability**

Absolute accuracy is an alternate measurement approach that is preferable for detecting variability over longer time periods. This approach relies on instruments having sufficiently low uncertainties on an absolute scale that solar-variability trends can be detected via direct measurements, which may be disparate in time. The absolute-accuracy approach does not rely on continuity, so is also more robust for maintaining a long-term climate data record despite potential spacecraft or instrument anomalies and varying science-budget priorities that could lead to measurement gaps.

Current TSI-instrument requirements for both approaches are given in Table 6.1 [2], [10], [154].

Table 6.1 TSI Measurement Requirements ($k = 1$)

Measurement Parameter	Requirement
Absolute Accuracy	< 0.01 %
Stability	< 0.001 % yr^{-1}

6.1.4 The TSI Record

Because of changes in the Earth's atmospheric transmission, which, on average, only allows ~2/3 of the top-of-atmosphere sunlight to reach the surface, accurate TSI measurements must be made from space. This record commenced in 1978 and has been uninterrupted since then thanks to the overlap of successive instruments on NASA, NOAA, and ESA missions. The current 43-year-long measurement record is shown in Figure 6.1.

6.1.5 The Space-Based Measurement Record

TSI instruments provide the most accurate and stable radiometric measurements of the Sun; and yet, even lower uncertainties than currently achieved are desirable for the climate-study

> **Measurement continuity is critical in maintaining the solar climate data record**

applications needed, as such studies rely on detecting small levels of solar variability over extremely long timescales.

Prior to the launch of the SOlar Radiation and Climate Experiment's (SORCE's) Total Irradiance Monitor (TIM), which was a newly-designed instrument incorporating many improvements over prior

TSI instruments [155], the accepted value of the average TSI was 1366 W m^{-2}. The new design of this TIM and subsequent reevaluations of artifacts in prior instruments established the now-accepted lower TSI value of 1361 W m^{-2} [35], having implications for Earth energy-balance studies [68] and the resulting effects on global warming/cooling. Corrections have now been retroactively applied to prior flight TSI instruments, particularly the SoHO/VIRGO and the ACRIMSat/ACRIM3, giving the consistency of contemporary measurements shown in Figure 6.1.
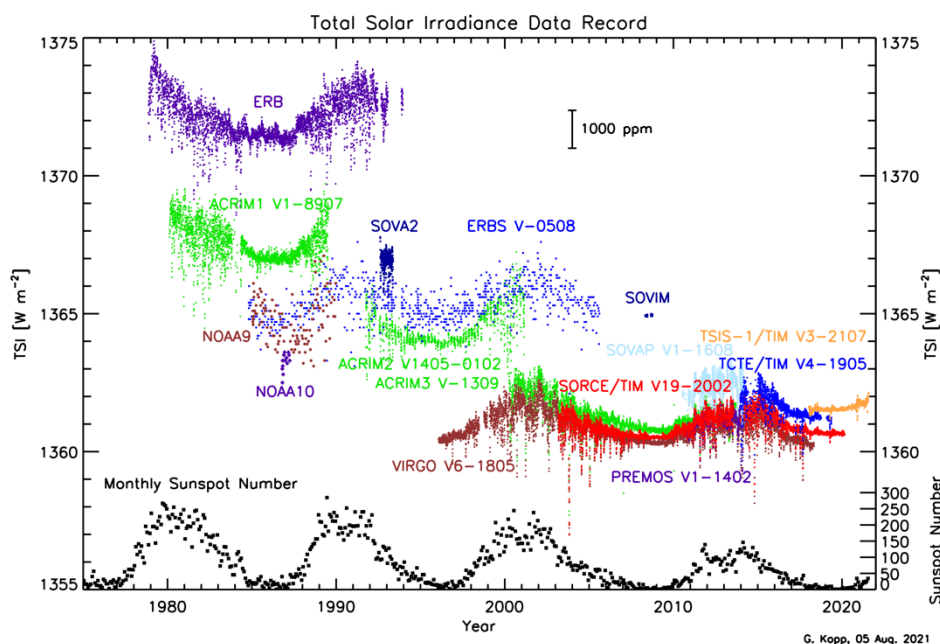
Figure 6.1 The space-based TSI instrument record has been uninterrupted since its beginning in 1978 thanks to the overlap of more than a dozen instruments. The measurements from each are plotted. Offsets are due to different instrument calibrations on an absolute scale. (from http://spot.colorado.edu/~koppg/TSI)

6.1.6   TSI Composites

Combining the many individual-instrument records shown in Figure 6.1 into a single timeseries, as desired for users of these data, requires assumptions of which instrument(s) to favor at which times. Traditionally, such composites have been created by individuals, often being the PIs of a particular instrument, and, as such, have biases favoring that individual's instrument. These traditional composites, with the most prominent being the PMOD [156], ACRIM [157], and Dewitte [158] composites, suffer from the following issues:

- They contain biases, typically favoring the individual's instrument
- Instruments are selected binarily, using only one instrument at any one time and thus ignoring the added information provided by other co-temporal measurements
- There are discontinuities in the TSI value or slope at instrument transitions
- Uncertainties are generally not provided

To circumvent these issues, a newer, statistics-based approach was created [70]. This method avoids individual-instrument biases, weights all available instrument values by data-driven estimates of each instrument's uncertainties and uses scale-wise smoothings to avoid abrupt instrument transitions. Time-dependent uncertainties are provided. An update to the example composite given by Dudok de Wit *et al.* [70] is shown in Figure 6.2. This composite has the support of most active TSI instrument teams as being the best currently available composite and composite-creation approach.
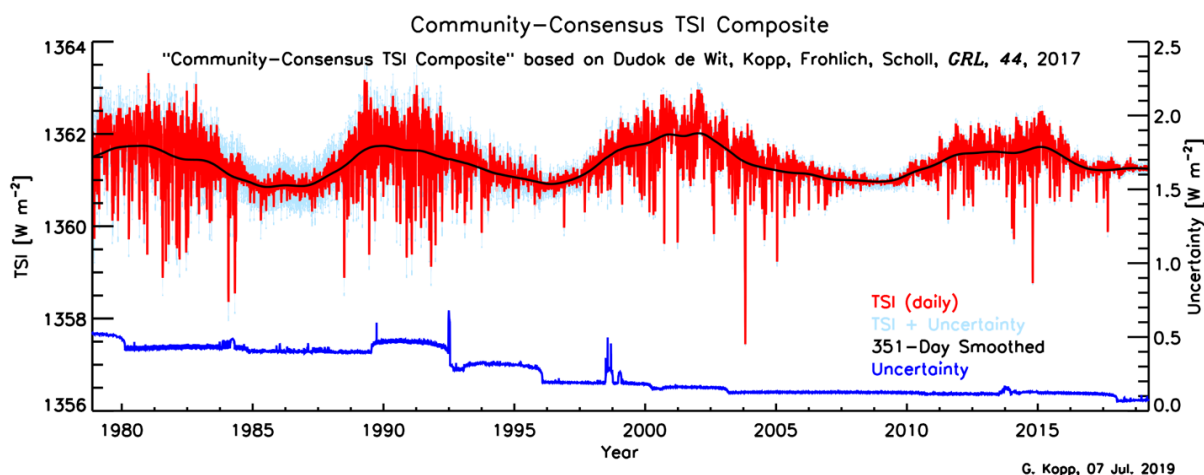
Figure 6.2 This "Community-Consensus TSI Composite," using the unbiased, statistics-based methodology of Dudok de Wit et al. [70], has several advantages over prior composites, one of which is that it has the consensus of most of the currently-active TSI instrument teams.

6.1.7   TSI Models and Historical Reconstructions

TSI models can extend the measurement record to historical times, as needed for comparisons with long-term Earth-climate records for climate research. These models correlate spacecraft-era

> **Proxies extend the solar-irradiance record to historical times for climate studies**

TSI measurements with other indicators of solar variability, such as sunspot-number, -area, and -position; measurements of faculae or their proxies; and magnetic-field measurements. Historical measurements of those solar-proxy records then enable historical TSI reconstructions via empirical and/or semi-empirical solar models. The two most prominent such TSI-reconstruction models, the Naval Research Laboratory TSI (NRLTSI) [159] and the Spectral And Total Irradiance reconstructions (SATIRE) [160] models, estimate the TSI from 1610 to the present using, among other indicators of past solar-magnetic activity, the 400-year sunspot record. Reconstructions going back even further in time are achieved via comparisons with cosmogenic isotopes [71], [161], as shown in Figure 6.3.
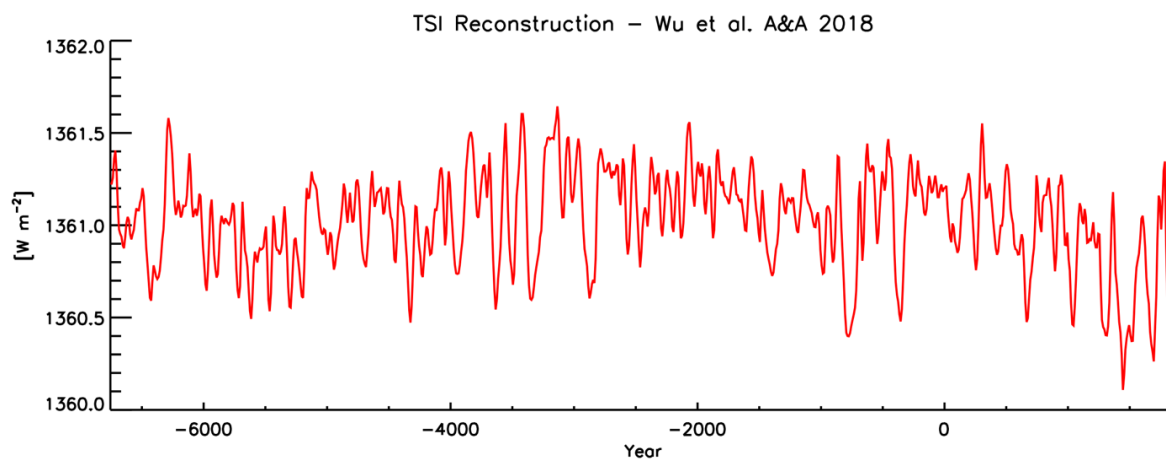
6.1.8   Future TSI-Record Needs

Kopp [24] assesses the space-borne TSI measurement-record for climate research and discusses the current record's limitations, quantifying the noise and stabilities of various instruments. He suggests future needs with regard to measurement accuracy, stability, and continuity. Although updated with newer data now, those overall requirements, given in Table 6.1, remain the same and progress is being made to achieve these levels.

Modern ground-based test facilities, particularly the TSI Radiometer Facility (TRF) [162], now enable end-to-end calibrations of TSI instruments under flight-like conditions by operating in vacuum with full solar-irradiance power levels. No such facility existed prior to its construction in 2007, and all early TSI instruments were merely calibrated at the component level rather than calibrated or validated end-to-end at the instrument-system level. This TRF has improved consistency between the most recent on-orbit TSI instruments. It has been used for calibrations of the ESA's Picard/PREMOS [163] and CLARA spaceflight instruments as well as for validations (but not calibrations) of other flight instruments, including the NASA's STPSat3/TCTE/TIM and the TSIS–1/TIM. Diagnostics enabled by the TRF have also allowed corrections for the already-on-orbit flight SoHO/VIRGO and ACRIMSat/ACRIM3 instruments, which previously reported erroneously-high TSI values.

The future TSI-measurement record and resulting climate studies relying on solar variability will benefit from the following improvements:

- Continued improvements to *absolute accuracy* will help maintain the uninterrupted spacecraft TSI measurement record in the undesirable event of a gap in measurements and will help discern long-term changes in the TSI.
- The TSI record still relies on *measurement continuity with stable instruments*. A series of TSIS/TIM instruments is intended to provide this continuity in the immediate foreseeable future. International instrument teams provide further robustness of this record in the event of a single-instrument failure.
- Smaller versions of the current TSI instruments, such as the 6U CubeSat Compact Total Irradiance Monitor (CTIM), are in development for flight. Such smaller and less-expensive instruments should help maintain the space-based TSI measurement record needed for Earth-climate studies.
- Improvements to historical reconstructions via better TSI models and historical proxies will improve knowledge of past solar variability, as needed for climate studies.

6.1.9   Chinese Contribution to TSI

To detect small and long-term changes in the Sun, an instrument for measuring the total solar irradiance should meet the following criteria: To detect small and long-term changes in the Sun, an instrument for measuring the total solar irradiance should meet the following criteria:

> **The Chinese Fengyun-3 satellite will monitor total solar irradiance for climate studies**

- The uncertainty of solar radiation on an absolute scale is $\leq 0.02\%$ and ideally $\leq 0.01\%$ for solar radiation data over ten or even a hundred years.
- Long-term stability is better than 0.005% yr^{-1}, with 0.001% yr^{-1} preferable, from continuous measurements.

> **FY¬3E TSI measurement goals are 0.02% accuracy and 0.005% / 10 years stability**

Since 2016, CIOMP/CAS and PMOD/WRC have jointly developed an international comparative solar radiation monitor, which will carry the Fengyun 3 (05 satellite) for long-term space-based total solar irradiance observations.

As described in §11.3.1.2, the high-accuracy Sun-Earth-Moon observation instrument in the solar-reflected spectrum has a solar-observation mode. This space cryogenic radiometer benchmark is transferred to the total solar irradiance monitor by synchronous solar observations for improving the uncertainty and long-term stability of space-based total solar irradiance measurements and supplementing the international solar radiation observation sequence.

6.2   Spectral Solar Irradiance

6.2.1   Introduction

The incoming solar radiation powers the complex and tightly coupled physical and chemical processes that establish the interactions among the atmosphere, oceans, land, and ice. Although relative variations in the Sun's radiative inputs are

> **Solar-forcing mechanisms are spectrally dependent**

small, the climate sensitivity uncertainties from solar forcing remain large; in some cases, these uncertainties are comparable to those associated with greenhouse gases and aerosols [107]. Accurate, long-term measurements of the TSI constrain the total energy available to drive the climate system (Section 6.1). However, it is the spectral solar irradiance (SSI) measurements that provide the additional wavelength-dependent details to elucidate the underlying mechanisms and terrestrial interactions responsible for solar-induced climate changes [69], [164]–[166]. Therefore, an accurate SSI spectrum is vital in remote-sensing algorithms that rely on accurate specification of the solar energy entering the Earth system as a function of wavelength. Furthermore, accurate and long-term SSI measurements are vital inputs for climate models used to advance scientific understanding of the wavelength specific processes of climate variability and change. Accurate and long-term SSI measurements are also vital for validating and constraining solar irradiance variability models (both empirical and physical), that interpolate and extrapolate the variability to time periods and spectral ranges beyond those covered by the measurement record(s). Ultimately, SSI measurement continuity plays a critical role in evaluating and improving these models to quantify processes and establish the pace and scale of the climate response to both natural and anthropogenic changes [69]. As these Earth-climate spectral models become more sophisticated, absolute measurement accuracy has become a more stringent measurement requirement toward the goal of unequivocal attribution of causes [8], [167].

To this end, long-term accurate SSI monitoring extends to the fundamental objectives related to a broad Earth science community that includes studies on the global energy budget, process-oriented remote-sensing applications, climate and atmospheric modeling, and atmospheric composition. For example, one of the three CLARREO benchmark measurements, high-accuracy spectrally-resolved reflected-solar radiation from Earth, is bounded by the accuracy and SI-traceability of the SSI since the reflectance is a measurement of reflected radiance relative to SSI in absolute units [6].

While short-wavelength SSI measurements (predominantly in the EUV and UV) have been measured from space for over four decades, a newer record of SSI covering the UV, visible, and near IR commenced with the launch of the Solar Radiation and Climate Experiment (SORCE) in 2003. The SORCE SSI measurements, while crucial in evaluating and improving spectral models on short timescales at most ultraviolet and visible wavelengths, are not yet of sufficient accuracy, precision, and spectral stability to definitively establish long-term (decadal) solar impacts at all wavelengths [168].

This has consequences for producing a definitive solar reference spectrum, for constraining short- and long-term solar variability at all wavelengths, and on improving our understanding of wavelength-dependent climate processes. Therefore, because of the reliance on multiple data sets spanning long timescales (linking of multiple instrument data into a continuous data record), an important requirement moving forward for the validation of SSI climate data records is continuous calibration in which the characterization of measurement uncertainties can be established (and maintained) against fundamental international (SI) standards.

6.2.2   Spectral Solar Irradiance Measurement Requirements and Data Record

The current implementation for continuous, long-term SSI monitoring is from the Spectral Irradiance Monitor (SIM) on the Total and Spectral Solar Irradiance Sensor (TSIS-1) mission that began operations from the International Space Station (ISS) in March 2018. The TSIS-1 SIM measurements (covering 200-2400 nm, or approximately 96% of TSI) will secure the SSI data record continuity for the near-term. The SORCE mission ended in February of 2020 and overlapped with the TSIS-1 mission for two full years. The TSIS-1 SIM instrument is the latest state-of-the-art spectral solar irradiance radiometer – and represents the most accurate and stable spectral radiometer developed to meet the demanding long-term measurement requirements to quantify the input solar signal and track SSI variability for the climate record [25], [159].

> **TSI and SSI are required Climate Data Records**

The Solar Irradiance Environmental Data Record (EDR) requirements were originally specified in the *NPOESS Integrated Operational Requirements Document* (IORD) and updated in version II and in the *NOAA Climate Sensors Project TSIS Requirements Document* [169], [170]. Through these efforts, the SSI (along with the TSI) is now recognized as a Climate Data Record (CDR) rather than an Environmental Data Record (EDR) to distinguish it from higher-latency, lower-accuracy requirements of operational weather (short-term) data [159].

Table 6.2 TSIS-1 SSI Level-1 requirements.

Parameter	SSI Requirements	
	Baseline	Threshold
Spectral Range	200-2400 nm	
Uncertainty	0.2%	1%
Stability	0.05%/yr (<0.4 µm) 0.01%/yr (>0.4 µm)	0.1%/yr (<0.4 µm) 0.02%/yr (>0.4 µm)
Spectral Resolution	2 nm: (< 0.28 µm) 5 nm: (0.28 µm to 0.4 µm) 45 nm: (>0.4 µm)	
Reporting Frequency	2 spectra per day	

There has been much effort over the last decade devoted to establishing the fundamental principles and calibration guidelines for future climate measurement strategies [171], [172]. The dominant issue for calibration of CDR's is establishing traceability to internationally recognized standards pre-launch and maintaining the on-orbit calibration over the life of the instrument. The full traceability definition here requires a full radiometric analysis of measurement uncertainties through an uninterrupted chain of

calibrations tied to primary metrology standards [173], [174]. Therefore, central to the creation of a reliable SSI record is the establishment of the full instrument response with SI traceability.

SSI accuracies are traceable to NIST

Achieving the desired absolute accuracies to meet the climate-data requirements for SSI measurements and provide the necessary tie to existing and future SSI data records involved developing new, state-of-the-art detector-based calibration facilities. This was done in close partnership with the NIST using recent developments in the techniques used to establish primary spectral radiometer scales, which make it possible to significantly improve the accuracy and traceability of spectral irradiance measurements and assure quantification of absolute measurement uncertainties near 0.1% [60], [62]. The comprehensive Spectral Radiometer Facility (SRF) was developed at the Laboratory for Atmospheric and Space Physics (LASP) at the Univ. of Colorado, Boulder in collaboration with the NIST to ensure the ties to primary spectral SI-standards in power and irradiance [25], [175]. Laser sources provide the needed high intensities and accurate wavelengths. By using these sources, the traceability to SI is achieved via direct electrical substitution radiometer (ESR) detector calibration against a cryogenic radiometer either in optical power (W) responsivity or irradiance (W m^{-2}) responsivity. At present, the LASP SRF has an absolute uncertainty of 0.018 % in power and an end-to-end absolute uncertainty of < 0.15 % in irradiance for instrument calibrations and validations operating in vacuum and at solar input power levels. This new calibration facility now enables SI traceability in absolute accuracy for spaceflight SSI instruments such as the TSIS-1/SIM.

Long-term stability limits for SSI measurement requirements are based on the magnitude of the estimated near-decadal trends in the SSI variability. Those specified for the SORCE SIM are given by [166]. Newer instruments, such as the TSIS-1 SIM, are stiving for yet more stable measurements. For the two SIM instruments, the long-term maintenance of the calibration relies on an on-board, detector-based reference electrical substitution radiometer (ESR). An ESR is a bolometric detector that accurately compares the heating effect of absorbed optical radiation with that of electrical power heating via an accurate, high-stability standard-watt circuit. The calibration maintenance approach involves establishing (pre-flight) the ESR as an absolute detector and then (on-orbit) using the Sun as the common calibration source to track relative channel-to-channel changes. This offers the unique advantage of adhering to the "like-to-like" rule of radiometry in that the solar calibration optical geometry is identical to the measurement optical geometry [176]. The ESR is established as an SI-traceable power calibration standard detector by pre-launch spectral calibrations against an absolute cryogenic radiometer traceable to the NIST Primary Optical Watt Radiometer (POWR), the primary US standard for radiant power measurements [177]. Verifying the invariance of the ESR calibration over time is a key foundation to maintaining on-orbit stability. By utilizing the three independent SIM channels in a solar exposure duty-cycling mode it is possible to quantify and correct the on-orbit long-term exposure-related degradation changes in the final irradiance data products. Sophisticated spectral radiometric models, maintained and continually updated throughout mission life, are important components of the on-orbit recalibration procedure.

Meeting these demanding absolute and stability SSI measurement requirements involves a complete instrument characterization and calibration approach, including extensive unit-level and pre-launch end-to-end calibrations, post-launch stability tracking, instrument inter-calibration and complete documentation of algorithm product development. This complete characterization of instrument stability is required in order to ensure that any potential changes over time (either discrete offsets or systematic trends) can be quantified with respect to any instrument performance changes [2]. Based on an absolute measurement equation approach, each independent contribution must be quantified with an associated uncertainty and verified by characterization measurements.

Individual characterization uncertainties at the component level propagated through the full measurement equation allows validations against an SI-traceable, end-to-end spectral irradiance measurement against the cryogenic radiometer. For the TSIS-1/SIM, this validation showed a $< \pm 1$ % systematic bias common to all three SIM channels, indicating a missing contribution to the measurement equation from the unit-level calibrations. Based on the calibration accuracy of the SRF in irradiance (0.14%, k=1), we apply a spectral functional calibration correction to achieve an instrument absolute irradiance calibration against the cryogenic radiometer irradiance values at the ~ 0.25 % level of uncertainty across the full spectrum (Figure 6.4).
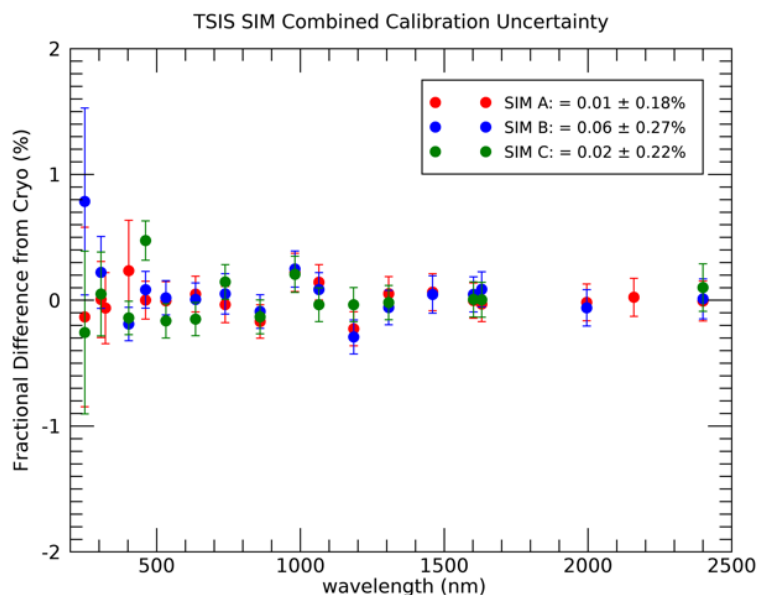

Figure 6.4 Results of the final pre-launch spectral calibration of all three TSIS-1 SIM channels against the SRF cryogenic radiometer irradiance values. Reported combined uncertainties (k=1) include the channel level offset and spread in the spectral distribution and the 0.14 % SRF-cryogenic radiometer absolute irradiance uncertainty.

6.2.3   2018 Solar Minimum SSI Reference Spectrum

With the launch and early observations of the TSIS-1 SIM during the solar cycle 24 – 25 minimum, we have been successful at obtaining a new SSI reference spectrum at high calibration accuracy and can compare to other known SSI reference spectra used by the Earth science community. Figure 6.5 shows the spectrally-dependent differences from 300 – 2400 nm from the TSIS-1 SIM reference spectrum with several established solar reference spectra. While typical differences are in the 2 to 4 % range, there are significant differences to the ATLAS3 reference spectrum in the near IR that are in the 5 to 8 % range; the majority of these previous SSI reference spectra are higher in irradiance for most of the visible and near IR [178]–[181].
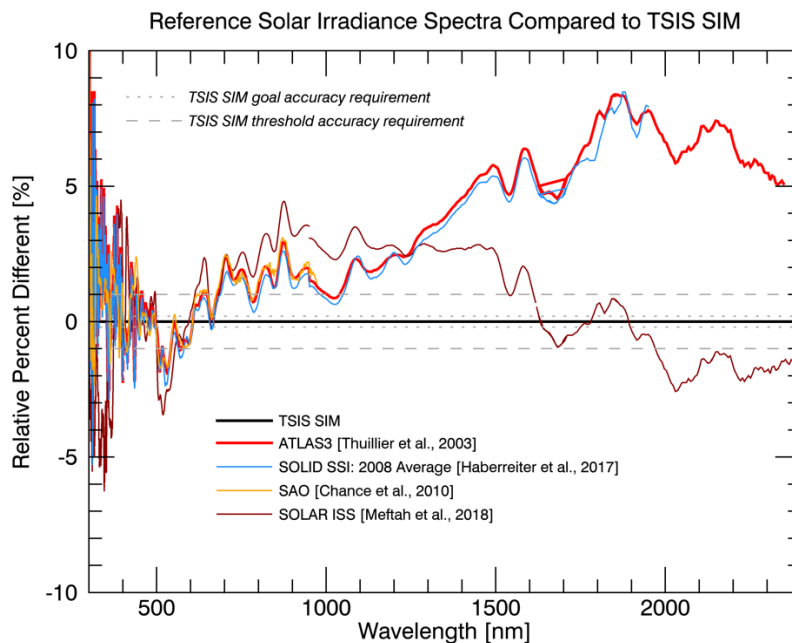
Figure 6.5 Comparisons of the differences between the TSIS SSI reference spectrum with several well-established SSI reference spectra used by the remote sensing community. For most of the spectrum, the new TSIS-1 SSI reference spectrum is lower in spectral irradiance than previous spectra. In particular, the ATLAS3 reference is significantly higher (by 5-8 %) in the atmospherically important near-IR solar spectral region.

6.2.4   Long-term SSI Data Records

Based on a three-channel, duty-cycled solar exposure approach, we can correct the primary measurement channel for solar exposure optical degradation and recover true solar variability at the 100-200 ppm level. Figure 6.6 shows the long-term relative stability performance of the TSIS-1 SIM SSI measurements for ~1.5 years of operations. The data here are presented in four integrated wavelength regions spanning the UV through the near IR. Also shown for comparison are the modeled SSI integrated results from the NRLSSI2 solar irradiance empirical model over this same time period [182]. By utilizing a three-channel degradation correction approach, where each SIM channel has decreasing duty cycle in solar exposure, we are able to correct the optical degradation of the primary measurement channel (SIM A) and recover true solar variability near the 0.01% levels (as seen in the near IR where solar variability is near the limit of detection). Maintaining this correction stability over the coming years with the onset increased solar activity in solar cycle (SC) 25 will provide an unprecedented SSI data record in absolute accuracy and measurement stability that will serve the broader science community to advance improvements in Earth-process studies as well as solar irradiance modeling.
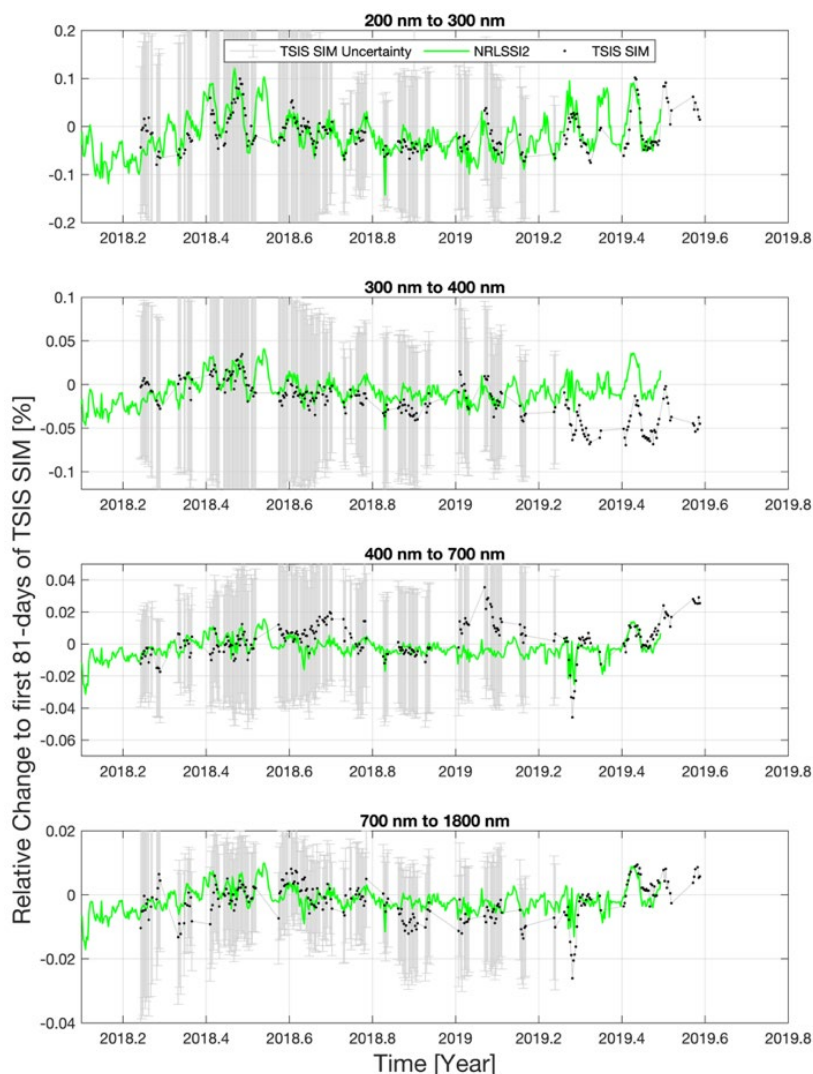
Figure 6.6 Plot of the long-term spectral stability of the TSIS-1 SIM SSI data record (March 2018 – September 2019). The data (black dots) are plotted relative to the percent change from the average of the first 81 days of measurements. Shown for comparison are the results of the NRLSSI2 empirical model (green line) for the same time period and spectral regions.

6.2.5   Addressing the Measurement Continuity Challenges for the Future

> **New concepts for a low-risk, cost-efficient observing strategy to maintain the solar irradiance record for decades to come should be a priority for new continuity mission programs**

There are both scientific and programmatic motivations for addressing the challenges of maintaining the SSI data record over the coming decade. The science rests on well-founded requirements of establishing a trusted climate-observing network that can monitor trends in fundamental climate variables – is this case, the energy available for the entire Earth system. Programmatically, the continuous and long-term monitoring of solar irradiance must be balanced within the broader goals of the international observation community and, in this example, that of NASA Earth Science. In keeping with the mission strategy described above, new developments to reduce the size of these instruments will advance their adaptability to smaller spacecraft and a broader range of launch opportunities.

The Compact Spectral Irradiance Monitor (CSIM) developed under a NASA Earth Science Technology Office (ESTO) program represents a new approach to acquiring spectral solar irradiance measurements to meet future needs for compact, robust measurement systems [183]. CSIM covers a continuous wavelength range of 200-2800 nm (> 97 % of the TSI) and was designed to meet the required SI-traceable SSI-measurement accuracy and on-orbit stability but with reduced size and cost. Ultimately, these successful concepts will mitigate data continuity risks associated with future mission delays by providing implementation flexibility for alternative flight opportunities, including ride-share and hosted payloads, small satellites, and dedicated CubeSat missions [184]. New concepts for a low-risk, cost-efficient observing strategy to maintain the solar irradiance record for decades to come should be a priority for new continuity mission programs.

6.3　Earth Radiation Budget (ERB): Continuity of ERB Measurements

6.3.1　Background and Need

Top-of-atmosphere Earth radiation budget (TOA-ERB) measurements have been made nearly continuously since the dawn of the space age [72], [185]. These have largely consisted of measurements of the entirety of two radiation streams: the solar radiation reflected from the Earth's

> **Outgoing Earth radiation budget measurements complete the energy-balance assessment**

surface and atmosphere and the thermal infrared radiation emitted by the Earth surface and atmosphere. These measurements, coupled with measurements of the total solar irradiance, allow for assessment of the energy budget of the entire planet. While space-based measurements of the ERB have almost exclusively been made from low-Earth orbiting satellites, the Geostationary Earth Radiation Budget instruments [77], [186] have been observing from the Meteosat Second Generation series of geostationary satellites since 2003.

The longest-running, continuous, global ERB measurements are those made since 2000 by the Clouds and Earth Radiant Energy System (CERES) instruments [76]. At present, there are six instruments operational in low Earth orbit on multiple satellites: two instruments each on the NASA Terra and Aqua satellites (launched 1999 and 2002); one instrument on the Suomi-NPP satellite (launched 2011); and one on the NOAA-20 satellite (launched 2017). ERB measurements prior to 2000 were primarily focused on understanding fundamental properties of the Earth's climate system (e.g., planetary albedo; magnitude of equator-to-pole heat transport; and the net effect of clouds in heating or cooling of the Earth). Today, with clear evidence of climate change as a result of increasing carbon dioxide and other infrared-active greenhouse gases, continuous TOA-ERB measurements are essential for monitoring Earth's response for decades into the future. Some scientific questions for which TOA-ERB measurements are essential include understanding Earth's energy imbalance [73]; quantifying the magnitude of cloud radiative effect [10]; and understanding planetary uptake of energy and ocean heat storage [74].

Measurement of the planetary heat uptake is particularly critical because it provides a clear metric of Earth's response to increased greenhouse gases and the associated energy trapped by them. While Earth's surface temperature is a common metric for assessing the planet's response, the recent "hiatus" in the first decade of the 21st century illustrated that it is an unreliable metric for assessing the Earth's response on short (decadal) timescales. Specifically, from ~ 2001 to 2014, the rate of increase in the global mean surface temperature slowed relative to the prior three decades. This led to much debate about the veracity of climate change models and their projections for future warming.

However, CERES observations showed no "hiatus" in planetary heat uptake since the year 2000 when observations began [74]. These observations are consistent with model simulations [73], which show a

direct relation between ocean heat storage and Earth-system energy change and a much weaker correlation between Earth-system energy change and the rate of surface temperature change. The surface temperature will ultimately reflect the magnitude of the energy change; however, on shorter (~ decadal) timescales, natural variability of the Earth system may obscure its rate of change.

6.3.2   Requirements for TOA-ERB Continuity

The current CERES sensors will continue to operate into the foreseeable future. The Aqua and Terra satellites will likely be de-orbited by 2025 before they run out of fuel for orbital maneuvers. A new ERB sensor must be launched by ~ 2026 in order to minimize

> **Measurement continuity and stability are currently relied upon for maintaining the ERB data record**

the risk of a gap between the current CERES and new sensors. Gap avoidance is essential for the current CERES-class instruments. The nominal calibration accuracy of CERES is 1 % in the "longwave" or thermal emission measurement and 2 % in the measurement of reflected solar radiation. Both accuracies are specified as $k = 2$ values [78]. At these accuracies, a gap at this point in the record would require the new instrument to have extraordinarily high (< 0.3 %) accuracy in order to yield scientifically useful trends derived from the ongoing ERB record [6], [10], [12], [78].

This result is taken directly from [78], who simulated a 30-year record of net cloud radiative effect (CRE^{net}), which is the sum of shortwave and longwave CRE, using the first seven years of CERES data. In the middle of this simulated record, a 1-year gap was placed and known calibration errors (2 % shortwave, 1 % longwave, mentioned above) were applied to the post-gap record. The uncertainty in the CRE^{net} for this 30-year record was then required to be equal to 25 % of the anthropogenic radiative forcing, 0.15 W m^{-2} decade^{-1}. Trend analyses were conducted on the 30-year record with uncertainties applied post-gap, adjusting downward the instrument accuracy post-gap until the required trend accuracy was met. The results are in Figure 6.7, which shows the shortwave channel accuracy (abscissa) and the required longwave channel accuracy (ordinate) required to achieve the uncertainty in trend accuracy given in the contours. For a trend accuracy of 0.15 W m^{-2} decade^{-1}, a new instrument operating after a one-year gap would require shortwave accuracy of 0.3 % and a longwave accuracy of 0.1 %, both nearly one order of magnitude better than the current CERES accuracy. In essence, a gap in the current record would require a restart of the entire CERES record, rendering the existing record more or less obsolete.
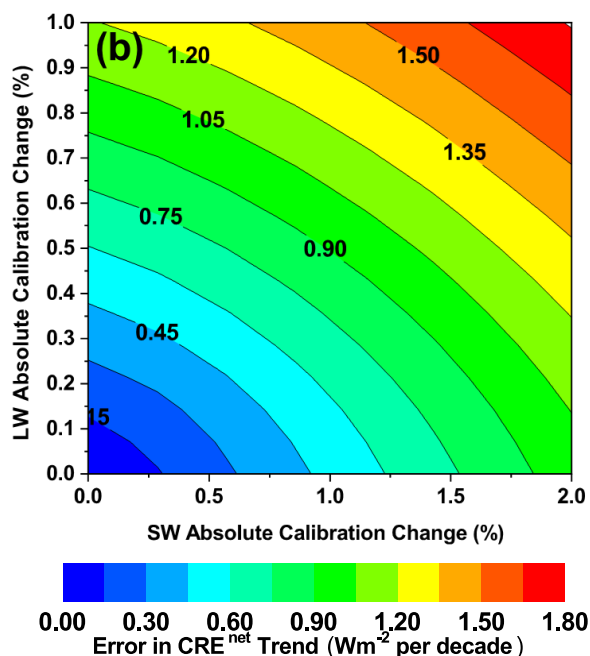
Figure 6.7 Required shortwave (SW) and longwave (LW) accuracy in a new radiation budget instrument to meet trend uncertainty in net CRE given in the various contours. From [78].

In addition, because of the current calibration accuracies, not only must gaps in the record be avoided, but overlap of at least one year is required to place the new and current records on the same radiometric scale [78]. The current record cannot admit a gap and new sensors must have a significant period of overlap.

6.3.3   The Future of ERB Measurements

Continued measurement of the TOA-ERB has been endorsed in many recent community reports [3], [10], [12]. NASA plans to continue the CERES record via its new Earth Venture Continuity space flight mission program and the European Space Agency will soon launch the Broadband Radiometer (BBR) instrument [187] on the EarthCARE satellite [188].

A key step forward for TOA-ERB measurements will come with the launch of the CLARREO Pathfinder (CPF) mission [6], [21], [38] in 2023 and the TRUTHS mission [8] in the mid-2020's. The goal of these missions is to measure the Earth's spectral ERB at high accuracy with instruments and techniques that are traceable on orbit to Système Internationale (SI) standards at accuracies of 0.3 % to 0.6 % (k=2). The CPF and TRUTHS instruments will function as metrology labs in orbit for the purpose of performing a reference intercalibration (RI) of other sensors, including the ERB sensors. The RI will enable detection of long-term drifts in calibration of instruments like CERES, including changes in electronic gains, offsets, non-linearity, and spectral response. RI will provide a more accurate climate record from the ERB (and other) sensors and will reduce the need for overlap between successive ERB sensors. The future climate observing system [13] that realizes the advantages of high-accuracy, on-orbit metrology sensors like CLARREO and TRUTHS will significantly shorten the time to observe changes in the climate system, providing actionable data for government policy makers, and yielding significant economic value [19].

§6.1   Author: **Greg Kopp**, Univ. of Colorado / LASP

§6.1.9 Authors: **Xin Ye, Xuejun Zhang, Xiaolong Yi, Chao Lin, and Long Wang**, Changchun Institute of Optics, Fine Mechanics and Physics, Chinese Academy of Sciences

§6.2   Authors: **Erik Richard, Odele Coddington, Peter Pilewskie**, Univ. of Colorado / LASP

§6.3   Author: **Marty Mlynczak**, NASA / LaRC

§6   Editor: **Greg Kopp**, Univ. of Colorado / LASP

7   Reflected Solar Passive

7.1   Introduction

The impact of human activities on the Earth's ecosystem is gradually intensifying and the world is facing severe environmental challenges. Pure fresh water is increasingly scarce, soil erosion is aggravated, and ecosystem degradation, glacier melting, and greenhouse gases are increasing. Climate change is closely linked to human causes and is expected to be even more dramatic and precarious in the future.

Solar radiation is the main external energy source of the Earth. The solar radiation reflected back into space from the Earth's atmospheric system is sensitive to changes of snow cover, sea glaciers, land use, and aerosol and cloud characteristics. Time series of systematic, spatially resolved observations of solar-reflected radiation in the ultraviolet, visible, and near infrared bands can provide reliable analysis data of the highly variable climate system.

> **Spatial and spectral knowledge of reflected solar radiation is needed for understanding the effects of climate drivers**

In order to scientifically understand the impacts of land, ocean, atmosphere, and human activities on the global environment and climate change, countries around the world have carried out research on the Earth's outgoing spectral radiation. Fully using the advantages of global coverage from satellite platforms, the spectral radiation observation instruments were developed to obtain the spectral information of the reflected-solar spectrum and provide key data for climate modelling, weather forecasting, disaster prevention and mitigation, and resource exploration. Climate models require extremely high-stability measurements of spectral radiation across the reflected solar bands. For observing the relatively small radiation changes from space, spectral radiation observation instruments require extremely high observation accuracies and long-term stabilities. The measurement uncertainties of these observations need to reach 0.3% within the next ten years, driving new measurement challenges across this spectral region. Radiometric calibration is an important factor in achieving these requirements. The necessary calibrations can be divided into laboratory calibrations before launch and on-orbit calibrations after launch, such as via use of vicarious calibration sites and using on-orbit references like the Moon. This section discusses these on-orbit calibration approaches as well as their implementations on some currently operating reflected-solar imagers.

7.2   Reflected-Solar Narrowband Imagers: MODIS and VIIRS

The MOderate Resolution Imaging Spectroradiometer (MODIS) instrument was developed in order to meet the increasing need of the remote sensing community and users worldwide in late 1980s and early 1990s to further extend and enhance the data records developed based on the

> **MODIS and VIIRS provide spectral knowledge with high spatial resolution**

measurements made by a number of legacy sensors, such as the AVHRR, Landsat TM, CZCS, HIRS, and SeaWiFS. It was designed with an overall improvement in terms of its spectral and spatial characteristics, temporal coverage, calibration requirements, and on-orbit calibration capability [189], [190]. Developed and designed by the same instrument vendor, the VIIRS has a strong MODIS heritage, including a number of improvements based on the experience and lessons learned from MODIS instrument design, operation, calibration, and performance [191]–[193].

The MODIS, shown in Figure 7.1, is one of the key instruments for the NASA's Earth Observing System (EOS), currently operated onboard the Terra and Aqua spacecraft launched in December 1999 and May 2002, respectively [189], [194]. MODIS observations are made in 36 spectral bands from the

visible to the thermal infrared (0.4-14.4 μm). The MODIS has 20 reflective solar bands (RSB), covering wavelengths from 0.41 μm to 2.2 μm and collecting data at three spatial resolutions (nadir): 250 m for 2 bands, 500 m for 5 bands, and 1 km for the remaining 13 bands. Nearly 40 data products are routinely generated from each MODIS instrument and widely distributed to the remote sensing community and users worldwide in support of their studies of the Earth's system and its land, oceans, and atmosphere, including the land, cloud, and aerosol properties, ocean colour, land/sea surface and cloud temperatures, water vapor, and cloud-top altitude. To date, high-quality data records of more than 20 and 18 years have been successfully generated from the Terra and Aqua MODIS observations, respectively.
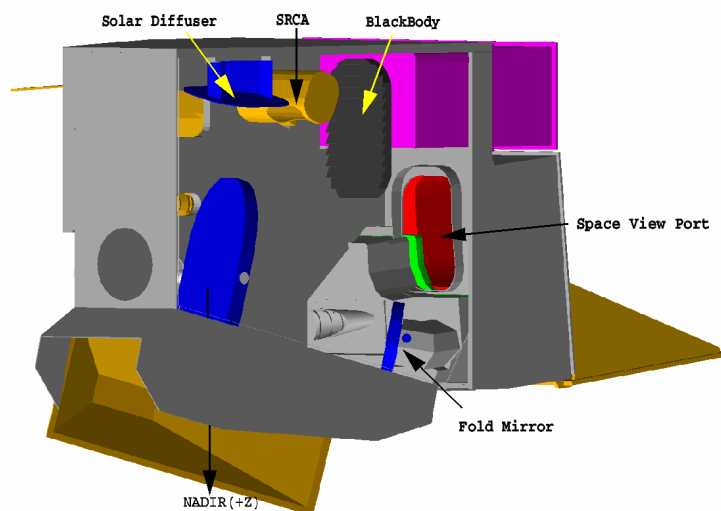

Figure 7.1: MODIS instrument and its on-board calibrators

The Visible Infrared Imaging Radiometer Suite (VIIRS), shown in Figure 7.2, was originally developed as a key instrument for the National Polar-Orbiting Environmental Satellite System (NPOESS)[191], [195], [196]. Due to cost overruns and schedule delays, the NPOESS program was phased out and transitioned to the Joint Polar Satellite System (JPSS) in 2010. Currently, there are two VIIRS instruments in space: one onboard the S-NPP satellite launched in October 2011 and the other onboard the NOAA-20 satellite launched in November 2017. As a MODIS follow-on instrument, the VIIRS collects data in 22 spectral bands covering wavelengths from 0.4 to 12.2 μm. The VIIRS has 14 RSB channels, covering the same spectral wavelength range as MODIS. It should be pointed out that some VIIRS spectral bands can collect data at both high and low gains, depending on the scene radiances. VIIRS observations are made at two spatial resolutions (nadir): 375 m for the imaging (I) bands and 750 m for the moderate (M) resolution bands. Listed in Table 7.1 are the bandwidths and spatial resolutions of VIIRS spectral bands as well as their corresponding MODIS spectral bands. As expected, most of the MODIS data products and associated long-term data records can be extended further using VIIRS observations, including various applications, such as disaster monitoring and weather forecasting.
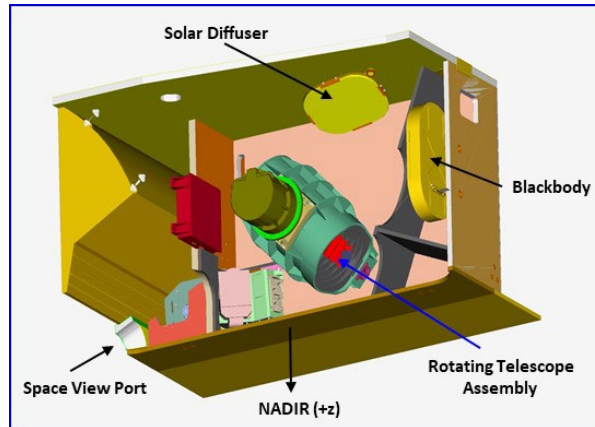
Figure 7.2 VIIRS instrument and its on-board calibrators.

Two major contributors to making the MODIS and VIIRS data extremely valuable are that both sensors are well calibrated, from pre-launch to on-orbit, and that their observations are made concurrently with other Earth-observing sensors operated on the same platforms which maintain constant orbit-equator crossing times. For example, the Aqua spacecraft also includes the Atmospheric Infrared Sounder (AIRS), the Advanced Microwave Scanning Radiometer for EOS (AMSR-E), the Advanced Microwave Sounding Unit (AMSU), the Clouds and the Earth's Radiant Energy System (CERES), and the Humidity Sounder (HSB) working together with the MODIS instrument. Because of this, the long-term data records from MODIS and VIIRS observations, as well as those from other complementary sensors, provide significant contributions to and support for a space-based climate observing system.

Table 7.1 MODIS and VIIRS band spectral ranges and nadir-looking horizontal sampling resolution (HSR)

VIIRS Band	Spectral Range (um)	Nadir HSR (m)	MODIS Band(s)	Range	HSR
DNB	0.500 - 0.900				
M1	0.402 - 0.422	750	8	0.405 - 0.420	1000
M2	0.436 - 0.454	750	9	0.438 - 0.448	1000
M3	0.478 - 0.498	750	3 10	0.459 - 0.479 / 0.483 - 0.493	500 / 1000
M4	0.545 - 0.565	750	4 or 12	0.545 - 0.565 / 0.546 - 0.556	500 / 1000
I1	0.600 - 0.680	375	1	0.620 - 0.670	250
M5	0.662 - 0.682	750	13 or 14	0.662 - 0.672 / 0.673 - 0.683	1000 / 1000
M6	0.739 - 0.754	750	15	0.743 - 0.753	1000
I2	0.846 - 0.885	375	2	0.841 - 0.876	250
M7	0.846 - 0.885	750	16 or 2	0.862 - 0.877 / 0.841 - 0.876	1000 / 250
M8	1.230 - 1.250	750	5	SAME	500
M9	1.371 - 1.386	750	26	1.360 - 1.390	1000
I3	1.580 - 1.640	375	6	1.628 - 1.652	500
M10	1.580 - 1.640	750	6	1.628 - 1.652	500
M11	2.225 - 2.275	750	7	2.105 - 2.155	500
I4	3.550 - 3.930	375	20	3.660 - 3.840	1000
M12	3.660 - 3.840	750	20	SAME	1000
M13	3.973 - 4.128	750	21 or 22	3.929 - 3.989 / 3.929 - 3.989	1000 / 1000
M14	8.400 - 8.700	750	29	SAME	1000
M15	10.263 - 11.263	750	31	10.780 - 11.280	1000
I5	10.500 - 12.400	375	31 or 32	10.780 - 11.280 / 11.770 - 12.270	1000 / 1000
M16	11.538 - 12.488	750	32	11.770 - 12.270	1000

7.2.1   SI Traceability for MODIS and VIIRS – Pre-Launch Calibrations

The MODIS Terra and Aqua and the VIIRS SNPP and JPSS-1 through JPSS-4 instruments will ultimately produce a continuous multispectral Earth remote-sensing data set spanning approximately 38 years. The first step in assuring consistency in that multi-instrument, multi-decadal data set

> Reflected-solar narrowband imagers require meticulous pre-launch calibrations

and, by inference, its ability to be used with data produced by other international remote-sensing instruments depends on the pre-launch calibration and characterization, and consequential post-launch Cal/Val, of those instruments against common, internationally recognized physical scales and consequential post-launch Cal/Val. Ideally, instruments' pre-launch radiometric calibration is accomplished using sources, detectors, and artifacts with calibrations traceable to the physical scales maintained by national measurement laboratories (NMLs) defined by the International System of units, or SI. For MODIS and VIIRS, calibrations are traceable to standards maintained by the National Institute of Standards and Technology (NIST), the NML for the United States. For MODIS and VIIRS instruments currently on-orbit and the VIIRS JPSS-2 instrument being readied for launch, a series of radiometric tests were performed in the laboratory to determine the coefficients used to convert the digital numbers produced by the instruments to radiance and to characterize overall instrument performance. These tests were performed in ambient and thermal vacuum conditions to simulate the

anticipated range of on-orbit operating conditions at the subsystem and system levels. These tests will also be performed on the VIIRS JPSS-3 and JPSS-4 instruments.

Extensive efforts were made during MODIS and VIIRS pre-launch calibration and characterization under various operating conditions to evaluate and verify their performance compared to the specified sensor design requirements, including calibration traceability and uncertainty requirements [197], [198]. Key sensor performance parameters derived from pre-launch testing include but are not limited to the following:

- Signal-to-noise ratio (SNR)
- Dynamic range
- Nonlinearity
- Calibration accuracy and stability
- Relative spectral response (RSR)
- Polarization sensitivity

At the full instrument system level, prelaunch radiometric tests include the determination of instrument spectral radiance responsivity, dynamic range, linearity, offsets, stability, and signal-to-noise (or noise-equivalent radiance) as a function of instrument on-orbit operating temperature, scan angle relative responsivity, and polarization sensitivity. For these MODIS and VIIRS radiometric tests in the visible through shortwave infrared, the Spherical Integrating Source-100 (SIS-100) is used (Figure 7.3). This is a 100-cm diameter integrating sphere source equipped with multiple quartz tungsten halogen filament lamps of various wattages and a radiance monitor. Depending on the number and wattage of illuminated lamps, the uniform radiance output of the sphere covers a radiance range encompassing the brightest to dimmest scenes which will be viewed by MODIS and VIIRS on-orbit.

The radiance calibration uncertainty of the SIS-100 for use in calibrating the moderate resolution bands of MODIS and VIIRS and the imaging bands of VIIRS is ±5.0% (k=1) for all lamp operating configurations with exception of the two lowest radiance levels below 412 nm and above 2100 nm. For the VIIRS Day Night Band (DNB) calibration, the SIS-100 is equipped with a low-radiance module containing two low-wattage lamps. The radiance uncertainty for the DNB SIS-100 configuration is also ±5.0% (k=1) for the 500 nm to 900 nm DNB operating range. The calibration of the SIS-100 is performed in the laboratory using an Analytical Spectral Devices (ASD) FieldSpec scanning spectroradiometer to transfer the measured radiance from a lamp-illuminated Spectralon diffuser to the SIS-100.

The resulting calibration uncertainty of this approach has been fully quantified and validated using stable transfer radiometers to be better than ±3.0% (k=1) [199]. SI traceability of this absolute spectral radiance calibration of the SIS-100 to NIST is achieved using a NIST-traceable irradiance standard lamp to illuminate the Spectralon panel with BRDF measured and validated against laboratory standard diffusers measured by NIST. The absolute radiance calibrated SIS-100 is used in combination with measurements of the relative spectral response (RSR) of the MODIS and VIIRS bands to determine the band-averaged absolute spectral radiance responsivity (ASR) of the bands of these instruments. Figure 7.3 and Figure 7.4 show the traceability of the reflected solar pre-launch gain and on-orbit reflectance/radiance calibrations for both MODIS and VIIRS.
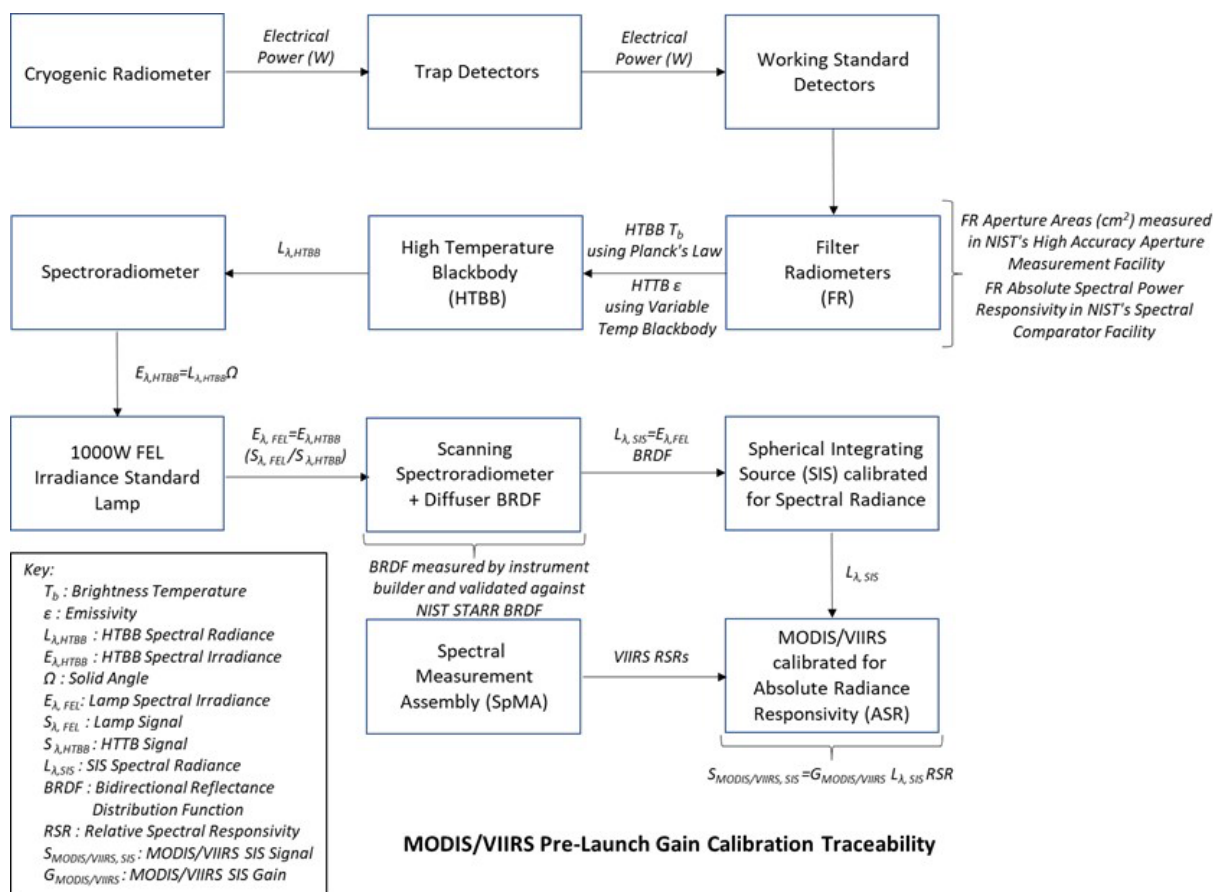
Figure 7.3 MODIS and VIIRS pre-launch gain calibration traceability

In addition to the SIS-100 radiance calibrations, the VIIRS instrument testing has incorporated a full-aperture spectral radiance calibration approach using intensity-stabilized, tuneable monochromatic lasers. In this approach, the output of the lasers is input to an integrating sphere equipped with trap reference detectors. The VIIRS instruments view the monochromatic output of the sphere while recording the signal from the reference detector as the laser is tuned across the VIIRS bands. Using this system, the relative spectral responsivity (RSR) and ASR are determined by sequentially stepping the laser across all VIIRS bands while recording the simultaneous signals from the reference detectors and from VIIRS. The resulting monochromatic ASRs can be used to determine the responses of the instrument bands to broadband radiance sources directly, eliminating the need for calibrated broadband light sources such as the SIS-100. SI traceability of this absolute spectral radiance calibration is accomplished through NIST measurements of the ASRs of the trap reference detectors using their Spectral Irradiance and Radiance Responsivity Calibrations using Uniform Sources (SIRCUS) laser system. To date, the ASRs produced by this approach have not been used in the production of the VIIRS sensor data record (SDR). However, when implemented, this promising, new, full-aperture, laser-based calibration approach has the capability to lower the absolute radiometric calibration uncertainty of VIIRS and other remote sensing instruments by an order of magnitude [200].

The tuneable, intensity-stabilized laser approach described above moves SI traceability of radiometric calibration from the SIS-100 source-based system to a reference trap detector-based system while producing lower overall calibration uncertainties. For the calibration of absolute spectral radiance responsivities of remote-sensing instruments, systems incorporating supercontinuum (i.e. white light) laser sources with laser-line tuneable filters (LLTF) are being developed [201], [202]. In these systems, the intensity-stabilized, monochromatic output of a tuneable supercontinuum laser with LLTF is input

to an integrating sphere whose output is monitored using trap reference detectors calibrated for absolute spectral radiance responsivity. In one approach, the satellite instrument under test directly views the monitored, stabilized, tuneable output from the integrating sphere in a similar fashion to that used in the tuneable laser-based approach described above [202]. In a second approach, a stable, fully-characterized transfer standard spectrometer views the monitored, stabilized, tuneable sphere output and transfers that radiance calibration scale to a lamp-based calibration source such as the SIS-100 [203]. In both approaches, SI traceability of absolute radiance calibration is achieved through calibration of the sphere trap reference detectors against absolute cryogenic radiometers located at national measurement laboratories. When fully commissioned, these detector-based approaches employing tuneable supercontinuum lasers show the potential of realizing absolute calibration uncertainties approximately 3 times lower than those using conventional source-based approaches (e.g. SIS-100). These approaches also show promise of lowering overall required calibration times.
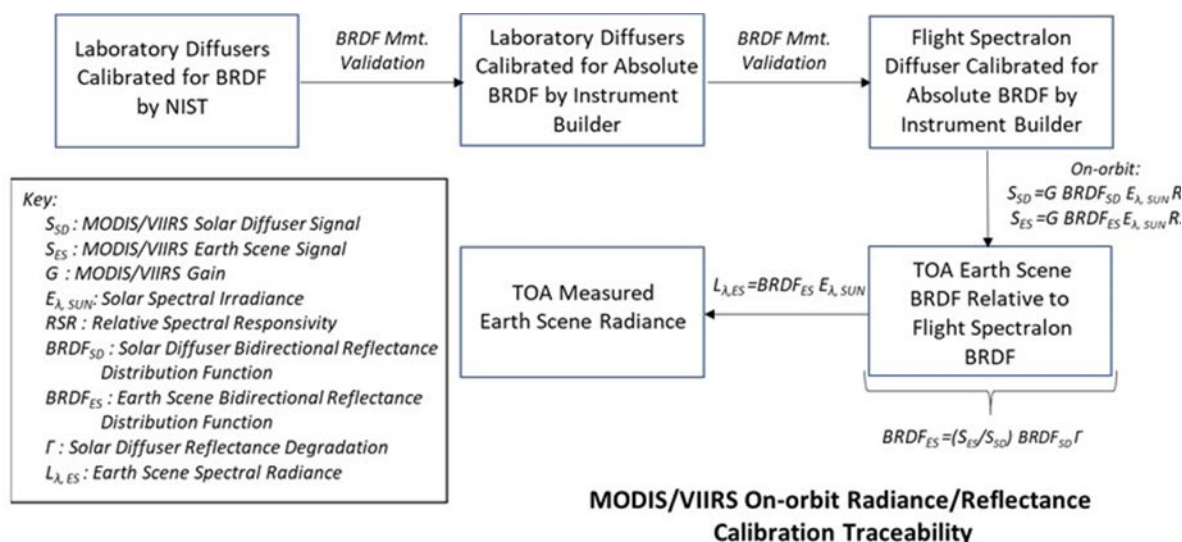

Figure 7.4 MODIS and VIIRS on-orbit reflective solar reflectance/radiance calibration traceability

MODIS and VIIRS calibration traceability was established through extensive pre-launch testing with measurements referenced to the national and/or international standards. Their calibration accuracy is maintained throughout entire missions. In addition to similar pre-launch testing, both instruments have nearly identical on-orbit calibration capability through the use of a set of on-board calibrators that include a solar diffuser (SD) and a blackbody (BB).

Special measurement assemblies were used for sensor RSR and polarization sensitivity characterization. Both MODIS and VIIRS are whisk-broom scanning radiometers and collect the Earth view data over a wide range of scan angles. Since on-orbit calibration is typically performed at a fixed scan angle. T, the sensor's response versus scan angle (RVS), is therefore a key calibration parameter that needs to be accurately determined pre-launch. For the same reason, the sensor polarization sensitivity characterization also needs to be performed at different scan angles.

7.2.2   SI Traceability for MODIS and VIIRS – On-Orbit Calibrations

Specified calibration requirements at typical scenes are 2% in reflectance and 5% for radiance for both MODIS and VIIRS RSB. Although the traceability chain to SI standards of some aspects could be weakened by the change in operating conditions associated with launch, in reality it is the uncertainty level that can be achieved that is affected, their on-orbit calibration is traceable to the BRDF of the on-board solar diffuser, shown in Figure 7.5. The SD BRDF was characterized pre-launch using reference samples that are traceable to NIST reflectance reference samples or measured directly and then

validated with the NIST traceable reference samples. An assessment of MODIS RSB on-orbit calibration uncertainty and its key contributors, such as SD BRDF uncertainty, SD on-orbit degradation, and detector SNR, has been made and documented by the MODIS Characterization Support Team (MCST) [28]. Figure 7.6 shows the on-orbit calibration uncertainties in reflectance (k=1) for Aqua MODIS RSB at nadir Angle of Incidence (AOI) and typical radiance levels. Most bands continue to meet the 2% calibration requirement in reflectance (k=1).

On-orbit calibrations track *relative* changes in sensitivity

On-orbit change in SD BRDF is tracked by an on-board solar diffuser stability monitor (SDSM). For MODIS, the SD/SDSM operation is scheduled on a regular basis. An SD door is used to prevent the SD from unnecessary solar exposure when no SD calibration is scheduled. The VIIRS design did not include a MODIS-like SD door. As a result, its SD calibration is performed each orbit and the VIIRS SDSM operations are scheduled more frequently than MODIS. Illustrated in Figure 7.7 is the S-NPP VIIRS SD on-orbit degradation derived from its SDSM observations. MODIS and VIIRS RSB use the same calibration strategies that also include regularly scheduled lunar observations. Lunar observations of each instrument are made at the same lunar phase angles through its SV port and via spacecraft roll manoeuvres. In order to ensure that high-quality data products can be continuously generated, calibration parameters, or look-up tables (LUTs), are updated on an as needed basis to account for on-orbit changes in sensor responses.

Figure 7.5 MODIS on-board solar diffuser (SD)

MODIS is also equipped with an on-board spectral-radiometric calibration assembly (SRCA). It can be used to track and characterize the RSB spectral and spatial performance [204], [205]. The VIIRS design did not include the SRCA. Because of this, lunar observations are used for VIIRS spatial characterization. This is accomplished using an approach developed and validated based on MODIS SRCA and lunar observations [206], [207].
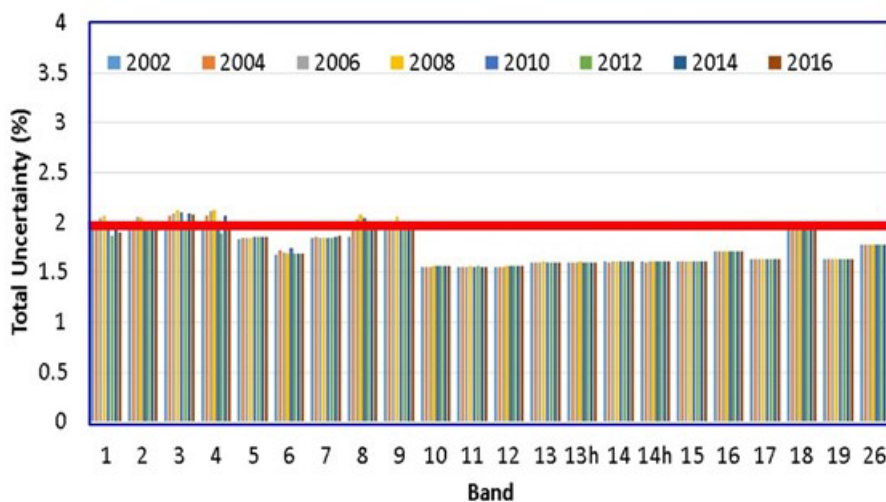
Figure 7.6 Aqua MODIS RSB calibration uncertainty at typical radiance and nadir (horizontal red line: calibration requirement).
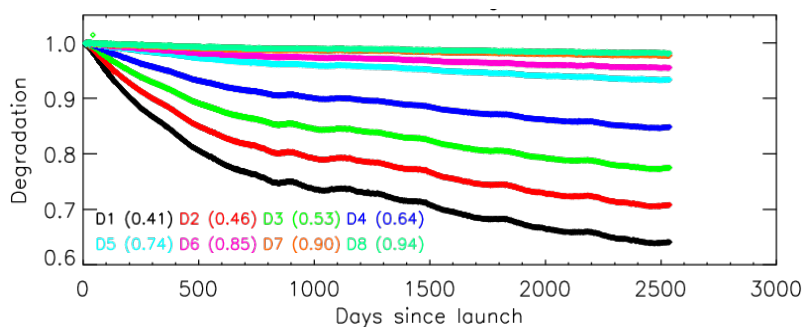

Figure 7.7 S-NPP VIIRS solar diffuser on-orbit degradation at wavelengths from 0.41 to 0.94 μm.

For MODIS, on-orbit changes in the RSB RVS are monitored and determined using the SD and lunar observations, coupled with the Earth view (EV) trends at different AOIs [208]. In general, large changes are observed in the bands at short wavelengths. For Terra MODIS (launched in 1999), the EV observations have also shown that its polarization sensitivity has experienced large on-orbit changes for a few short wavelength spectral bands and at the large AOIs, especially after 2007. To date, no changes in polarization sensitivity have been seen in Aqua MODIS. On-orbit changes in the polarization sensitivity, if not accurately characterized and corrected, could significantly increase the radiometric calibration uncertainty and impact the science data product quality, especially for the ocean colour products. Because of this, the NASA Ocean Biology Processing Group (OBPG) has formulated and implemented an approach to derive the Terra MODIS polarization correction parameters using SeaWiFS and Aqua MODIS as a combined reference and, therefore, produced high-quality ocean colour products from Terra MODIS observations [209], [210]. An alternative approach has been developed and applied by the MCST to derive the polarization correction parameters using from desert observations using top-of-atmosphere (TOA) reflectances at multiple AOIs over the select desert sites [211].

For S-NPP and N-20 VIIRS, no noticeable changes in the RSB RVS and polarization sensitivity have been observed since launch. The polarization correction parameters have remained the same as those derived from pre-launch measurements. In addition to calibration accuracy and data product quality, the correction for the polarization sensitivity, which is scene-dependent, needs to be implemented in order to achieve highly accurate calibration inter-comparison among sensors [212].

7.3 Lunar Spectral Irradiance

The Moon is well known to be an exceptionally stable diffuse reflector of sunlight, and this property has been exploited to develop a radiometric reference standard from moonlight at reflected solar wavelengths. Using the Moon as a reference can provide the sensor calibration stability and inter-consistency needed by a space-based Climate Observing System to separate actual changes in terrestrial observables from drifts in instrument sensitivity. The subtle signatures of climate change can take decades to detect, longer than the expected lifetimes of most Earth-observing satellites. The capabilities offered by lunar calibration can support on-orbit calibration requirements for climate measurements, but this will require further development of the lunar reference and refining lunar radiometry techniques.

> **The Moon provides an on-orbit calibration source having similar radiance levels to Earth scenes**

Having no atmosphere, the Moon has been subjected to eons of space weathering that has pulverized the lunar regolith, stabilizing the reflectance and nearly completely erasing all spectral structure of the surface constituents [213]. This inherent photometric stability leads to several important capabilities that lunar calibration can provide: (1) a common target for high-precision sensor inter-calibration; (2) an identical reference for matching calibrations of non-overlapping sensors, e.g. to bridge gaps in climate measurements; (3) updating historical instrument calibrations using archived image data that include lunar views, such as from geostationary meteorological imagers; and (4) a reliable standard to stabilize sensors' radiometric response over satellite lifetimes, meeting a critical requirement for climate measurements.

Studies using the Moon as a radiometric reference have concluded that the most useful quantity for sensor calibration is the spatially-integrated spectral irradiance [36]. The lunar irradiance varies substantially with the familiar change of phase, and the Moon's non-Lambertian reflectance properties mean the irradiance at 50% illumination is about one tenth that of the full Moon. The observed irradiance also varies with the inverse square of the Sun-Moon and Moon-observer distances, and with the particular lunar hemispheres that are illuminated and viewed, known as the lunar librations. To render this continuously changing quantity into a reference standard requires the capability to predict it for the specific circumstances of a sensor's lunar measurements, i.e., the Sun-Moon-observer geometry. This predictive capability takes the form of an analytic model that can be queried for any observational conditions of lunar views, thus the reference is manifest as the model representation.

Currently the most commonly used lunar reference is the Robotic Lunar Observatory (ROLO) model, developed at the United States Geological Survey (USGS) under NASA sponsorship [36]. The ROLO lunar calibration system provides the lunar spectral irradiance corresponding to Moon views acquired by an instrument for the time and location of the observations and with the spectral content of the sensor's bands. The ROLO model has an analytic form that is a function of only the phase angle and the lunar librations, with the latter specified as the sub-solar and sub-observer selenographic longitude and latitude. The model was developed empirically from an extensive set of lunar measurements derived from images of the Moon acquired by the ground-based ROLO telescopes over a period of more than 8 years. ROLO operations included numerous star observations each night, used primarily to derive atmospheric corrections for the lunar data, but also to specify the responsivity of the telescope cameras using measurements of the star Vega. This calibration also specifies the absolute scale of the ROLO model. The atmospheric correction and the Vega calibration are the two largest error sources in the ROLO model and the USGS lunar calibration system.

To utilize the lunar irradiance as a calibration reference, imaging sensors must capture the complete lunar disk. The irradiance E is measured from spatial integration of radiance pixels L_i in Equation 2, where Ω is the pixel IFOV, η is the oversampling factor, and the sum covers all pixels i on the Moon

disk image. Achieving high accuracy for such measurements from images requires careful evaluation of all the parameters in this equation.

$$E_{\text{meas}} = \Omega/\eta \sum_{i=1}^{N} L_i$$

The summation involves net radiance, and the space-viewing regions surrounding the disk can be used effectively to quantify the zero-radiance background level. Line-scanning sensors typically acquire complete Moon images as concatenations of multiple scans, with some amount of oversampling. Processing these scanned images into lunar irradiances requires precise evaluation of the actual oversampling of the Moon disk, which can differ significantly from nominal oversampling factors calculated from slew and sampling rates. Incomplete accounting for actual disk oversampling can lead to biases in lunar irradiance measurements taken with line scanning imagers. Comparisons of these sensors' lunar measurements to their corresponding ROLO reference values often exhibit differences that exceed the known uncertainties in both the sensor radiometric calibrations and the lunar model outputs.

The lunar irradiances generated by the ROLO model have uncertainties that are generally considered too large to use this reference for absolute calibration of space-based sensors. But these uncertainties reflect a limitation of the current model, whereas the Moon's brightness potentially can be known to the accuracy limits achievable with radiometry conducted outside the lab. The capacity for relative precision is far greater in terms of consistency of a lunar model's outputs over its valid geometric range, particularly when instruments' Moon observations are constrained to small ranges of phase angle and/or narrow spectral regions.

But reaching the full potential of the Moon as a radiometric reference requires collecting a new set of lunar characterization measurements to use as a basis for modelling. Such a collection must span the practical ranges of phase angle and lunar librations viewable from low Earth orbit with sufficient density of the acquisitions to give an adequate radiometric and geometric specification of the lunar irradiance. Because the phase and libration geometries available for observations from LEO are constrained by the Moon's tilted orbit, a measurement campaign of three to five years minimum duration is required for representative sampling. Other important considerations include traceability to primary optical power standards and taking at least some measurements from above the atmosphere to eliminate (or greatly reduce) atmospheric corrections.

A precise spectral specification of the lunar irradiance will require spectrally resolved measurements and modelling. The variegated lunar surface albedo corresponds to a diversity of lunar terrains, all having distinct spectral reflectance signatures [214], [215]. Moon observations at different phase angles and libration states sample different distributions of terrains, and thus have different spectral compositions. Advances in lunar irradiance models are required to capture these composite spectral contents.

The slightly polarized nature of moonlight will impact lunar irradiance measurements taken by polarization-sensitive instruments. To achieve the highest accuracy lunar calibrations for these sensors requires developing a moonlight polarization model, separate from the radiometric one. The required basis dataset for this supplemental model will consist of complete-disk polarization measurements of the Moon that are spectrally resolved and span the full valid range of phase angles.

Efforts are currently underway at several institutions worldwide to acquire new lunar radiometric measurements that eventually will enable redeveloping the lunar calibration reference with improved absolute accuracy and SI traceability. Three currently active NASA-sponsored projects have high-

accuracy lunar irradiance measurements as objectives: air-LUSI, CLARREO Pathfinder, and ARCSTONE.

The airborne Lunar Spectral Irradiance (air-LUSI) project has the goal of acquiring spectrally resolved irradiance measurements of the Moon with sub-percent absolute accuracy from the NASA ER-2 aircraft flying at 70,000 feet (21.6 km) above sea level. The instrument is a variant of the NIST ground-based LUSI system [216], which measures irradiance directly using a non-imaging telescope with a small integrating sphere at the focal point, feeding a field spectrograph via a fibre-optic cable. Spectral sampling is about 0.8 nm over the wavelength range 300-1100 nm. The flight acquisition system employs an autonomous robotic tracking subsystem to lock onto the Moon disk and compensate for aircraft motion during flight. Active thermal controls are installed on critical optical components. A series of technology demonstration flights were successfully conducted in 12-17 November 2019. Data analysis is in progress.
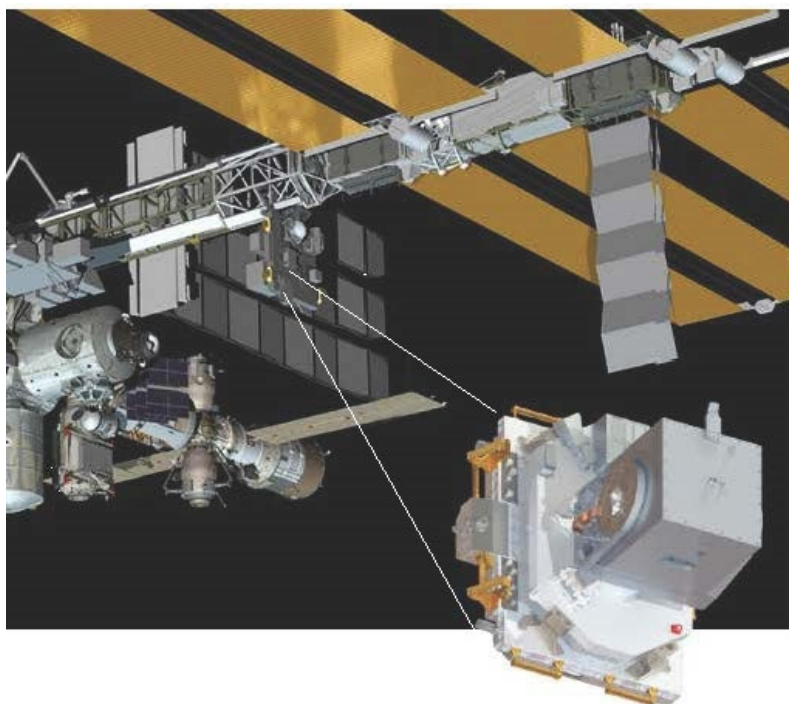

Figure 7.8: CLARREO Pathfinder on ISS

The Climate Absolute Radiance and Refractivity Observatory (CLARREO) Pathfinder (CPF) project has mission objectives to demonstrate measurement technologies for Earth reflectance with unprecedented absolute accuracy, ≤0.3% (k=1), and for reference inter-calibration of other satellite sensors. The CPF's reflected solar instrument, the HyperSpectral Imager for Climate Science (HySICS, [38]), is to be deployed on the International Space Station in the 2023 timeframe. Nominal CPF operations specify nadir-view spectral imaging in pushbroom mode from the ISS Express Logistics Carrier 1 (ELC-1) Site 3, as illustrated in Figure 7.8. Moon observations by CPF are planned as acquisitions of opportunity. Because the CPF RS scan platform has a 2-axis gimbal, across-slit scans over the Moon will trace a curved path, leading to differential oversampling of the lunar disk. To process these spectral images into lunar irradiance measurements will require precise knowledge of pointing to the Moon, the gimbal positions, and sampling and slew rates, all referenced to inertial space. Numerous Moon viewing opportunities are anticipated during the nominal one year of CPF on-orbit operations, providing the potential for broad sampling of the phase and libration space.
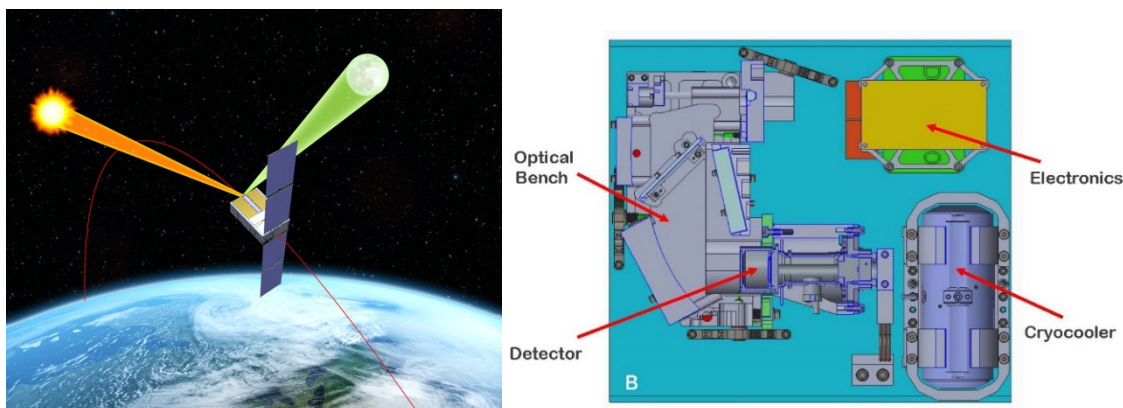
Figure 7.9(A) ARCSTONE measurement concept: acquiring lunar and solar irradiance from low Earth orbit (spacecraft image courtesy of Blue Canyon Technologies) (B) spectrometer instrument layout, sized to fit into a 6U CubeSat form factor.

ARCSTONE (not an acronym) is a CubeSat mission in development with the objective to measure the lunar spectral reflectance with an accuracy ≤0.5% (k=1) absolute [95]. The measurement concept is to radiometrically sample the whole disk of the Moon and the Sun through the same optical path, with no change of optics. The known solar spectral irradiance will be used to calibrate the lunar measurements to reflectance and transfer SI traceability. The ARCSTONE instrument is a compact spectrometer spanning the wavelength range 350-2300 nm with 4 nm to 8 nm spectral sampling. Figure 7.9 shows the reflectance acquisition concept and the spectrometer layout, fitting into a 6U form factor. Lunar measurements will be acquired every 12 hours to obtain adequate phase and libration coverage and will span phase angles up to 135°, providing the ability to extend lunar calibration capabilities to 3 weeks per month. Development of ARCSTONE is currently on track for potential spaceflight demonstration in the 2024 timeframe.

Calibrated lunar irradiances can enable intercalibrations between non-overlapping Earth-viewing sensors

The outcomes of these three activities can be applied immediately to reduce uncertainties in the current lunar calibration system. Redeveloping an absolute lunar reference with SI-traceability and minimum achievable uncertainties will require collecting multiple years of high-accuracy Moon characterization measurements to use as a basis for advanced modelling. This is essential to fully realize the potential offered by lunar calibration, but also critical are detailed examinations of irradiance measurements from Moon images, particularly the built-up images acquired using line-scanning sensors.

7.4   Vicarious Surface Sites

7.4.1   Introduction and Definition

Vicarious calibration of optical remote sensing satellite sensors involves using methodologies to perform absolute radiometric calibration and long-term trending/stability analysis using information obtained remotely by the satellite sensor. In the broadest sense, these include using sources of radiance such as the Earth, the Moon, and stars. However, for purposes of this paper, the focus will be on those methods that use the Earth only. (Lunar-based calibration is covered in §7.3.)

Earth-based vicarious calibration methods can generally be divided into two approaches. The first, often referred to as the "surface reflectance" method, involves in situ measurements of the

Ground sites provide another means of inter-comparing Earth-viewing sensors

upwelling radiance from the Earth and characterization of the atmosphere at the time the satellite is observing the calibration site [217]. These direct, ground-based measurements from the surface are used to predict the radiance, or apparent reflectance, that the satellite would measure during its observation of the site. This value is then used to generate calibration coefficients for the sensor.

The second major approach uses sites on the Earth's surface that are essentially unchanging over time [218]. These are commonly called Pseudo Invariant Calibration Sites, or PICS. The idea here is that each observation of the site should produce the same response in the sensor over time. Thus, PICS were initially used as a measure of satellite stability over time. However, the use of PICS has been extended to include absolute radiometric calibration through the use of a reference spaceborne radiometer. Details on both methods of vicarious calibrations follow, along with a discussion of limitations, uncertainties, and benefits of an SI-traceable spaceborne radiometer.

7.4.2   Methodologies and Uncertainties

Vicarious calibration using the surface reflectance method is dependent on an accurate measurement of the upwelling radiance from the surface of the calibration target or site [219]–[221]. This is generally measured with either a portable spectrometer carried by an operator (as in Figure 7.10) or a fixed spectrometer that stares at the same location on the ground continuously. These devices can be multispectral or hyperspectral in nature and can cover the electromagnetic spectrum from approximately 400 – 2400 nm. In practice, measurements are often obtained in a simultaneous, or near simultaneous, fashion of a known reflectance panel used for calibration. This allows the radiance measurement to be quickly converted to a reflectance measurement. These measurements are made at a time as close to the satellite observation of the site as possible.

Measurements of the atmospheric transmittance are also acquired using a Sun-photometer simultaneously with the surface measurements Figure 7.11. This is normally a multispectral device that tracks the Sun and measures its downwelling radiance at several spectral channels. These measurements are used as inputs to a radiative transfer code and are needed to characterize the optical properties of the atmosphere such as atmospheric optical depth, water vapor absorption, and ozone absorption. Additional meteorological inputs, in particular temperature and pressure, are also used as part of the development of an atmospheric model at the time of a satellite overpass.

Figure 7.10 Surface reflectance measurements with a handheld spectrometer

Figure 7.11 Cimel Sun photometer and met station

All of the above data are used as inputs to a radiative transfer code that, once optimized for the measurements, makes a hyperspectral estimate of either the top-of-atmosphere radiance or apparent reflectance. This estimate that is then integrated over the spectral bandpasses of the satellite sensor to predict what the satellite would observe. Lastly, the satellite image is obtained and pixels from where the surface measurements were made are identified. Using the mean value of the corresponding pixels, either a calibration gain (such as radiance/digital number or reflectance/digital number) can be obtained, or the estimated at-sensor radiance/reflectance can be compared to the current sensor calibration to determine if an update is needed for the calibration of the sensor.

> **Site selections must balance several important criteria**

As can be surmised from the basic methodologies, a key aspect for success of the surface reflectance method is selection of an appropriate calibration site or target. In general, for high signal-to-noise ratio (SNR), a bright, highly reflective, site or target is desired. For high spatial resolution sensors, these can be developed from manufactured materials. For coarser spatial resolution sensors, natural sites are used. Very often these are desert sites that are quite bright at all wavelengths. Perhaps the most famous of these is the Railroad Valley, Nevada, USA site [222]. The major advantage of such sites is the potential for minimizing uncertainties in the methodology because of high SNR. They also tend to be of large extent and are therefore useful for coarser spatial resolution sensors. Drawbacks are that they are often in places with poor accessibility and extreme environments, making the in-situ characterizations difficult.

One criticism of deserts sites is that they do not represent areas of the Earth's surface that are most often studied. Thus, calibration using vegetated sites has also been developed. Difficulties with these sites are low SNR since the targets are relatively dark, larger variability both spatially and temporally, and atmospheres that are more difficult to characterize than for desert sites. However, they are often much more accessible than desert sites. Combined together, bright desert sites and darker vegetative sites can provide two calibration points on the dynamic range of the sensor and represent two relatively independent methods.

In the past few years, automated monitoring of these calibration sites has been developed. The best-known approach, CEOS RadCalNet (https://radcalnet.org), has developed automated monitoring capabilities at several locations including Railroad Valley (USA), La Crau (France), Baotou (China), and Gobabeb (Namibia). RadCalNet, not only provides automation but also follows a rigorous process of assessing and documenting uncertainties and methods and is one of an increasing set of measurements that are being called Fiducial Reference Measurements (FRM) to make clear the SI-Traceable rigour https://earth.esa.int/web/sppa/activities/frm [90]. This approach has a tremendous advantage of not requiring people on site during satellite observations. However, at the time of this writing, uncertainties associated with the automated approach are somewhat larger [223].

The uncertainties associated with the surface reflectance method are summarized in Table 7.2 [224]. While actual uncertainties are dependent on the target/site and details of the methodology, these data are quite representative of the current capability.

Table 7.2 Uncertainties of the Surface-Reflectance Vicarious Calibration Method in the Visible Spectral Range

Source of uncertainty	Source	TOA spectral radiance
Ground reflectance measurement	—	2.1%
Reference panel calibration (BRF)	1.8%	—
Site measurement errors	1.0%	—
Optical depth measurements	—	$<0.1\%$
Extinction optical depth	0.5%	—
Absorption computations	—	—
Ozone Monitoring Instrument (OMI)	3.0%	—
Column water vapor	5.0%	—
Choice of aerosol complex index	100%	0.5%
Choice of aerosol size distribution	—	0.3%
Ångström's exponent	0.3%	—
Non-Lambertian surface	10%	—
Others	—	—
Nonpolarization vs. polarization	—	0.1%
Inherent accuracy of MODTRAN 5	—	2.0%
Uncertainty in SZA	—	0.2%
Total Uncertainty RSS	—	**3.0%**

The table clearly shows that the largest source of uncertainty is the measurement of the surface reflectance at 2.1%. Reasons for this include the use of differing instruments, differing operators, and repeatability of technique [225]. The second largest source of error is the radiative transfer code that is used. Although several codes are in use, uncertainties tend to be around 2% for all. It should also be emphasized that the overall uncertainty estimate of 3% is a 'best case' scenario. That is, there are no clouds present, the atmosphere is relatively clear, and the site is in good shape (no recent large moisture or wind events, or anthropomorphic change).

PICS-based calibration was initiated to monitor the long-term stability of an optical satellite sensor. The basic concept is that there are locations on the Earth's surface where the surface does not change as a function of time. Obviously, this cannot be precisely true, but variations can hopefully be small enough to be of value for satellite calibration. This normally requires very little vegetation (due to its inherent variability) be present, thus PICS are almost always in desert regions. The most common location is the Sahara Desert, but PICS have been identified worldwide [226]. In addition, sites have also been identified in polar regions such as Antarctica and Greenland.

Major factors that affect the precision of using PICS for trending the stability of satellites include illumination and viewing geometry and atmospheric changes [227]. Even though these sites are quite stable with respect to time, their reflectance properties do change with respect to Sun location and viewing angle of the satellite. Thus, a bidirectional reflectance distribution function (BRDF) model must be developed [228]. With respect to the atmosphere, a characterization based on meteorological observations or Sun photometer measurements is nearly always impossible due to lack of instrumentation close enough to the site to actually be representative of site conditions. As a result, a correction for it is not developed and the atmosphere is often considered as simply an additional source of uncertainty. Precision of these methods is currently in the 2-3% range.

Absolute calibration of optical satellite sensors using PICS has also been developed [229], [230]. These models are often based on the observation of the site(s) by one or more satellite instruments that is used as a calibrated radiometer. An example is MODIS Terra. The accuracy of this method is fundamentally limited by the accuracy of the reference radiometer. Because a hyperspectral model is needed to make this useful for a variety of sensors, inclusion of a hyperspectral satellite sensor is also a requirement— EO-1 Hyperion has been used for this purpose.

A PICS absolute calibration model is specific for a particular site and consists of an absolute scaling component based on a satellite used as a reference radiometer, a spectral model of the site based on an instrument such as SCIAMACHY or Hyperion, a BRDF model based on multi-angular and multi-year observations by a sensor such as MODIS or Landsat, and occasionally an atmospheric model to compensate for annual or other predictable variations. The model can then be applied to any optical sensor with a spatial footprint that allows at least several pixels to fit within the calibration site.

Figure 7.12 shows the results of using an absolute PICS-based calibration for Landsat 8 OLI using six different sites in the Sahara Desert. Since Landsat 8's calibration is well known (uncertainty of 3%, k=1), these data can be thought of as a validation of the PICS absolute calibration model [231]. Results indicate agreement of 3% or better at several sites, with the Niger sites showing somewhat worse agreement.

An uncertainty estimate for this method of calibration is shown in Table 7.3 [231]. This estimate spans all six sites from Figure 7.12, so the uncertainties extend across a range of values based on site and spectral coverage. The largest contributors are the 'K-scale factor' which is the uncertainty from the reference satellite radiometer, followed by the uncertainty in the spectral portion of the model. Both of these are due to using other spaceborne instruments to build the model and, therefore, include the uncertainties of their calibration as well as the measurement uncertainties. Site variation is a fundamental limitation to the accuracy of this approach. 'Satellite Calibration' in the table refers to the uncertainty of the instrument being calibrated. The upper end of the total uncertainty is driven by the poorer performance of the Niger sites which may be due to limited available observations.
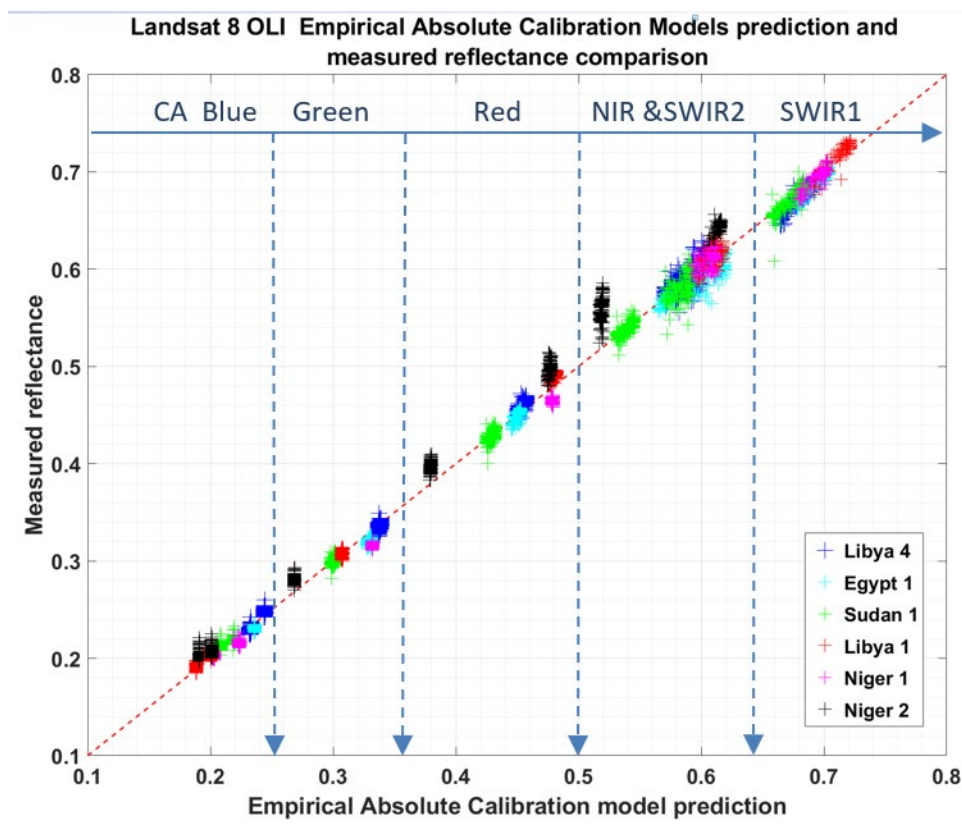
Figure 7.12 Examples of Absolute PICS-based Model results using Landsat 8 OLI for validation.

Table 7.3 Uncertainties associated with absolute PICS-based calibration.

Uncertainty Sources	% Uncertainty	Remarks
K-scale Factor	0.1-8.7%	For all Bands & all Sites
Hyperion Spectra	1.3-4.8%	
SZA	0.1%	
VZA	0.5%	
Site Variation	1-3%	
Satellite Calibration	3-5%	S2A, S2B, L7 = 5% L8 = 3%
Total Uncertainty	1-9%	For all Bands & all Sites

7.4.3   Current Limitations and Value of an SI-Traceable Radiometer

Fundamental limitations for the surface reflectance method of vicarious calibration begins with the surface reflectance measurement itself [225]. This is a fundamental limitation and significant improvements are not envisioned in the near future. Spectral solar irradiance models are also used with this approach and currently have an uncertainty of approximately 2% at some wavelengths of interest. Improvements in this area are expected as our spaceborne solar measurements progress. The third major sources of uncertainty are the radiative transfer codes that are used. Progress will continue in this area and small improvements are likely.

For PICS-based absolute calibration, the fundamental limiting factor is the uncertainty associated with the reference radiometer. Availability of regular measurements of PICS from an SI-traceable reference radiometer would fundamentally reduce the largest uncertainty in this methodology. If this radiometer were hyperspectral in nature, it would address the second largest uncertainty in the method. Thus, the overall uncertainty using absolute PICS calibration would be reduced to essentially the uncertainty associated with the site itself; so potential exists to reduce the uncertainty of this method to the 1 % - 3 % range given an SI-traceable, on-orbit reference.

7.5   Polarimetry – Solar Radiation Polarization Distribution Models for the SI-Traceable Space-based Climate Observing System

Reflected solar radiance from the Earth-atmosphere system can be significantly polarized by the Earth's surface and by atmospheric components such as air molecules and aerosols. Radiance measurements can be adversely affected by the state of polarization of the

> **Instrument sensitivity to polarization affects radiometric accuracy from potentially polarized scenes**

observed light if the radiometric sensor itself is sensitive to polarization. To enable highly accurate measurements for the SI-Traceable Space-based Climate Observing System, the polarization state of the light must be known with sufficient accuracy so that the polarization-induced measurement errors could be corrected if the measurement instrument has polarization dependence. For example, to use the highly-accurate data from the Climate Absolute Radiance and Refractivity Observatory (CLARREO) Pathfinder mission [6] to calibrate imagers like MODIS [232] or VIIRS as well as geostationary imagers, the polarization state of the reflected solar light must be known with sufficient accuracy, e.g. better than 5% rms. Empirical polarization distribution models (PDMs) [233], [234] based on the PARASOL data [235] can be used to correct radiometric biases in an imager's measurements [79]. However, the incidence and viewing geometries of pertinent scene types of these empirical PDMs are limited by the specific sensors and their satellites' orbits and equator-crossing times, etc., which may not always be applicable to other imagers on different satellites. Currently, PARASOL is the only polarimetric sensor in-orbit that is suitable for empirical PDM development. However, since PARASOL is in the A-train Sun-synchronous orbit and its CCD array has no cross-track scan function, its solar zenith angle (SZA) and viewing angles are limited. Although this may not be a problem for VIIRS, since it is also in the A-train Sun-synchronous orbit with an equator-crossing time of 1:30 pm, for imagers not in this orbit, such as geostationary ones, the empirical PDMs based on the PARASOL polarimetric data will be insufficient to cover all viewing and solar geometries. Also, as a pilot mission for the full CLARREO, the HySICS on the CLARREO Pathfinder is designed to measure spectra from 350 to 2300 nm with a spectral sampling of 3 nm (Science and Mission Requirements Document, Requirement #RS.21000 and RS.21015 [236]), providing the potential to inter-calibrate spaceborne sensors at nearly all of the solar wavelengths. Thus, the PDMs for the inter-calibration applications should be made over the broad solar spectra, and this cannot be achieved by using the available polarimetric measurements from PARASOL at only its three wavelengths (i.e. 490, 670, and 865 nm).

Sensitivity to polarization of imaging radiometers such as MODIS and VIIRS is obtained during instrument characterization before launch and expressed in a polarization factor (diattenuation). These factors are corrections of the baseline (unpolarized) gain and depend on the instrument band, scan angle, and angle of polarization [237]. Taking account of this framework, the PDMs are developed in a consistent manner, providing information on the degree of polarization (DOP) and the angle of linear polarization (AOLP) of the reflected solar radiation at the top-of-atmosphere (TOA). Modeling the polarization of the reflected light from the Earth-atmosphere system must comprehensively consider all these issues, as well as detailed physics in radiative transfer. For this purpose, the polarized solar radiation from the ocean-atmosphere system is studied with an adding-doubling radiative transfer model (ADRTM). The Cox-and-Munk ocean-wave slope-distribution model [238], [239] is used in calculation of the reflection matrix of a wind-ruffled ocean surface. An empirical foam spectral reflectance model and an empirical spectral reflectance model for water volume below the surface are integrated in the ocean surface model. For other scene types such as desert, trees, and snow surfaces, empirical models and theoretical models are developed to approximate the surface reflection of the polarized solar radiation. Polarization properties of reflected solar radiation from the ADRTM are compared with those from the PARASOL satellite data. Sensitivity studies are conducted for various ocean-surface and atmospheric conditions for the stratification of polarization distribution models (PDMs), which are to be used in the inter-calibration of the polarization-sensitive imager measurements with the CLARREO data.

We summarise here and, in more detail, in [212] the first accurate approach for making spectral PDMs over broad solar spectra, which cannot be achieved by empirical PDMs based on the data from polarimetric sensors. In [212] we see that the major uncertainty factors related to solar radiation polarization are aerosols, thin ice clouds, and complexity of surfaces. Aerosols and ice clouds must be carefully accounted for in making the CLARREO PDMs. The major problem with thin cirrus clouds and aerosols related to the polarization of reflected solar light from the Earth-atmosphere system is their optical thickness. However, although thin cirrus clouds and aerosols could significantly affect DOP, their effect on AOLP is not significant. Our results provide a reliable approach for calculating the spectral CLARREO PDMs over the broad solar spectra, which cannot be achieved by empirical PDMs based on the analysis of available data from current polarimetric sensors in orbit.

§7.2 Authors: **Jack Xiong** and **Jim Butler**, NASA / GSFC

§7.3 Authors: **Thomas C. Stone[1], Constantine Lukashin[2], Kevin Turpie[3]**, [1]U.S.G.S., [2]NASA / LaRC, [3]NASA / GSFC

§7.4 Author: **Dennis Helder**, S. Dakota St. Univ.

§7.5 Authors: **Wenbo Sun[1], Yolanda Shea[2], Bruce A. Wielicki[2], Rosemary R. Baize[2], Constantine Luskashin[2], and Gary A. Fleming[2]**, [1]Science Systems and Applications Inc., [2]NASA /LaRC

§7 Editor: **Greg Kopp**, Univ. of Colorado / LASP

8   Thermal Infrared Passive

The thermal infrared radiation (TIR), wavelengths > ~3 µm, are the result of direct emission from the parameter/surface being observed and simplistically characterise its effective temperature or the scattering/absorption properties of a medium to a surface emitting at that temperature. In some sense, remote observations in this spectral region are the most direct measure of the concept of global warming and in general relate to the use of planks law to correlate an observed spectral radiance to one of 'brightness' temperature. Measurements of the Ocean and Land then allow the prospect of detection of subtle signatures of change/warming. The relativity uniform emissivity of the Oceans compared to the land make it one of the best targets to observe but the large mass makes it very slow to respond requiring perhaps a few tenths of a degree C per decade, making it a highly challenging measurement.

> **Satellite observations of the Earth in the thermal infrared provide the only direct global measurement of the Earth's temperature and its change**

TIR can of course also be used in a similar way to the solar reflective, to observe properties of other parameters using it as a source of radiation, e.g. selective absorption by gas molecules provides an indicator of their presence and concentration (carbon dioxide and water vapour being some of the most important in the context of climate change) and also scattering of aerosols another. Here spectroscopic change from the nominal TIR continuum provides the means for this analysis also.

The TIR is thus clearly an important domain for remote sensing and one with many challenges similar to those of other parts of the electromagnetic spectrum, however it should be noted that one additional challenge in this spectral region is that special care needs to be taken in any observation since the sensor itself if often also an emitter radiation in the same spectral band of the signal it is trying to detect.

8.1   Challenges for In-Flight Calibration of Thermal-Infrared Imaging Instruments for Earth Observation

8.1.1   Abstract

Satellite instruments operating in the thermal infrared wavelength range > 3 µm, such as the Sea and Land Surface Temperature Radiometer (SLSTR) on Sentinel-3, the Infrared Atmospheric Sounding Interferometer (IASI) on Metop, the Visible Infrared Imaging Radiometer Suite (VIIRS) on NOAA-20 and the Landsat-8/9 Thermal Imager, provide information for applications such as profiling atmospheric temperature, humidity and composition, land surface temperature (LST), sea surface temperatures (SST), land surface emissivity, land classification, soil composition, volcanology, fire radiative power, cloud masking, aerosols, and trace gases.

All these instruments are dependent on blackbody (BB) calibration sources to provide the traceability of the radiometric calibration to SI. An ideal black body source consists of an isothermal thermal radiator that emits Planck radiation and perfectly absorbs all incident thermal radiation that falls on it, a view to deep space would be a black body or around 3K typically used as a cold or 'zero reference'. Practical laboratory black bodies can closely reproduce the performance of an ideal source. The accuracy of the measured temperature of the radiating surface is fundamental to the operation of the black body calibrator. Developing blackbody sources for flight applications is demanding because of the constraints placed on mass, power and volume, and the requirement to survive the launch and orbital environments. This in turn affects the thermal uniformity, emissivity and thermometry that are essential for high accuracy calibration sources.

A key issue for flight BB sources is to maintain the traceability of the radiometric calibration from ground to orbit. For example, the temperature of the BB is measured by a number of precision thermometers that are calibrated against a reference Standard Platinum Resistance Thermometer (SPRT) to provide the traceability to the International Temperature Scale of 1990 (ITS-90). However, once calibrated, the thermometer system is subject to drifts caused by on-ground thermal vacuum testing and the launch and space environments. At best the uncertainties due to thermometer ageing can only be estimated as there is at present no direct method for recalibrating on orbit. Comparisons with other satellite sensors are useful for placing an upper limit on calibration drifts but do not themselves provide a traceable link to the SI, as these other sensors are also prone to unpredictable change.

8.1.2   Introduction

The Planck radiation law predicts that for temperatures that cover the typical range of Earth scenes from 180 K to 350 K, the peak of the radiation distribution occurs within the range 3 µm – 20 µm. Also, the radiances cover a wide dynamic range, particularly at wavelengths < 5 µm. This makes observations in the thermal infrared range particularly useful for measurements of the Earth's surface temperatures and atmospheric sounding. Thermal infrared measurements from satellite instruments have a range of applications ranging from global climate change monitoring to monitoring urban pollution. Table 8.1 and [240] provide a summary of applications beyond those normally associated with climate .

Table 8.1: Applications of high resolution, hyper-spectral thermal infrared instruments [240].

Domain	Application	Domain	Application
Volcanoes and Earthquakes	Detection of Earthquakes and Pre-eruptive volcanoes	Urbanisation	UHI: Surface temperature maps, Vegetation maps, Land cover/Land Use, Building Information, Air Quality
	Hot spots and active lava flows		Security and surveillance
	Post eruptive studies on lava flows		Industrial/power plant monitoring
	Eruption clouds and Tropospheric plumes		Air pollution
			Differentiate between urban and industrial zone
Fires	Detection of fires, potential coal fires, coal mine fires		Detection of Oil spill and Plume
			Mapping malaria and/or cholera potential regions
	Estimation of burnt area, fire intensity and severity		Arthropod vector ecology and disease distribution
Hydrology	Detection of water stress in crops and forests		Mapping meningitis outbreak
	Detection of evapotranspiration in crops, river basins, and continents		Asbestos-cement detection (non-accessible areas)
	Prediction and monitoring of floods		Detection of minefields
	Mapping irrigated land		Trafficability (off-road soil moisture content)
	Cooling Degree Day estimations	Surface Variability	Soil composition
			Identifying geothermal resources
	Growing Degree Day estimations and mapping		Mapping geothermal anomalies
			Mapping dynamic variability of surface temperature and emissivity

There are many IR instruments on-orbit and planned to cover these and other applications. It is not practical to provide an exhaustive list in this section. Instead the WMO OSCAR tool provides a comprehensive searchable list of sensors [241]

In the context of climate, a particular use of thermal infrared instruments has been to measure global sea-surface-temperatures (SST) for monitoring warming. Sea surface temperatures are an important indicator of

> **Observation of change in ocean temperature is a key indicator for climate change**

climate change, Figure 8.1. Satellite instruments are particularly useful because they can provide global coverage within a few days and are operational for several years. Series of Polar orbiting filter radiometers such as the Advanced Very High-Resolution Radiometer (AVHRR), the Along Track Scanning Radiometer (ATSR), the Moderate Imaging Spectroradiometer (MODIS), the Visible and Infrared Imaging Spectroradiometer (VIIRS) and more recently the Sea and Land Surface Temperature Radiometer (SLSTR) have provided a near continuous record of global sea-surface temperatures since the 1970s. It is interesting to note from Figure 8.1 that the warmest period since 1880 has been during the era of satellite observations. Thus, for satellite measurements of SSTs to contribute to long-term climate records it is essential that the measurements are consistent and are traced back to the same temperature standards that were used for the historical records. For temperature, these measurements need to be expressed in terms of the International Temperature Scale of 1990, ITS-90, which provides a practical approximation to the SI unit of temperature, the kelvin.

Global Land and Ocean
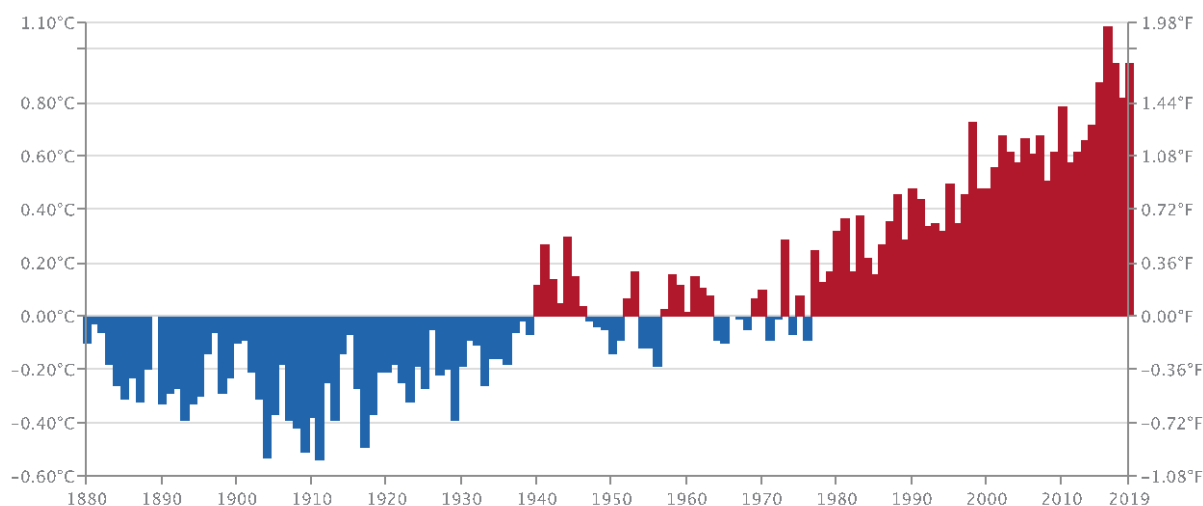**January–July Temperature Anomalies**

Figure 8.1: Global Land and Ocean Temperature anomalies since 1880 from NOAA National Centers for Environmental Information, State of the Climate: Global Analysis, published online September 2019, retrieved on 6-September-2019 from http://www.ncdc.noaa.gov/sotc/global/time-series/globe/land-ocean/ytd/7/1880-2019

To measure such changes requires satellite instruments to be capable of observing atmospheric and surface temperature trends as small as 0.1 K decade^{-1} [1]. The measurement precision and accuracy requirements needed to support the capability to retrieve sea surface temperature changes for climate change monitoring are of the order of 0.1 K – 0.3 K [242] (k=1) as a minimum reflecting the slow inertia and thermal mass of the oceans but ideally but ideally in common with other IR measurements of the Earth impacting radiation balance an order of magnitude further improvement would be desired. .

To achieve observational requirements, the instrument system design has to ensure that it can be calibrated, such that any remaining errors can be measured to a known accuracy either before launch or in-orbit. This process must start from the initial assessments of the mission performance in order place limits on the uncertainties of individual components, such that in the absence of any knowledge of the integrated system performance, there is a reasonable (1σ) expectation that the combined performance of the components and subsystems can meet the mission performance requirements.

An example of the flow-down from the mission performance requirements to component measurements is illustrated for SLSTR in Figure 8.2 below. For SLSTR the main objective is to measure sea surface temperature to an absolute accuracy of < 0.3 K traceable to ITS-90. The SST measurement is based on top-of atmosphere measurements of the Earth's brightness temperature at 3.7 μm, 10.8 μm and 12 μm to an uncertainty < 0.1 K. This is further broken down into specifications for the individual components including radiometric noise, spectral response, non-linearity, stray light limits.
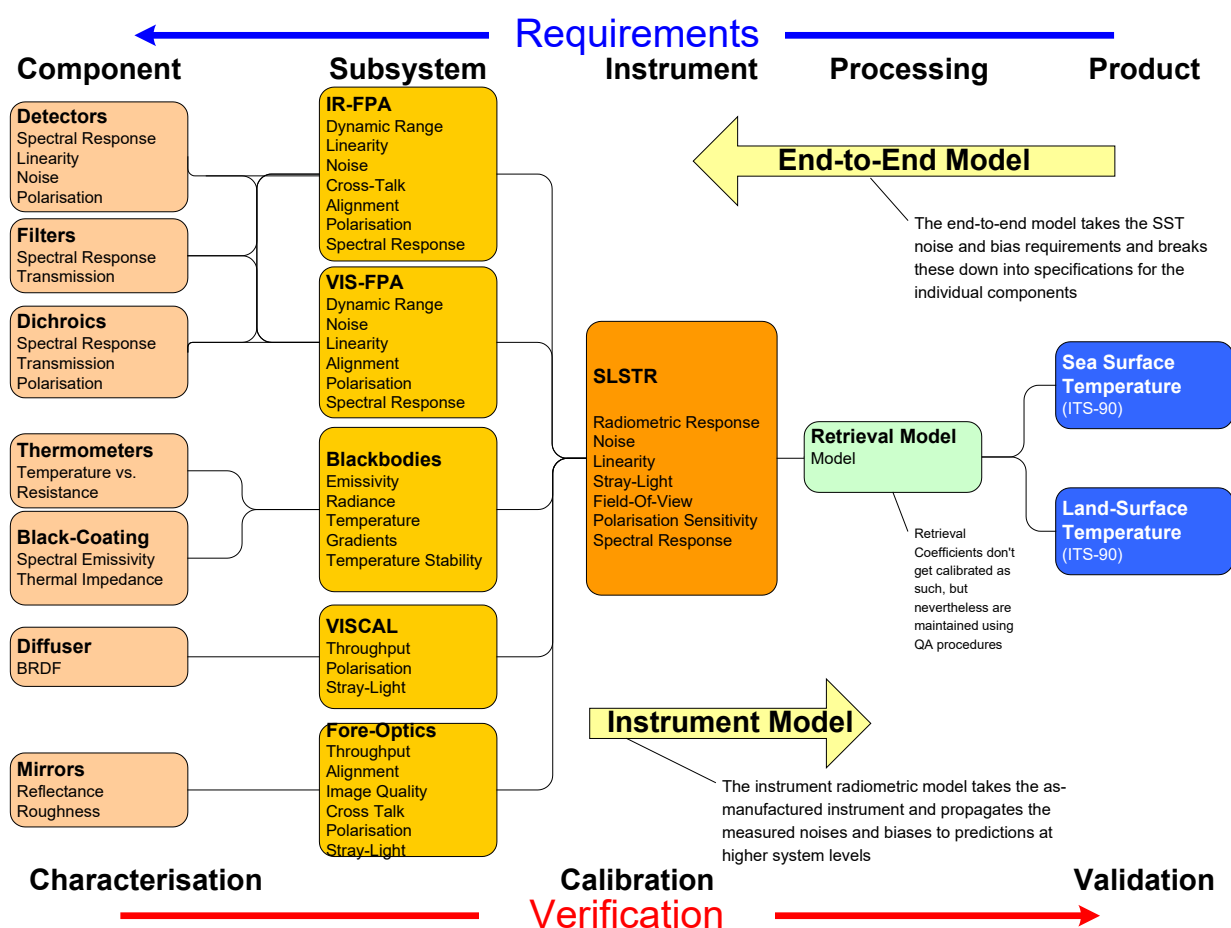

Figure 8.2: Diagram showing the concept of flow of the SLSTR performance requirements down to instrument, subsystem and eventually component level accuracy requirements, and the subsequent calibration & characterisation measurements to be performed in order to provide a fully calibrated system.

The calibration of the system response requires a combination of on-board calibrators (blackbodies) to provide stable on-orbit calibration, measurements performed at subsystem and/or component level, on ground measurements performed at instrument level to characterise and validate the end-to-end calibration, and sustained post launch calibration and validation activities.

The traceability chain needs to be developed during instrument design phase to identify all calibration effects. Here the instrument calibration model is defined, and all uncertainty effects contributing to the calibrated Level-1 data are traced through to their original sources. For most thermal infrared instruments, the primary effects will be due to uncertainties in the calibration source thermometry and emissivity, instrument spectral response and non-linearity effects. Data processing effects must also be considered, for example where averages of several measurements from calibration sources are used to reduce random noise effects.

8.1.3   Calibration Systems for IR instruments

Thermal infrared instruments are notoriously difficult to calibrate. Calibrations are required for field of view, wavelength selection and radiance response. The field of view and wavelength selection are relatively stable over time by design and can be calibrated pre-flight, but

Blackbodies provide a convenient and reliable method for calibrating TIR sensors

radiance signals at the instrument detector include the thermal self-emission of the instrument. This self-emission combined with the temperature sensitivity and degradation over time of components such as the infrared detectors and other electronic parts causes an instrument's radiometric gain and offset to vary continuously. Consequently, the instrument must be re-calibrated repeatedly in orbit.

For IR instruments such as (A)ATSR and SLSTR, traceability to SI is achieved via internal blackbody calibration sources. For an ideal blackbody source, the Planck radiation law can be used to derive the emitted spectral radiance (W.m^{-2}.µm^{-1}.sr^{-1}) from the temperature and wavelength since:

$$B(\lambda, T) = \frac{2hc^2}{\lambda^5} \frac{1}{e^{\frac{hc}{\lambda kT}} - 1}$$

Equation 3

SLSTR utilises two cavity blackbody sources with emissivity > 0.998 based on the design originally used for ATSR [243]. The emissivity, in flight is assumed to be stable based on previous ageing tests on the black coating. One blackbody 'floats' at the optical enclosure temperature of 260 K and the other is heated to 302 K to provide two calibration points. Platinum Resistance Thermometers (PRTs) embedded in the base of each cavity are used to measure the temperature. The blackbody sources are 'viewed' by the instrument every scan thereby providing a continuous calibration to minimise effects due to the orbital and long-term temperature variations of the instrument optics. Other IR instruments typically include views of deep space to provide a cold blackbody calibration source, close to absolute zero.

Figure 8.3: Flight blackbody calibration sources for AATSR (left) and SLSTR (right)

Although the calibration principle is relatively straightforward, the actual process from raw data to calibrated radiances/brightness temperature involves several processing stages and requires several inputs. For example, for SLSTR, calibration coefficients are computed for each spectral band (five thermal bands) and each detector element (2x2) and for each Earth view (separate for nadir and oblique views). These coefficients are derived from data recorded on-orbit and parameters contained in the Satellite Characterisation Database Document. Each source of error contributes to the overall uncertainty of the instrument calibration budget.

An analysis of the SLSTR level-1 processing has identified the following primary sources of uncertainty in the IR radiometric calibration.

1. Blackbody Temperature Measurement

These are measured by PRTs and calibrated pre-flight at subsystem level and are traced to ITS-90 via a Standard Platinum Resistance Thermometer (SPRT).

2. Blackbody Temperature Gradients

These are determined by thermal analysis of the cavity [244] and measurement at different positions across the cavity baseplate.

3. Blackbody Cavity Emissivity

The emissivity of the blackbody is < 1.0 because of the constraints of the instrument design and the non-blackness of the coating material. The emissivity of the cavity is determined by spectral reflectance measurements of the black coating material by NIST and NPL, and modelling.

4. Spectral Response

These are measured for all channels pre-launch at RAL and are assumed not to change.

5. Non-Linearity Response

Measured during instrument pre-launch tests at RAL and assumed not to change.

6. Detector Noise

Measured during instrument-level calibration tests and on-orbit using signals from on-board blackbody sources

Pre-launch calibration testing at the instrument level against accurate reference sources is essential for thermal infrared instruments. The principle for (A)ATSR and followed for SLSTR is to validate the on-board calibration systems and processing under flight representative thermal vacuum conditions with

the instrument fully operational in its flight configuration in a purpose-built calibration facility [245]. SLSTR-A was tested between March-May 2015 and SLSTR-B between October 2015 to February 2016. Measurements were performed at different thermal environment conditions and for different instrument configurations. Data are processed using the same algorithms and characterisation data that are used for flight. Furthermore, raw data generated during the tests are used to validate the flight L0-L1 processing chains.
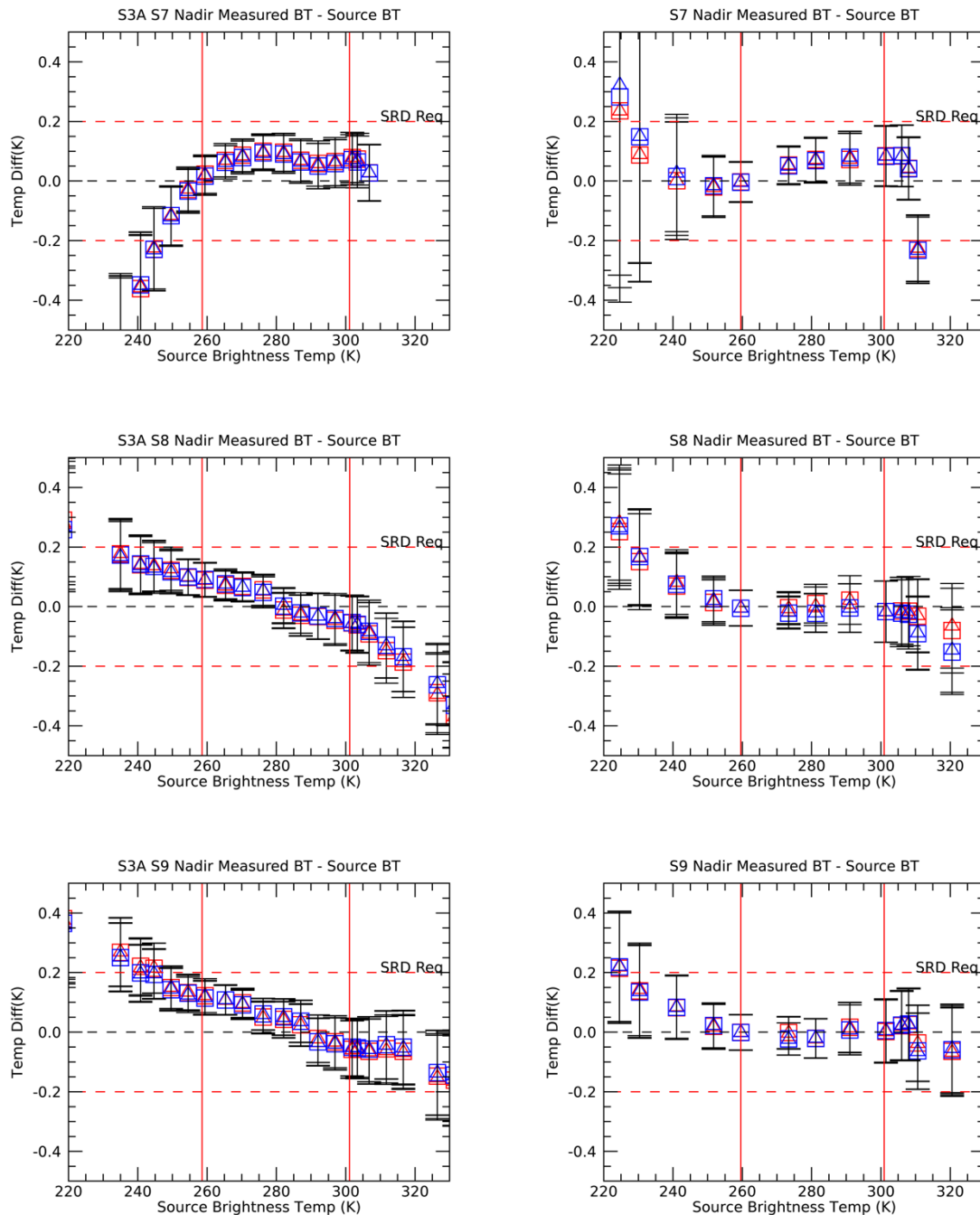
Figure.8.4: Pre-launch calibration results of SLSTR-A (left) and SLSTR-B (right) showing differences between brightness temperature measured by SLSTR and the brightness temperature of the reference blackbody derived from the thermometer measurements.

Typical results, as shown in Figure.8.4, demonstrate that the SLSTR calibration is within requirements over the expected dynamic range of the instrument. They also revealed an issue with SLSTR-A that requires a further processing step to account for a scan dependent offset error [246].

Unless pre-launch calibration tests are performed it is not possible to demonstrate the radiometric calibration of thermal infrared (TIR) instruments within the required uncertainty levels.

8.1.4   On-Orbit Verification

After launch, establishing the absolute calibration to uncertainties < 0.1 K becomes far more challenging. Vicarious calibration methods such as those used for instruments operating in the visible to short-wave infrared range [88], [247], [248] are restricted by a number of factors including knowledge of the surface emissivity, non-uniformity of the surface, contribution of the atmosphere to the measured signal, and temporal variations over very short timescales due to the effect of surface wind and clouds. Hence, post launch activities are currently limited to monitoring of instrument parameters, satellite to satellite intercomparisons, and the validation of the retrieved products by comparison to in situ-measurements.

On-orbit monitoring of critical parameters, in particular the radiometric noise, gains and offsets derived from the on-board calibration sources and/or deep space views, the black-body and instrument temperatures provide a useful indication of the instrument's stability. While monitoring is used to provide an assessment of some components of the on-orbit calibration uncertainty budget, for example radiometric noise and temperature gradients, with no on-orbit reference standard such as a phase change cell, it is not possible to quantify and then correct for any on-orbit changes of absolute temperature values.

Currently, the only method available to evaluate the overall absolute calibration is via comparisons with other satellite sensors operating in the same wavelength range. An example is comparisons of SLSTR with respect to IASI on Metop. Here, Simultaneous Nadir Observations (SNOs) are performed by comparing spectrally averaged IASI BTs over the spectral responses of the SLSTR bands, and spatially aggregated SLSTR BTs over the IASI footprint, based on algorithms recommended by GSICS (see WR§4). These comparisons have been performed for both SLSTR-A and B. and show that SLSTR and IASI agree within 0.1K for homogenous scenes [127]. However, there are some limitations to the approach.

1. The spectral range of IASI does not cover the full range of SLSTR bands. So only two channels at 10.8 µm and 12 µm can be covered unambiguously. (Monitoring the 3.7µm channel in this way requires estimating extensions to IASI's spectral coverage, which introduces small additional uncertainties.)
2. The presence of clouds and sea ice within the IASI footprint increases the noise in the measurements.
3. Because of the temporal variability of the IR measurements, the matchups have to be performed within a 5-minute window.
4. Agreement does not signify SI-traceable accuracy – they could both be in error

Another example of direct comparisons has been the Sentinel-3 tandem phase where the S3A and S3B satellites flew on the same ground track 30s apart for 4 months. This provided a unique opportunity to compare the radiometric calibrations of all SLSTR channels. The results from this phase are still under assessment but have been useful for verifying that the radiometric calibrations of the two sensors are consistent with each other. Nevertheless, this does not demonstrate the absolute radiometric accuracy of either.

8.1.5   Towards On-Orbit Traceability

Despite the efforts described in the previous sections, there are currently no operational IR sensors with the means to provide a calibration reference that is unequivocally traceable to ITS-90 on orbit at the uncertainty levels required for climate.

One step towards a solution is to employ phase change cells within the calibration system. Under laboratory

> **Use of fixed point blackbodies at the phase transition of materials like gallium, water, and mercury can provide more robust SI traceability of the thermometers used to define the temperature of in-flight blackbodies**

conditions low uncertainty calibration is achieved using phase changes of pure materials e.g. triple point, freezing point, and melting point, as these are extremely reproducible and have well characterised temperatures specified by the International Temperature Scale of 1990 (ITS-90). Key references for the TIR range are the triple point of mercury (-38.8344 °C) and water (0.01 °C), and the melting point of gallium (29.7646 °C). Typically, the temperature of on-board satellite BB calibrators can be changed in flight, so if Phase Change Cells (PCCs) are embedded in a BB structure in close proximity to the temperature sensors and the BB is warmed or cooled, then during the phase change the material will absorb or release heat without a significant change in temperature, and the thermometer output will show a 'plateau' at the phase change temperature. As this temperature is known, the thermometer can be calibrated *in situ*. Such miniature PCCs for use within blackbody sources have been developed and tested under the CLARREO project [249].

A joint study with RAL Space, NPL and Surrey Nano systems funded by the United Kingdom Space Agency, UKSA, has sought to improve the on-orbit traceability of satellite IR instruments, [250]. The aim of the Next Generation InfraRed Source (NGenIRS) was to demonstrate the performance of novel readout electronics, carbon-nanotube black coatings and a phase-change cell within an existing SLSTR like blackbody cavity geometry with the goal of reaching Technology Readiness Level-5/6, Figure 8.5.
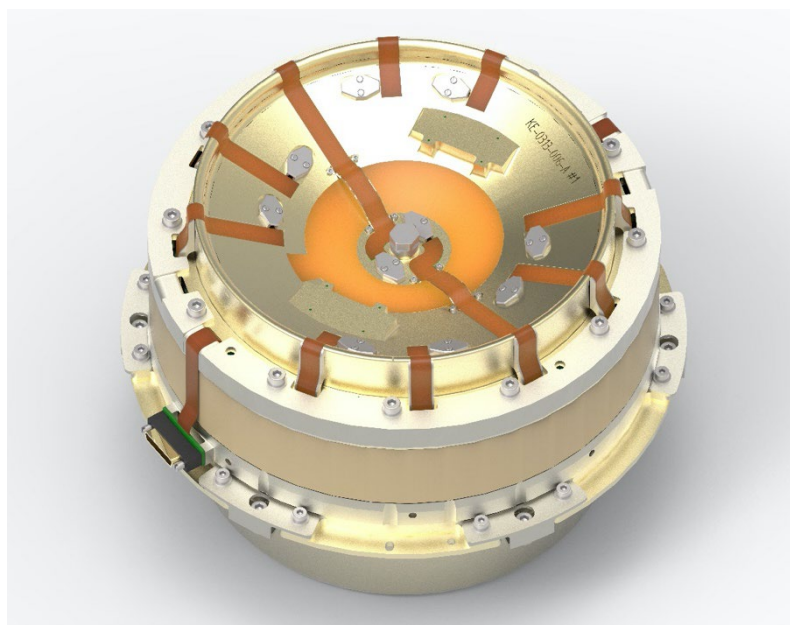

Figure 8.5: CAD model of NGenIRS source.

The PCCs developed for NGenIRS use less than 2 grams of Gallium. Early attempts found that there was a problem with excessive undercool, but the team have now achieved repeatable phase changes and

simple freezing procedure (only requires 2-3 °C undercool). Results from the prototype cells have achieved melt durations of 3-12 hours with a repeatability of < 5 mK independent of orientation. Furthermore, methods have been developed to ensure the long-term robustness of the PCCs that make them suitable for high levels of vibration and long-term use (many years) without leakage or contamination due to reaction between the gallium and the container, Figure 8.6 [251].
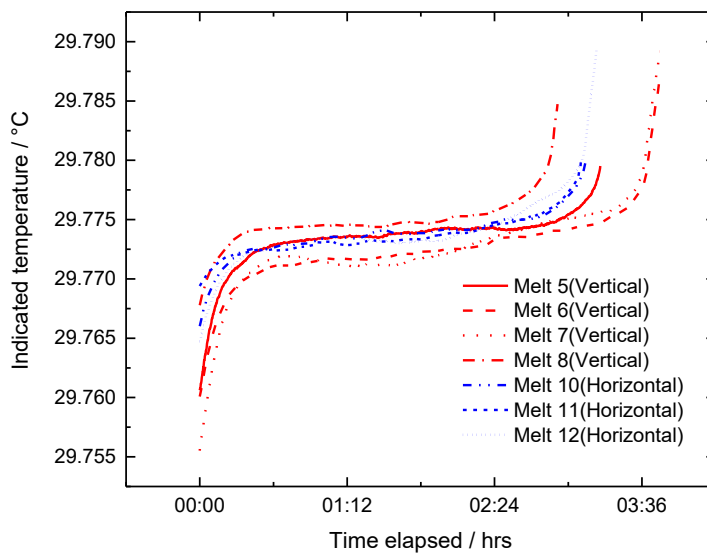

Figure 8.6: Repeatability of the melting plateaux for different orientations of the cell; 'vertical' means upright.

A PCC has since been integrated into a blackbody cavity with the same geometry, thermal and mechanical interfaces as the flight SLSTR black-body cavities. Tests under flight thermal vacuum conditions have verified that the phase change transition can be measured by the cavity thermometers to an uncertainty < 10 mK, Figure 8.7 [250].
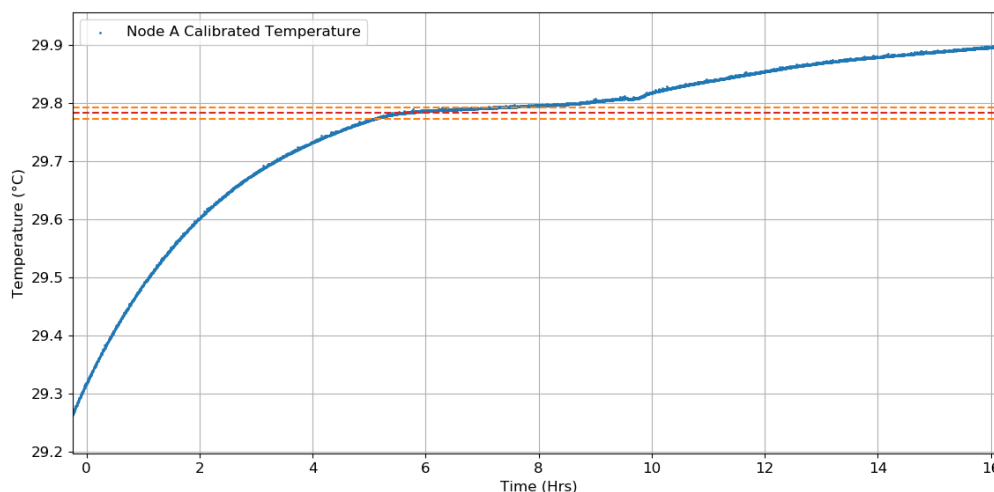
Figure 8.7: Early results for a melting point plateau of a phase change cell in the NGenIRS blackbody calibration source. The plot shows the temperature of a calibrated thermometer mounted on the base of the blackbody next to the phase change cell for a single melt during thermal testing of the prototype source.

8.1.6   Conclusions

To realise the potential of satellite instruments in the TIR wavelength range for providing climate quality data records, it is essential that they be calibrated with uncertainties < 0.1 K to standards that are traceable to ITS-90 and with associated evidence that this is also representative of the emitting surface of known emissivity in-flight. Instrument design is also fundamental to achieving traceable measurements. This includes control of internal and external stray light sources to a level that they do dominate the uncertainty budget.

The instrument traceability chain needs to be developed during instrument design phase to identify all calibration effects, including data processing as well as from on-board calibration sources.

Pre-launch calibration is essential to validate end to end calibration model, particularly at thermal infrared wavelengths. Because TIR instruments are highly sensitive to their thermal environment, testing must be done with the instrument in flight representative thermal vacuum conditions, where the temperatures of all thermal surfaces are controlled and measured.

The primary route to SI-traceability in the TIR range is through the use of on-board black-body sources. Here the measured radiance is linked to the measured temperature via the Planck function.

A limitation with all blackbody sources flying on all current TIR instruments missions is that the uncertainty is based on pre-flight measurements of the thermometry system and estimates of the long-term drift through analysis and predictions.

Recent developments of miniature phase change cells provide a route to direct traceability of the on-orbit calibration of the blackbody thermometers to uncertainties < 20 mK. Further work is in progress to advance this technology in a flight blackbody source.

8.2   Infrared Narrowband Imagers: MODIS

8.2.1   Introduction

16 of the 36 MODIS spectral bands are referred to as the thermal emissive bands (TEB), covering wavelengths from 3.5 μm to 14.5 μm. All MODIS TEB observations are made at 1 km nadir spatial

resolution. MODIS TEB are located on two cold focal plane assemblies (CFPA) that are nominally controlled at 83 K. The VIIRS has 7 TEB covering wavelengths from 3.5 to 12.2 µm: 5 M bands (750m resolution) and 2 I bands (375 m resolution). It does not, however, have similar MODIS bands with wavelengths above 12.2 µm that are could be used for cloud top height. Like MODIS, the VIIRS TEB are also located on the CFPAs. The S-NPP and N-20 VIIRS CFPAs are controlled at 80 K.

The MODIS and VIIRS TEB calibration traceability was established pre-launch using a blackbody calibration source (BCS) of high emissivity and temperature measurement accuracy (similar to the on-board BB shown in Figure 8.9), which was operated together with the ground-based BCS (reference source) over a range of temperatures. This enabled the TEB calibration traceability to be transferred from the BCS to the on-board BB. Key sensor TEB performance parameters, similar to those described in §6 for RSB, were characterized and derived from various pre-launch measurements [197], [198].

For MODIS TEB, the specified calibration requirements at typical scenes (or temperatures) are 1% in radiance, with the exception of band 20 (3.75 µm) at 0.75%, band 21 (3.95 µm), used for fire detection, at 10%, and bands 31 and 32 (11 and 12 µm), which are used for sea surface temperature (SST) measurements, at 0.5%. The VIIRS calibration requirements are similar and slightly higher (or more stringent) compared to that of MODIS.

8.2.2   Pre-launch Calibration

The pre-launch calibration of the MODIS and VIIRS thermal emissive bands between 3.75 µm and 12.02 µm employs a large aperture blackbody calibration source (BCS) with high emissivity and accurately measured temperature operated in thermal vacuum conditions. The BCS is a trap-type blackbody with thermally controlled specular black surfaces. The radiance temperature scale for the BCS is established by the instrument builder using contact thermometry provided through the use of high precision platinum resistance thermometers (PRTs) with SI calibrations traceable to the NIST realisation of the International Temperature Scale-90 (ITS-90) over the full 190 K to 345 K BCS temperature operating range [252]. The emissivity of the BCS is computed to be 0.9996 using a geometric model of the BCS and knowledge of the bidirectional reflectance of the blackbody specular black surface. With knowledge of the effective BCS cavity temperature provided by a weighted average of the temperatures from the calibrated PRTs and the emissivity, the Planck radiation formula is used to determine the BCS emitted spectral radiance over the MODIS and VIIRS bands. Figure 8.8 shows the traceability of MODIS and VIIRS thermal infrared calibration, from pre-launch to on-orbit.
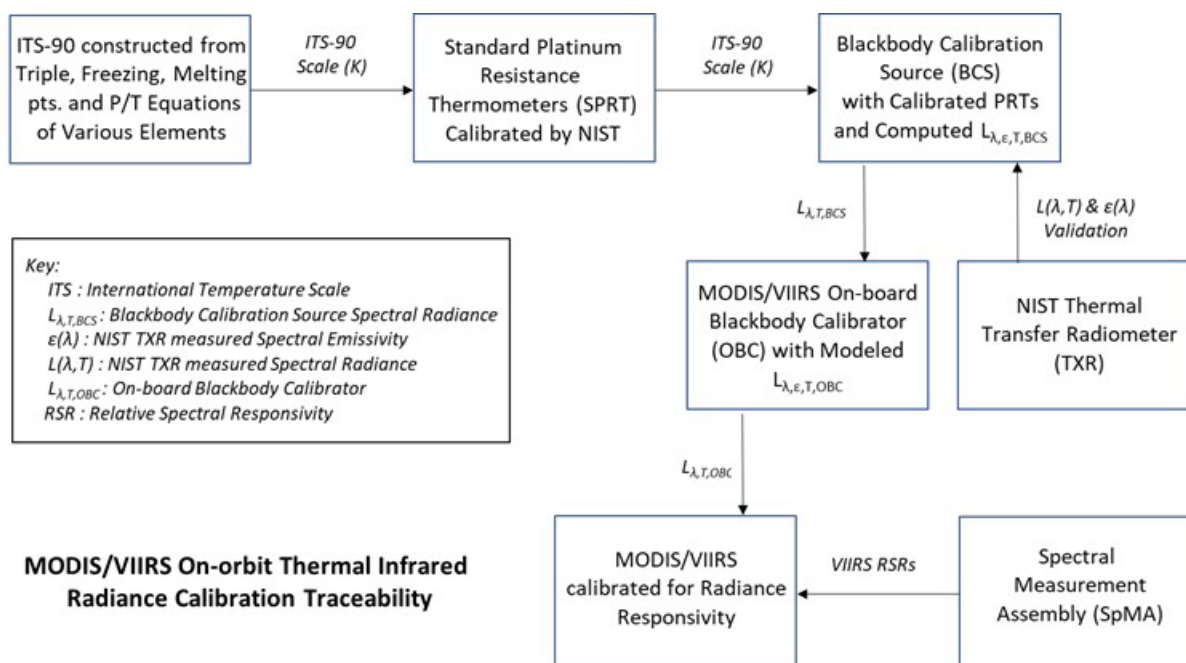
Figure 8.8: MODIS and VIIRS on-orbit thermal infrared radiance calibration traceability

In an effort to validate the BCS radiance scale used in the MODIS (and later, VIIRS) calibrations, NASA's Earth Observing System (EOS) enlisted NIST to design, build, and test the Thermal Transfer Radiometer (TXR) and to deploy the TXR to instrument builder facilities [116]. Briefly, the TXR is a liquid-nitrogen cooled, portable filter radiometer with two channels centred at 5 μm and 10 μm, both with bandwidths of approximately 1 μm. Prior to deployment of the TXR, the TXR absolute radiance temperature scale is transferred to the radiometer by having the TXR view the NIST Water Bath Blackbody (WBBB) at NIST's Ambient Infrared Radiometry and Imaging (AIRI) facility [253], [254]. The WBBB implements the NIST radiance temperature scale based upon the ITS-90 temperature scale. For lower temperatures, the radiance scale of the TXR was calibrated by placing the TXR in a NIST cryogenic vacuum chamber and having it view a large-area cryogenic blackbody with radiation temperature calibration tied to the NIST detector-based radiometric scale [255]. The radiance temperature scale of the TXR is maintained using a stable travelling blackbody, called the Check Source, between its calibration at NIST and its viewing the BCS.

8.2.3   Post-launch On-Orbit Calibration

The MODIS and VIIRS TEB on-orbit calibration is performed using the on-board BB with its temperatures measured by a set of thermistors that are traceable to the NIST temperature standard. The TEB calibration is performed on a scan-by-scan basis. During normal operations, the BB temperature is constantly controlled at pre-determined set points. For example, the Terra MODIS BB is set at 290K whereas the Aqua MODIS BB at 285K. MODIS and VIIRS on-board BB temperatures can vary from instrument ambient to 315 K via electric heaters. This allows TEB detectors' nonlinearity to be monitored and updated if necessary during on-orbit operations. In addition to BB, space view observations are made each scan for measuring the instrument thermal background. Details of MODIS and VIIRS TEB on-orbit calibration and performance can be found in a number of references [100], [256]–[258].

Figure 8.9 MODIS on-board blackbody (BB)

Similar to RSB, an assessment of MODIS TEB calibration uncertainty and its key contributors, such as its on-board BB emissivity, BB temperature, and detector NEdT, has been made [28] and an example is shown in Figure 8.10 for Aqua MODIS TEB on-orbit calibration uncertainties at nadir and typical radiance levels. Not included is band 21, which was designed for fire detection. All TEB bands continue to meet their calibration requirements for Aqua MODIS.
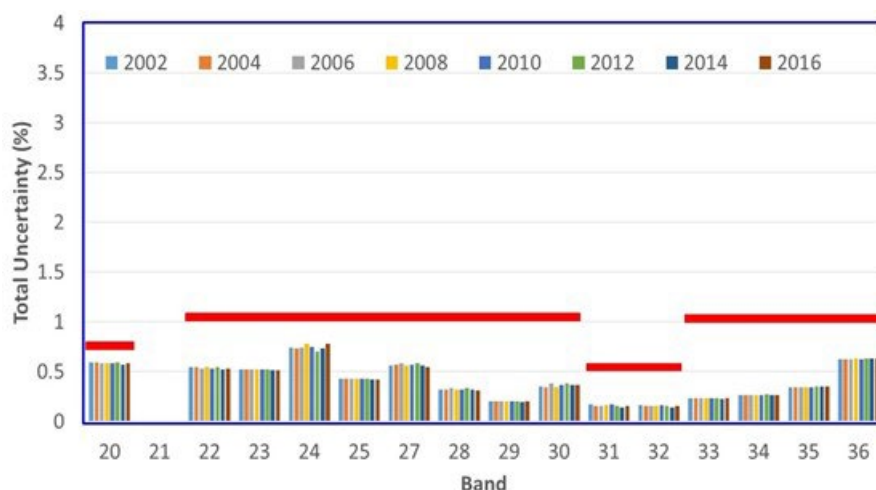

Figure 8.10 Aqua MODIS TEB calibration uncertainty at typical radiance and nadir (horizontal red lines: calibration requirements).

8.3 Improving the Longest SI-traceable Hyperspectral Infrared Record from Space from the AIRS

8.3.1 Contribution of IR Sounders to the Global Hyperspectral Infrared Radiance Record

Infrared (IR) sounders measure the upwelling spectrum of the Earth's atmosphere with high spectral resolution as shown in Figure 8.11. This enables profiling of temperature and water vapor and measurement of concentrations of trace gases from the surface to the stratosphere. The IR sounders, operating today

> **TIR allows analysis of the composition of the Earth's atmosphere**

include the Atmospheric Infrared Sounder (AIRS) on the NASA Aqua Satellite, the Cross-track Infrared Sounder (CrIS) on the NASA/NOAA Suomi NPP and NOAA JPSS Satellites, the Infrared Atmospheric Sounding Interferometer (IASI) on the EUMETSAT MetOp Satellites, and the Hyperspectral Infrared Atmospheric Sounder (HIRAS) on the CMA FY-3 Satellites. All of these instruments are 'hyperspectral', having very high spectral resolution (>1000) to resolve CO_2 and H_2O absorption

features used to make temperature and water vapor profiles. The instruments also measure trace gas constituents including O_3, CO, CH_4, SO_2 at various altitudes from the surface to the stratosphere, depending on constituent. The sounders also measure surface temperature and emissivity, cloud top height, cloud liquid water and cloud fraction. The data from these instruments has demonstrated amongst the highest forecast improvement in NWP models of all data types. The data are regularly used in studies of processes affecting weather and climate as well as validation of weather and climate models. The data are also used in applications including volcano alerts, drought prediction, air quality prediction, and influenza forecasting.
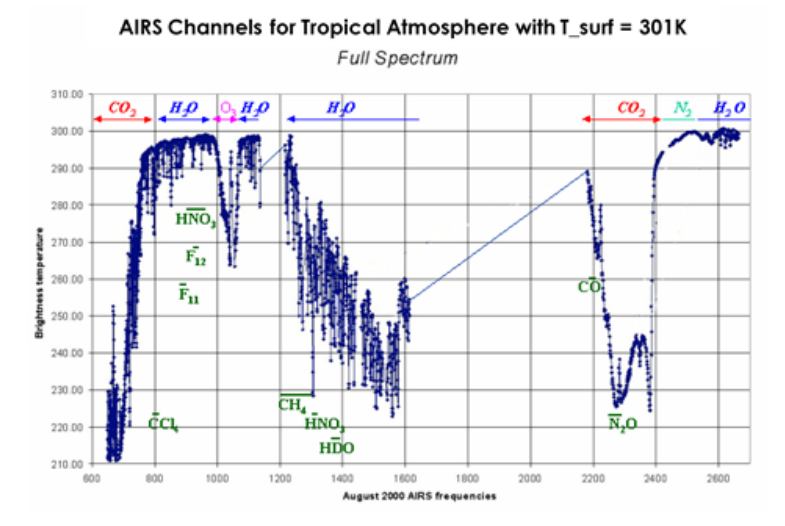

Figure 8.11 IR Sounders measure the upwelling spectrum with high spectral resolution. Radiances shown are simulated at the AIRS resolution and sampling.

8.3.2 The Atmospheric Infrared Sounder (AIRS) on Aqua

The Atmospheric Infrared Sounder (AIRS), shown in Figure 8.12, is a "facility" instrument developed by NASA as an experimental demonstration of advanced technology for remote sensing and the benefits of high resolution infrared spectra to weather forecasting and science investigations [259]. It was launched into a 1:30 pm polar orbit on May 4, 2002 on the EOS Aqua Spacecraft, and is expected to provide highly calibrated data beyond 2024. AIRS has 2378 infrared channels ranging from 3.7 μm to 15.4 μm and a 13.5 km footprint. The AIRS data are used for weather forecasting, climate process studies and validating climate models [260]. For more information see http://airs.jpl.nasa.gov. AIRS is a vital IR reference sensor for the Global Space-based Inter-Calibration System (GSICS) and is used by the Japan Meteorological Agency (JMA) for comparison to Himawari 8/9 AHI [261], the Korean Meteorological Administration (KMA) for comparison to COMS [262], NOAA for comparison to CrIS [43] and GOES [263], and EUMETSAT for comparison to IASI [98].

Figure 8.12 The Atmospheric infrared Sounder (AIRS) prior to integration with the Aqua Spacecraft.

The AIRS was the first hyperspectral IR sounder designed originally for weather forecasting. The long life of AIRS and the excellent stability of the radiances make them invaluable for climate studies on the seasonal, annual and inter-annual timescales. Use of AIRS in multi-decadal timescales relies on the SI-traceability of the AIRS since a continuous overlap of follow-on sounders cannot be guaranteed indefinitely, and operational sounders may not have the necessary stability and accuracy to propagate the record. The radiances from AIRS are traceable to SI-standards through temperature sensors in the pre-flight calibration Large Area Blackbody (LABB) and Space View Source (SVS) viewed by AIRS during pre-flight testing. During the stepped linearity test, the LABB and SVS are viewed along with the AIRS On-Board Calibrator (OBC) blackbody enabling the AIRS to transfer the calibration of the LABB and SVS to the OBC blackbody.

The AIRS instrument, developed by BAE SYSTEMS, includes a temperature-controlled grating spectrometer and long-wavelength cut-off HgCdTe infrared detectors. AIRS scans the Earth scene up to ±49.5° relative to nadir with a spatial

> **Blackbodies provide the means to calibrate TIR sensors used for spectroscopic analysis of the Earth system**

resolution of 13.5 km. The key to the high accuracy and SI traceability of AIRS is the full aperture OBC blackbody and four full aperture space views, both viewed every scan. The OBC is a specular coated wedge design with an internal angle of 27.25°. The care taken in the design and development of the AIRS instrument has led to its long life and excellent radiometric stability. Testing performed at BAE systems characterized the spatial, spectral, radiometric and polarimetric response of the instrument. The accuracy of the radiometric characterization and the accuracy of the LABB and SVS contribute to the overall accuracy of the system relative to SI-traceable standards.

8.3.3   AIRS Radiometric Calibration Approach

The AIRS radiometric calibration approach is straightforward using a nonlinear polynomial fit to observed radiances from the LABB, and a correction for the polarization coupling between the scan mirror and spectrometer that is scan angle dependent. The AIRS Level 1B algorithm converts digital counts to calibrated radiances as follows [264]:

$$L_{ev} = L_o(\theta) + \frac{c_0 \ + \ c_1'(dn_{ev} - dn_{sv}) \ + \ c_2(dn_{ev} - dn_{sv})^2}{[1 + p_r p_t cos2(\theta - \delta)]} \qquad \textit{Equation 4}$$

Where the radiance offset term depends on the polarization product and phase difference of the scan mirror and spectrometer:

$$L_o(\theta) = \frac{L_{sm}p_rp_t[cos2(\theta - \delta) - cos2(\theta_{sv,i} - \delta)]}{[1 + p_rp_t cos2(\theta - \delta)]}$$

<div align="right">Equation 5</div>

In-flight, the gain is then recalculated on-orbit for every scan using the OBC blackbody as

$$c_1' = \frac{[\varepsilon_{obc}P_{obc}(T_{obc}) - L_o(\theta_{obc})][1 + p_rp_t cos2\delta] - c_2(dn_{obc} - dn_{sv})^2 - c_0}{(dn_{obc} - dn_{sv})}$$

<div align="right">Equation 6</div>

where

L_{ev} = *Spectral Radiance in the Earth Viewport (W/m2-sr-μm)*
c_0 = *Instrument offset (W/m²-sr- μm)*
c_1' = *Instrument gain (W/m²-sr- μm-counts)*
c_2 = *Instrument nonlinearity (W/m²-sr- μm-counts²)*
dn_{ev} = *Digital counts while viewing Earth for each footprint and scan (counts)*
dn_{sv} = *Digital counts while viewing Space for each scan (counts)*
$L_o(\theta)$ = *Polarized Mirror Emission Offset. (W/m²-sr-μm)*
L_{sm} = *Spectral Radiance of the Scan Mirror for Unity Emissivity at T_{sm} (W/m²-sr-μm)*
p_rp_t = *Product of scan mirror and spectrometer polarization diattenuation (unitless)*
θ = *Scan Angle measured from nadir (radians)*
δ = *Phase of spectrometer polarization (radians)*
ε_{obc} = *Effective Emissivity of the blackbody*
P_{obc} = *Plank Blackbody function of the OBC blackbody at temperature T_{obc} (W/m²-sr-μm)*
T_{obc} = *Telemetered temperature of the OBC blackbody (K) with correction of +0.3K.*
dn_{obc} = *Digital number signal from the AIRS while viewing the OBC Blackbody*

The radiometric calibration pre-flight involves measuring the instrument response while viewing the LABB stepped from 205K to 310K. The calibration enables computation of the coefficients and from these and the instrument telemetry we can drive the effective emissivity of the OBC blackbody, OBC temperature correction, and contribution to the radiance from the coupling of the polarization of the scan mirror and the spectrometer, L_o. The calibration is applied independently for all channels and a 5 point running smooth is then applied for each of the 17 independent detector modules of the AIRS instrument. Updates to the calibration have been made recently using pre-flight and in-orbit data to improve the accuracy of the product. These include smoothing of the blackbody emissivity, updates to the polarization parameters, and separate nonlinearity coefficients for the A side and B side detectors. The calibration coefficients computed pre-flight are still used today in the Version 5 Level 1B radiance product delivered at the GES/DISC.

8.3.4   AIRS Radiometric Uncertainty

The radiometric uncertainty of the AIRS is calculated by varying each term in the calibration equation in a numerical model and computing the resulting uncertainty due to that term. The uncertainties are then RSS'd to provide a total uncertainty for the radiances. Figure 8.13 compares the predicted absolute radiometric uncertainty for a scene temperature of 250K of AIRS for radiances from the version 5 L1B, and a future improved version under development (Version 7k). The uncertainty shown is 1-sigma and includes the SI-traceability of the pre-flight calibration target, and the transfer of that to the OBC blackbody of the AIRS instrument. Version 7k has improved the accuracy up to 200 mK in some channels and was made available to the public in late 2020. Results shown here are preliminary since the uncertainty in the individual terms is still being assessed. They do, however highlight the high accuracy in the current product, and the potential improvement that can be expected in a future version.
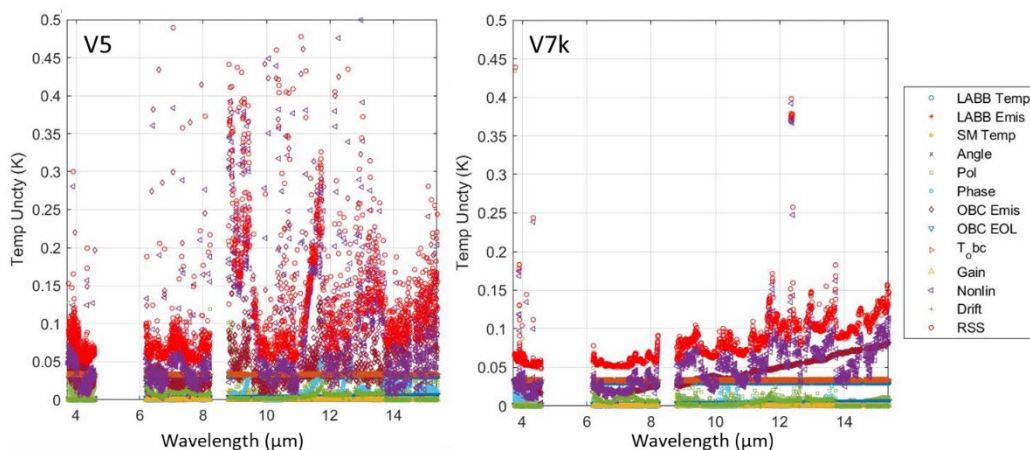
Figure 8.13 Estimate of the absolute radiometric uncertainty for a scene temperature of 250K for the AIRS L1B radiance product Version 5 (current operational version) (left), and a future Version 7k (right).

Table 8.2 lists the radiometric uncertainty for the AIRS module centered at 9.14 µm for a scene temperature of 260K. This is one of the worst case modules in V5 due to the uncertainty in the nonlinearity. The high uncertainty arrives from the recent realization that separate A side and B side detector nonlinearity are required for those channels with A-only or B only detectors operating (the average of A side and B side values were used for all channels in Version 5).

Parameter	Parameter Uncty	Radiometric Uncty (K)
Uncertainty in LABB Temperature	0.03K	0.03K
Uncertainty in LABB Emissivity	0.00005	0.002K
Uncertainty in Scan Mirror Temperature	1.25K	0.006K
Uncertainty in Polarization Amplitude	.0009	0.04K
Uncertainty in Polarization Phase	.08	0.005K
Uncertainty in OBC Blackbody Emissivity	.002	0.07K
Uncertainty in OBC Blackbody Emissivity (EOL)	0.0001	0.004K
Uncertainty in OBC Blackbody Temperature	0.05K	.04K
Uncertainty in Nonlinearity	2.7%*	0.21K
Uncertainty in drift in space view	0.04dn	0.001K
Total Uncertainty at 260K		0.24K

Table 8.2 AIRS radiometric uncertainty (1-sigma) for the worst-case module centered at 9.14 µm.

The radiometric uncertainty expressed in terms of temperature depends on the temperature of the scene. Figure 8.14 shows the dependence of the AIRS radiometric accuracy on scene temperature for the Version 5 product averaged over each module in the

Uncertainty of spectroscopic observations varies with scene temperature

AIRS. The centre wavelength of the module is shown in the legend. At cold scene temperatures, the uncertainty of the polarization terms begin to dominate. A minimum occurs around 308K for most modules since that is the temperature of the OBC blackbody and the nonlinearity uncertainty vanishes at this temperature.
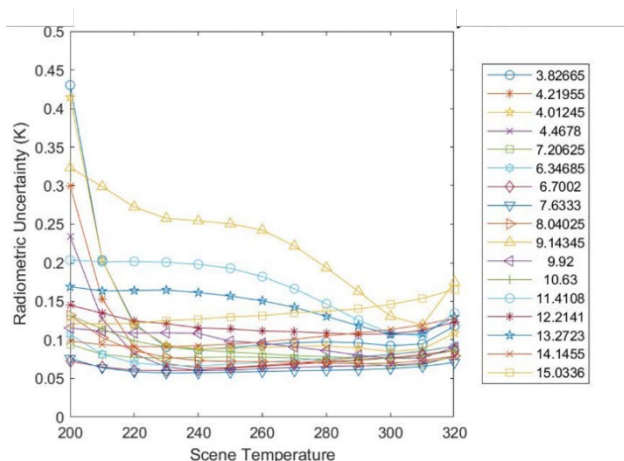
Figure 8.14 Temperature dependence of the AIRS radiometric uncertainty for each of the AIRS 17 modules.

8.3.5   Radiometric Stability and Spectral Calibration

The excellent radiometric stability of the AIRS is discussed in several prior publications [265]. Comparison of AIRS brightness temperatures with sea surface temperatures from the NOAA floating buoy network measured under clear non-frozen ocean conditions shows less than 10 mK/year drift. The AIRS spectrum is calibrated using spectral absorption features in the upwelling spectrum. At present, we have shown the ability to both calibrate to better than 1 ppm and correct the spectra for time varying spectral calibration including Doppler corrections [266]. These corrections along with cleaned and gap filled radiances (using PC reconstruction) will be available in a new Level 1C product. For the Level 1B, spectral calibration data are provided separately in calibration properties files by epoch. More information is found in the AIRS Level 1B user guide [267].

8.3.6   Conclusions

The AIRS instrument on the EOS Aqua spacecraft provides over 17 years of hyperspectral infrared radiances traceable to SI-standards. The accuracy of the Version 5 product available operationally is 100-400 mK depending on channel, while we expect that a 2x improvement or more is possible in the next version (V7). AIRS V7 L1B is expected to be available in the late 2020 or early 2021 timeframe. While AIRS provides SI-Traceable radiances, the SI-traceability is transferred from the external LABB pre-flight to the OBC blackbody. The transfer adds 50-100 mK of uncertainty to the calibration. This uncertainty can be recovered if the instrument was cross-calibrated in-orbit with an On-orbit SI-Traceable IR Sounder reference sensor. Radiance differences seen between AIRS, CrIS and IASI, that are on the order of 100mK -200 mK, could be reconciled with such a system, facilitating use of multiple instruments in a single application. Improving the accuracy of AIRS radiances reduces errors in science investigations and when compared to model radiances. Reducing errors and biases in the calibration enables reanalysis systems to differentiate instrument biases from model biases. With an expected 20+ year record of SI-traceable, highly accurate, hyperspectral infrared radiances, with global daily coverage, the AIRS radiance record is expected to be extremely valuable to the climate science community. All efforts to improve the accuracy of AIRS and the other hyperspectral IR sounders should be continued and is supported by the IR sounding community.

8.4   CLARREO TIR measurements: ARI spectrometer

8.4.1   Abstract

The benefits of implementing a passive IR reference spectrometer on-orbit are based on the need for providing higher information content and higher accuracy climate data for making earlier long-term climate trend detections. Here we describe the approach chosen for the NASA Climate Absolute Radiance and Refractivity Observatory (CLARREO) infrared high spectral resolution measurements, starting with the use of an SI-traceable reference source on orbit, and leading up to defining the uncertainty traceability for intercalibration with other spaceborne sensors. The Absolute Radiance Interferometer (ARI) IR prototype employs a highly stable, flight-proven, 4-port FTS interferometer for broad spectral coverage with a small number of detectors and an On-orbit Absolute Radiance Standard (OARS), developed under the NASA Instrument Incubator Program for CLARREO, for on-orbit calibration verification to better than 0.1 K k=3 brightness temperature at scene temperature. The OARS consists of a variable temperature, high emissivity blackbody with temperature calibration established to better than 10 mK on-orbit and provision for on-orbit emissivity monitoring. The temperature scale is established using miniature melt cells of Ga, H_2O, and Hg. Transferring the high accuracy of ARI measurements to other IR instruments, especially the high spectral resolution operational sounders (AIRS, CrIS, IASI, and HIRAS), should be an important objective of any new SI-traceable climate observing system. The natural property of uniform Nyquist sampling from FTS interferometers is highly valuable for this intercalibration process as well as for other applications. The mathematical approach to rigorous traceability of sampling uncertainties is derived and applied in simulations of the intercalibration process. Results show that it will be possible to make intercomparisons to CrIS and AIRS of better than 0.05 K k=3 with just 6 months of observations from a single CLARREO in true polar orbit.

High accuracy SI-traceable 'benchmark' observations of the Earth in the TIR are an essential perquisite to a comprehensive climate observing system

Note that throughout this section the CLARREO infrared spectrometer referred to is the instrument originally planned for the 2007 Decadal Survey CLARREO mission. That instrument has not yet been funded for flight. The reflected solar spectrometer portion of the CLARREO mission is funded for flight on the International Space Station for launch in 2023 and is discussed in section 11 of this report.

8.4.2   Introduction

For ultimate societal acceptance, new missions to monitor decadal climate trends need to achieve higher irrefutable accuracy by employing the principles of metrology to implement highly accurate on-orbit measurement standards for radiance and reflected solar observations and by rigorously assessing their uncertainties [2]. They also need to provide careful uncertainty traceability when transferring the accuracy of these standards to other spaceborne measurements (intercalibration) and when flowing down uncertainties to climate products. While on some level this has always been done for spaceflight measurements, the level of accuracy needed for decadal climate trending observations (and the level of public scrutiny expected for these key societal records) requires more rigor and fewer assumptions of stability. The NASA Climate Absolute Radiance and Refractivity Observatory (CLARREO) mission has emphasized these principles from its inception, especially requiring the use of fundamental measurement standards that can be used for on-orbit calibration verification, not just evoking stability arguments after pre-flight testing [6]. Such a system can be used to upgrade the accuracy of other climate and weather sensors already in orbit or planned.

This subsection provides an overview of areas where metrological principles are employed in the CLARREO concept for high spectral resolution observations of the Earth emitted spectrum (4 to 50 microns or 200-2500 cm^{-1} at 0.5 cm^{-1} resolution). Much more detailed information about the infrared spectrometer prototype for CLARREO, the Absolute Radiance Interferometer (ARI), has been given elsewhere [268]–[270]. Its proven ability to implement broad spectral coverage, achieve an uncertainty of < 0.1 K k=3 brightness temperature at scene temperature with an FTS interferometer providing Nyquist sampling is described there. The key for this white paper is that the ARI makes use of a well-understood measurement standard, the On-orbit Absolute Radiance Standard (OARS), to verify its measurement accuracy of better than 0.1 K k=3 on-orbit. The body of the paper consists of two major parts, the first presenting the metrological principle of the OARS, the second describing the rigorous traceability of the intercalibration process for transferring the ARI radiance calibration accuracy to operational sounding instruments.

Before proceeding, we provide the definition of metrological categories from Howarth and Redgrave [271], along with an example for temperature that is relevant to our OARS application.

1) The definition of units of measurement that are internationally accepted. e.g. The kelvin for thermodynamic temperature that is now defined by fixing the value of the boltzmann constant (https://www.bipm.org/en/measurement-units/)
2) The realization of units of measurement by community agreed scientific methods. e.g. the International Temperature Scale (ITS-90), based on the melting points of mercury, water, and gallium, coupled with measurements of well characterized temperature sensors to establish the practical scale from about -40 to +30°C.
3) The establishment of traceability chains by determining the value and accuracy of a measurement compared to a standard. e.g. Temperature intercomparisons using transfer standards with associated uncertainty analysis.

Examples for the CLARREO infrared application are included in the following discussion.

8.4.3   On-orbit Metrology Considerations for the CLARREO IR Sensor Radiance

The On-orbit Absolute Radiance Standard (OARS) is a measurement standard that provides traceability to the SI, the International System of units [249], [272], [273]. It is a variable temperature, high emissivity (> 0.997 - 0.999), cavity blackbody that serves as a standard radiance source based on the fundamental quantum mechanical theory of the Planck function. The Planck function radiance that applies to a perfectly emitting blackbody (unit emissivity) and depends only on temperature and wavenumber (or wavelength). For ARI, the wavenumber scale is accurately maintained by the Fourier Transform Spectrometer (FTS) operating principle and is calibrated using the signatures of atmospheric absorption lines with well-known spectral locations. In addition, the spectral instrument line shape (ILS) is measured on-orbit.

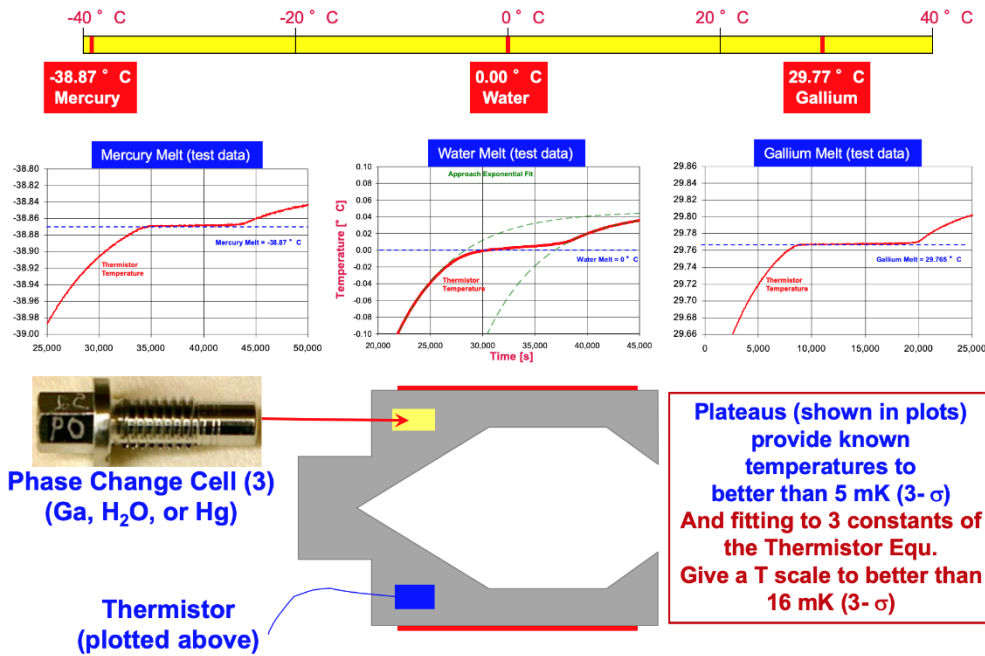The principle that the OARS uses to establish the temperature scale is illustrated in Figure 8.15.

Figure 8.15: Illustration of the new approach for establishing a fundamental temperature scale on orbit used in the On-orbit Absolute Radiance Standard (OARS) blackbody for CLARREO.

The temperature scale needed to establish a radiance standard for the ARI is based on detecting the melting points of Hg, H_2O, and Ga, similar to the principle used by international standards laboratories. The difference is that the OARS uses only very small quantities of phase change material (<0.3 grams) encapsulated in a cell of the same design as that used to house the basic thermistor temperature sensors. The phase change cells and thermistors are embedded within the aluminium cavity. The scheme works because of the very sensitive thermal control system for the blackbody cavity and the high degree of iso-thermality that minimizes thermal gradients during a melt. The melt signatures defining the temperature to better than 5 mK shown in Figure 8.15 are achieved while a low level of constant power is applied after reaching a temperature just below a substance's melt point. A continuous temperature scale accurate to better than 16 mK is established by using each of the three melt points to constrain the three coefficients of the well-established Steinhart-Hart thermistor sensor equation [249].

> Si traceability in the TIR requires not only reliable temperature measurements of a reference blackbody with phase change cells but also the means to assess its emissivity in flight

Finally, the small deviation of the OARS radiance from a Planck function because of its non-unit emissivity is handled by knowing its emissivity quite accurately (order 0.1%) and accounting for its reflection of background radiation. Because of the high emissivity, an uncertainty of several degrees in the effective background radiative temperature is acceptable. To avoid having to assume emissivity stability on-orbit, a system called the heated halo has been devised to measure the emissivity on-orbit (see Figure 8.16).
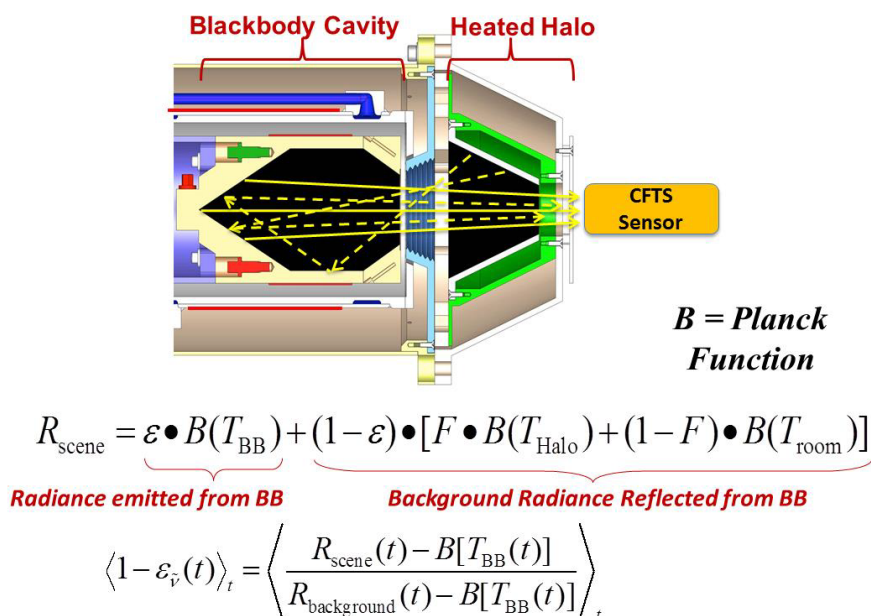
$$R_{\text{scene}} = \varepsilon \bullet B(T_{\text{BB}}) + (1-\varepsilon) \bullet [F \bullet B(T_{\text{Halo}}) + (1-F) \bullet B(T_{\text{room}})]$$

Radiance emitted from BB   *Background Radiance Reflected from BB*

$$\langle 1 - \varepsilon_{\tilde{v}}(t) \rangle_t = \left\langle \frac{R_{\text{scene}}(t) - B[T_{\text{BB}}(t)]}{R_{\text{background}}(t) - B[T_{\text{BB}}(t)]} \right\rangle_t$$

Figure 8.16: Illustration of the CLARREO approach for measuring blackbody hemispheric-to-normal spectral emissivity on orbit. The heated halo is a conically shaped body with a hole at the apex through which the FTS views the OARS blackbody. The heated halo can be heated to 10s of degrees above the cavity temperature and fills a large fraction of the blackbody's view to the environment (about 70%). Therefore, it provides a known, broadband source of background radiation to the OARS from which the reflected spectrum can be accurately measured by the ARI spectro-radiometer.

Test results and a careful uncertainty analysis of the heated halo implementation for ARI show that the emissivity can be measured to about 0.06 %, better than the 0.1% required for CLARREO [120], [274].

8.4.4 Radiance Intercalibration Traceability for Improving the Accuracy of Operational IR Sounding Instruments

Once a new climate quality radiance standard is provided by CLARREO, a natural application is using it as an on-orbit transfer standard to improve the absolute calibration and consistency of other IR spaceborne sensors. The natural uniform spectral spacing and Nyquist sampling of the FTS-based ARI is an important property for being able to achieve rigorous intercalibration.

In addition to improving the accuracy and consistency of the international fleet of IR instruments, combining ARI observations with those from the international high spectral resolution operational sounders will provide a highly valuable climate benchmark. The combination of orbits (with ARI on a true polar, precessing orbit or on the International Space Station, ISS, at 52 degree inclination, IASI on MetOp at 0930 local time, CrIS on JPSS at 1330 and HIRAS on FY3E at 1730) will allow achieving important climate radiance products free of spatial biases to the 0.1 K k=3 level (0.1 K k=2 total uncertainty combining measurement and sampling errors).

The basic intercalibration process has already been successfully demonstrated by several researchers [102] and is currently used by the WMO sponsored Global Space-based Inter-Calibration System (GSICS) program with IASI or CrIS as standards. The ARI sensor will improve the accuracy of this IR radiance transfer standard by temperature dependent factors of about 3-10, as outlined in §3.

The process of performing intercalibration of operational sounding instruments with CLARREO has been simulated and the potential for very high accuracy demonstrated [81]. This simulation uses high spatial resolution MODIS data to evaluate the realistic intercalibration challenges. It shows that both of

the orbits planned for CLARREO (the 52° degree inclination of the ISS orbit planned for the Pathfinder and the true polar 90° orbit of the full mission) would provide many Simultaneous Nadir Overpasses (SNOs) with Sun-synchronous operational sounders, thereby offering comparisons with an excellent assortment of representative Earth spectral radiances.

Here we present the metrology considerations for quantifying the traceability of the intercalibration process. The fundamental challenge to achieving optimized comparisons and ascribing accurate uncertainty estimates is defining how to handle errors related to spatial and temporal mismatches. The key properties of spatial mismatches from the simulations using MODIS images are illustrated in Figure 8.17.
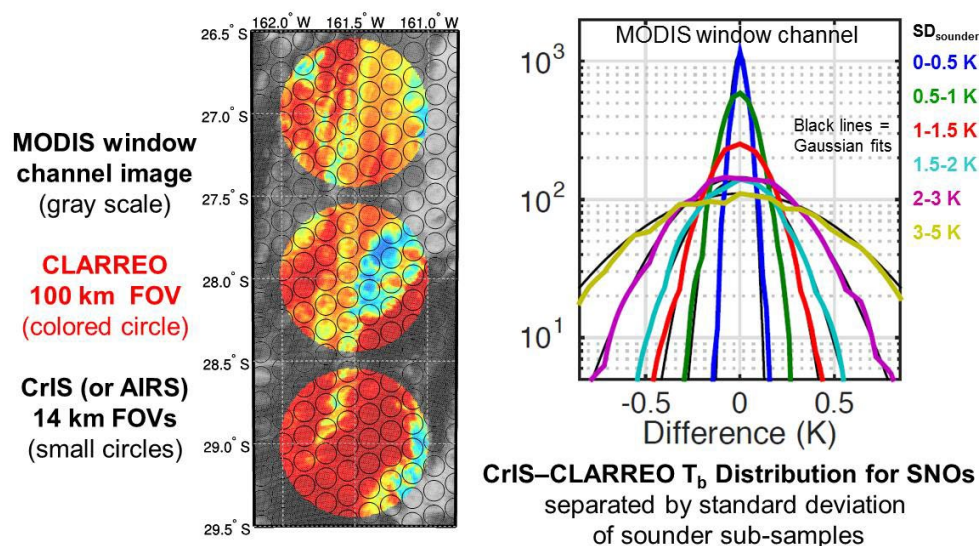

Figure 8.17 Illustration of the properties of the CLARREO intercalibration approach for comparison to operational sounding instruments. On the left, a black-and-white MODIS image is shown with the large CLARREO footprints colour enhanced to illustrate individual Simultaneous Nadir Overpasses (SNOs). The much smaller sounder footprints are overlaid as black circles. On the right, the key statistical properties of SNOs are shown, demonstrating that the distribution of radiance differences is composed of a summation of Gaussian distributions, each well characterized by the standard deviation of sounder sub-samples in the SNO.

The mathematical approach to quantifying the radiance uncertainty of each SNO due to sampling differences, based on the properties shown in Figure 8.17, is quite straight forward (although, beware that the result in our first two publications is incorrect [81], [275]). Assume that the mean of M sounder samples that fall within the jth ARI circular footprint are used to represent the coincident sounder estimate of the ARI measurement, Equation 7, where the spatial uncertainty associated with each spectral sample y is Gaussian with standard deviation σ_j.

$$C^{SDR} = \frac{\sum_{i=1}^{M} y_i}{M}$$

Equation 7

Then, to make use of the statistical properties of sounder samples, it is assumed that the Big Circle representing the ARI measurement can be exactly filled by N sounder samples (think of it as geometrically a big square with aligned square sounder FOVs). The Big Circle mean measurement representing ARI can be written as:

$$C^{ARI} = \frac{\sum_{i=1}^{N} y_i}{N}.$$

The variance of the difference for a given intercomparison j is then:

$$Var(C^{SDR} - C^{ARI}) = Var\left[\frac{\sum_{i=1}^{M} y_i}{M} - \frac{\sum_{i=1}^{N} y_i}{N}\right] = \frac{s_j^2}{M} - \frac{s_j^2}{N} = \left(1 - \frac{M}{N}\right)s_j^2/M$$ *Equation 9*

Note that this form for the variance (or square of the uncertainty due to sampling differences) makes physical sense, because the sampling uncertainty goes to zero when M = N and blows up when there are no sounder samples ($M = 0$).

This spatial sampling error formalism can be used, combined with noise and similar temporal sampling error estimates, to optimally weight mean SNO differences [81]. The weights are the normal inverse of the total error variance [w_j = 1/(total error variance for SNO$_j$)], and yield a rigorous uncertainty estimate [$=1/\Sigma w_j^{1/2}$]. This approach results in a rigorous mean difference and uncertainty, *with no clear sky selection or other SNO filtering*.

Finally, applying this technique shows that a single CLARREO in a true polar orbit can achieve intercalibration uncertainties for the CrIS and AIRS sounders (for which *M/N* =0.55) of less than 0.05 K in 6 months, even assuming a reasonably large CLARREO noise and for a window channel where spatial non-uniformity is largest (see Figure 8.18). Similar levels of performance would be expected when applied to intercalibrate IASI.
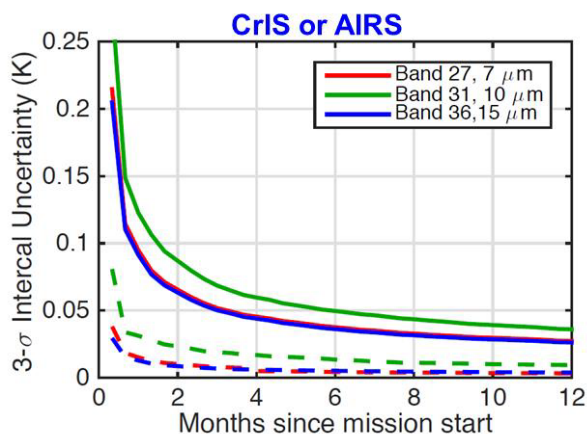

Figure 8.18 Simulated Intercalibration Uncertainty as a function of time since mission start for a single CLARREO polar orbit with 50 km IR footprints and 20 seconds between samples.

This shows that intercalibration can be used to transfer the higher CLARREO accuracy, proven on-orbit, to other concurrent sensors with rigorous traceability, and that a single ARI Pathfinder instrument could lead to a very important climate benchmark. Future ARI launches could then establish long-term trends with unprecedented accuracy.

§8.1 Authors: **Dave Smith[1]**, **Dan Peters[1], Tim Nightingale[1], Jonathan Pearce[2], Radka Veltcheva[2]**, Science and Technologies Facilities Council / RAL Space, [2]National Physical Laboratory, Acknowledge funding from ESA and Eumetsat for SLSTR and UKSA CEOI for black body development work

§8.2 Authors: **Jack Xiong** and **Jim Butler**, NASA / GSFC

§8.3 Author: **Thomas S. Pagano[1]**, **Evan M. Manning[1], Steven E. Broberg[1] , Hartmut Aumann[1], Sharon Ray[1], Eric Fetzer[1], Joao Teixeira[1], Larrabee Strow[2]**,
[1]NASA / JPL, [2]University of Maryland under contract to NASA (80NM0018D004

§8.4 Authors: **Hank Revercomb, Fred Best, David Tobin, Joe Taylor, Jon Gero, Robert Knuteson, Douglas Adler, Claire Pettersen, Mark Mulligan, Robert Holz, Fred Nagle,**
University of Wisconsin-Madison / Space Science and Engineering Center

§8   Editor: **Nigel Fox**, National Physical Laboratory

9   Passive Microwave Measurements

9.1   Laboratory SI-Traceable Calibration Methods

Traceability of microwave-radiometer-measured brightness temperature to the SI physical temperature unit of kelvin is possible by laboratory and/or thermal-vacuum chamber measurements. This path of traceability can be achieved in three ways: (1) through calibrated temperature sensors embedded in a calibration target/load/blackbody; (2) through calibration with a brightness temperature source (noise diode) traceable to a primary or transfer standard that is, in turn, traceable to the SI unit of kelvin; (3) through inter-calibration of a common target with an SI-traceable radiometer. The challenge of these approaches is the rigorous uncertainty analysis required in propagating the added uncertainties associated with the pathway from the traceable reference to the resulting calibrated brightness temperature of the radiometer being calibrated.

According to the "Guide for Expression of Uncertainty in Measurement (GUM)" by the Bureau International des Poids et Mesures, the type B evaluation of uncertainty is:

> *method of evaluation of uncertainty by means other than the statistical analysis of series of observations*

which includes systematic errors. Traceability includes this type of uncertainty because it cannot be estimated from statistical analysis, and it relates a measurement back to fundamental units or constants. The following discussion uses type B uncertainty as the metric to estimate the potential error between the units of brightness temperature in kelvin to the fundamental physical temperature unit kelvin.

We begin with a discussion of the free-space or blackbody calibration method, then we discuss the guided-wave noise diode calibration methods, and we end with a mention of inter-calibration with a traceable radiometer.

9.1.1   Laboratory Traceability through Free-space Measurements

Maintaining traceability from a physical temperature sensor to the calibrated brightness temperature of a radiometer involves: firstly, a thorough characterization of the source uncertainty; secondly, a detailed understanding of the uncertainty arising through the coupling of the antenna and the source; and thirdly, a detailed understanding of the radiometer's uncertainty characteristics. Figure 9.1. shows a diagram depicting the traceability path from a free-space calibration target to the measured radiometer units of brightness temperature.
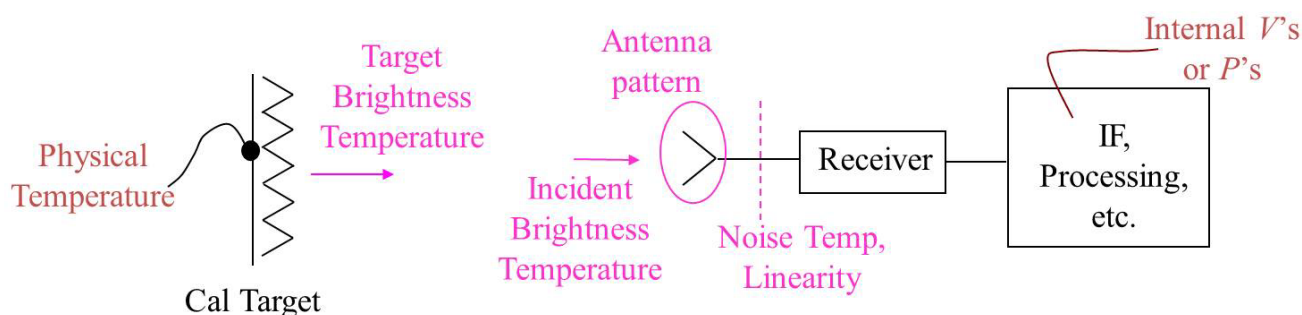

Figure 9.1. Diagram of Free-space Calibration Traceability Path

Quantifying the uncertainty associated with the brightness temperature radiating from a blackbody calibration source depends on the emissivity of that source and possible reflections off of this source,

as well as the physical temperature gradients in and on the absorber from which the microwaves are radiated.

Measuring the emissivity of a blackbody is perhaps the least understood aspect of blackbody characterization. To date, most characterizations of blackbody emissivity have been based on normal incidence monostatic reflectivity measurements such as in [276]. By making the assumption that a blackbody source is isotropic, one can infer the emissivity as the complement of the monostatic reflectivity. In reality, the validity of this assumption is geometry and frequency dependent and a monostatic reflectivity of -40 dB does not necessarily imply an emissivity of 0.9999 [277].

Electromagnetic simulations can provide the bistatic reflectance distribution function of a blackbody, which can then be integrated to estimate the total emissivity, but experimental measurement of this parameter is not fully realizable due to hardware geometry limitations. Finite-element electromagnetic simulations of blackbodies are computationally expensive and may be beyond the ability of even state-of-the-art high-performance cluster (HPC) computing at higher microwave frequencies [278]. The method-of-moments is the preferred EM solving method for simulating blackbody emissivity, and has shown promising results with lower computational expense [279]. Accurate quantification of a calibration blackbody source's emissivity remains one of the prevailing challenges to achieving SI traceability.

Emissivity is always a frequency-dependent parameter and is highly dependent on the absorber and blackbody geometry [280], [281]. Typical blackbodies use arrays of absorber-coated pyramidal structures, but these configurations are frequency dependent as a function of their pyramid physical dimensions. Alternative geometries such as the hollow inverted cone [282] or wedge [283] can provide high broadband emissivity, but come with the trade-off of high mass and volume (dis-advantageous for space-borne instruments). Figure 9.2 shows some of the aforementioned calibration target geometries. Even a high-performance blackbody source needs to establish traceability between an embedded temperature sensor and the calibrated brightness temperature of a radiometer. The theoretical groundwork for the brightness temperature uncertainty analysis of a hollow conical blackbody was demonstrated in [284], but the simulations have not been experimentally verified.
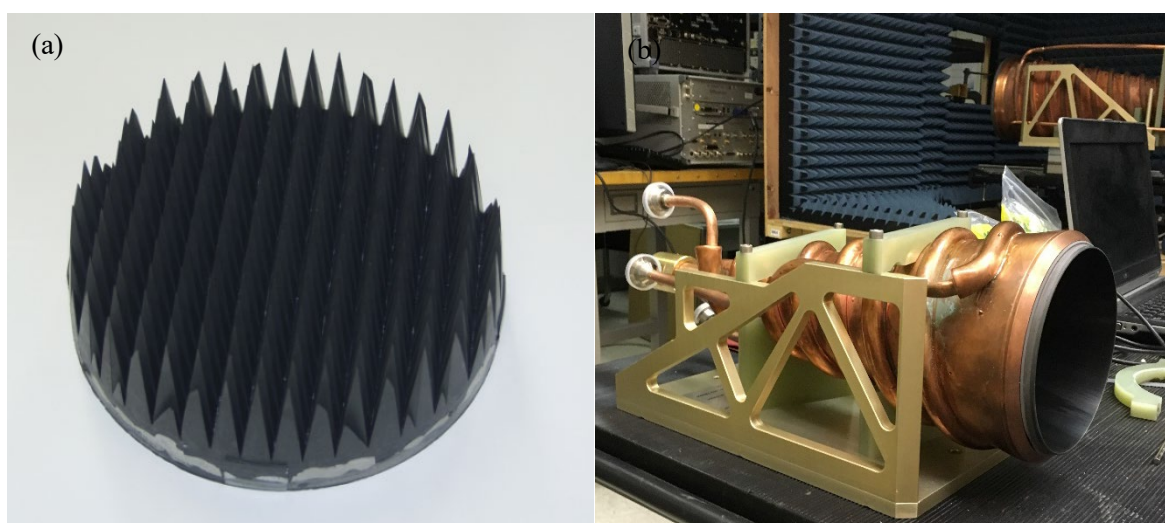

Figure 9.2: Blackbody calibration target geometries, (a) pyramid array (b) hollow inverted cones

Physical temperature gradients on and in the radiating volume are the second major concern and focus of the uncertainty analysis for achieving SI brightness temperature traceability. Temperature gradients

on space-borne calibration sources have been recognized and studied previously [285], [286]. In the lab, there is less concern of solar intrusion and more stable temperatures can be achieved, but physical temperature gradients on calibration loads are still of great concern and must be treated in an uncertainty analysis. Numerical finite element analysis [287], [288] or infrared imaging may also help in characterizing these gradients. In the vacuum chamber, reducing radiative heat exchange is of primary concern. Decoupling the IR radiation from the environment can be done with shrouds, insulation, and IR black microwave reflectors.

Though the uncertainty analysis for emissivity, physical temperature, and antenna coupling is time-consuming, this approach will likely result in the lowest type B uncertainty as it provides an in-depth understanding of the system, which allows for design optimisation. The following sections outline other approaches to achieve traceable brightness temperature measurements.

9.1.2   Laboratory Traceability through Noise Source Calibration

Traceable calibration of a radiometer can be achieved in the laboratory by using a noise source that is traceable to noise standards of a metrology institute. Two main challenges of performing guided-wave radiometer calibration are that the antenna and antenna switch path are not considered, and that noise sources can drift in time, increasing the uncertainty of the calibration. The antenna, cables, and switch must be well characterized including quantified antenna efficiency and spillover factor (also known as illumination efficiency [289]) and their associated uncertainty must also be known. The impedance difference between the noise source and the antenna will also vary the reflection of self-emission of the radiometer itself, causing a possible bias in the measured antenna temperature. A thorough description of noise-source calibration uncertainty is provided in [290].

9.1.3   Laboratory Traceability through Inter-Calibration with a Traceable Radiometer

The NIST-traceable noise radiometers were used to demonstrate traceable free-space brightness temperature measurements of a microwave calibration load in [291]. The multiple uncertainty contributors to the brightness temperature radiometric measurement results in a best-case uncertainty of 0.7 K in the 18-26.5 GHz band. This can be slightly improved by further decreasing the measurement distance as demonstrated in [292]. Still the minimum uncertainty from calibration with a traceable radiometer is on the order of 0.4 K at these frequencies. This is insufficient for any climate measurements where traceable calibration uncertainty is required at levels of <0.1 K, e.g. for SST.
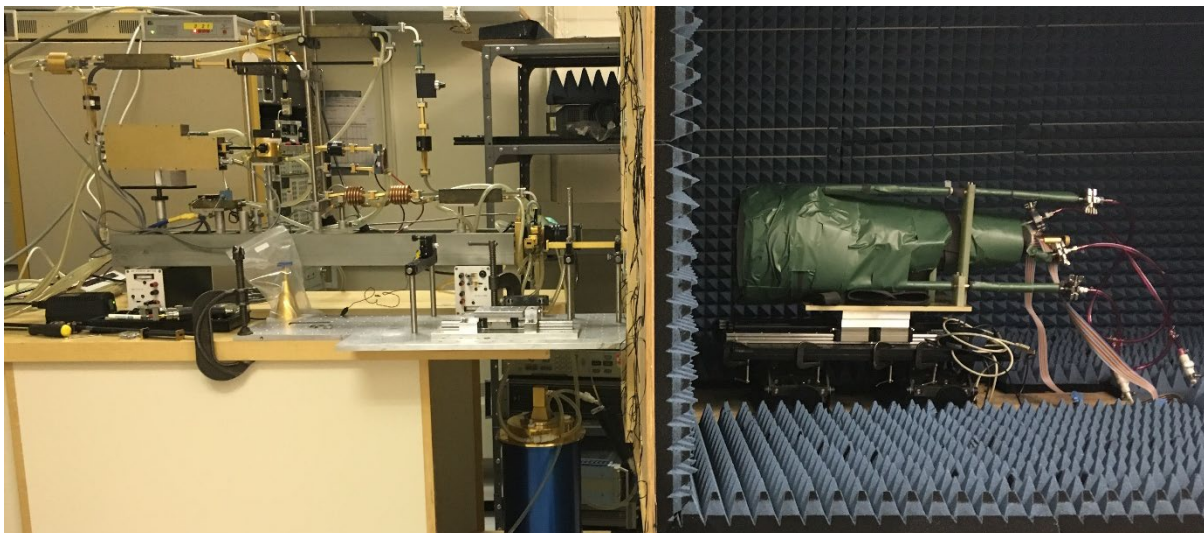

Figure 9.3. The NIST WR-42 waveguide radiometer viewing a conical blackbody target

9.2 Microwave Imagers and Sounders

9.2.1 On-board Calibration

Although microwave sounding instruments on weather satellites have been used to monitor global trends in atmospheric temperature (see the discussion by [293]), they were designed to observe weather phenomena. The requirements for the two types of measurement are different. Weather observations benefit from good spatial resolution (i.e. narrow antenna beams) and radiometric resolution (i.e. low noise) because individual measurements are assimilated into a numerical prediction model. For monitoring of climate, the measurements are spatially averaged and temporally smoothed, so calibration-related issues predominate in the error budget. For example, any non-linearity in radiometer response introduces scene-dependent errors with adverse consequences for the determination of long-term trends [294]. Therefore, a microwave radiometer designed as a reference instrument in a space-based climate observing system would differ in several respects from weather-satellite instruments. The antenna should have extremely low sidelobe levels; there is no trade-off with respect to a narrow beamwidth requirement as in the case of weather satellites. The radiometer should have excellent linearity and stability in both frequency and calibration accuracy, with on-orbit SI traceability.

> **Microwave sounders on current weather satellites are not optimised for climate applications**

> **Low sidelobes and high linearity & frequency stability are essential for climate applications**

To achieve those goals, the following design features [295], [296] are desirable:

a. A phase-locked local oscillator to prevent frequency drifts.
b. A low-sidelobe horn antenna without a reflector eliminates spillover of energy at the edge of the reflector. Then the radiometer section would rotate along with the antenna, to scan the Earth and also view cold space and an on-board blackbody target, as sketched in Figure 9.4.
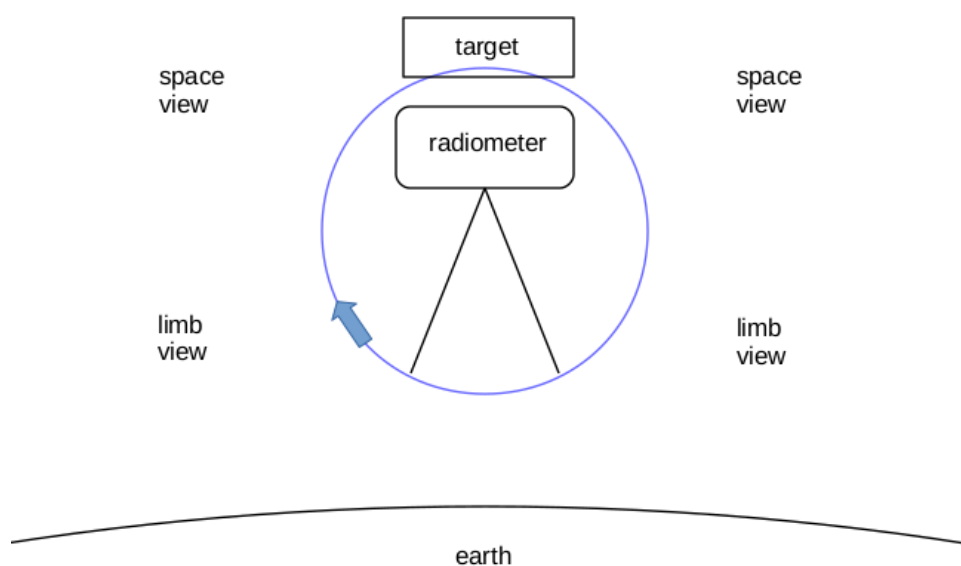

Figure 9.4 Radiometer/antenna/target scanning configuration.

c) Very linear amplifiers and detectors, with an internal noise diode to provide correction of residual non-linearity. Firing the noise diode at high and low calibration temperatures measures gain compression, without prior knowledge of the excess noise temperature of the diode [297].

d) Dual-polarization measurements, using two radiometers coupled to orthogonal modes of the antenna, to allow exact calibration of rotating-polarization instruments like ATMS, for channels sensitive to surface polarization. For channels not sensitive to the surface, the two polarization measurements would be averaged together.

e) Sensitivity to short-term gain fluctuations within the calibration cycle should be reduced by Dicke-switching or by some other means (instead of total power detection).

f) The scan should include the Earth limbs, for comparison of limb radiometric measurements to GPS radio-occultation (RO) measurements [295], as discussed below in Section 0. The use of radiometric measurements at the limb instead of closer to nadir will avoid the difficulties associated with a different geometry for radiometry than for RO (e.g., see [22]).

g) The orbit should be stabilized in altitude and facilitate inter-satellite calibration of instruments on several weather satellites. A 90°-inclination orbit [6], [81] samples the entire diurnal cycle, unlike the very slow diurnal drift which created problems with MSU and AMSU data [298]. Compilation of a climatology for the diurnal variation could reduce uncertainties in the trends of tropospheric temperature inferred from MSU measurements starting from 1979.

Non Sun-synchronous polar orbits can sample the entire diurnal cycle

Inter-calibration reference instruments do not need high spatial resolution

Reference instruments designed in this way could calibrate instruments on other satellites by combining several footprints of the other instrument, so the antenna beamwidth could be as large as several degrees. Except for (f), the above features would facilitate inter-satellite transfer calibration of microwave imagers as well as sounders. To serve as a calibration reference for ATMS, the reference instrument may need to duplicate only a few ATMS channels for each target on ATMS.

For the 50-60 GHz band, the radiometer characteristics listed in the table below should be achievable with currently available technology. This band has the advantages of smaller quasi-optic beam sizes and antenna apertures than the lower frequencies discussed in §9.1, allowing close coupling between the antenna and smaller on-board black body calibration targets, so that the target illumination efficiency is very nearly unity, which reduces the overall calibration uncertainties. In this case, the antenna aperture is the reference plane for calibration of antenna temperature; hence ohmic loss in the horn antenna does not contribute anything to the uncertainty budget. The first four values in Table 9.1 are $k=1$ uncertainties, while the last three should be interpreted as upper limits. Radiometer noise for a 400-MHz passband is 0.05 K at 1-s integration, but the actual integration time τ will depend on the scan rate. The long-term stability of calibration is discussed in the next subsection.

Table 9.1: Radiometer Characteristics for Microwave Radiometer Temperature Sounding Channels

Parameter	Value	Comments
(noise-equivalent ΔT) $\cdot \tau^{\frac{1}{2}}$	≤ 0.05 K s$^{\frac{1}{2}}$	for dual-polarization average
accuracy of calibration at launch	± 0.1 K	for antenna temperature
(long-term stability of calibration)·(time interval)$^{\frac{1}{2}}$	± 0.01 K yr$^{\frac{1}{2}}$	from [46]
lifetime frequency stability	± 1 MHz	with phase-locked LO
antenna 3-dB beamwidth	3-5°	from [295]
antenna stray factor $(1-\eta)$	≤ 1 %	>15° from center
antenna off-Earth stray factor	≤ 0.03 %	for nadir view
non-linearity max. deviation (before correction)	≤ 0.1 K	for $3 \leq T_A \leq 300$ K

9.2.2   GPS-RO Calibration Reference

The limb measurements in §9.2.1(f) would be referenced to microwave brightness temperatures inferred from simultaneous radio-occultation (RO) measurements of refractivity at the same elevation and azimuth angles, thus obtaining similar horizontal averaging of the atmosphere, as illustrated by Figure 9.5. (Elevation is equivalent to scan angle, and azimuthal alignment of the radiometer beam could be achieved either by adjustment of spacecraft yaw, or with a gimbal mount for the radiometer, see for example https://atmospheres.gsfc.nasa.gov/meso/index.php?section=121). This will measure long-term stability of the target's emissivity and temperature sensors, and also provides another way to monitor possible scene-dependent error over time, because limb brightness temperature varies with angle over a wide range.

> Microwave sounders scanning the Earth's limb can be tied to radio occultation measurements
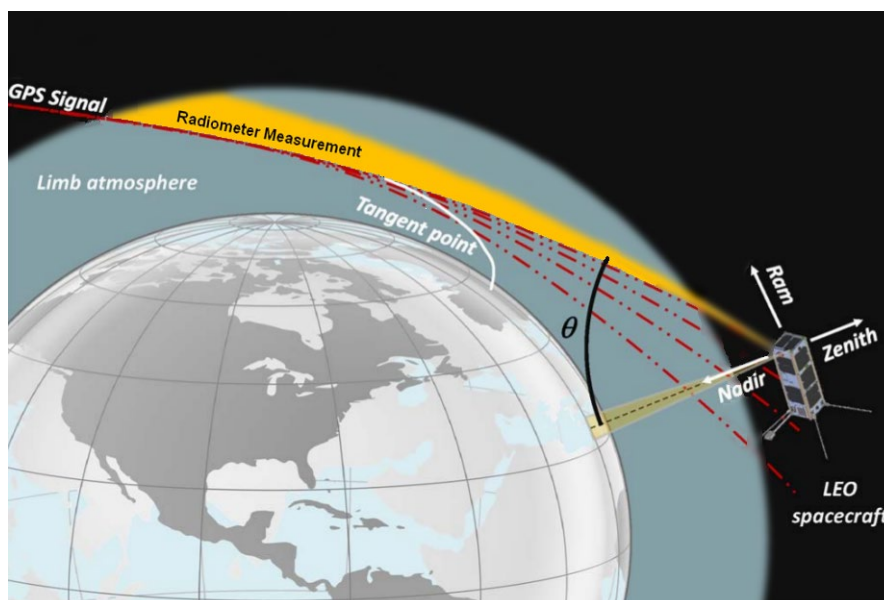
Figure 9.5 Basic geometry of GPS-RO microwave radiometer calibration [295].

Comparison with occulted GPS signals would depend on the atmospheric refractivity model and on the microwave transmittance model used to calculate brightness temperature. The refractive index of the atmosphere is typically modeled by an equation like this:

$$n = 1 + K_1 \frac{P_d}{T} + K_2 \frac{P_w}{T} + K_3 \frac{P_w}{T_2},$$

Equation 10

where K_1, K_2 and K_3 are constant coefficients, P_d is the dry-air partial pressure, P_w is the partial pressure of water vapor, and T is temperature in kelvin. In the stratosphere, where the atmosphere is very dry, refractivity is unambiguously related to the profile of temperature vs. pressure, which also determines the limb brightness temperature for opaque microwave frequencies. The troposphere generally contains more moisture, which varies independently of P_d and T. Consequently, these comparisons would be useful for channels in an O_2 band but less so for water or window channels. Surface emissivity is not a significant factor at the limb. Leroy *et al*. (2018) [299] recommend some changes to current RO retrieval algorithms to improve their tracking of temperature trends. However, the underlying measurement in RO is the additional Doppler shift of the GPS signal relative to that which would be observed in the absence of an atmosphere [300]. That Doppler shift is the time-derivative of phase delay due to refractive index along the atmospheric path, and it can be accurately measured [301]. The absolute accuracy of calibration would be attributable to the on-board target as launched, but if the computer algorithms are applied in a uniform way to a time series of measurements, then RO provides a stable reference to determine whether the on-board target's calibration is also stable. Rosenkranz *et al.* (2020) [46] show that calibration stability could be tracked to 0.01 K rms in a year, or 3 mK rms over a decade, using only a fraction of the potentially-available GPS occultations.

Although no physical mechanism causing changes in target components has been identified, their long-term stability in the space environment cannot be verified without reference to an independent standard. Ideally, GPS-RO comparisons would verify that the on-board calibration is stable over many years. But if those comparisons diverge over an instrument's lifetime, the trend derived from the radiometer could be adjusted accordingly. For the purpose of creating a multi-decadal time series, the traceability of radiometric calibration to RO will aid the precision of inter-satellite comparisons between reference microwave radiometers, when replacement is needed. Overlapping of instrument lifetimes would be less important and probably not even necessary.

9.2.3   Lunar Calibration for Microwave Instruments

9.2.3.1   Introduction

Lunar radiation is highly stable in the microwave spectrum because of the geophysical properties of the Moon's surface. Most space-borne microwave-sounding instruments can collect lunar radiation data from space-view observations during so-called lunar intrusion events that usually occur several days a month. For some miniaturized microwave instruments, a special lunar observation mode has been designed to enable lunar irradiance being taken as an important microwave source for on-orbit calibration. The NASA Time-Resolved Observations of Precipitation structure and storm Intensity with a Constellation of Smallsats (TROPICS) mission is a follow-on constellation of six 3U CubeSats based on the MicroMAS-2 design that is scheduled for launch in 2022. Each Space Vehicle (SV) includes a 12-channel scanning passive microwave radiometer in W-band, F-band, and G-band. The TROPICS mission's dual-spinner configuration provides a unique opportunity for solar and lunar calibration, as solar and lunar intrusions are periodic and occur every orbit [302]. In the future, if an SI-traceable microwave source is available and can be transferred to an instrument like MicroMAS, the Moon can be used as an SI-traceable calibration reference for microwave instruments to evaluate the calibration accuracy and assess the long-term calibration stability. The goal of this paper is to establish a general framework for microwave lunar calibration, based on lunar observations from current operational microwave radiometers. The method and results developed here could be further improved when more reliable and accurate observations are available from an advanced traceable microwave radiometer in the future.

Major challenges of using the Moon as a radiometric standard source for microwave sensors include the reliability of measurements of the microwave brightness temperature (T_b) spectrum of the lunar surface, knowledge of the lunar phase lag because of penetration depths at different detection frequencies and accurate knowledge of radiometer's antenna pattern. Microwave radiation can penetrate the lunar sub-surface, so microwave thermal emission in terms of T_b can be different from the skin temperature. Previous studies have shown that due to the special structure of the Moon's surface and the penetration characteristics of microwave radiation, the maximum microwave emission from the Moon typically lags behind the maximum temperature when the Moon is full. The lag angle depends on the ratio of the physical thickness of the emission layer to the penetration depth [303]. Satellite-based lunar observations are valuable because of the high accuracy and stability of space-borne microwave instruments. Unlike ground-based observations, spaceborne microwave radiometers can cover a wide range of frequencies and experience less contamination from their surroundings. In the most recent studies by Yang et al. [304], [305] and Burgdorf et al. [306], [307], well-calibrated satellite observations were used to derive the lunar microwave T_b spectrum from 23 GHz to 183 GHz. Their results show that the maximum lunar disk-integrated T_b varies from 270 K at 23 GHz to 300 K at 183 GHz. The phase lag also changes from 40° at 23 GHz to 12° at 183 GHz.

The following subsections provide an overview of microwave lunar calibration studies. The general retrieval algorithm for microwave lunar T_b is introduced and the T_b spectrum and Moon phase lag derived from different satellites are presented. The uncertainties in satellite-observed lunar Tbs are also discussed.

9.2.3.2   General Description of Satellite Lunar Microwave T_b Retrieval Algorithms

When the Moon appears in the satellite observation field of view, the effective microwave radiance of the Moon's disk, R_{moon}^{eff}, can be derived from the receiver output counts difference between the clean space view and the space view with the lunar intrusion [304]:

$$\Delta R = \frac{1}{G} \cdot \Delta C \qquad \textit{Equation 11}$$

where G is the instrument calibration gain, and ΔR is the difference between R_{moon}^{eff} and the cosmic background microwave radiance R_C:

$$\Delta R = R_{moon}^{eff} - R_C \qquad \textit{Equation 12}$$

For most weather satellites with an orbital altitude of ~830 km, the apparent angle of the lunar disk is ~0.55°, which is much smaller than the antenna beam width. In this case, the effective lunar disk radiance can be expressed as a function of the antenna response G_{ant}, the normalized solid angle of the Moon Ω_{moon}, and the average disk-integrated lunar radiance as follows [304]:

$$R_{moon}^{eff}(\theta, \varphi) = \frac{\Omega_{moon}}{\Omega_p} \cdot G_{ant}(\theta, \varphi) \cdot R_{moon}^{disk} \qquad \textit{Equation 13}$$

The antenna solid angle Ω_p and antenna gain term G_{ant} on the right side of Equation 13 are instrument-related parameters and will not change over time after the instrument is in orbit. The lunar solid angle term Ω_{moon} slightly depends on the position of the satellite in the orbital plane, which is highly predictable. Burgdorf et al. [307] showed that the $\frac{\Omega_{moon}}{\Omega_p}$ term could be determined by performing an analytical integration of the Gaussian function over the lunar disk when the Moon passes through the center of the antenna beam,

$$\frac{\Omega_{moon}}{\Omega_p} = \eta \cdot \left(1 - e^{-4 \cdot ln2 \cdot \left(\frac{r_{moon}}{FWHM} \right)} \right), \qquad \textit{Equation 14}$$

where η is beam efficiency, r_{moon} is the apparent angle of Moon, and FWHM is the full width at half maximum of the antenna beam. Therefore, once the effective lunar radiance is known from calibrated lunar observations, the lunar disk-integrated radiance R_{moon}^{disk} can be determined from Equation 13.

9.2.3.3 Retrieval Results of the Lunar Microwave T_b Spectrum

NOAA-20 is the follow-on satellite program of the Suomi National Polar-orbiting Partnership (SNPP) operated by NOAA, successfully launched on 18 November 2017. The Advanced Technology Microwave Sounder (ATMS) onboard NOAA-20 is a 22-channel passive microwave radiometer with frequencies ranging from 23 GHz to 183 GHz. Soon after launch, a spacecraft pitch maneuver operation was carried out, during which a perfect 2D lunar disk in a full-moon phase was captured by the ATMS deep-space scan. Based on well-calibrated lunar antenna temperature datasets, the disk-integrated lunar surface microwave T_b spectrum with frequencies from 23 to 183 GHz can be derived. Table 9.2 lists the microwave T_b retrieval results at the full-moon phase for each ATMS frequency. The retrieved Moon-disk-averaged T_b spectrum shows a strong frequency-dependent feature, i.e., increasing from 240 K at 23 GHz to 2930 K at 183 GHz at the full-moon phase [308].

Table 9.2 Lunar Microwave Tb 23.8–183-GHz Retrieval Results from AMSU-A/B/MHS

Center Frequency (MHz)	Beam Width (°)	$\mathbf{T_{b\,moon}^{Disk}}\ (\boldsymbol{\phi = 0^o})$ (K)
23.8	5.1	239
31.4	4.9	246
50.3–55.5	2.2	264
57	2.2	267
88.2	2.1	275
165.5	1.1	290
183.3	1.1	293

The Fidelity and Uncertainty in Climate data records from Earth Observations project and the Global Space-based Inter-Calibration System considers the MHS onboard NOAA-18 a reference instrument, i.e., the biases of microwave sounders refer to the T_bs that the MHS onboard NOAA-18 would measure. This instrument was operational from May 2005 through October 2018. AMSU-B is part of the ATOVS sounding instrument suite. It is the precursor of the MHS onboard NOAA-18/19 and EUMETSAT's Metop satellites.

Satellite Channel / Centre Frequency (GHz)	ATMS	AMSU-B	MHS
89	16	16	H1
150/165	17	17	H2
183.3±7	18	20	H5
183.3±4.5	19		
183.3±3	20	19	H4
183.3±1.8	21		
183.3±1	22	18	H3

AMSU-B and MHS use the same method to measure the T_b of the Moon. Processing starts with the signal from the deep space view (DSV) from each scan taken during a time interval of several minutes around the appearance of the Moon. Because DSV signals are recorded in every scan at four different positions, there are four such curves, two or three of which receive enough flux from the Moon to fit a Gaussian with high accuracy. It is possible to convert the amplitude of the Gaussian to the radiance of the Moon if the full width at half maximum (FWHM) and the efficiency of the beam are known. Burgdorf et al. [306] provide details about the retrieval algorithm. Figure 9.6 shows lunar T_b retrieval results for 89 and 183 GHz from AMSU-B/MHS onboard NOAA-16,18,19 as well as Metop-A.
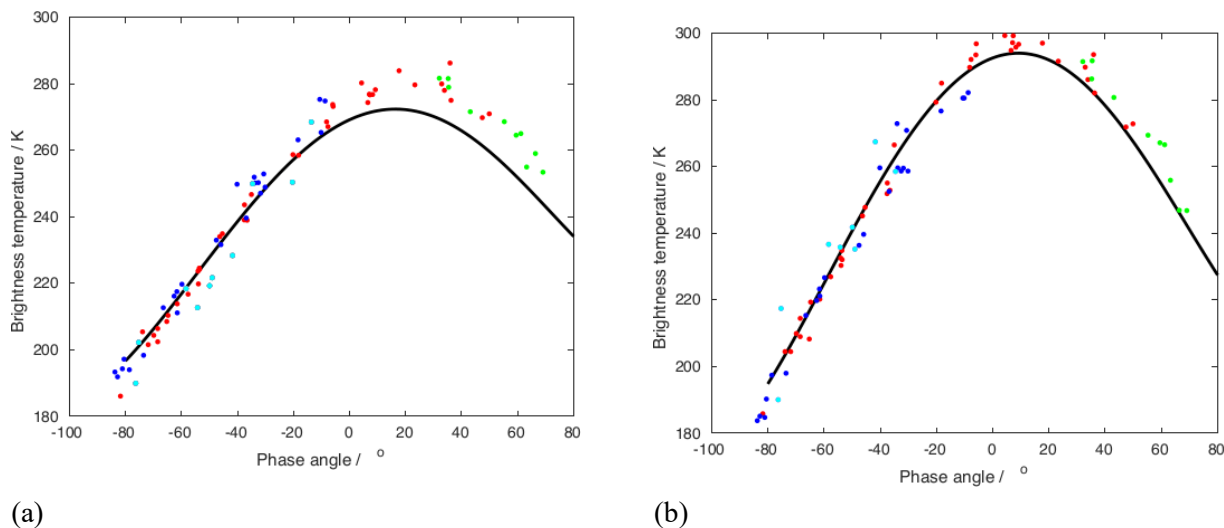
(a)   (b)

Figure 9.6 Disk-integrated T_bs of the Moon for different phase angles relative to the full Moon. Green: AMSU-B onboard NOAA-16, red: MHS onboard NOAA-18, magenta: MHS onboard NOAA-19, violet: MHS onboard Metop-A, black solid line: model by [309]. Frequencies are (a) 89.0 GHz (channel 16 or 1) and (b) 183.31 GHz (average of channels 18–20 or 3–4).

Measured Tbs were compared with model-simulated [309] disk-integrated T_bs of the Moon. At both frequencies shown here, the values measured with the microwave sounders show a higher maximum temperature and a larger phase lag between the full Moon and the occurrence of this temperature than the model. Subsequent analysis of the same observations with a more recent brightness temperature model of the Moon [310] reveals a further improved fit, with standard deviation of 2.0 K at 89 GHz, compared to 3.5 K from the above plots, and much reduced bias.

9.2.3.4   Lunar Phase Lag Angle Observed from the Drifting Satellite Orbits

For a Sun-synchronous, polar-orbiting Earth satellite, the Right Ascension of the Ascending Node (RAAN), equivalent to the local time of the ascending node (LTAN), determines the orientation of its orbital plane. For most current cross-track-scanning microwave-sounding instruments, the scan plane of instrument is perpendicular to the orbital plane. When the orbital LTAN is kept stable, lunar radiation can only be collected within a narrow range of lunar phase angles. With the rotation of the orbital plane around its orbital axis, lunar phase angles collected in the lunar intrusion (LI) events of the scanning instruments change consistently with the orbit LTAN. Taking an example of AMSU-A onboard NOAA-18 satellite, the mean lunar phase angle captured at each LI event changed from around -80° in 2005 to about 45° in 2019. Lunar radiation data samples collected over a large range of lunar phase angles enable the study of phase-angle-dependent features of lunar radiation, and more importantly, increasing knowledge about lunar phase-angle lags at microwave frequencies. To obtain information about lunar phase angle lags, all space-view data samples from different satellite orbits were collected. For each LI event, only those LI samples collected when the Moon passed through the antenna beam center were kept. Clean DSV counts were then identified and used to calculate the instrument calibration gain and do the internal warm calibration. Table 9.3 lists the lunar phase lags at different frequencies from low to high derived from AMSU/MHS [311].

Table 9.3 Moon phase lag angles and the maximum lunar disk Tb at microwave frequencies.

Center Frequency (GHz)	Peak Tb (K)	Phase Lag Angle (deg)
23.8	247	37
31.4	253	34
50.3	265	31
57	268	28
89	280	20
183 (MHS)	296	12

9.2.3.5 Conclusions and Future Work

The microwave T_b and phase-angle-dependent features of the Moon's disk are studied based on NOAA-20 ATMS and NOAA-16, -18, and -19 and Metop AMSU-A and AMSU-B/MHS lunar observations. Presented are retrievals of the T_b spectrum from 23 to 183 GHz. A strong frequency-dependent feature of the Moon's surface T_b was found. By examining lunar radiation samples collected from the drifting orbits of NOAA/Metop satellites, the phase lag feature of the Moon's surface microwave T_b was also studied at different frequencies. Current work shows that based on accurate spaceborne microwave radiometer observations, taking the Moon's disk as an SI-traceable calibration reference is possible and promising by building up a reliable microwave lunar radiation model. Future work will focus on studying the surface temperature conductivity and microwave emission properties of the Moon's surface and developing a comprehensive, physically based microwave T_b model for microwave calibration. In the future, if an SI-traceable microwave source is available and can be transferred to instrument like MicroMAS, the Moon can be used as an SI-traceable calibration reference for microwave instruments to evaluate the calibration accuracy and assess the long-term calibration stability. The method and results developed here could make further improvements when more reliable and accurate observations are available from advanced traceable microwave radiometers in the future.

§9.1　Author: **Derek Houtz**, Swiss Federal Institute for Forest, Snow and Landscape Research (WSL)

§9.2　Authors: **Philip Rosenkranz[1], William Blackwell[2], R. Vincent Leslie[2],**
[1]Massachusetts Institute of Technology (retired), [2]MIT Lincoln Laboratory

§9.2.3　Authors: **Hu Yang[1], Martin Burgdorf[2], Robert Vincent Leslie[3], William Blackwell[3], Edward Kim**[4],
[1]Cooperative Institute for Satellite Earth System Studies, University of Maryland,
[2]Universität Hamburg, Meteorological Institute, [3]MIT Lincoln Laboratory,
[4]NASA Goddard Space Flight Center, Maryland, USA

§9　Editor: **Tim Hewison**, EUMETSAT

10 Additional Applications

10.1 Weather

10.1.1 On the Need for SI-Traceable Calibration in Support of NWP and Reanalysis

Satellite level 1 calibrated radiances have been used by numerical weather prediction (NWP) centres since the early 90's to drive down errors in forecasts, analyses, and reanalyses. The initial state of the atmosphere from which the NWP model starts, also known as the

> **Satellite radiances used to initialise and constrain Numerical Weather Prediction**

analysis, is derived from Bayesian theory that gives the probability of the atmospheric state vector having a value x when the observation has the value y and can be expressed as:

$$P(x|y) \propto P(y|x)\,P(x) \qquad \text{\textit{Equation 15}}$$

where $P(y|x)$ is the probability that the observation has the value y given an atmospheric state x, and $P(x)$ is the prior probability of the atmospheric state, referred to as the background information. Here the prior probability of the observation is assumed constant (any y is equally probable).

Porting the Bayesian formulation into vector notation, assuming Gaussian distributed observation and background errors, Equation 15 can be decomposed as quadratic terms in a cost function $J(x)$ whose minimisation will give the most probable value of x, such as:

$$2J(x) = \left(x - x^b\right)^T B^{-1}\left(x - x^b\right) + \left(y - H(x)\right)^T R^{-1}\left(y - H(x)\right) \qquad \text{\textit{Equation 16}}$$

with

$$y = H(x^t) + \varepsilon^{obs} \qquad \text{\textit{Equation 17}}$$

and

$$x^b = x^t + \varepsilon^b \qquad \text{\textit{Equation 18}}$$

where x^t is the true value, H is the observation operator, and ε^{obs} and ε^b the errors in the observation and the background, respectively. R and B are the observation and background covariance errors, respectively, such as $B = <\varepsilon^b\left(\varepsilon^b\right)^T>$ and $R = <\varepsilon^{obs}\left(\varepsilon^{obs}\right)^T>$.

> **Empirical bias correction applied when assimilating observations into NWP**

Because the theory assumes that both model and observations are free from systematic error (i.e. $<\varepsilon^{obs}> = 0$ and $<\varepsilon^b> = 0$), observational datasets are supposed to be corrected before or during the assimilation process, while model errors are simplistically assumed small and neglected. In practice, the correction is applied on the difference between the observation and the model, which may include errors from both sides. Systematic errors in satellite observations can arise from calibration or instrumental issues, pre-processing, and/or the observation operator. Variational bias correction schemes (e.g. [312]) correct satellite radiances during the data assimilation cycle by adding a correction term to the observation operator based on bias coefficients β that are estimated during the variational analysis. The cost function is then solved simultaneously for x and β as follows:

$$2J(\boldsymbol{x}, \boldsymbol{\beta}) = (\boldsymbol{x} - \boldsymbol{x}^b)^T \boldsymbol{B}^{-1}(\boldsymbol{x} - \boldsymbol{x}^b) + (\boldsymbol{\beta} - \boldsymbol{\beta}^b)^T \boldsymbol{B}_\beta^{-1}(\boldsymbol{\beta} - \boldsymbol{\beta}^b)$$
$$+ \left(\boldsymbol{y} - \widetilde{H}(\boldsymbol{x}, \boldsymbol{\beta})\right)^T \boldsymbol{R}^{-1}\left(\boldsymbol{y} - \widetilde{H}(\boldsymbol{x}, \boldsymbol{\beta})\right)$$

Equation 19

with

$$\widetilde{H}(\boldsymbol{x}, \boldsymbol{\beta}) = H(\boldsymbol{x}) + b(\boldsymbol{x}, \boldsymbol{\beta})$$

Equation 20

and

$$b(\boldsymbol{x}, \boldsymbol{\beta}) = \sum_{i=1}^{N} \boldsymbol{\beta}_i \boldsymbol{p}_i(\boldsymbol{x})$$

Equation 21

where $\boldsymbol{p}$ is the vector of N bias predictors (e.g. constant offset, scan angle, or atmospheric thickness), $\boldsymbol{\beta}^b$ is the prior value of bias predictor coefficients, and $\boldsymbol{B}_\beta$ is the error covariance of the bias predictor coefficient.

Such a correction scheme performs well for the observations sensitive to well-defined atmospheric components and regions where the model bias is small and presents little variation. An important caveat

> **Unbiased observations assimilated without bias correction to anchor NWP model**

however appears where the model bias is not negligible. As the observations are corrected towards the analysis and the bias correction cannot disentangle model biases from biases in the observations, the bias correction will try to correct for a bias that originates from both the model and the observation and drift off in time to unrealistic values and propagate biases in the analysis [313]. To balance this effect, observations whose biases are much smaller than that of the model are assimilated without correction, adding a basic constraint on the bias correction. These are often referred to as anchor observations. In practice however, the current anchor observations are not sufficiently abundant (and/or not sufficiently unbiased) and bias correction drifts are still observed.

The optimal use of anchor observations could be guided by a better understanding of model biases. These biases are being investigated in radiance space through the mapping of temperature and humidity fields with a fast radiative transfer model [314]. Simulated top-of-atmosphere brightness temperatures derived from NWP model fields are compared to those derived from radiosondes traceable reference measurements of the Global Climate Observing System (GCOS) Reference Upper-Air Network (GRUAN). The propagation of both model and radiosonde uncertainties in radiance space allows the evaluation of the statistical significance of the observed bias following the methodology described by [315]. Here, the ratio of the brightness temperature difference between NWP and GRUAN, noted δy, and the square root of the total covariance, noted $S_{\delta y}$, is evaluated for each matchup such as:

$$\left| S_{\delta y}^{-1/2} . \delta y \right| < k$$

Equation 22

where k is the coverage factor that determines the confidence interval for normally distributed error probability. Here, we take $k=2$ to reflect a confidence interval of 95.5% or 2σ. Note that this test assumes that $S_{\delta y}$ is correctly defined.

Figures 10.1 and 10.2 show an example of ~15000 mid-latitudes matchups obtained between 2011 and 2017 simulated in the microwave and infrared domains together with the percentage of occurrences satisfying Equation 22 (i.e. no significant bias, NWP and GRUAN are in agreement). Statistics are summarised in Tables 10.1 and 10.2. For this example, NWP fields are from the Met Office global model and some profiles are discarded to avoid short or partial profiles. There is also a discrimination

between day/night due to a radiation sensitivity of the RS92 sonde to daytime radiation. In the spectral domain sensitive to temperature, the model is significantly biased in 14 % to 53 % of the comparisons, while in the spectral domain sensitive to humidity, a significant bias is found in less than 7 % of the matchups, owing to the much larger model uncertainty in humidity fields.

 Potential anchor observations should therefore demonstrate a bias significantly smaller than 0.01 K – 0.19 K in channels sensitive to temperature and significantly smaller than 0.12 K – 0.54 K in channels sensitive to humidity, with total radiometric uncertainty less than 0.06 K and 1.68 K, respectively.

The correctness of $S_{\delta y}$ can be further evaluated by the mean of a reduced Chi-square test (noted χ^2) as in Newman et al. (2020, Eq. 13) [316]. This test aims to evaluate the overall agreement between NWP and GRUAN profiles, for all channels under consideration including the inter-channel correlation. Results arising from a smaller albeit more recent sample (January – June 2020 from Sodankylä, Lindenberg, Singapore, Lauder, and Ross Island) suggest that in polar and mid-latitudes, the calculated χ^2 is close to its theoretical distribution. This reflects an overall good estimation of the total uncertainty, noting however that compensating effects may remain (for example, the lack of correlation term in GRUAN uncertainty is likely balance by a slightly overestimated NWP model uncertainty). In the tropics, the calculated χ^2 is significantly different (not shown) to its theoretical distribution, a sign that one or more component of χ^2 have been under-estimated, and/or there are missing unforeseen sources of uncertainty. More work is however needed to pinpoint the origin of this discrepancy.

Table 10.1 Microwave. Statistics showing (for left to right) the frequency (GHz) simulated (based on ATMS RTTOV coefficients), the number of collocations, the mean and standard deviation of δy for this sampling (K), the total uncertainty (K) (square root of $S_{\delta y}$ diagonal), the background uncertainty (K), GRUAN uncertainty (K), and the fraction of the sampling satisfying Equation 22.

| Frequency	Matchups	Mean	StDv	Total Uncertainty	NWP Uncertainty	GRUAN Uncertainty	Success rate (%)
54.94	13410	0.08	0.15	0.06	0.06	0.01	63.4
55.50	14860	0.13	0.17	0.07	0.07	0.02	66.5
57.29	15646	0.19	0.23	0.10	0.09	0.02	66.8
57.29±0.21	14795	0.19	0.25	0.11	0.10	0.03	54.1
183.31±1.0	13501	-0.54	1.98	6.32	6.30	0.15	98.1
183.31±1.8	13914	-0.38	1.78	4.86	4.84	0.14	97.2
183.31±3.0	14181	-0.24	1.55	3.44	3.43	0.14	95.5
183.31±4.5	14244	-0.18	1.36	2.50	2.47	0.20	95
183.31±7.0	14281	-0.12	1.18	1.78	1.68	0.37	93.6
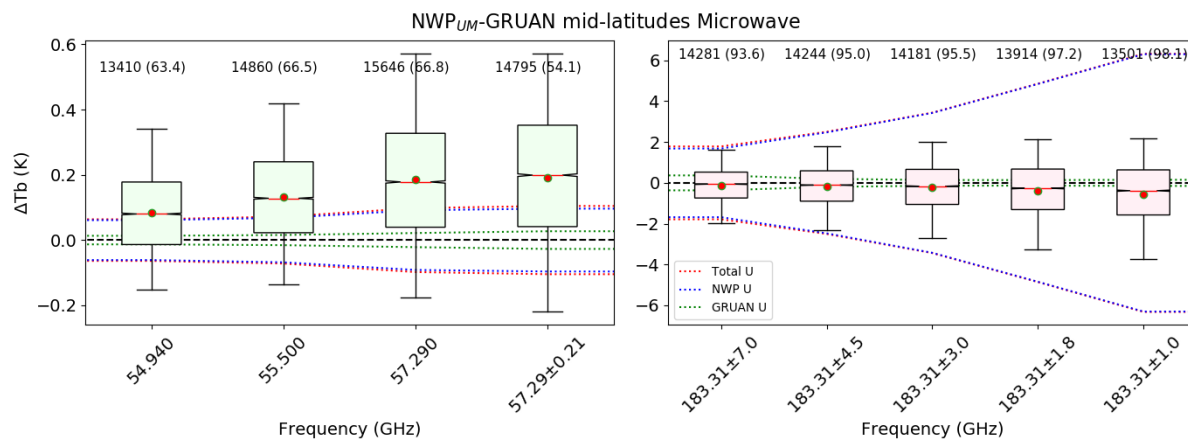
Figure 10.1: Microwave. Box plots showing the median (red line), mean (red dot), Q1 and Q2 quartiles, and 5-95% distribution (whiskers) of the difference NWP-GRUAN for mid-latitudes sites. Green boxes (left) show temperature sensitive frequencies, red boxes (right) show humidity sensitive frequencies. Dotted lines show the total uncertainty (diagonal of $S_{\delta y}$, red), the NWP component of the uncertainty (blue), and the GRUAN component of the uncertainty (green). Numbers on top of the boxes show the number of matchups and, between brackets, the percentage satisfying Equation 22.

Table 10.2: Infrared. Statistics showing (for left to right) the frequency (cm^{-1}) simulated (based on IASI RTTOV coefficients), the number of collocations, the mean and standard deviation of δy for this sampling (K), the total uncertainty (K) (square root of $S_{\delta y}$ diagonal), the background uncertainty (K), GRUAN uncertainty (K), and the fraction of the sampling satisfying Equation 22.

| Wavenumber	Matchups	Mean	StDv	Total Uncertainty	NWP Uncertainty	GRUAN Uncertainty	Success rate (%)
657.5	15513	0.17	0.22	0.09	0.08	0.02	47.9
696.0	14983	0.11	0.16	0.08	0.07	0.01	67.0
697.75	14888	0.09	0.15	0.08	0.08	0.01	89.5
706.25	15001	0.02	0.14	0.08	0.08	0.01	84.1
731.5	14925	-0.01	0.19	0.20	0.20	0.02	86.1
1367.0	14403	-0.15	1.24	1.91	1.90	0.13	93.2
1402.0	14403	-0.20	1.46	2.97	2.97	0.11	96.4
1408.0	14419	-0.17	1.37	2.49	2.48	0.11	93.0
1540.25	9901	-0.51	0.91	3.21	3.17	0.15	98.4
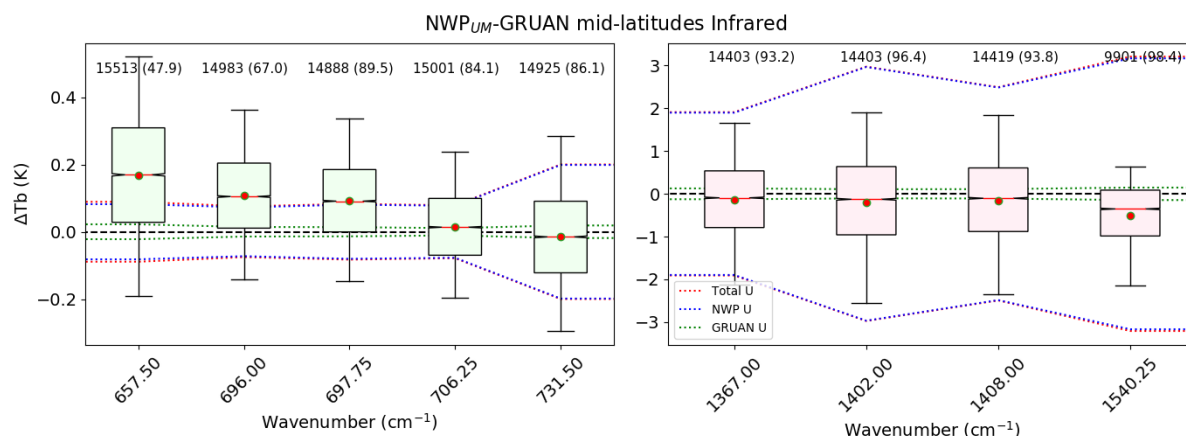
Figure 10.2: Infrared. Box plots showing the median (red line), mean (red dot), Q1 and Q2 quartiles, and 5-95% distribution (whiskers) of the difference NWP-GRUAN for mid-latitude sites. Green boxes (left) show temperature sensitive frequencies, red boxes (right) show humidity sensitive frequencies. Dotted lines show the total uncertainty (diagonal of $S_{\delta y}$, red), the NWP component of the uncertainty (blue), and the GRUAN component of the uncertainty (green).

Alternative strategies to mitigate bias correction drift are also being investigated in NWP centres. Constraining the variational bias correction with a term that penalises the size of the correction has been shown to be effective in limiting the drift while allowing for some correction of previously un-corrected observations [317]. This constraint takes the form of an additional term in the cost function that is tied to the bias uncertainty in the observation as follows:

$$2J(x,\beta) = \left(x - x^b\right)^T B^{-1}\left(x - x^b\right) + \left(\beta - \beta^b\right)^T B_\beta^{-1}\left(\beta - \beta^b\right)$$
$$+ \left(y - \widetilde{H}(x,\beta)\right)^T R^{-1}\left(y - \widetilde{H}(x,\beta)\right)$$
$$+ \gamma^2\left(b_o - b(x,\beta)\right)^T R_b^{-1}\left(b_o - b(x,\beta)\right)$$

Equation 23

where b_o is the prior value of the bias, R_b the covariance errors of b_o, and γ a regularization parameter. [317] suggests, for example, to link R_b to the uncertainty in the instrument absolute calibration.

> **Traceable observations with uncertainties needed to optimise NWP bias correction**

With this formulation, small observational bias uncertainties (R_b) result in a penalty term limiting the growth of the bias correction, while for large bias uncertainties, the variational correction has the freedom to evolve as if not constrained. For this approach to be applicable there is a clear need for traceable calibration with uncertainty characterisation of satellite datasets. The recent ECMWF-NWPSAF Workshop on Error Characterisation [318] emphasised that some existing observing systems, effectively treated as references, are still missing rigorous traceable uncertainty estimates (e.g. GNSS-RO). The Fidelity and uncertainty in climate data records from Earth Observations (FIDUCEO) project (http://www.fiduceo.eu/) aims for example to reprocess existing observations from raw satellite data to geolocated and calibrated radiances with traceable uncertainties from a set of different references at the pixel level. FIDUCEO uncertainty characterisation accounts for the physical basis of the sensing process, the on-board calibration system, and an estimate for the uncertainties arising from the processing, and therefore can be used in a constrained variational bias correction scheme for e.g. reanalysis. For near real time applications however, the estimation and distribution of data with uncertainties still needs further coordination between space agencies and data providers.

10.2 Cloud Radiative Forcing Feedback Uncertainty

10.2.1 Introduction

The uncertainty in climate sensitivity has remained nearly constant over the past 40 years, [107], [319], despite notable advancements in climate system modelling and research. Reducing uncertainty in equilibrium climate sensitivity (ECS) will provide humanity with greater confidence in climate change projections and their predicted accompanying economic

> Uncertainty in Earth's climate sensitivity is driven by uncertainty in cloud feedback: how the radiative effects of Earth's clouds will change over decades

impacts. ECS is the global annual mean surface temperature change in response to a doubling of atmospheric carbon dioxide concentration after the system has returned to equilibrium. Cloud feedback, in particular, the shortwave (SW) cloud feedback, is the dominant contributor to uncertainty in equilibrium climate sensitivity (ECS) [320]. Cloud feedback is the response of Earth's radiation budget to cloud changes in response to perturbations in surface temperature. Reducing uncertainty in SW cloud feedback will contribute to significant reductions in ECS and, ultimately, improve confidence in climate projections.

Observed cloud feedback can be estimated from trends in cloud radiative effect (CRE), that is, the difference between clear and all-sky top of atmosphere irradiance. Additionally, an understanding of the physical basis of CRE trends is dependent on understanding how the cloud properties that govern trends in CRE respond to changes in Earth's climate. Cloud properties that dominate the impact on SW CRE trends, and therefore SW cloud feedback, include cloud fraction, optical depth, and cloud microphysical properties. For LW CRE trends, cloud height is an additional critical cloud property. Consistency between these two methods of estimating observed cloud feedback would increase confidence in measured cloud feedback estimates. Studies have been conducted to better constrain climate sensitivity uncertainty and cloud feedback uncertainty from both of these perspectives. From those studies, some of which we summarize below, suggested measurement requirements for SW and LW instruments can be gleaned to ensure that future observations are sufficiently accurate to detect trends in critical climate change variables.

10.2.2 Challenges to Reducing Climate Sensitivity Uncertainty

An abundance of cloud property and TOA irradiance measurements have been made over the past two to three decades; however, the community has struggled to observationally constrain cloud feedback. There are several obstacles to this challenge, including Earth's natural variability dominating during mission lifetimes, absolute calibration verification on orbit, instrument calibration drifts, and differences in satellite viewing geometry and retrieval algorithms spanning different missions [321].

> Uncertainty of decadal change in cloud properties and radiative effects is dominated by uncertainty in instrument calibration

Recent advancements have improved our understanding of the physical bases of cloud feedback using techniques such as radiative kernels [322] and directly computing cloud effects [323]. Although some observational data sets and climate models agree on the sign of the global or regional SW cloud feedback, widespread disagreement remains regarding its magnitude. This remaining uncertainty suggests that there is a need for more accurate measurements of both cloud properties and top-of-atmosphere irradiance to better constrain cloud feedback uncertainty and verify the physical drivers for the sign and magnitude of observed and modelled cloud feedback [1], [323], [324]. This raises the question of the required measurement accuracy needed to accomplish the science target. We used a framework developed to

quantify the measurement requirements for climate change observations [6], [20], [325] [10] to estimate the calibration uncertainty needed to reduce climate sensitivity uncertainty over various periods of time. This method evaluates the impact calibration uncertainty has on climate variable trend detection times and takes into account the impact of data record gaps and instrument calibration drift.

10.2.3   Determining Climate Observation Requirements

The CLARREO Pathfinder (CPF) instrument (see §11.1) is being designed to have a radiometric uncertainty of 0.3% *(k=1)*. Additionally, the inter-calibration approach [79] that will be demonstrated as a part of the mission (see §11.1.4) has a requirement of 0.3 % uncertainty. A mission like CPF is a crucial step toward reducing trend detection times in critical climate variables that are needed to confront longstanding challenges such as the ECS and SW cloud feedback uncertainty. The TRUTHS mission (see Section 11.2) and potentially the CRABS mission (ref report section) will enable independent verification of the new accuracy level.

Figure 10.3 shows the time needed to achieve various trend uncertainties in cloud optical thickness trends and its estimated relationship to ECS [21]. The grey shaded region in Figure 10.3 shows the AR5 90% uncertainty ECS range [107]. The figure also shows a sample science objective, to reduce ECS uncertainty by a factor of two [12], denoted by the horizontal dashed lines. This ECS uncertainty range has been determined assuming that the optical depth trend uncertainty is reduced to the point such that ECS uncertainty is reduced by a factor of 2. The different curves in Figure 10.3 illustrate the impact that instrument calibration uncertainty (in the 0.65 μm band) can have on trend uncertainty and trend detection time. We focus on calibration uncertainty because it dominates among uncertainties in instrument noise, orbit sampling, and absolute calibration for global and annual climate trends [6].
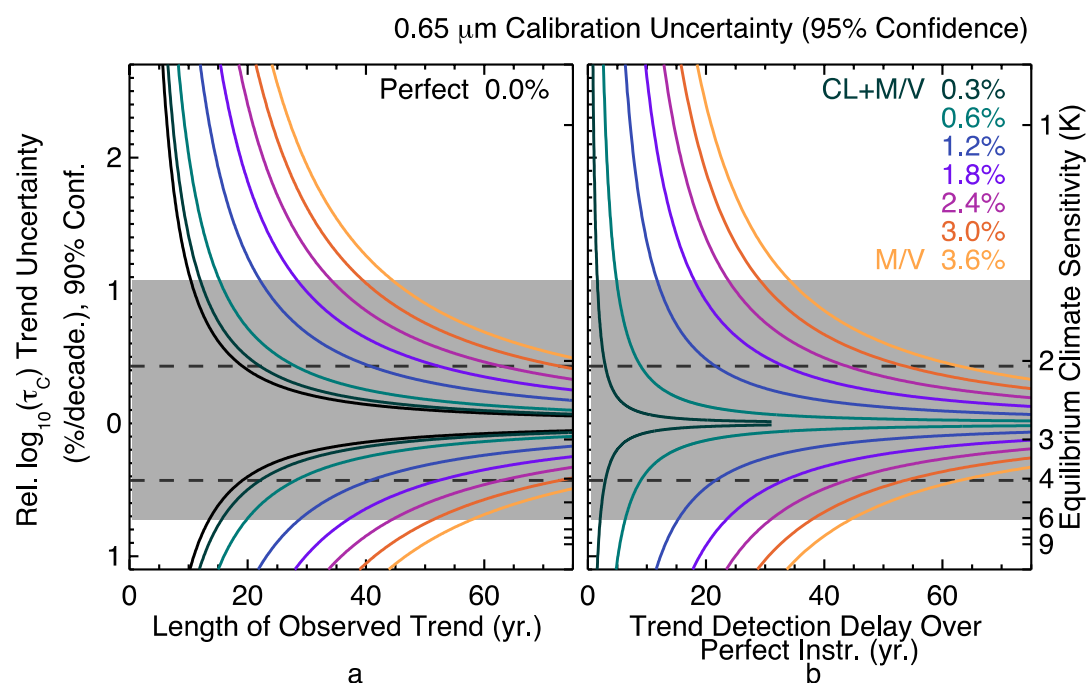

Figure 10.3 Cloud optical depth trend uncertainty and trend detection times based on radiometric uncertainty in 0.65 um band [21]. M/V indicates MODIS/VIIRS, CL+M/V indicates MODIS/VIIRS with intercalibration to CLARREO Pathfinder SI Traceability in orbit.

These results show that if only limited by natural variability (no other uncertainty sources) it would take about two decades to detect a trend in cloud optical depth that would achieve our sample science target. Continuing with measurements from existing process study-focused cloud imagers such as MODIS (Moderate Resolute Imaging Spectroradiometer) or VIIRS (Visible Infrared Imaging Radiometer Suite) it would take about six decades longer than the natural variability limit to detect such a trend. However, using a cloud imager inter-calibrated with an instrument maintaining an SI-traceable accuracy of 0.3%, (k=1) that delay would be reduced to only one decade longer than the natural variability limit. [21] demonstrated this approach for other cloud properties and other RS and IR cloud imager bands. The results for different cloud properties illustrate a similar reduction in trend detection time with notably improved radiometric calibration [21]. For example, infrared imager observations of cloud height or cloud top temperature require an accuracy of 0.03K *(k=1)*.

[6] conducted similar studies and showed that for broadband SW Cloud Radiative Effect (CRE) a 0.3% (k=1) radiometric calibration requirement would enable a factor of two reduction in CMIP3 SW CRE climate model simulation uncertainty and within about three decades (Figure 10.4) trends in CRE would be monitored using a broadband radiometer such as the Clouds and the Earth's Radiant Energy System (CERES) [76]. A comprehensive climate observing system likely needs to continue to include cloud imagers and broadband radiometers but must be augmented with SI-traceable on-orbit calibration standards.

> **Uncertainty in decadal trends of cloud properties and cloud radiative effects are used to determine key accuracy requirements of reflected solar and thermal infrared instruments**
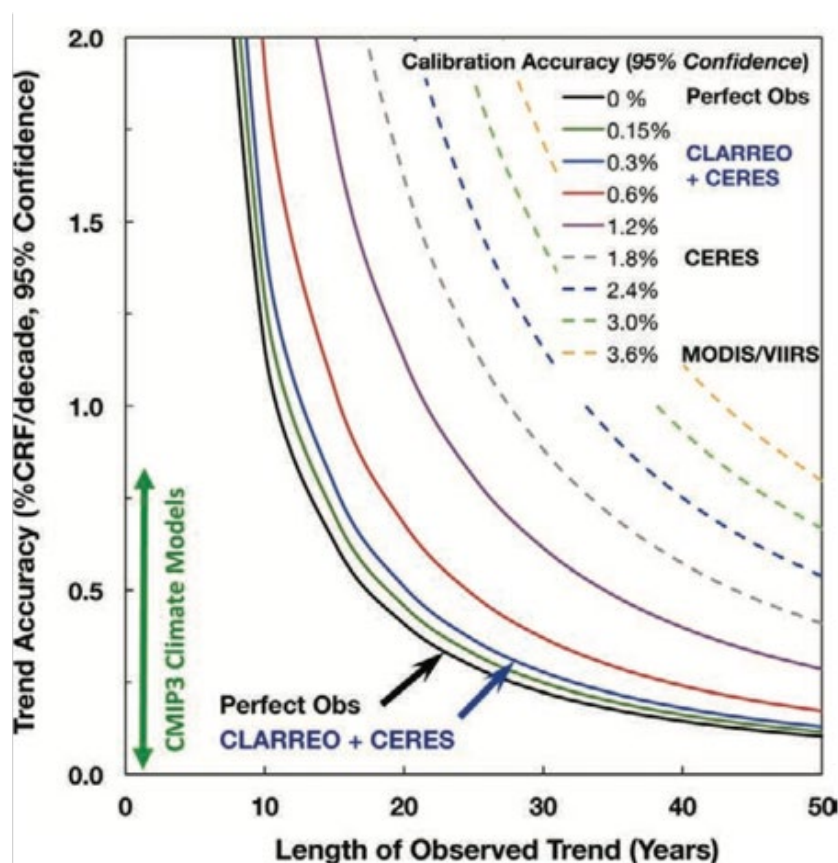

Figure 10.4 Trend uncertainty and detection times for shortwave (SW) cloud radiative effect based on broadband radiometric uncertainty.

This approach can be applied to other climate variables to quantify requirements for future climate missions. Additionally, the approach can be modified to determine requirements based on the natural variability and interactions of multiple climate variables simultaneously using multivariate analysis. To determine requirements, a science target or objective should be clearly stated, such as in our case reducing uncertainty in climate sensitivity with a focus on SW cloud feedback. A justification for a timeframe within which to achieve the stated science objective is also needed. That timeframe applied to this framework helps to define the relevant trade space for mission requirements needed to reach the stated science objective. This framework can be used to provide a clear quantitative justification for the resulting requirements and the impact of descopes.

As a final note, the results above do not include uncertainties due to satellite retrieval algorithm biases changing over decades. This is an additional source of uncertainty discussed in the NASEM 2015 Continuity Report [10], but to date, little research has been conducted on this topic. Such biases would have to be reduced using improved algorithms and not through satellite calibration improvements.

10.3   Land-Imaging Constellations

10.3.1   Mission Description and Current Calibration Methodologies

Land imaging constellations exist to monitor the land surfaces of the Earth in order to detect changes that may be occurring on both a short term (daily) and long term (decadal) basis [326], [327]. They may consist of only one or two instruments, such as MODIS which has two instruments [328], or of large numbers of similar instruments, such as Planet Doves which number in the hundreds [329]. Most of these sensors are in low Earth polar orbits with inclinations of around 98 degrees which allows them to maintain Sun-synchronous equatorial crossing times. Spatial resolutions vary, ranging down to a few meters/pixel to as large as one kilometre/pixel footprints. Temporal resolution also varies. Coarse resolution sensors such as MODIS can view the entire globe in only two days, while the Planet flock of Doves, by virtue of large numbers, observes the Earth on a daily basis. Systems such as Landsat and Sentinel 2 observe the globe on an approximately weekly basis. Much effort is being focused on harmonizing data from multiple sensors so that temporal resolution can be increased. This places an obvious and extreme emphasis on accurate calibration of sensors. Spectral coverage by these sensors varies widely. Small, low-cost sensors are based on silicon detectors and image in the visible and near-infrared (VNIR) portion of the spectrum—about 400-1000nm. Larger, more expensive sensors will image in the VNIR and shortwave infrared (SWIR) from 1000-2400nm. There are also several instruments that image in the thermal regions from 8000-12,000nm. In general, most of the sensors are multispectral in nature, though a few hyperspectral instruments have flown and more are expected in the near future.

A subset of land imaging sensors are those whose main purpose is to obtain observations of the Earth's surface for scientific analysis. Examples include Landsat, MODIS, and Sentinel 2. These instruments are designed and built for long term use and a high degree of radiometric accuracy and stability [33], [330], [331]. They have onboard calibration systems consisting often of diffuser panels, lamps, and stability monitors. Current prelaunch capabilities can provide a laboratory calibration on the order of 2-3% for these devices [332]. Recent advances in laser-based calibration, such as NASA's Goddard Laser for Absolute Measurement of Radiance (GLAMR) shows promise to improve uncertainties further [333]. However, despite ever improving ground-based calibration, the launch event adds uncertainty to the calibration of any spaceborne sensor.

As an example of these sensors, Figure 10.5 shows the degradation that has occurred in Landsat 8, Band 1, over the lifetime of the instrument [334]. In this example multiple calibration devices and methods are shown including lamps, diffusers, and lunar calibration. It can be seen that after almost five years

of operation there has been about a 1.5% decrease in sensor responsivity. Furthermore, there are indications that the working lamps and working solar diffuser are beginning to show signs of aging as compared to the backup lamps and diffuser that are used more sparingly. It is clear that even with an instrument built for long term science research, it is necessary to monitor its calibration on a regular basis. In addition, the only tie to SI traceability is prelaunch measurements.
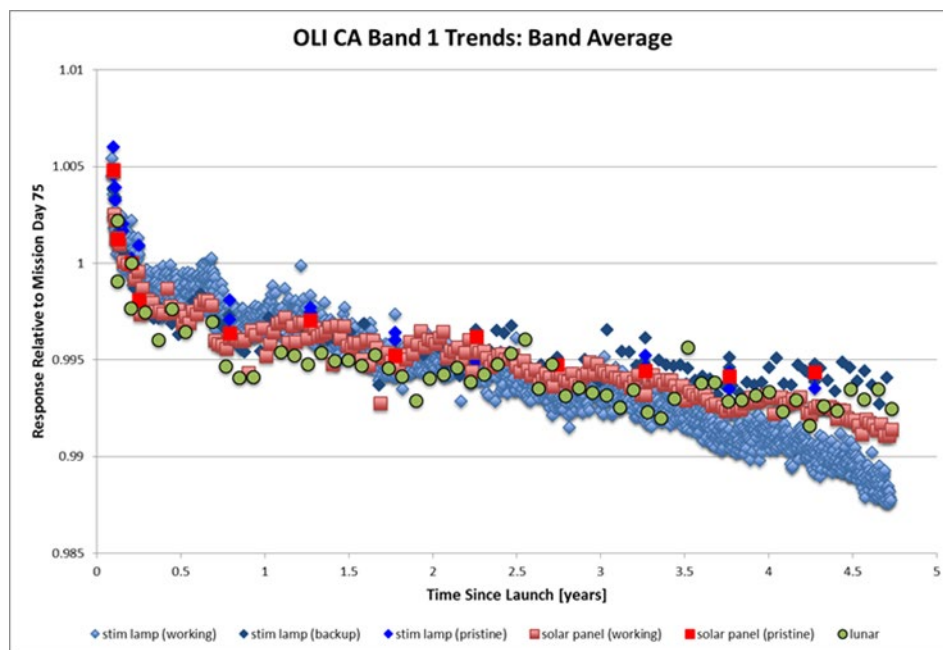

Figure 10.5: An example of long-term sensor stability using Landsat 8 OLI. Note the overall change in responsivity, about 1.5%, is quite small, but still represents a need for both on-orbit stability monitoring as well as a need for continuous absolute radiometric calibration.

> **The best land-imaging sensors have SI-traceable uncertainty of 2 to 5% ($k=1$)**

Commercial sensors often fly with limited onboard calibration capability, with many of the smaller sensors solely relying on vicarious methodologies (see Section 7.4) for both absolute radiometric calibration as well as stability monitoring. These sensors must closely monitor stability as well as radiometric accuracy in order to establish accurate calibration of their observations. This need is further compounded due to size and cost constraints that lead to significant drift in sensor responsivity as well as short lifetimes. Development of an SI traceable spaceborne radiometer would be especially attractive for these systems.

A major effort by the global remote sensing land surface monitoring community is directed towards data harmonization [335], [336]. The idea is to combine data from as many sensors as possible to improve the number of measurements being made over sites of interest. Accomplishing this requires development of methodologies to compensate for differences in sensor design, view times and angles, illumination differences, and spatial resolution to name a few. One of the most important is to have consistent radiometric calibration between sensors. Currently this is often performed through inter-comparisons between sensors with one sensor ultimately being chosen as the reference sensor. Launch of an independent reference radiometer would be a major step forward in developing harmonized data sets that are not only consistent, but also SI traceable.

Currently capabilities for the major science quality sensors in orbit are on the order of 2-5% absolute radiometric calibration, with precisions that can be significantly better (see Figure 10.5) [33], [34], [337]. However, each of the sensors in this category is calibrated to its own standard; this often leads to

greater uncertainties in the cross-calibration of sensors. Only limited efforts exist to date towards developing prelaunch cross-comparisons. With regard to commercial sensors, the claims on absolute radiometric calibration vary widely; some claim accuracies in the 3-5% range while others claim no better than 15%. A spaceborne calibration capability would serve this community especially well.

10.3.2   Science Drivers

As land surface imaging sensors have improved over the years, science capabilities have improved as well. Current requirements on the calibration of these sensors are driven by several science areas; two are briefly presented as representative of the opportunities that would exist with improved calibration.

Surprisingly, with calibration uncertainties pushing into the 2-3% range, those who are studying water are beginning to use land remote sensing systems to pursue their science [338]. In a recent workshop it was stated that a 1% calibration offset in the blue bands will yield a 10% error in retrieved reflectance over water [336]. Figure 10.6 shows an example of the difficulties in deriving standard water products from Landsat and Sentinel 2 sensors. Driving the calibration of land remote sensing instrument down to 1% will be virtually impossible without a spaceborne radiometer that can be used in-orbit on a regular basis.
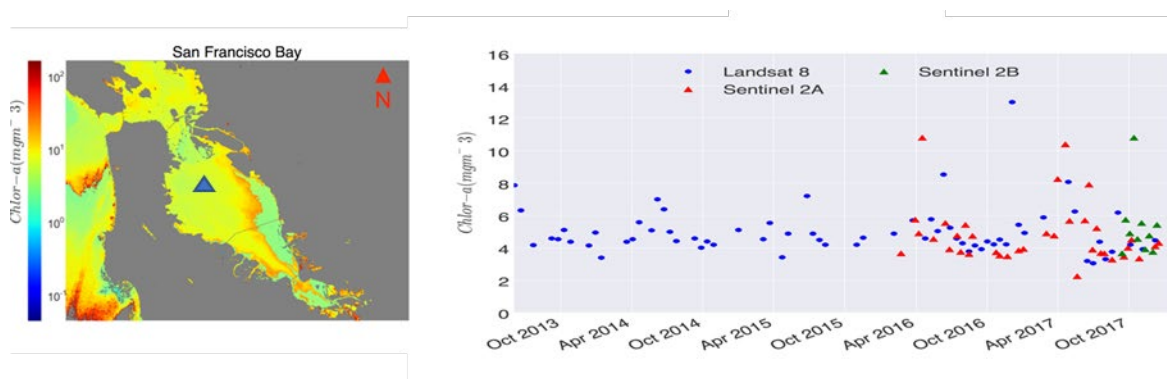

Figure 10.6 Time-series of chlorophyll-a products derived from Landsat-8 and Sentinel-2A/B [336]

A second area of science that would benefit significantly with improved calibration is the data harmonization community [339]. In many cases, sensors are calibrated prelaunch to differing standards, and then drift after launch exacerbating the calibration problem. An example is shown in Figure 10.7 where Landsat 8 and Sentinel 2 sensors are being used to study alfalfa cropping patterns. It is very clear that with the increased temporal resolution available from multiple sensors, it is much easier to ascertain the growing and harvesting events. However, close examination also reveals a consistent offset between the sensors. Most groups looking at Landsat/Sentinel 2 cross-calibration agree that the differences are in the 1 % - 3 % range depending on spectral band. A spaceborne reference radiometer could greatly improve data harmonization.
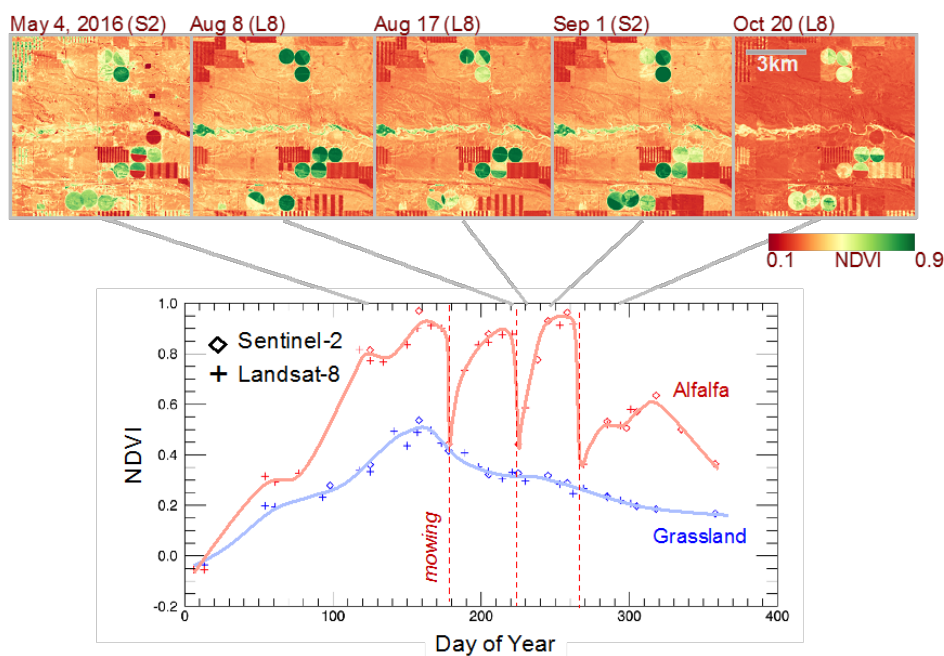
Figure 10.7 Data harmonization of Landsat 8 and Sentinel for alfalfa [327].

10.3.3   Opportunities with an SI-Traceable Satellite Radiometer

From the land remote sensing point of view, several highly desirable outcomes occur with the availability of a spaceborne SI traceable reference radiometer. Chief among these is the obvious cross-calibration capability that will exist with such an instrument. If the reference radiometer is placed in an orbit that complements common polar orbits for most of these sensors, the opportunity for simultaneous nadir overpasses (SNO) exists. These occur when the orbit paths intersect between the reference radiometer and the land remote sensor at the same location and at nearly the same time. This ensures that the same illumination occurs for each sensor, and the atmospheric effects are common to them as well. If the two sensors also have similar viewing angles, then a very accurate cross calibration can be performed; theoretical analyses have indicated an uncertainty of 1% or less. The limiting factor for this opportunity will be the frequency of these occurrences and the similarity of viewing angles. Thus, for small, low-cost sensors, SNO opportunities should be designed to occur with regularity and at varying latitudes in order to track sensor stability as well as calibration.

A second major area of improvement that would occur with a spaceborne reference radiometer is long term stability monitoring. All sensors degrade over time, and much effort is put into minimizing the degradation or carefully monitoring it. If a reference radiometer were in space whose performance was based on laboratory standards, stability could be monitored much more accurately than with existing methods where the stability of the onboard monitoring device is always a part of the total uncertainty of the measurement. Once again, depending on the sensor, temporal regularity will be key to successful stability monitoring.

Data harmonization, which was discussed briefly in the preceding section, will also improve dramatically. This can happen from two perspectives. First, as already described, sensors can be cross-calibrated to a standard SI-traceable sensor. This will eliminate two sources of uncertainty—differing prelaunch references, and uncertainty in degradation in space. With an appropriate reference sensor (<< 1% uncertainty), obtaining cross-calibration uncertainties of 1% or less will be achievable. Secondly, the reference radiometer itself will be imaging the surface of the Earth. If it is a hyperspectral instrument (i.e. with spectral bands useful for characterizing the atmosphere), it will be capable of providing surface

reflectance estimates of high quality. Most land remote sensing scientists today are interested in surface reflectance as opposed to top-of-atmosphere (TOA) reflectance. The reference radiometer will provide regular observations of the land surface that will be particularly useful for data harmonization purposes.

One of the limitations of a single reference radiometer in space will be the limited number of SNO opportunities. This will be especially significant for those sensors that are low cost, limited lifetime, with no onboard calibration, and exhibiting significant drift. One potential solution to this problem would be to develop a primary calibration capability with an SI-traceable radiometer in space, and then to develop a number of transfer calibration radiometers that would be placed in orbits to highly increase SNO opportunities for land remote sensors. These transfer radiometers would be built in a manner similar to the primary SI-traceable reference radiometer, but with relaxed calibration accuracy and stability requirements. The transfer radiometers would receive their calibration regularly from the primary radiometer and then through many SNO opportunities daily transfer their calibration to both science quality and commercial sensors. Because of the single function of these transfer radiometers, and their relaxed calibration requirement (~1% absolute radiometry, k=1), they can be built small and light, and be fairly low cost to place in orbit. A tier of transfer radiometers would be especially helpful to low-cost sensors with poor stability; and their presence could enable cheaper development of future sensors, both science quality and commercial.

10.4 Ocean Colour: Radiometric Uncertainty Requirements for Ocean Colour: Essential Climate Variable (ECV) Representing the Oceanic Natural Sink of Carbon

10.4.1 Requirements and Benefits

The oceans and land absorb more than half of the anthropogenic emitted carbon with the global ocean accounting for more than half of this total, largely through photosynthesis with microscopic lifeforms near the surface of the ocean. Reliable monitoring of this is a key requirement for climate science and mitigation strategies.

> **Ocean Colour is an ECV representing the aquatic natural sink of carbon**

Measurements of the sunlight reflected in the ocean, coastal and inland water bodies (water-leaving spectral reflectance) in the visible to near infrared region are used to map biogeochemical properties of aquatic ecosystems at temporal and spatial scales that are commensurate with scales relevant for the various ecosystem processes. Concentration of the main phytoplankton pigment, chlorophyll-a, is a pivotal product from ocean-colour data to study the carbon cycle, but additional products such as suspended particle concentration, absorption by coloured dissolved organic matter and phytoplankton diagnostic properties such as accessory photosynthetic pigments or size classes can also be derived from spectrally resolved water-leaving reflectance/radiances. These key products are used to assess aquatic primary production, sediment fluxes and the suitability of coastal and inland waters for bathing, food production and water extraction.

Phytoplankton absorb light through their pigments, and most of the absorbed energy is dissipated as heat, thereby influencing the depth at which solar heating occurs. Phytoplankton are at the base of the pelagic food chain, and are the food source, directly or indirectly, for all larger marine organisms, including fish. The variability in primary production and in phytoplankton seasonal dynamics has been shown to be relevant for understanding fisheries' variability.

Table 10.3: Specification for minimal spectral requirements for an ocean colour sensor

# 0	1024 – 1064 nm	width	30 nm
			(possible width 40 nm)
# 1	855 – 890 nm	width	20 nm
			(possible width 35 nm)
# 2	744 – 757 nm	width	14 nm
# 3	704 – 713 nm	width	10 nm
# 4	550 – 565 nm	width	10 nm
# 5	485 – 495 nm	width	10 nm
# 6	438 – 448 nm	width	10 nm
# 7	407 – 417 nm	width	10 nm

For global oceanic observations a spatial sample scale of around 300 m is generally adequate to meet sampling requirements but for coastal zones and inland waters higher spatial resolution becomes essential to not only deal with land boundaries but also to differentiate structures and features in the water bodies. Obviously, the higher spatial resolution the better but of course there is a trade-off against Signal to Noise. Similarly, from increased spectral discrimination, both in terms of spectral resolution and also number of bands.

Ocean Colour requires an extreme calibration effort

In order to help establish a coherent long-time base Climate Data Record for Ocean colour, the international community have defined a minimal set of observation requirements for ocean colour sensors, in particular, the choice of spectral bands: number, centre wavelength and bandwidth, see Table 10.3, [340].

Of all the ECVs related to surface waters that are amenable to remote sensing, water-leaving reflectance is the only one that pertains to the living component. For further details and applications, see [341]. It is vital to learn to make the best use of ocean-colour data, improve interpretation of the rapidly increasing volume of relevant satellite data and products, and to reduce uncertainties in products. One of the major challenges here is to ensure high fidelity in the radiometric quantities retrieved at the level of the water surface.

The uncertainties associated with state-of-the-art ocean-colour and lake water-leaving reflectance do not yet meet the GCOS requirements for climate-quality data records.

SITSats can complement efforts in ways that have not previously been possible

In particular, the uncertainty associated with removal of the atmospheric signal from at-sensor radiance records is high. Deriving a full uncertainty budget is challenging because of the large optical variability in global water bodies, while in situ reference data are relatively scarce and the separation of atmospheric and water-leaving radiance signals is subject to ambiguity (many potential solutions) and inter-sensor bias determination is limited to overlapping observation periods. The OC-cci and Lakes-cci projects of ESA will, in the course of their lifetime, produce refined versions aimed at better uncertainty characterization. However, well-calibrated high accuracy SI traceable sensors such as TRUTHS and CLARREO can complement these efforts in ways that have not previously been possible.

Requirements for the generation of a CDR of satellite-derived *water-leaving radiance* L_w from multiple ocean colour missions [342], include (a) Radiometric uncertainty of L_w lower than 5 % (equivalent to ~0.5% at sensor) in the blue and green spectral regions in oceanic waters (downscaled with respect to the spectrally independent 5 % uncertainty mentioned in several ocean colour missions); and (b) Stability of L_w better than 0.5 % over a decade. The uncertainty requirement is needed to understand

climate-driven processes and changes, while the stability requirement is essential to determine long-term changes or trends [1]. Achieving these requirements is limited by the uncertainty of the absolute radiometric calibration of satellite optical sensors (e.g., [343]–[345] indicates uncertainties >3 %) and by uncertainty affecting the quantification of atmospheric perturbations in top-of-atmosphere radiance L_T (e.g., [346] also indicates values exceeding several percent).

The effects of such uncertainties are currently minimized through the System Vicarious Calibration (SVC, [347]): that is the determination of vicarious adjustment gain-factors g (i.e., g-factors) for the absolute radiometric calibration coefficients of satellite sensors. These g-factors are given by the ratio of simulated to measured L_T values and aim at minimizing: (a) uncertainties due to the absolute pre-flight radiometric calibration and characterization of the satellite sensor after correction for sensitivity change with time; and (b) inaccuracy of the models and algorithms applied in the atmospheric correction to determine L_w from L_T.

Note that simulated TOA L_T are currently determined: (a) from *in situ* L_w reference measurements collected at ideal SVC sites (e.g., MOBY and BOUSSOLE); and (b) using the same atmospheric models and algorithms embedded in the atmospheric correction code applied to satellite data. It is important to recall that SVC leads to the determination of L_w with the lowest uncertainty when satellite observation conditions are equivalent to those characterizing the data applied for the calculation of g-factors. SVC also requires the re-computation of g-factors after any change in the models or algorithms applied for the atmospheric correction.

Thus, availability of L_T data with SI traceable uncertainties lower than 0.3 % (k=2) from a space sensor (e.g., TRUTHS) would permit calibration transfer to any ocean colour sensor looking at the same region with equivalent geometry, satisfying the absolute uncertainty GCOS criteria and moving some way to that required for decadal stability. The latter may be accomplished through a robust transfer of absolute calibration to a temporally stable source like the Moon, which may be able to deliver the longer-term stability requirement. This calibration-transfer through adjustment factor (i.e., a-factors) could be systematically performed at several ocean colour sites exhibiting high temporal and spatial stability and by virtue of its hyperspectral nature (allowing e.g. aerosols to be determined) may additionally permit investigating uncertainties in the atmospheric correction process as a function of the viewing geometry and marine/atmospheric properties. An analysis [348] has shown that a spectral bandwidth of 3 nm is ideally required to ensure a good spectral match for an OLCI like sensor and 1 nm for PACE when comparing surface-based measurements to satellite over oligotrophic waters, this relaxes by a factor of three for more complex waters. An analysis needs to be carried out to assess any variation on this requirement for similar ToA observations. An illustration showing the mathematics of this process can be found below.

10.4.2   Uncertainties in Water-Leaving Radiances

To investigate ocean colour calibration needs, the relationship linking uncertainties in L_w and L_T is examined through the use of its associated 'measurement equation'. Specifically, in the absence of atmospheric gaseous absorption, Sun glint and foam perturbations, the top-of-atmosphere radiance L_T can be related to the water-leaving radiance, L_w through the following simplified model:

$$L_T = L_R + L_A + L_w t_d \qquad \textit{Equation 24}$$

where L_R and L_A indicate the Rayleigh and aerosol atmospheric radiance contributions, and t_d is the diffuse atmospheric transmittance that varies with atmospheric path-length and constituents. By assuming the values of L_R and L_A are exactly determined for any given observation condition, following the *Guide to the Expression of Uncertainty in Measurement* [93], Zibordi and Voss [349] and Zibordi

et al. [347], provided equations linking relative uncertainties $u(L_T)/L_T$ to $u(L_w)/L_w$. Following their work, $u(L_T)/L_T$ is given by:

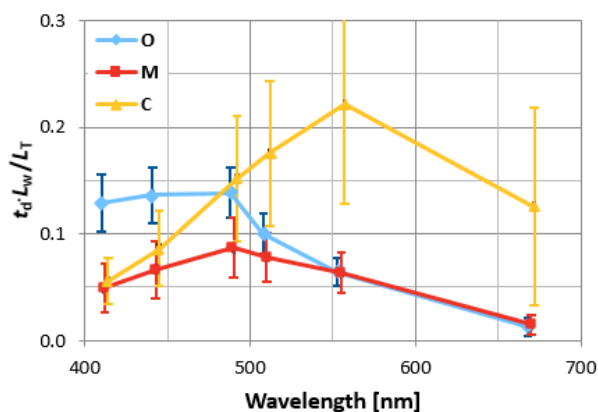$$\frac{u(L_T)}{L_T} = \frac{u(L_w)}{L_w} t_d \frac{L_w}{L_T}$$

Equation 25

Figure 10.8 Spectral values of td·Lw/LT for oligotrophic (O), mesotrophic (M) and coastal (C) waters. Mean values and standard deviations σ (indicated by the vertical error bars), result from the analysis of 814, 1487 and 1045 SeaWiFS data extractions, respectively. The centre-wavelengths between spectra have been shifted by ±2 nm to increase readability (after) [347].
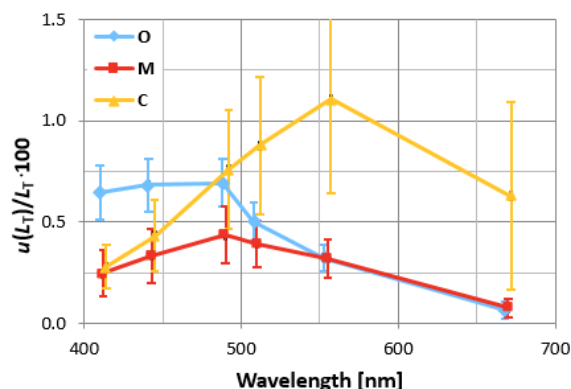
Figure 10.9 Relative uncertainties u(LT)/LT determined assuming a spectrally independent 5% uncertainty value for Lw with the mean values of td·Lw/LT given above for different water types: oligotrophic (O), mesotrophic (M) and coastal (C). The vertical bars refer to values determined with $t_d \cdot L_w/L_T \pm \sigma$ [347]

Equation 25 (and Figure 10.8 shows that relative uncertainties $u(L_T)/L_T$ and $u(L_w)/L_w$ are related to both marine and atmospheric optical properties which affect the term $t_d \cdot L_w/L_T$.

From Zibordi et al. [347], Figure 10.9 summarises the results from the application of Eq. 2 using identical spectrally independent relative uncertainties for *in situ* L_w (i.e., 5%). The derived values of $u(L_T)/L_T$ exhibit a significant spectral dependence and, as expected, are smaller when $t_d \cdot L_w/L_T$ is smaller (i.e., in correspondence with the lower values of L_w). Specifically, the lowest $u(L_T)/L_T$ are observed for mesotrophic waters with values included in the range of approximately 0.2-0.5% in the blue-green spectral regions and dropping below 0.1% at 670 nm. The values observed for the oligotrophic waters are higher in the blue spectral region with values approaching 0.7%. Using the higher values of L_w, $u(L_T)/L_T$ computed for the coastal waters reach 1.1% at 555 nm and 0.6% at 670 nm. It should be noted that differences in the observation conditions at the various sites or in the spectral values of $u(L_w)/L_w$, may lead to $u(L_T)/L_T$ different from those presented in Figure 10.9. Additionally, the relative combined uncertainty value of L_T determined from a number N of *in situ* L_w data obtained with equivalent observation conditions would decrease with respect to the value of $u(L_T)/L_T$ from an individual L_w due to the statistical averaging of the random component of uncertainties.
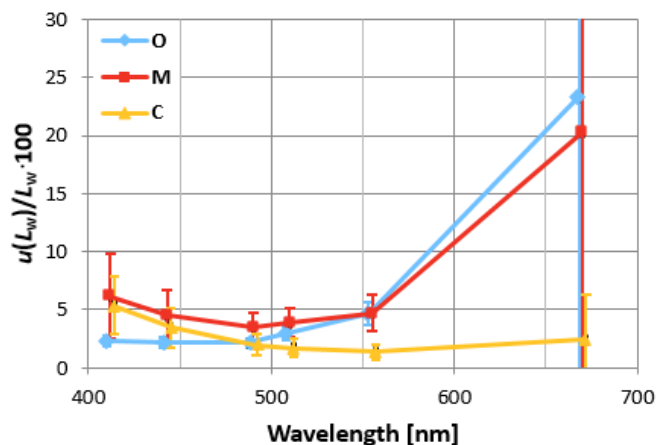
Figure 10.10 Relative uncertainties u(L$_w$)/L$_w$ determined assuming a spectrally independent 0.3% uncertainty value for L$_T$ and the mean values of t$_d$·L$_w$/L$_T$ given above for different water types: oligotrophic (O), mesotrophic (M) and coastal (C). The vertical bars refer to values determined with t$_d$·L$_w$/L$_T$ ± σ (after [347])

Rearranging Equation 25, relative uncertainties in satellite-derived L_w, can be investigated as a function of $u(L_T)/L_T$. By assigning a spectrally independent value of 0.3% to $u(L_T)/L_T$, results displayed in Figure 10.10 indicate that the 5% uncertainty requirement in satellite-derived L_w generally cannot be met in the red for oligotrophic and mesotrophic waters, and is challenging in the blue mostly at 412 nm for mesotrophic and coastal waters. Because of this, the 0.3% value assigned to $u(L_T)/L_T$, could be considered a rough upper threshold for the uncertainties of g-factors required to meet the 5% WMO [350] requirement for $u(L_w)/L_w$ in the blue-green spectral regions in oligotrophic waters.

> **SITSats could advance the achievement of GCOS requirements for the absolute uncertainty and decadal stability of ocean colour parameters**

The 0.5% stability requirement over a decade [350] for L_w accuracy entails maximum uncertainties of approximately 0.05 and 0.025 in a-factors, when assuming generic values of 0.10 and 0.05 for the term t_d·L_w/ L_T in the blue and green spectral regions. This result indicates the need for a long-term high accuracy reference with inherent stability in terms of radiometric performance from a space-based calibration reference such as TRUTHS/CLARREO to minimize perturbing effects in the determination of a-factors over time for different or successive missions. Whilst the stability requirements in radiometric gain from a space sensor are effectively limited to its absolute uncertainty at end of life, which for TRUTHS is 0.3 % (k=2), and is about a factor 3 greater than that desired for climate trend detection, the use of more stable references such as the Moon may enable this stability metric to be met.

If such a-factors are determined over different ocean locations and conditions whilst maintaining the oligotrophic criteria some statistical benefit from combining values may also be obtained. The hyperspectral nature of TRUTHS will help to provide improved consistent characterisation of the atmosphere, helping to constrain and anchor the retrieval algorithms of different sensors placing their results on the same SI scale. Additionally, comparisons can be carried out in coastal waters where more tailored a-factors can be obtained.

10.5   Atmospheric Trace Gases

10.5.1   Impact of Trace Gases (CO$_2$ and Water Vapour) on Climate

Trace gas retrievals from satellites also benefit from the improved SI-traceability made available from SITSats. Here we focus on the trace gases CO_2 and H_2O retrieved from near-infrared and shortwave-infrared sensors. These two are important atmospheric essential climate variables (ECV) which are needed to observe and understand the evolution of the Earth's climate.

Atmospheric trace gases such as carbon dioxide and water vapor are often observed using reflected-solar satellite sensors

CO_2 is the primary anthropogenic greenhouse gas and is of key relevance for climate. Its concentration in the atmosphere has increased due to human activities from a preindustrial level of 280 ppm to more than 400 ppm today, which has led to a change in the radiative forcing of 1.82 Wm^{-2} between 1750 and 2011 (out of a total radiative forcing of 2.83 Wm^{-2} [107]). The atmospheric growth of CO_2 is the result of an imbalance between emission (from both natural and anthropogenic sources) and sinks (which are currently purely natural). On average, only 44% of anthropogenic emissions remain in the atmosphere; the rest are taken up by the world's oceans and land ecosystems [351]. Thus, we need to understand the role of natural and anthropogenic contributions to the carbon cycle, their response to a changing climate on decadal timescales, and the future pathways for CO_2 emissions required to prevent damaging climate change. In response to the latter challenge, during the 2015 United Nations Climate Change Conference held in Paris, participants agreed to reduce global emissions of greenhouse gases to limit the increase in global surface temperature to 1.5°C. Amongst other actions, this includes the implementation of a transparent framework for monitoring the impact of the Nationally Determined Contributions (NDCs) and the global stock take be evaluated every 5 years beginning in 2023.

Water vapour is an essential greenhouse gas in the Earth climate system whose role in atmospheric processes extends over a broad range of spatial and temporal scales [352]. With a predominant capacity for positive feedback of around 2 $W m^{-2} K^{-1}$ [353] water vapour provides the largest amplification for anthropogenic climate change relative to other greenhouse gas radiative forcings [354]. Critical to the development of cloud and precipitation, water vapour also has a significant influence and impact on surface fluxes and radiative balance. Water vapour, however, is considered to be under natural control as it is sufficiently abundant and short-lived [355] but remains, nevertheless, a critical variable for climate studies [356], [357].

10.5.2   Operational and Research Uses

10.5.2.1   Research Climate Applications of Relevant Trace Gases

The first space-based observations of CO_2 columns became possible with the launch of the SCIAMACHY instrument onboard ENVISAT in 2002 followed by the first dedicated CO_2 missions, GOSAT and OCO-2, launched in 2009 and 2014, respectively.

The key measurement principle adopted by these missions is to measure spectrally resolved radiances over near-infrared and shortwave-infrared of O_2 and CO_2 bands, allowing the inference of CO_2 columns using the O_2 band to extract information needed to correct the variable path-length of light. To infer accurate CO_2 columns from the space-based measurements requires sophisticated retrieval methods (so-called full-physics retrieval algorithms) which have been developed by a number of groups around the world, including NCEO-Leicester (e.g. Cogan et al., 2012 [358]). These missions have for the first-time given global data on the distribution of atmospheric CO_2 with the coverage, sampling, and precisions required to constrain regional CO_2 surface fluxes via assimilation into an atmospheric transport model ('surface flux inversion'). In the UK National Centre for Earth Observation (NCEO), we use the Ensemble Kalman Filter data assimilation approach for the GEOS-Chem chemistry transport model

developed at NCEO-Edinburgh [359], which has already successfully demonstrated the new science insights that can be obtained from such datasets [360].

The information on surface fluxes resides in small spatial and temporal gradients of the CO_2 column distribution and already-small biases of the order of 1 ppm will substantially impact the inferred fluxes. Thus, high-quality and well-characterised datasets are needed, which is the goal of the GHG project of the ESA Climate Change Initiative (CCI). This project has produced ECV datasets from SCIAMACHY and GOSAT [361] and in the CCI+ phase includes also OCO-2 and TanSat. Furthermore, to fulfil the needs of the climate modelling community, an ensemble dataset EMMA and a Level 3 product (Obs4MIPS) has been generated (see Figure 10.11; [362]).
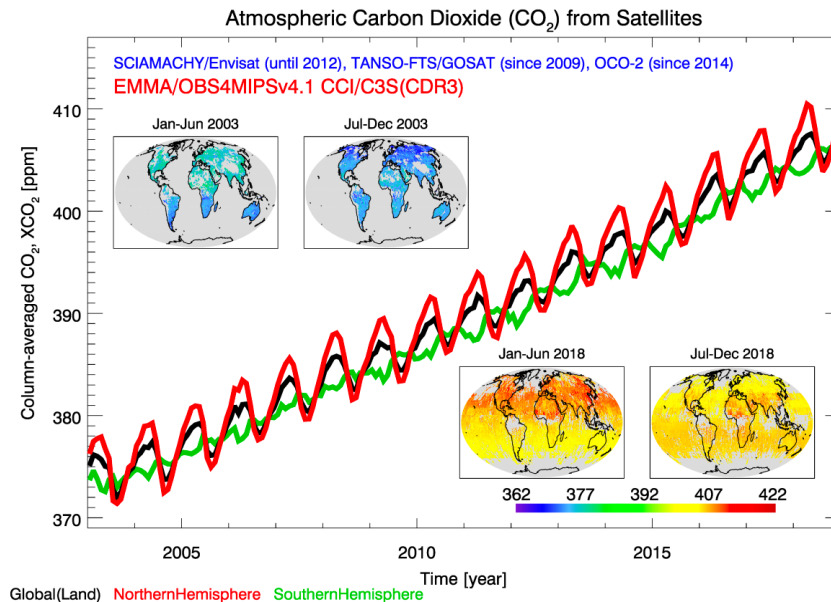

Figure 10.11: Time series over land for three latitude bands (global, black line; northern hemisphere, red; southern hemisphere, green) and global maps (half-yearly averages at 1×1 obtained by gridding (averaging) the merged Level 2, i.e., EMMA, product). From Reuter et al., 2020

Atmospheric humidity has been observed from satellite measurements since the launch of Nimbus-2 in 1966. With the first single channel instruments operating around 6.5 µm in the thermal infrared (IR), additional water vapour sensitive channels in the microwave (MW) were added in 1972. This combination of IR and MW instruments continues to this day (with evolving sophistication), forming the backbone of operational missions (e.g., Metop) used by numerical weather prediction (NWP). With water vapour absorption found throughout the electromagnetic spectrum, measurements of column amounts have also been made from satellite instruments observing in the ultraviolet/visible (UV/Vis) as well as the near-infrared (NIR) and the shortwave infrared (SWIR).

For total column water vapour measurements, GCOS-200 requirements demand climate products have temporal and spatial resolutions of 4 hours and 25 km respectively, with measurement uncertainties within 2%, and maintain stabilities of 0.3% per decade. Meeting these targets is extremely challenging, requiring a constellation of platforms that operate over multiple spectral bands. This challenge is made more complex as these different measurements employ a variety of retrieval algorithms (e.g., DOAS, optimal estimation, linear regression) to solve the inverse problem. This approach of combining different instruments observing different regions of the electromagnetic spectrum has been the focus of recent efforts from the ESA GlobVapour (http://due.esrin.esa.int/page_project120.php) and current ESA water vapour climate change initiative (http://cci.esa.int/watervapour). Both products have combined microwave ocean measurements of total column water vapour (TCWV) with those made in

the NIR from ESA platforms. Looking forward, there is an increasing number of NIR/SWIR instruments/missions becoming 'operational' (in a non-NWP sense) through the Sentinel program (e.g., MSI/Sentinel-2, OLCI/Sentinel-3, TROPOMI/Sentinel-5p, UVNS/Sentinel-5), which will have a significant impact on the temporal sampling of TCWV over land, which has been a limitation of the current combined observation systems.
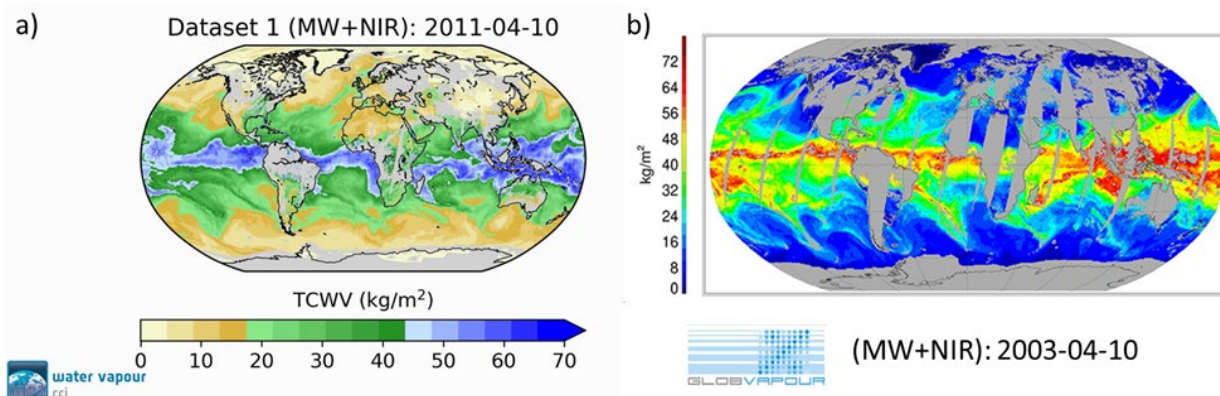

Figure 10.12: Examples of the merged microwave and near-infrared daily products of Total Column Water Vapour (TCWV) from (a) ESA Water Vapour CCI, and (b) ESA GlobVapour (Lindstrot et al. 2015) for 10 April (2011 and 2003 respectively). Maps represent the 10 AM UTC mean field of TCWV from merged SSM/I and MERIS L2 products

10.5.2.2 Operational Climate Applications of Relevant Trace Gases

Satellite-based CO_2 datasets from SCIAMACHY, GOSAT, and OCO-2 are now contributing to operational services. Near –real-time data streams are fed into the Copernicus Atmosphere Service (CAMS) to support short-term forecasts while space-based CO_2 climate datasets are included in the Copernicus Climate Change Service (C3S) to enable climate change mitigation and adaptation strategies by policy makers and businesses.

In support of the global stock take, Copernicus is in the process of establishing an operational Monitoring & Verification Support (MVS) capacity to quantify anthropogenic CO_2 emissions (Figure 10.13; [363]). The space component of this system will be provided by the Copernicus Carbon Dioxide Monitoring (CO2M) constellation, whose main objective is to measure images of CO_2 with the resolution, accuracy, time sampling, and spatial coverage required to provide information on CO_2 emissions. This European system will eventually become part of a wider, international constellation provided by multiple space agencies contributing missions [364].

Operational satellite-based observations of water vapour currently exist within the NWP framework, with IR and MW radiances routinely assimilated by NWP centres all over the world. Currently, water vapour measurements from the NIR are not used as input to NWP; however, through C3S water vapour products are now being ingested for operational climate use (Joaquín Muñoz Sabater, private communication) Therefore, it is highly likely that these products will be looked at for NWP purposes in the future.
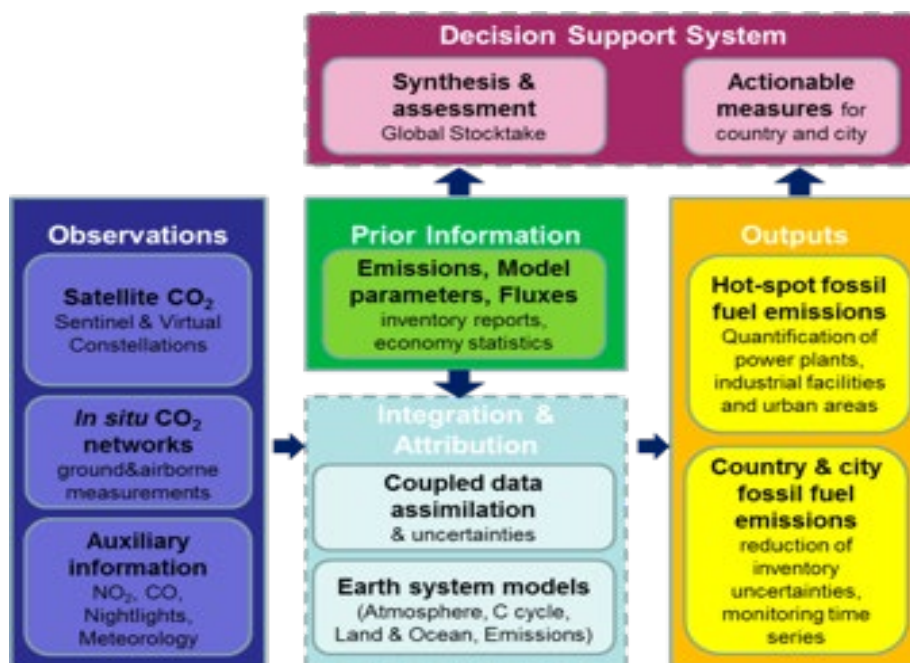
Figure 10.13: Schematic overview of the planned anthropogenic CO_2 Monitoring & Verification Support capacity. From Janssens-Manhout et al., 2019 [363]

Water vapour climate data records are periodically assessed by the Global Energy and Water Exchanges (GEWEX) Water Vapour Assessment (G-VAP). The primary focus of this international working group is to characterise the current state of the art in satellite water vapour products with the overall goal to conduct consistent evaluations and inter-comparisons in order to point out strengths, differences, and limitations of long-term satellite data records, in particular with respect to stability. Additionally, no ranking is given to the datasets; rather, the findings are directly reported back to dataset PI's before being published on the World Climate Research Programme (WCRP) website. This effort also further supports the selection process of suitable water vapour data products by the general (climate analysis) community and in particular by GEWEX Data and Assessments Panel (GDAP). The next cycle of G-VAP ends in November 2021.
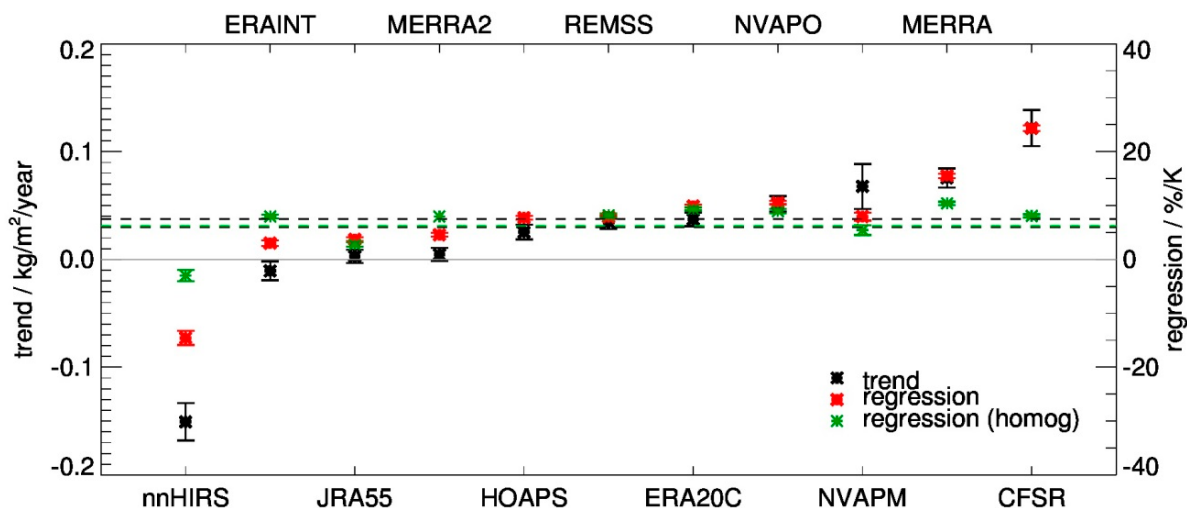
Figure 10.14: Trend estimates in TCWV in kg/m2/year and regression coefficients (correlation of amount of TCWV with change in, temperature) in %/K for eleven data records (satellite and reanalysis). Also shown are regression coefficients which have been computed using homogenised TCWV data records. TCWV values been averaged over the global ice-free ocean within 60 N/S and cover the common period 1988-2008. The vertical bars show the estimated uncertainty of the trends and the regression coefficients. The black dashed lines mark the typically expected range of regression values given in, e.g., Wentz and Schabel, (2000) [365], while the green dashed line marks the expectation, computed using observed SST. The light grey line marks the zero line. The use of the trend analysis here is to identify issues in the data records and it is not claimed that these are the trends occurring in nature. Figure taken from Schröder et al. (2019) [366].

10.5.3   Benefits of SITSats for Trace-Gas Missions

10.5.3.1   CO₂ Missions

> **Sensor accuracy is key for reliable observations of CO₂ monitoring from space. SITSats will provide a powerful tool to improve CO₂ and H₂O monitoring**

The requirements on the Level-2 CO_2 dataset are high since surface flux inversion systems are sensitive to small regional biases in the CO_2 column data already (e.g., Chevallier et al., 2014 [367]). The user requirement document [368] for the ESA CCI projects gives a precision requirement of better than 1 ppm goal with an 8-ppm threshold and systematic errors of better than 0.2 ppm goal/ 0.5 ppm threshold. The requirement for the CO2M mission on precision is 0.7 ppm for a single sounding to allow observing small-scale emission plumes from localised sources with a requirement on systematic biases of 0.5 ppm [369].

The retrieval methods for CO_2 rely on the absolute radiance values of measured spectra, and therefore consistency of radiometric calibration and bias correction of these sensors at the appropriate radiance level is needed to achieve the Level-2 requirements on systematic errors. This is even more critical when utilising CO_2 data combined from multiple sensors of a constellation as is planned for CO2M or from a heterogeneous constellation of sensors adopting different measurement techniques and orbits including LEO and GEO [364]. It is important to highlight that the radiometric calibration needs of these missions includes not only the overall radiometric gain but also the relative radiometric gain between the different bands and even within bands.

Individual instruments might achieve their required calibration accuracy, but this will still need a substantial and sustained effort for in-orbit calibration and verification to enable traceable results. Many satellite missions are known to suffer from significant calibration issues in the early phase of the mission due to previously unknown or unexpected effects (e.g., Crisp et al., 2017 [370]). SITSats such as

TRUTHS and CLARREO can become a powerful part of these systems in principle to achieve and verify their requirements and potentially even to overachieve them, with the prospect of improved performance and/or relaxation of other constraints. It can also enhance interoperability and coherence of Copernicus and multi-agency CO_2 constellations through cross-calibration at different parts of the orbit.

The primary benefit of a SITSat like TRUTHS would be its capability to improve the absolute accuracy of vicarious calibration sites and similar non-instrumented sites by reference calibration from space. SITSats can also allow simultaneous nadir (or angle matched) overpasses of sensors at many Earth locations, thus complementing the limited number of existing vicarious calibration sites and accounting for potential intra-orbit variances in sensor performance. TRUTHS has the added advantage that it will also provide calibrated solar irradiance measurements that can benefit the retrievals of missions like CO2M.

10.5.3.2 Total Column Water Vapour (TCWV)

Currently ESA has three Sentinel instrument series in space that provide daily estimates of global TCWV distributions in cloud-free conditions, with a fourth planned for launch in 2021. While these measurements are not currently used by NWP, they are all important data sources for climate data records. On their own, no single sensor record can meet the requirements for a water vapour climate data records (Table 10.4), therefore, integration of numerous records is required to meet these demands. A key benefit of a SITSat like TRUTHS or CLARREO is that it would act as a common calibration reference for all these sensors as they operate between 400-2400 nm. Long-term water vapour records also rely on the instrument stability characterisation, as changes in performance introduce step functions to the time series (Schröder et al. 2016) [371]. Another benefit of SITSats is that all Sentinel TCWV products and indeed those of other international missions such as VIIRS, offering different observation times, will have a common SI-traceable reference from which to harmonise against accounting for both L1 bias removal and at L2 assuming a robust internationally accepted retrieval is also established.. This is crucial when considering combining these records for climate products.

Table 10.4: Requirements for TCWV climate data records, adapted from Hegglin et al. (2019) [372].

Frequency	Spatial Resolution	Measurement		Stability
		Uncertainty	Accuracy	
GCOS				
4 hr	25 km	2%	-	0.3% dec^{-1}
Climate-AOPC				
6 hr	200 km	3 kg/m^2	-	
4 hr	100 km	1.4 kg/m^2	-	Not available
3 hr	50 km	1 kg/m^2	-	
GEWEX				
3 hr	10 km	2%	-	0.3% dec^{-1}
ESA GlobVapour				
Daily/monthly	≤ 0.5°, 55 km	-	5 kg/m^2	Not available
		-	2 kg/m^2	
		-	1 kg/m^2	

A secondary benefit of an agile SITSat with high spatial resolution such as TRUTHS is to enable calibration across an imager's swath, allowing for the removal of striping artefacts and inter-calibration of different detector spectral response functions. This is especially important for spatially high-resolution measurements, as they are able to provide NWP with features currently not resolved by the models. Figure 10.15 shows how reanalysis models will lose/smooth out detail from the source data here from the relatively spatially course OLCI. This resolution and missing data due to cloud, will be greatly improved by higher spatial resolution data with high reliability allowing the models to take greater dependence on the observation. SITSats, of course, also characterise ground truth sites. This is especially important to help define the representativeness uncertainty during the collocation process.

Figure 10.15: Example scene from OLCI (S3A) relative to ECMWF reanalysis demonstrating how reanalysis fields do not always resolve all features and so the higher the resolution of the starting image the more detailed the model can interpret it. Missing data in OLCI image due to cloud is coloured dark grey. (Rene Preusker, private communication)

10.5.4   User Requirements for SITSats

10.5.4.1   Requirements for CO_2 Missions

In the case of CO_2, we focus on the Copernicus High Priority Anthropogenic CO_2 Monitoring Mission CO2M. CO2M will be a constellation to be launched in 2025-2026 and serves as the space component of the European anthropogenic emissions monitoring and verification system. To achieve its mission objectives, CO2M needs to fulfil the Level-2 requirements of 0.7 ppm precision with less than 0.5 ppm systematic errors for a 250 km wide swath with 4 km^2 ground pixels (Figure 10.16).
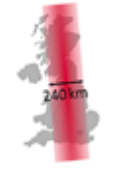
Requirements for XCO₂	GOSAT2 (Japan)	OCO-2 (USA)	TanSat (China)	CO₂M (EU)
Random Error and systematic biases	≤0.5 ppm (CO₂) ≤5ppb (CH₄)	≤0.5 ppm	≤1-4 ppm	≤0.5-0.7 ppm
Spatial resolution	74km²	2.3x1.3km²	2x2km²	2x2km²
Swath width	5-point sampling on 1000km track	10km	10km	240 km
Revisit	3 days	16 days	16 days	2-3 days with 3 satellites
Orbit equator crossing	13:00 (ascending)	13:36 (ascending)	13:39 (ascending)	11:30 (descending)

Figure 10.16: Comparison of the technical specifications of the Copernicus CO2M satellite to some currently available sensors. From Janssens-Manhout et al, 2020

The need for highly-accurate Level-2 products drives demanding Level-1 requirements including those on radiometric calibration.

- Absolute radiometric accuracy: 3% over the dynamic range at the continuum level for each band given by NIR: 747–773nm; SWIR-1: 1590–1675nm; SWIR-2: 1990–2095nm (Figure 10.17).
- Inter-band relative gain: radiometric accuracy between any two bands needs to be better than 1%
- Relative radiometric accuracy: Relative radiometric accuracy of the ratio of the radiance and the irradiance measurements of CO2M for each band and applied to each radiance measurement with the swath needs to be better than 0.5%.
- CO2M has a 10-year lifetime and calibration will be needed over the whole duration of the mission, with a criticality to the start of the mission.
- Spatial requirement: Radiometric calibration will have to consider the full FOV of a CO2M pixel with a ground area of 4 km². It is also important to evaluate the whole swath (250 km), especially as many push-broom spectrometers show significant striping patterns along the flight path (see e.g., TROPOMI).
- Temporal calibration: Many cooled spectrometers suffer from build-up of ice on the detectors, which can lead to rapid changes in relative radiometric response. To correct this effect will require frequent radiometric re-calibration

The translation of Level-1 into Level-2 requirements is described in the ESA CO2M-REB study. For the application of CO_2 imaging, it is found that absolute multiplicative gain errors contribute 0.1 ppm to the total error budget and relative radiometric errors contribute 0.2 ppm. Thus, radiometry is a significant contributor to the total error budget with an overall systematic error of 0.5 ppm.
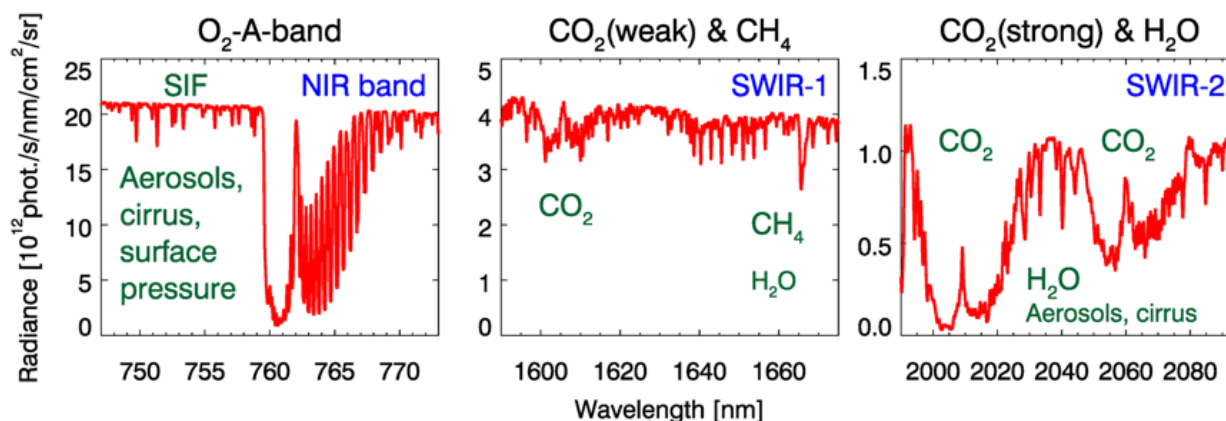
Figure 10.17: Simulated example spectrum for CO2M for all 3 band (figure by M. Buchwitz)

10.5.4.2 Requirements for H₂O Missions

Another key area where SITSats can readily contribute to is the harmonisation of water vapour channels used on Sentinels 2, 3 and 5p/5. All water vapour records are impacted by not only their performance (radiometric calibration) but also changes in their sensor/spectral response function with time [366]. Accurately accounting for these changes is needed to characterise whether L2 TCWV products are meeting the uncertainty requirements for NWP of 2-5 kg/m² at spatial resolutions between 25-250 km, and climate applications where the requirements are 1-3 kg/m² at spatial resolutions of 50-200 km [372]. Furthermore, TCWV climate records also require stabilities of 0.3% dec^{-1} (GCOS-200). Being made up of a number of individual sensor records, harmonisation at the radiance level using a SITSat like TRUTHS or CLARREO would ensure performance could be traced through to product levels 2, 3U, 3, and 4.

The Ocean and Land Colour Instrument (OLCI) instrument on-board Sentinel 3 (S3) uses bands Oa19 (900 nm) and Oa20 (940 nm) to retrieve TCWV. This places the following requirements on a SITSat used for harmonisation:

- **Spectral coverage:** Range needed to cover OLCI bands is between 890-960 nm, OLCI channels are broadband so a SITSat spectral resolution of <5 nm can be readily convolved with the OCLI SRFs.
- **Radiance inter-calibration**: OLCI requires 2-5% absolute radiometric accuracy/0.2 % relative radiometric accuracy across bands. SITSats can be used to assess this through collocations:
  - o 1:1 match-ups required within 5 minutes of OLCI measurement, sample a range of viewing/SZA angles and cover different surface types. Analysis would then be performed at the monthly/seasonal level, rather than the individual matches (similar to GSICS approach).
  - o Collocations need to sample whole OLCI pixels (300 x 300 m) as well as all detectors on each platform (S3a, S3b, S3c, and S3d). A minimum overlap of 2 years between platforms is usually used for harmonisation.

Multispectral Instrument (MSI) on-board Sentinel 2 (S2) is now being used to produce 60 m resolution TCWV using bands 9 and 10, which are in the near infrared (NIR) and shortwave infrared (SWIR) respectively. Requirements for harmonisation by a SITSat include:

- **Spectral coverage**: Range needed to cover MSI bands is between 920-1408 nm at. Bands 9 and 10 are reasonably broad at 66 nm, therefore a SITSat bandwidth of <10 nm can be convolved with MSI SRFs.

- **Radiance inter-calibration**: MSI requirements are 3-5% absolute radiometric accuracy/0.5 % relative radiometric accuracy across bands. SITSats can be used to assess this through collocations using the same criteria as OLCI.

The TROPOMI and Sentinel 5 UVNS instruments (Sentinel 5p, Metop-SG respectively) have water vapour sensitivity in their SWIR band(s) at 1600 (SWIR-1) for Sentinel 5 and 2300 nm (SWIR-3) for both. Unlike OLCI and MSI, these instruments take spectra at a much higher resolution than that of a typical SITSat however they can still provide support: .

> **Requirements for reflected-solar trace gas sensors are for SI accuracy better than 2-5% and relative accuracy across spectral bands of 0.2-1.0%**

- **Spectral coverage**: Bands SWIR-1 and SWIR-3 cover the spectral range between 1590-2385 nm. However, the strong H_2O and CH_4 absorption bands in SWIR-3 are found after 2362 nm and so sensitivity to ~2400 nm is required, but the spectral bands will not be resolved and so spectral smoothness between SITSats sampling resolution will need to be assumed.
- **Radiance inter-calibration**: SWIR-1 performance (Sentinel 5 UVNS only) requires an absolute radiometric accuracy of 6%, while SWIR-3 has an increased dependence of 3%. Both bands require a relative radiometric accuracy of less than 0.2%. Again, collocations with a SITSat for radiometric calibration are the same as OLCI and MSI. The spatial resolution of TROPOMI SWIR-3 pixels is 7x7 km^2.

10.5.5   Conclusions

Traceable radiometry from a space-based mission can play an important role for achieving, verifying, and potentially over-achieving radiometric requirements for NIR/SWIR trace gas missions. The key requirements will be on spectral coverage over the NIR and SWIR bands used by these trace gas sensors, an absolute radiometric calibration of better than 2-5 %, and a relative radiometric accuracy of 0.2 - 1%.

§10.1 Authors: **Fabien Carminati** and **Chawn Harlow**, Met Office, Exeter
§10.2 Author: **Yolanda Shea**, NASA / LaRC
§10.3 Author: **Dennis Helder**, Univ. of S. Dakota
§10.4 Authors: **Stefan Simis[1], Thomas Jackson[1], Giuseppe Zibordi[2],** [1]Plymouth Marine Laboratory, Plymouth, UK, [2]Joint Research Centre of European Commission, Ispra, Italy
§10.5 Authors: **Hartmut Boesch** and **Tim Trent**, Univ. of Leicester
§10   Editor: **Bruce Wielicki**, NASA / LaRC

11 SITSats Anticipated for Launch Within the Decade

The impact of human activities on the Earth's ecosystem is gradually increasing. The world faces significant environmental challenges. The phenomena of glacier melting, sea level rise, land drought and more extreme weather shows that the climate system is changing. Climate change is closely related to human reproduction. In the future, climate change will be more noticeable and even more dangerous. The solar radiation, which is reflected from the Earth's surface, clouds, etc, back to space, constitutes a powerful and highly variable feature of the climate system through changes in snow cover, sea ice, land-use, aerosol, and cloud properties. Systematic, spatially resolved observations of time series of the reflected solar spectral radiation can provide reliable analytical data for the changing climate system.

The space-based remote sensing technology has made great achievements and plays a key role in meteorological prediction, disaster prevention and mitigation, resource exploration and other fields. However, climate change models need the reflected solar spectral radiation with high accuracy and long-term stability. The solar radiation changes 0.1% within a solar cycle, and changes 0.2% on weekly timescales. The measurement uncertainty of reflected solar spectral radiation needs to achieve <1% and long-term stability is needed to research climate-change trends. The stability needs to be less than 0.3% per decade. Although optical remote sensors are calibrated with high accuracy before launch, their post-launch calibration can lose some traceability to SI and cannot currently meet these absolute-accuracy requirements.

Efforts to re-establish post-launch validation of performance and/or correction of calibration coefficients in an SI-traceable manner are pursued both on the spacecraft and through vicarious methods. In the latter, increased focus on the need for SI-traceable rigour has led to the terminology of 'Fiducial Reference Measurements' (FRM) which is used to represent measurements with clearly documented evidence of SI-traceability, transparent and open access procedures [90]. Typically, a subset of many in-situ or similar measurements, these have a status implying greater reliability. They also provide a framework to encourage upskilling of the global community and generally involve some element of comparisons e.g. www.FRM4SST.org and www.FRM4SOC are examples for sea surface temperature and ocean colour. FRM's distinguish themselves from other post-launch cal/val or in-situ observation by virtue of rigorous documented evidence of traceability usually including some form of comparison but always with transparent accessible methods and uncertainty budgets. It should be noted that the FRM concept in relation to validation of the satellite product applies not only to the direct measurement of the specific 'in-situ' parameter but also the adequacy of its sampling, space/time, to correlate with the satellite and of course any method or algorithm or auxiliary data need to account for the atmospheric path, viewing angle or other sampling differences.

 CEOS RadCalNet (www.radcalnet.org) is another example where a network of test sites delivers SI-traceable Top of Atmosphere spectral radiances every 30 minutes derived from autonomous surface reflectance and auxiliary environmental measurements. However, whilst this type of measurement is important and can provide some on-going infrastructural support for the space element, the resultant uncertainties achievable on their own still typically remain significantly larger than is needed for climate.

In this section, we discuss future missions and instruments intended to meet these higher-accuracy requirements. These SI-Traceable Satellites (SITSats) are focused on what are currently accuracy-limited, but critical measurements of the Earth's outgoing energy, with expected improvements to be provided by the CLARREO Pathfinder HySICS, the TRUTHS, the CSRB, LIBRA, and FORUM. These types of sensor may also allow performance improvement in some of the FRM infrastructure so that they can better contribute to the overall goals.

11.1 The HyperSpectral Imager for Climate Science on the CLARREO Pathfinder Mission

11.1.1 CLARREO Radiometry

The 2007 U.S. Academy of Sciences Decadal Survey for Earth Science recommended the Tier 1 CLARREO (Climate Absolute Radiance and Refractivity Observatory) mission [6] to acquire high-accuracy, climate-benchmarking spatial/spectral radiances of the Earth's surface and to provide reference calibrations for other on-orbit sensors. The more recent 2018 Decadal Survey similarly prioritized reference radiance inter-calibrations as one of its "Most Important Targeted Observables", providing on-orbit SI traceability for other programs such as the Global Space-Based Inter-Calibration System. To achieve these climate-benchmarking and inter-calibration capabilities, the space-borne imaging spectrometer for the CLARREO requires radiometric-accuracy improvements that are 4 to 8x better than any currently flying spectrometer provides, necessitating innovative new on-orbit measurement techniques.

The HyperSpectral Imager for Climate Science (HySICS) is currently in development for the NASA CLARREO Pathfinder (CPF), a low-cost, Class-D mission planned for launch to the International Space Station (ISS) in 2023. This 1-year mission is intended to demonstrate both the CLARREO-needed on-orbit radiometric accuracies and provide reference inter-calibrations for other space-based assets. The two primary goals of this mission are to demonstrate: 1) on-orbit, high-accuracy, SI-traceable calibrations for measurements of Earth-reflected radiances in the solar-spectral region; and 2) the ability to transfer calibrations to other on-orbit sensors, in particular the VIIRS and CERES as proof-of-concept. The instrument will also acquire lunar radiances at various phase and libration angles to improve the knowledge of the Moon as an on-orbit calibration source. A two-axis HySICS pointing system, included with the CPF instrument package shown in Figure 11.1, enables target selection. The primary intended target is the Earth viewed at nadir, although the Moon and off-nadir Earth scenes needed for reference-calibration coincidence pointing with other instruments are targets as well, and both along- and cross-slit scans of the Sun are needed for instrument calibrations.

> **The HySICS will acquire spatial/spectral measurements with unprecedented radiometric accuracies of 0.3 % across the reflected-solar spectral range**

The CLARREO Pathfinder is currently in Phase C with intended installation in the ISS ExPRESS Logistics Carrier #1 Site #3.

The HySICS will acquire images of the Earth's surface and atmosphere with unprecedented radiometric accuracies of <0.3 % (k=1) achieved via on-orbit calibrations using the spectral solar irradiance. These high radiometric accuracies enable benchmarking of Earth radiances for climate studies (see §11.1.3) and provide reference calibrations for other on-orbit Earth-viewing sensors (see §11.1.4).
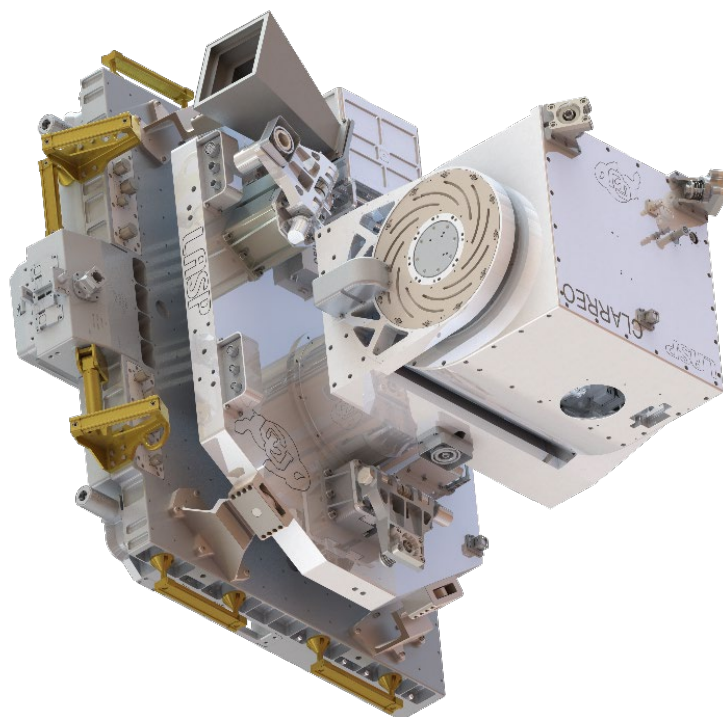
Figure 11.1: Drawing of the nadir-looking HySICS instrument (right-most box with downward-looking entrance aperture) and its two-axis pointing system as planned for installation on the ISS.

11.1.2   HySICS Optical Design

The HySICS is an Offner-based pushbroom imaging spectrometer that contiguously covers the spectral range from 350 to 2300 nm with 6-nm spectral resolution (3.1-nm sampling). The instrument's primary measurement requirements are given in Table 11.1. The nadir-looking instantaneous field-of-view is 130 m (instrument-intrinsic 67 arcsec), sampling a cross-track swath of 71 km with an effective IFOV of 0.5 km and an intrinsic 10.1° field of view from the ISS's orbit altitude. An orthogonal arrangement of the optical planes of the instrument's four-mirror anastigmat telescope (4MA), providing imaging for the spectrometer, and the Offner spectrometer reduces instrument-induced polarization to <0.1 % from 350 to 1800 nm and <0.2 % at wavelengths above 1800 nm. These low polarization sensitivities are needed for maintaining radiometric accuracy from scenes of unknown polarization. An aperture wheel prior to the imager's 4MA allows selection of Earth- and solar-viewing apertures needed for on-orbit calibrations using direct views of the Sun, as described briefly below and in more detail by Kopp et al. [38].

Cross-track nadir observations of the Earth acquire spatial/spectral information of the ground and atmosphere on a two-dimensional focal plane array (FPA). Cross-slit scans of the Sun give composite measurements of the spectral solar irradiance (SSI), to which the HySICS is radiometrically referenced to SI. Along-slit solar scans enable flat fielding in the instrument's solar-viewing configuration, while a transmissive diffuser in the aperture wheel enables Earth-viewing-geometry flat fielding. A Hg/Ar pen-ray lamp provides on-orbit wavelength calibrations across the spectral range.

This full spectral range is spanned by a single HgCdTe FPA with 100 % fill-factor pixels in a 640x480 format to acquire spatial/spectral images. The high-speed CMOS design includes an electronic global shutter allowing precise control of integration timing needed for known attenuation control. With 15-Hz sampling, ground images have an along-track smear-limited 500-m spatial resolution; cross-track pixels are binned to the same resolution in Level-1 data products. Operated at 150 K to reduce

uncertainties from dark current and thermal backgrounds to acceptable levels, the FPA's read-out noise is <100 e⁻.

Table 11.1: HySICS Measurement Requirements

Measurement Parameter	Requirement
Radiometric Accuracy	0.3 % (k=1)
Spectral Range	350 – 2300 nm
Spectral Resolution	6 nm
Field of View	10.1° (71 km nadir swath)
Spatial Resolution	0.5 km (nadir)

11.1.3 HySICS Achieves Radiometric Accuracies Using On-Orbit Solar Cross-Calibrations

The radiometric uncertainty goal for the CLARREO Pathfinder HySICS is 0.3 % (k=1), which is much better than any current spaceflight reference detector or calibration light source is capable of providing. Instead of either of these traditional detector- or source-based calibration approaches, the HySICS relies on on-orbit

> **The HySICS achieves SI-traceable radiometric accuracies on-orbit using spectral solar irradiance cross-calibrations**

calibrations provided by direct views of the SSI, which is known on an absolute SI-traceable scale to ~0.2 % from other space-based assets such as the TSIS-1 Spectral Irradiance Monitor [373].

Two signal-attenuation approaches enable the HySICS's direct views of the Sun for these SSI cross-calibrations: 1) knife-edged apertures of different sizes prior to the telescope entrance limit the amount of entering light by precisely-known amounts, giving ~10^3 attenuation due to geometric area between a 2-cm diameter Earth-viewing aperture and a 500-µm diameter Sun-viewing aperture; and 2) changes in FPA integration times coupled with well-characterized detector linearity provide similar levels of attenuation. In conjunction, these two attenuation methods enable viewing both the Earth and the Sun using the same optical system despite the 10^6 difference in radiances between these two targets. A prototype HySICS demonstrated these attenuation approaches and the desired radiometric accuracy improvements during two high-altitude balloon flights under a NASA Earth Science Technology Office program [38]. A sample ground-scene data cube from one of these flights is shown in Figure 11.2. Estimated CPF HySICS uncertainties across the spectral range using balloon-flight results and expected improvements to the space-flight instrument are plotted in Figure 11.3.
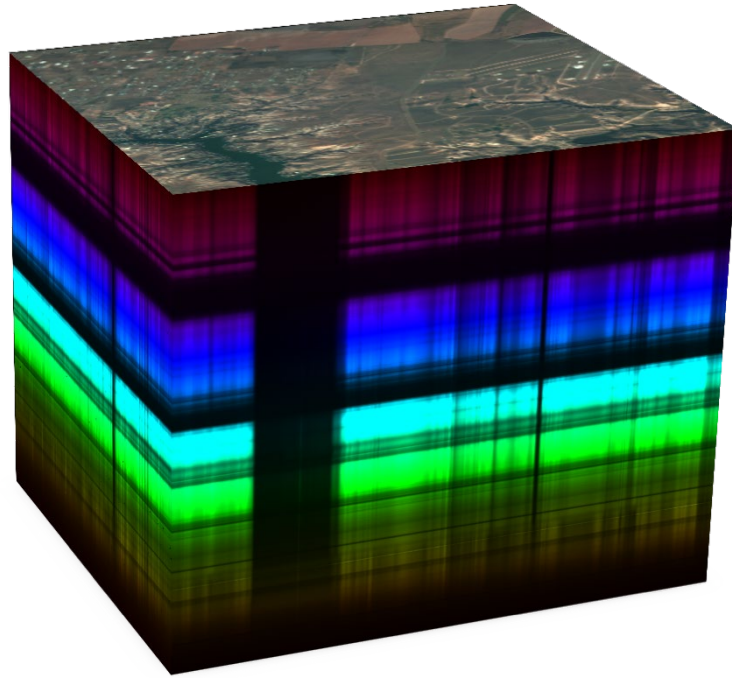
Figure 11.2: A nadir-viewed ground scene acquired during a high-altitude balloon flight gives full spectral coverage at each spatial position viewed.
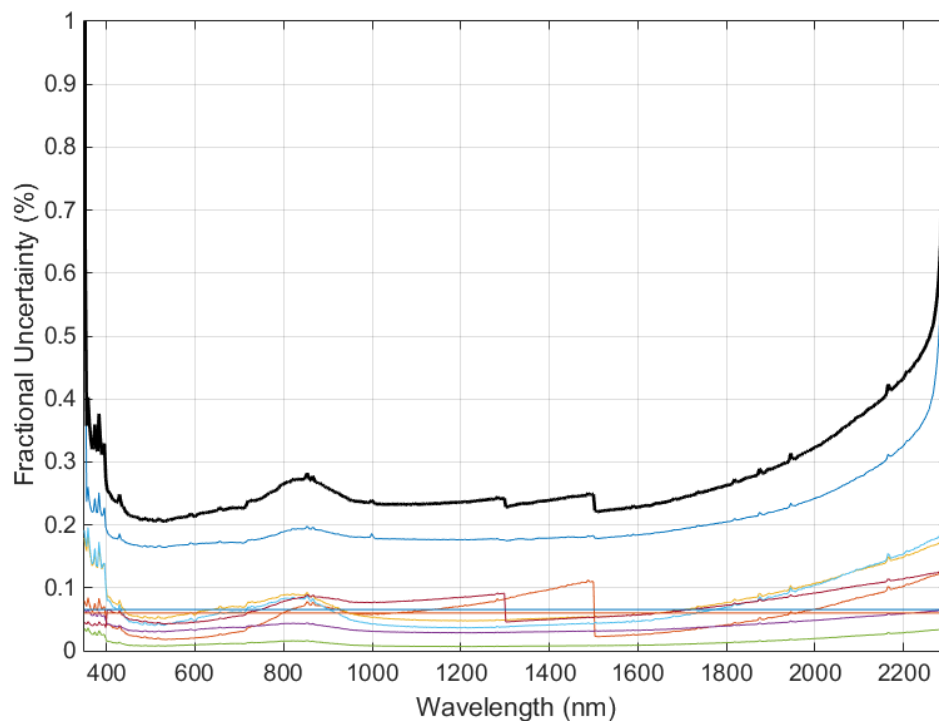
Figure 11.3: HySICS uncertainties from dominant contributors (coloured curves) are summed in quadrature (black curve) to give a mean radiometric uncertainty of 0.27 % across the spectrum.

11.1.4 CLARREO Pathfinder: On-orbit Data Matching and Sensor Inter-calibration

In this section, we describe in more detail the second of the two CLARREO Pathfinder objectives, namely to demonstrate an on-orbit sensor inter-calibration approach using the high-accuracy HySICS

to transfer calibrations to other on-orbit sensors. We use the example of inter-calibrating VIIRS by comparing observations matched in space, time and angle, as shown in Figure 11.4.
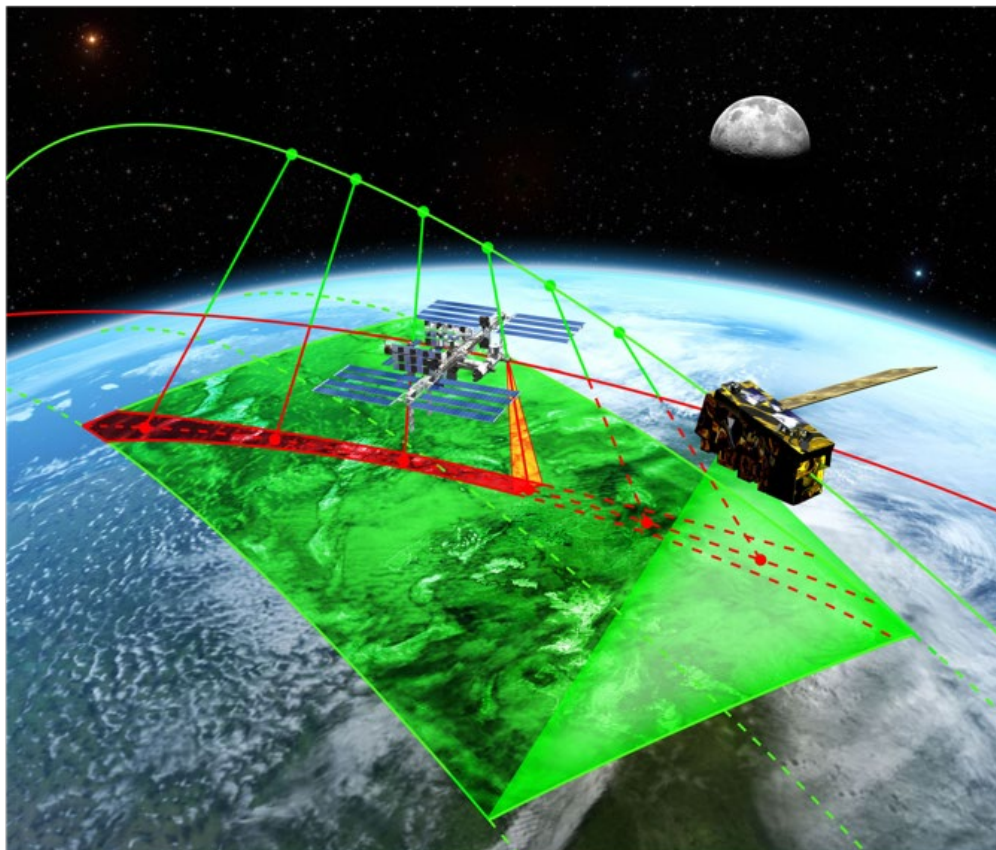
Figure 11.4 Concept of CLARREO Pathfinder special pointing operations: temporal and angular matching observations to the cross-track instrument on the JPSS satellite. The matched data is shown in red.

11.1.4.1 Data Matching and Sampling

Table 11.2 Summary of high-priority inter-calibration goals for VIIRS and relevant temporal periods.

Sensor	Parameter	Timescale
VIIRS	Baseline offset	monthly
VIIRS	Baseline gain	monthly
VIIRS	Non-linearity	bi-annually
VIIRS	Sensitivity to polarization	bi-annually
VIIRS	Band Spectral Shift	bi-annually

The CPF approach for inter-calibration is based on obtaining coincident highly accurate spectral reflectance measurements and establishing an on-orbit reference for existing Earth-viewing sensors. The mission goal is to be able to provide CPF reference observations that are matched in space, time, and viewing angles with measurements from the aforementioned instruments, with sampling sufficient

to overcome the random and systematic error sources from imperfect data matching [80], [374]. This is achieved by planning CLARREO Pathfinder instrument special operations on orbit using a roll-over-pitch pointing gimbal. An example of matching CPF measurements to cross-track sensors on the JPSS satellite, such as VIIRS, is shown in Figure 11.5, showing collocated observations between 52°S and 52°N latitude. Furthermore. Full coverage of the diurnal cycle can be achieved in approximately 1 month.
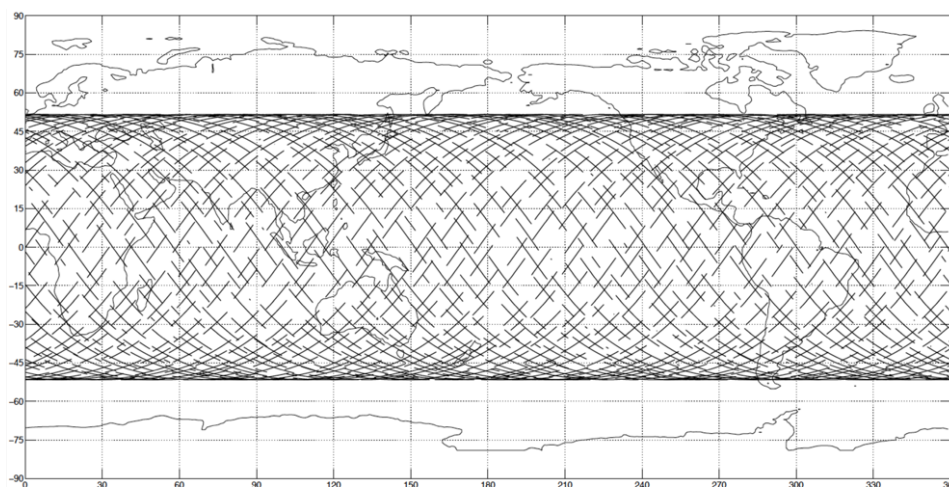
Figure 11.5 Geolocation of the ISS ground track during each opportunity to take measurements for inter-calibrating VIIRS sensor on JPSS.

The inter-calibration method is to monitor changes in the following response-function parameters of the targeted sensor over time as a function of instrument scan angle: effective offset, gain, non-linearity, spectral degradation, and sensitivity to polarization of optics. The CLARREO Pathfinder inter-calibration goals for the VIIRS instrument are summarized in Table 11.2. We plan to achieve collocation data with uncertainties matching noise of about 2 % [375] with the following matching requirements: ± 10 minutes of JPSS passing, angular match within 5° (over the entire CPF swath), SZA < 75°. Using simulation methods, we estimated realistic inter-calibration sampling over a one-year time period. The geolocation of the ISS ground track during each opportunity to take measurements for inter-calibrating VIIRS sensor on JPSS is shown in Figure 11.5. The inter-calibration duration per day over a one-year time period is shown in Figure 11.6a with 2 or 3 inter-calibration events occurring daily. Estimated monthly inter-calibration sampling is shown in Figure 11.6b. We conclude that the sampling is sufficient to meet CLARREO Pathfinder mission inter-calibration requirements.

Figure 11.6(a) The inter-calibration duration per day over a one-year time period, (b) Estimated monthly sampling for CPF/VIIRS inter-calibration. The red dashed line indicates minimum sampling required to meet the mission objectives.

Measurements of spaceborne imagers are often sensitive to the polarization of incoming light. Typical values of imager sensitivity to polarization are a factor of 2% to 5% depending on the spectral band, increasing for bands in the blue wavelength range [237]. We use a sensitivity to polarization term in sensor calibration in a way consistent with the definition by Sun et al. [237], [376]:Measurements of spaceborne imagers are often sensitive to the polarization of incoming light. Typical values of imager sensitivity to polarization are a factor of 2% to 5% dependin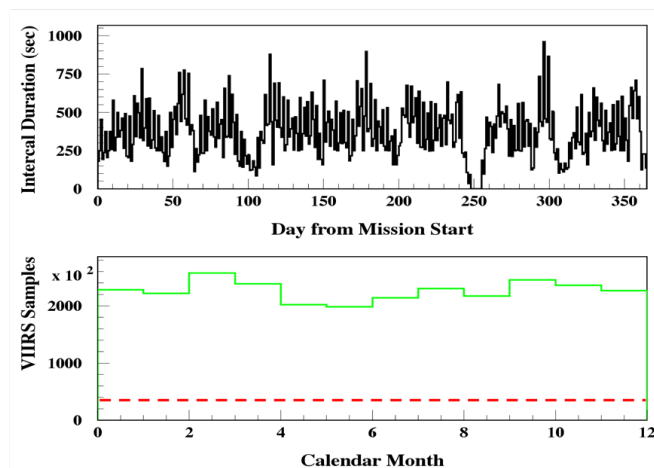g on the spectral band, increasing for bands in the blue wavelength range [237]. We use a sensitivity to polarization term in sensor calibration in a way consistent with the definition by Sun et al. [237], [376]:

$$\rho^{\text{imager}} = \frac{\rho_0}{(1 + mP)} \qquad \text{\textit{Equation 26}}$$

where ρ^{imager} is the measured reflectance including correction for polarization sensitivity, ρ_0 is the reflectance factor corresponding to the imager calibration model for non-polarized light, P is degree of linear polarization of reflected light at top-of-atmosphere, and m is the sensitivity to polarization. For simplicity, in this formalism the m dependence on polarization angle is implicit, and Equation 26 is defined for every sensor scan and polarization angle. The sensitivity to polarization affects the sensor effective gain, and this is the basis of the inter-calibration approach by the CLARREO Pathfinder described in [79]. The knowledge of polarization is provided by Polarization Distribution Models (PDM) [377], [378], After performing error propagation analysis, and assuming covariance coefficients to be zero, we have imager relative radiometric uncertainty:

$$\frac{\sigma^{\text{imager}}}{\rho^{\text{imager}}} = \sqrt{\left(\frac{\sigma_0}{\rho_0}\right)^2 + \frac{P^2 \sigma_{\text{m}}^2 + m^2 \sigma_{\text{p}}^2}{(1 + mP)^2}} \qquad \text{\textit{Equation 27}}$$

The uncertainty in the first term, σ_0, is radiometric uncertainty of inter-calibrated imager reflectance for unpolarized measurements:

$$\frac{\sigma_0}{\rho_0} = \sqrt{\left(\frac{\sigma^{\text{cpf}}}{\rho_0}\right)^2 + \left(\frac{\sigma_{\text{intercal}}}{\rho_0}\right)^2 + \left(\frac{\sigma_{\text{residue}}}{\rho_0}\right)^2} \qquad \text{\textit{Equation 28}}$$

where σ^{cpf} is the accuracy of CLARREO Pathfinder, $\sigma_{intercal}$ is the error contribution from inter-calibration noise, and $\sigma_{residue}$ is error associated with target sensor remaining error contribution (e.g. instrument instability within a one-month time period). These error sources are both types: systematic and random. Examples of numerical analysis of these equations are provided in [79].

Detailed uncertainty propagation for inter-calibration of VIIRS instrument, including explicit dependencies on the angle of linear polarization and phase angle of instrument, has been derived by Goldin et al. [212].
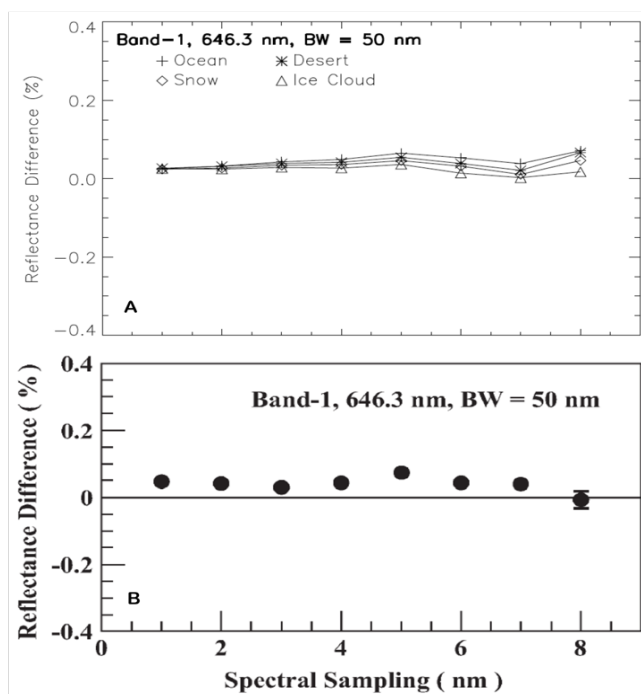
Figure 11.7 Expected reflectance differences at MODIS Band 1 as function of spectral sampling frequency: (a) MODTRAN simulations for ocean, desert, snow, and ice clouds. (b) Deep Convective Clouds in July 2004 SCIAMACHY instantaneous data.

An example of estimated bias due to different spectral sampling is shown in Figure 11.7 for MODIS Band 1: (a) MODTRAN simulations for ocean, desert, snow, and ice clouds. Sensitivity of inter-calibration uncertainty to the CLARREO reflected solar spectrometer features is reported in [379]. Top-of-atmosphere spectral radiances simulated by MODTRAN and measured from the SCIAMACHY instrument on Envisat are used to determine sensitivity of inter-calibration uncertainty to key design parameters of the CPF spectrometer: spectral range, sampling, and resolution. Their impact on inter-calibration uncertainty for MODIS and VIIRS imagers is estimated for various surface types (ocean, vegetation, desert, snow, deep convective clouds, clouds, and all-sky). Results indicate that for the visible to near-infrared spectral region (465 – 856 nm), the CPF instrument in the current design concept produces uncertainties of better than 0.16% (k=1). An example of estimated bias due to different spectral sampling is shown in Figure 11.7 for MODIS Band 1: (a) MODTRAN simulations for ocean, desert, snow, and ice clouds. (b) Deep Convective Clouds in July 2004 SCIAMACHY instantaneous data.

The CLARREO Pathfinder mission objectives also include: (1) demonstration of ability to inter-calibrate imagers in the geostationary orbits (GEO), (2) calibration of lunar spectral reflectance [see

Section 7.3], and (3) collecting near-nadir data over Pseudo Invariant Calibration Targets (PICTs), such as the Libya-4 desert site. The CPF mission configuration allows for the collection of a massive amount of inter-calibration matched data for GEO imagers and multi-angular sampling for the PICTs. However, at this time, these tasks are not included in the mission funding profile.

The objectives of the CLARREO Pathfinder mission include operations and collecting distributed data for inter-calibration of VIIRS and CERES instruments. Taking into account data volume and the variety of data archives, it is a significant challenge to design an efficient approach for inter-calibration data handling. To facilitate remote data access and inter-calibration analysis we are deploying the Multi-Instrument Inter-Calibration (MIIC) framework [380]. The key features of the MIIC framework include: (a) Support for inter-calibration of sensors in LEO-GEO and LEO-LEO. (b) Collaborative processing within the NASA Earth Science data system infrastructure. (c) Definition of inter-calibration events accounting for sensor data taking mode. (d) Efficient access to remote data. (e) Customized functions for data reduction on remote servers.

The essence of the MIIC framework efficiency is in performing necessary operations on-the-fly remotely, where the sensor data are stored. Only useful data are transferred to the local computing facility, and the user is insulated from the complex structure of the raw data and large volume data import. On the user's side, the framework includes science algorithms and statistics libraries, required for inter-calibration data analysis.

11.1.5　Summary of CLARREO Pathfinder HySICS

The Sun is the most stable accurately known radiometric light source in space. Using direct views of the spectral solar irradiance to provide on-orbit radiometric calibrations, the HySICS transfers this SI-traceable source to Earth reflectance measurements with 0.3 % uncertainty across the reflected-solar spectral region. This methodology is intended to provide needed radiometric accuracies for long-term climate studies and to improve, via reference inter-calibrations, measurements from other on-orbit sensors. The CLARREO Pathfinder is implementing the HySICS with this SI-traceable on-orbit calibration approach from the ISS starting in 2023. This mission is intended to demonstrate current state-of-the-art in establishing traceability in orbit; new observations and climate-sensitivity detection capabilities and concepts; needed measurements, timescales, and accuracies for long-term climate studies; and reference calibrations for other on-orbit assets using identical viewing geometries of vicarious targets.

11.2　TRUTHS: An Element of a Space-based Climate and Calibration Observatory

11.2.1　Introduction

This subsection describes a new satellite mission, recently selected to start formal phase A/B1 development in the ESA Earth Watch program, called TRUTHS (Traceable Radiometry Underpinning Terrestrial and Helio- Studies) which is expressly designed to meet the exacting needs of climate and fulfils similar goals to that of the solar reflective instruments of NASA CLARREO and its current pathfinder mission and the Chinese LIBRA mission. SI Traceable Satellites (SITSATS) like TRUTHS, CLARREO and LIBRA are intended to provide highly accurate and trusted climate records and to help constrain the uncertainties in predictions of climate forecast models. Their inherent SI traceability and high accuracy also enable them to upgrade the calibration performance of other sensors through in-flight reference calibration.

11.2.2 Mission Concept

11.2.2.1 Mission Objectives

TRUTHS has two primary objectives:

1. Provide datasets with sufficient accuracy to observationally detect the signals of climate change (in the solar reflective domain) in the shortest possible time. Needed to critically test climate models and attribute the effects of climate change to geophysical processes by providing Top of the Atmosphere (ToA) measurements of incoming and reflected total and spectrally resolved solar radiation appropriately sampled and with SI-traceable uncertainties optimised to minimise time to detect a trend- consistent with goals of GCOS specified requirements (See Table 16).

2. **Upgrade the performance of the EO system** through delivery of an operational high accuracy L1 nadir-looking hyperspectral Earth-reflected radiance product with sufficient spatial (Goal 50 m), spectral (<8 nm), accuracy (Goal 0.3%) and agility that allows it to match (or address) the observational radiometric characteristics of a wide range of Earth viewing sensors so that it can validate and/or upgrade their performance by 'reference calibration' from space, primarily to address climate measurement needs.

Derived from studies by the CLARREO team, choice of a 100-km swath, 90° precessing orbit at 609 km provides the opportunity for multiple near simultaneous nadir observations (SNO) of other polar orbiting sensors, the altitude difference extending the overlap time to increase the number of match-ups. An agile platform compliments this further allowing off-nadir angle matching so as to significantly reduce sources of error resulting from view/illumination angles and atmospheric variations. TRUTHS additionally assigns Top and Bottom of Atmosphere calibration coefficients to existing CEOS/GSICS calibration methods and stable targets such as deserts and the Moon, enabling not only in-flight sensors to be calibrated, but also back correction of heritage sensors that viewed these targets. Other reference targets such as oceans and vegetation also form part of the observation plan.

> **TRUTHS is designed to establish high-accuracy SI traceability in flight, on-board the spacecraft for the solar-reflective domain**

Through this reference calibration, SI traceability of the global Earth observing system (solar reflective domain) is established; robust sensor to sensor interoperability and bias removal achieved (essential for future constellations such as for Green-House Gas (GHG) monitoring, and for many, uncertainty improved- enabling more robust climate quality observations and resilience to potential data gaps.

As a secondary objective, TRUTHS' data set can be used to provide a source of global hyperspectral data to address a range of applications and, constrain and improve retrieval algorithms, such as atmospheric correction and aerosols.

In the context of the primary objective, climate, we take from GCOS [350], the specific requirements for radiation balance, in the 'short-wave' domain as these are the most demanding and arguably most urgent. The $k = 1$ values are presented in Table 11.3.

Table 11.3: GCOS requirements driving the radiometric performance drivers of TRUTHS. Values are $k = 1$.

Parameter	Accuracy	Stability (decade)
Total Solar Irradiance	0.04 %	0.01%
Solar Spectral Irradiance	0.3% (200 – 2400 nm)	0.1 - 1%
Reflected solar radiance (integrated)	1W/m2 =~ 1%	0.3W/m2 =~0.3%

Note:

1) Instantaneous accuracy, although demanding, is in general less than the requirement for long-term stability. In practice, to have confidence and remove dependencies on a continuous 'overlapping' time series it is preferable to target the stability requirement, which is taken to be with respect to similar phases of the solar cycle.

2) For Solar Spectral Irradiance the decadal stability requirement specified by GCOS is 1%. However, this value, whilst still demanding is given as a single value for the whole spectral range where in practise over an 11 yr solar cycle there will be significant (tens %) variation in the UV spectral region. §6.2 and references therein indicate a more demanding target of 0.1% per decade for wavelengths >400 nm but reflecting change for similar phases of the solar cycle.

3) In the context of reflected solar radiance, to aid understanding of attribution, mitigation and to constrain and test climate forecast models, the reflected solar radiance needs to be spectrally resolved (e.g., the key radiation feedbacks which drive uncertainty and variance in the models; cloud and albedo and natural carbon sinks such as the oceans and land vegetation).

11.2.2.2   Mission Data Products and Performance Requirements

The mission data products and associated performance requirements which have been derived to achieve the mission objectives are listed in Table 11.4 The driving requirements are shown in red. The evidence for these requirements, derived from user need and the propagation of required uncertainties to the operational geophysical product, is given in [14].

> TRUTHS can observe climate-relevant processes related to the atmosphere, the oceans, and the land surface

The most demanding of the driving mission requirements is uncertainty and this stems from TRUTHS' intrinsic space climate observatory dataset applications, including reference calibration for climate focused sensors. For more conventional, instantaneous applications e.g., imagery and to some extent cross-calibration- spectral bandwidth, Ground Instantaneous Field of View (GIFOV) and Signal to Noise Ratio (SNR) (all interdependent) become more critical whilst overall uncertainty can in general be relaxed.

It should be noted that SNR values in Table 11.4 are largely defined to be 'commensurate with the overall uncertainty required by the application and its observational characteristics and are, of course, in the case of non-climate applications, highly dependent on the choice of GIFOV and spectral bandwidth. For Earth viewing they are given as instantaneous values relative to a nominal average Earth albedo of 0.3, for the Sun/Moon it is with respect to several seconds of integration time, as the satellite points and stares. Simplistically, the higher the SNR, the smaller the bandwidth and highest spatial resolution the better but contrasted to this is the complexity of the camera, particularly driven by the size of the telescope needed to collect enough photons.

Unlike many conventional satellite missions where the instantaneous observation is the primary measurand and thus where SNR should be a key component of the overall uncertainty budget, for climate benchmark applications this is not the case as the product of interest will always be temporally/spatially averaged to remove effects of localized anomalies. Although a GIFOV of <250 m is desired, this is primarily to aid in assessing scene type and degree of cloud contamination. Most of the benchmark applications are concerned with scene aggregated observations over relatively large spatial and/or temporal scales. In these cases, effects of instrumental or observational noise, the dominant detrimental component of SNR, are effectively randomized and reduced significantly so that SNR makes little overall contribution to the uncertainty budget. Instead, instrument systematic effects and/or biases dominate the uncertainty achievable. Thus, the SNR for these applications can be <50 at GIFOV of 250 m. Similarly, for solar or lunar observations because the spacecraft and its sensors can effectively stare at its target and accumulate signal the instantaneous SNR does not need to be demanding. For some climate applications e.g., Ocean colour the SNR requirements can be more demanding i.e., >1000 but even here the spatial resolution can be > 1 km, reducing the need for high SNR at nominally high instantaneous spatial resolutions.

For applications where the instantaneous, spatially resolved measurement is of greater importance e.g., cross-calibration of a high-resolution land imager like Landsat or Sentinel 2 and associated imagery such as land use classification, the radiometric uncertainty levels can be relaxed towards those of existing sensors. However, there remains the proviso that for the reference

TRUTHS will establish benchmark measurements for the detection of decadal change in the most sensitive climate radiative forcings, responses, and feedbacks

calibration process to be of value the reference sensor (TRUTHS) uncertainty should not dominate. Here, SNR will play a more significant role in the overall uncertainty budget and will likely be the ultimate limiter in terms of number of applications that a mission like TRUTHS can address, when considering what is achievable for an affordable instrument design.

TRUTHS, with an agile platform can both spatially integrate and employ satellite motion compensation (rotating the satellite to compensate for its orbital movement to allow it to stare and temporally integrate over the target) to increase SNR for the specific measurement and also to sample targets with multiple view angles to improve surface characterization.

TRUTHS' measurements of ground-based reference sites (and the Moon) will allow retrospective improvements to the calibration of existing satellites and their data

Table 11.4**.** Mission performance requirements (climate and calibration) red indicates a driving requirement. SNR values are given with respect to an average Earth albedo of 0.3 and for the corresponding GIFOV.

Level 1 products	Mission Observational Requirement							
	Spectral range (nm)	Bandwidth (nm) Spectral sampling X0.5	Uncertainty (%) (k=2)		SNR (with respect to Earth albedo of 0.3)		GIFOV (m)	
Earth spectral radiance (Climate)	320-2400	8 – 25 nm	Goal	Threshold	>50		250	
			0.3	<1.0				
Solar Spectral Irradiance	<320 – 2400	<1 (<400), <5 (<1000), <10 (<2400)	0.3)	<1.0	>300		NA	
Total Solar Irradiance	Total	200-30000	<0.02)	<0.05	>500		NA	
					Goal	Threshold	Goal	Threshold
Earth Spectral radiance (Cal/Val/other)	<380-2400	<8 (< 1000 nm) <16 (>1000 nm)	0.3	<1.0	>300	>80 (<500 nm) >150 (500-1000 nm) >100 (>100 nm)	<50	100 (>500 nm) 250 (<500 nm)
Lunar Spectral Irradiance	<350 -2400	<8 (< 1000 nm) <16 (>1000 nm)	0.3	<2.0	>~300		NA	

11.2.3   Mission Architecture

This section briefly describes the key components of the mission architecture, which have evolved and simplified since the mission was first conceived in 2001 [7], [8].

11.2.3.1   System Requirements

The principal TRUTHS mission observational requirements are summarised in Table 11.4. Additional to these are those in Table 11.5.

Table 11.5: TRUTHS mission requirements

Mission requirement	Parameter
Polarisation sensitivity	0.5% (k=2) for λ<1000 nm 0.75% (k=2) for λ>1000 nm (Although for many applications these can be relaxed. They are primarily to support off-axis reference calibrations of other sensors and associated atmospheric corrections).
Orbit	polar 90-degree inclination with altitude of 609 km (±200 m)
Swath	50 - 100 km or larger
Scene Pointing	(reference calibration ability ~1 km, knowledge <2x GIFOV
Continuity of operation	Sufficiently continuous to not increase the sampling bias error contribution to represent a significant uncertainty contribution, Minimum 5 yrs with a target of > 8 yrs
Revisit	As frequent as possible but <61-day revisit as determined by the 90 deg polar orbit.
Coverage	Global nadir spectral radiances
Sampling time	Continuous during sunlit phase of the Earth
Quantisation	14 bit

The mission requirements Table 11.4, Table 11.5 are achieved through:

a) the payload instrument: a hyperspectral imaging spectrometer (HIS) which can be used to measure the Earth, Sun and Moon.
b) the radiometric calibration of that HIS directly, regularly and traceably to an on-board SI primary standard.
c) the choice of an orbit that supports climate benchmark measurements and increases the number of simultaneous cross-calibrations.
d) the use of a small, agile platform.

11.2.3.2 Payload

11.2.3.2.1 Overview

The main observational instrument of TRUTHS is a hyperspectral imaging spectrometer (HIS), with continuous spectral sampling extending across the UV-VIS-SWIR (320 nm to 2400 nm) and a planned 50 m GIFOV, not dissimilar in headline capability to the DLR EnMap, NASA Hyperion & HyspIRI, ASI PRISMA or future ESA CHIME missions.

> **TRUTHS will become a *standards laboratory in space* providing directly traceable measurements of unprecedented accuracy in orbit, through primary radiometric standard and calibration methodology**

The disruptive innovation of TRUTHS stems from incorporating a space-adapted primary SI-standard onto the satellite bus and its use with a novel on-board calibration system (OBCS). This mimics the method used terrestrially at NMIs, allowing TRUTHS to provide hyperspectral data immune from drift or biases for the lifetime of the mission and achieve the performance requirements of Table 11.5.

A summary of the payload instruments is provided below together with an overview of the on-board calibration method. It should be noted that the unusual asynchronous orbit of TRUTHS, whilst providing many observational benefits presents significant additional challenge to both the spacecraft and payload. Varying thermal and solar viewing (power) conditions add complexity to the mission. Thus, as part of the pre-flight calibration/characterisation and during the commissioning phase' calibrations of the HIS will be performed under a variety of simulated/real orbit conditions to assess any variances due to inadequate thermal stabilities.

11.2.3.2.2 Hyperspectral Imaging Spectrometer (HIS)

The HIS, through a novel approach, can be used both to image the Earth, measuring its spectral radiance, the Moon, measuring its spectral irradiance, and also to measure incident solar spectral irradiance. This concept not only minimises the instrumentation needed but also allows the derivation of ToA reflectance with the added confidence of exact spectral matching, through use of a common spectrometer. It also has the advantage that solar features can provide additional anchor points for spectral calibration. The design of the HIS is currently in progress as part of the phase A studies but an example of a potential realisation can be found in [8].

11.2.3.2.3 Cryogenic Solar Absolute Radiometer (CSAR)

The heart of the calibration system is the primary SI standard, the Cryogenic Solar Absolute Radiometer (CSAR). CSAR is a flight version of the primary standard cryogenic radiometer, adopted by most NMIs worldwide and recommended as the means to achieve SI traceability [55], [381]–[383]. The cryogenic radiometer is an extension of the Electrical Substitution Radiometer (ESR) concept, initially developed by the meteorologist Ångström (1893) [384] and the metrologist, Kurlbaum (1894) [385] and are in essence the basis of instruments currently flying in space measuring TSI, e.g., PMO6 on SOHO. Cooling the technology to cryogenic temperatures (originally <30 K) reduces uncertainty levels to <0.01 % (k=2) as first shown by NPL in the 1980s [53], [386]. Due to performance of space qualified cryogenic coolers, CSAR will operate at <~60K (higher temperature increases the time constant and

decreases sensitivity a little), when flown it will be the first cryogenic radiometer, and consequentially optical primary SI radiometric standard flown in space and is a key element of the calibration system of TRUTHS. It is through this On-Board Calibration System (OBCS) that the traceability of Earth spectral radiance measurements to SI to an absolute accuracy of <0.3 % (k=2) is achieved.

Apart from serving as a primary standard for radiance and irradiance, CSAR will also provide science measurements in its own right, TSI with an accuracy of 0.02 % (k=2) a significant improvement over existing ambient temperature radiometers.

Because CSAR is both critical to the TRUTHS missions' ability to achieve its aims and the key novel aspect of TRUTHS, the instrument was first prototyped (CSAR_v1) in 2010 and successfully undergone both laboratory and field tests (see below). A second version of the instrument (CSAR_v2), an evolved and simplified design, making direct use of an upgraded Airbus space cooler was built and demonstrated in 2016, see Figure 11.8. The operating principles of cryogenic radiometers and also CSAR are described in detail in many places e.g. [53], [381]–[383], [386] and so won't be repeated here.
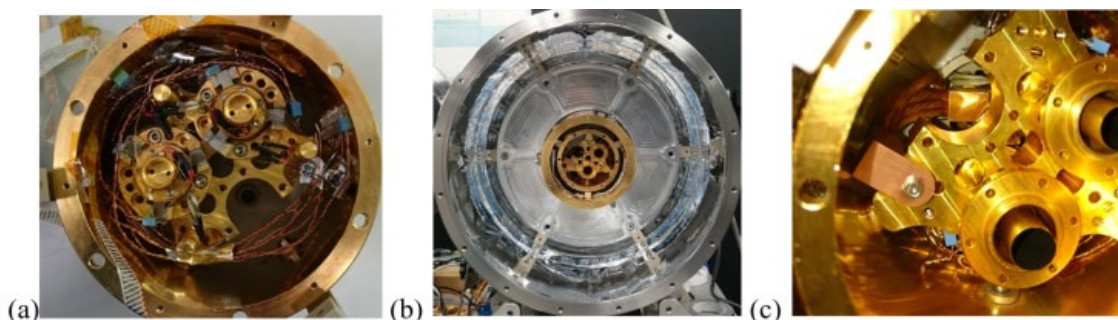
Figure 11.8: Photographs of the assembly of CSAR_V2 showing, from left to right, (a) two cavities mounted on the temperature reference block (b) the radiometer head coupled to the HPSC and mounted inside the cryostat and terrestrial vacuum can (c) close up of cavities showing thermal link to the HPSC

One of the principles underpinning CSAR's ability to establish SI-traceability in-flight is that the only optical interface that is subject to potential change is a blackened cavity. The use of a carbon nanotube black coating with resultant absorptance of >0.99995 makes it inherently insensitive to change.

11.2.3.2.4 On-Board Calibration System (OBCS) overview

The calibration system designed for TRUTHS has been simplified relative to those used at NMIs to minimise the number of components, and in particular, the number of moving parts compared to measurements in the laboratory and also to reflect the use, where possible, of heritage space components or heritage constituent technologies and is shown schematically and in manufactured breadboard form in Figure 11.9.
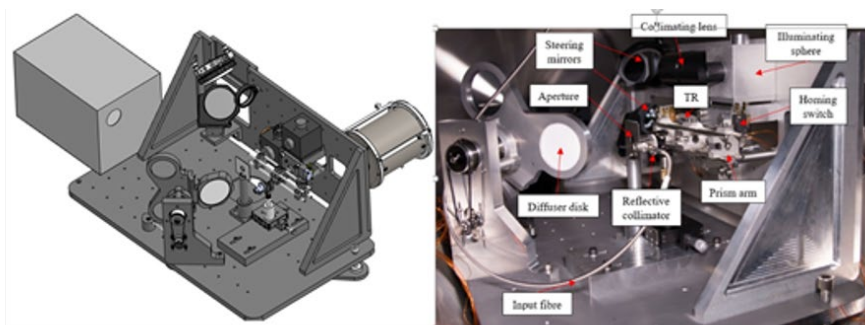
Figure 11.9: Computer Aided Design drawing of Laboratory breadboard of the TRUTHS calibration system together with a photograph of its engineering realisation before testing in vacuum tank.

The calibration of the HIS for Earth radiance and SSI measurements is performed, traceably to the CSAR, using a system that consists of a Transfer Radiometer (TR), a small number (~8-10) low power Laser Diodes (LDs), an Integrating Sphere (IS) and a diffuser wheel with two diffusers (D1, D2) for redundancy. Calibration generally takes place during the Earth shadow part of the orbit allowing the systems to be well-protected from solar and other radiation damage.

11.2.3.2.5   On-Board Calibration Procedure

A video representation of the OBCS and calibration procedure can be found here [387]. This is performed with just two mechanisms within the calibration system. A diffuser wheel, common on heritage sensors, and a rotating laser arm, used to distribute the laser power into three of the calibration sub-systems.
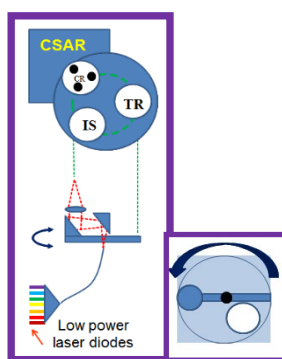
Figure 11.10: LD illumination system (schematic)

Here we discuss, in outline, the calibration steps. Note that the diagrams here are schematic, and in the actual flight implementation, for example, additional turning mirrors may be used, which do not affect the overall calibration principle. Similarly, the exact design of sub-systems such as transfer radiometer and laser illumination systems may also differ in detail. It is also likely that, without adding any additional rotational mechanisms, further redundancy can be achieved for all of the critical sub-systems.

An example layout, used as the breadboard is shown in Figure 11.9 and in a more cartoon style in Figure 11.10. The primary calibration is performed at a small number of wavelengths corresponding to the chosen LDs. These LDs can illuminate either of two (identical) cavities of the CSAR (providing redundancy), the TR and the IS (which is used as part of the illumination of the HIS during calibration). The LDs illuminate each instrument/sub-system in turn using an illumination system based on a rotating pair of rooftop prisms serving as mirrors, with the central axis (mirror) being fed by laser radiation from a common optical rod conjoiner linking LDs via optical fibre (Figure 11.10). An alternative realisation may involve the LDs or at least coupled fibres attached directly to the perimeter of the rotation wheel,

avoiding the prism mirrors. The optical fibre in either case is wound around the compressor of the cryocooler of CSAR where the micro-vibrations help to reduce the effect of speckle. The monochromatic radiation from the LDs illuminates the full aperture of HIS in a Lambertian manner via a flat plate diffuser in a similar manner to existing on-board systems, the difference being the use of monochromatic LD radiation rather than the Sun. The radiance of the diffuser can be measured directly inflight by the on-board calibrated TR. The responsivity at all other intermediate wavelengths is obtained using a white light source e.g., incandescent lamp, which is radiometrically anchored at the LD wavelengths. The following steps scope the calibration procedure which mimics that carried out terrestrially. It should also be noted that in addition to radiometric calibration the use of LDs allows wavelength accuracy of HIS to be checked and also of particular interest, stray light. The latter whilst not having enough LDs to provide a full calibration matrix as can be done on ground using tuneable lasers, does provide sufficient spectral sampling to allow the pre-flight correction matrix to be at least monitored in flight.

Step 1: Calibration of TR against CSAR using LDs. The optical power of the temperature-and-current-stabilised LD is measured absolutely by the CSAR Figure 11.11(a), the beam underfilling the CSAR irradiance defining aperture and then used to calibrate the response of the TR to this now measured power level by rotation of the prism assembly Figure 11.11(b). The TR in this illustration is a small integrating sphere with integral Si and InGaAs semiconductor photodiodes viewing its internal wall. The integrating sphere provides a convenient means to reduce any alignment or source non-uniformity issues (although alternative methods to achieve the same goal can be envisaged and may in practise be utilised). It has two field-of-view (FOV) defining apertures (radiance), but for this phase of the calibration they are underfilled. This step is repeated for each of the LD wavelengths in turn. The calibration process requires the LD output to be of known wavelength (controlled with an etalon) and stable in intensity (<0.1%) during the transfer from the CSAR to TR (about 1 minute, which is easily achieved). Individual wavelength calibrations can take place sequentially or on different orbits. However, it is probably likely to be optimum to perform the full calibration sequence step 1 and 2 for each wavelength individually.
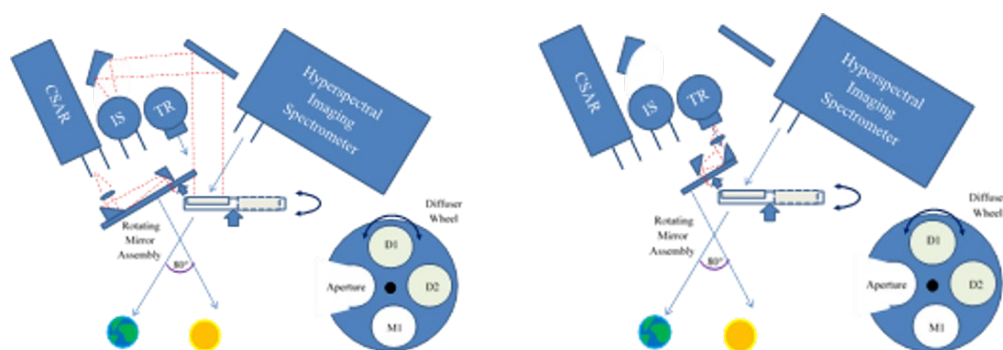
Figure 11.11: Schematic of step 1. The LDs illuminate (underfill) first (a) the CSAR cavity and then (b) the TR, by rotating the mirror assembly

Step 2: HIS (Earth Radiance view) calibrated against the TR at each LD wavelength (radiance mode). The radiance responsivity of the HIS is determined by comparison with the radiance responsivity of the TR using the LDs. In this step the LD source is allowed to expand and then collimated to create a uniform illumination on a flat plate Lambertian diffuser, using an IS and mirrors (for alignment purposes). The IS not only helps to pre-condition the LD radiation, removing effects of non-uniformity, but also reduces significantly the effect of speckle, from both spatial and temporal coherence. The diffuser can move in and out of the FOV of the HIS by rotation of its mounting plate shown in Figure 11.12 with a second redundant diffuser and also mirror. When illuminated, normal to

the diffuser as shown (Figure 11.12), the TR and HIS simultaneously view the diffuser at reciprocal angles.
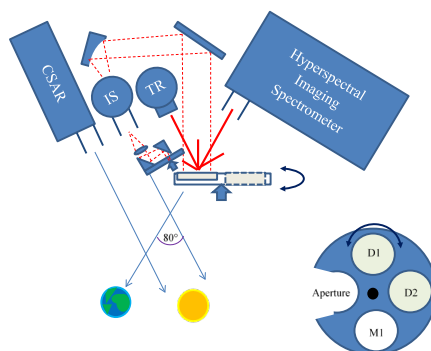
Figure 11.12: LD illuminates the diffuser, via the IS, and this is viewed by the HIS and IS

In this step, the TR measures the absolute radiance of the LD-illuminated diffuser. Its absolute radiance responsivity having been determined from its power responsivity (step 1) and knowledge of the areas of the two FOV-defining apertures, which are never directly exposed to the space environment. Note that, because the TR measures the radiance of the diffuser directly, the transmittance of the IS and reflectance of any turning mirrors (optics) do not need to be known. It is advantageous to limit the FOV differences between the TR and the HIS, but such differences and their effect is small and can be characterised pre-flight and therefore an exact match is not required.

Thus, the HIS is calibrated for radiance responsivity at the LD wavelengths. Note also that by comparing the TR signals in Step 1 and Step 2 (assuming a stable laser source between these two measurements) the TR also directly calibrates the throughput of the IS, mirrors and diffuser at these wavelengths. This provides an irradiance responsivity calibration of the system comprising the IS (underfilling an irradiance defining aperture on the entrance port), mirrors, diffuser and HIS (this allows it to become the SSI measuring system, when the aperture is overfilled by solar radiation, see step 4).

Step 3: HIS (Earth radiance view) calibrated at intermediate wavelengths with a lamp.
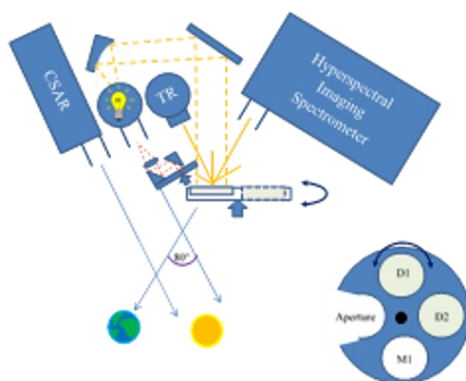
Figure 11.13: Lamp illuminates the diffuser via the integrating sphere and mirrors to provide calibration of the HIS at intermediate wavelengths

An incandescent lamp (with a smooth spectral output) illuminates the IS and consequently the diffuser and is viewed by the HIS in a similar manner to the LDs. At the end of step 2, the HIS has been calibrated at the wavelengths of the LDs for absolute radiance responsivity. It is now only necessary to interpolate between these laser wavelengths. This will be achieved using a white light source/lamp with a

broadband, smooth spectral output. Although the lamp will change during operation, it will do so in a spectrally smooth manner [59]. The absolute level and the basic spectral shape are determined at the LD wavelengths in step 2, this step, Figure 11.13, is primarily used for interpolation although at the extremes of the wavelength range of HIS, beyond the final anchoring wavelengths of the LDs the spectral shape is extrapolated. There are many examples of such lamps being used for space calibration, here we only need functionality and short term (< 10 s) stability and of course spectrally smooth output.

The HIS can then be considered calibrated for making spectral radiance measurements of the Earth. Similarly, the system comprising the IS, mirrors, diffuser and HIS can be considered calibrated for making spectral irradiance measurements of the Sun/Moon where the aperture on the IS is the defining aperture.

Step 4: Operational measurements of the Earth and Sun/moon.
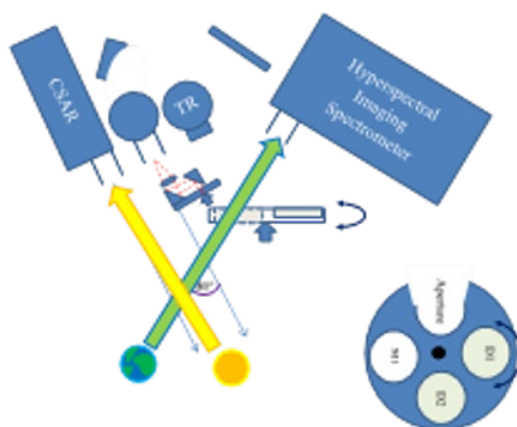
Figure 11.14: Measurements of the Earth and Sun

Measurements of the radiance of the Earth are made with the HIS directly. The diffuser disc rotates to allow light from the Earth to enter the HIS telescope, Figure 11.14. When the TRUTHS satellite is rotated to allow CSAR to face the Sun, then the CSAR can measure TSI and the IS (illuminating the mirrors, diffuser and HIS) can measure SSI and similarly for the Moon. For UV measurements of SSI, where the signal levels are very low, the mirror (M1) rather than diffuser (D1/D2) is used in the path between the IS and HIS.

These measurements are fully SI-traceable because of this calibration scheme for their radiometric responsivity. Full traceability to SI also needs traceability for the defining aperture areas (the two apertures on the TR, the aperture on the IS, and the aperture on CSAR). These apertures will be calibrated on the ground. In orbit, apertures on CSAR and IS will both be subject to direct exposure to space and the Sun and so there is a need therefore to monitor the stability of those aperture areas. CSAR will have redundant apertures (different apertures on each cavity, which can have varying degrees of exposure). For the IS and in principle the TR, a dedicated LD beam (at one wavelength since geometry has no spectral dependency) is expanded with optics to a size that overfills the defining apertures of CSAR and the IS. By illuminating each CSAR aperture (redundant options) in turn, it can compare these apertures and calibrate the IS in irradiance (rather than power) mode. The same LD irradiance beam can also be used to check the smaller TR aperture as a relative comparison. It is also envisaged that there will be two IS's on TRUTHS each with their own aperture and again these will be used in a manner that allows reduced solar exposure time for one of the redundant pair.

Calibration procedure summary. Figure 11.15 shows a schematic representation of the above calibration sequence for TRUTHS. Each complete iteration through the cycle (single wavelength) is estimated to take at most 5 minutes including time for any motions and stabilisation of the system.
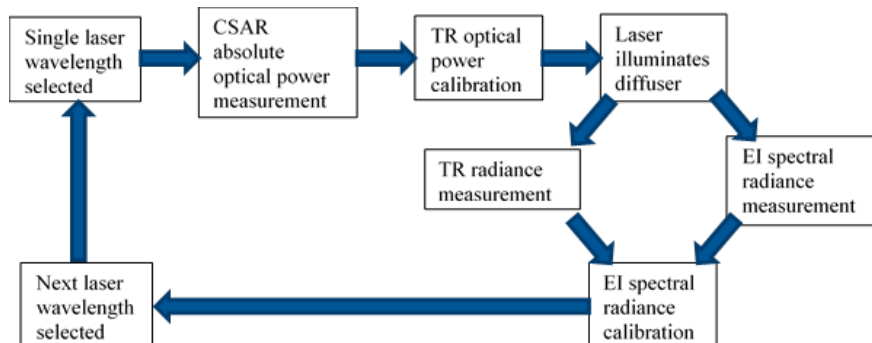
Figure 11.15: Schematic Showing Overall Calibration Sequence

All the sub-components of the calibration system, IS, TR, diffusers, detectors, optical fibres can in themselves suffer degradation. The effects of this are removed by the calibration process which effectively spectrally calibrates each component as part of the system. The Cal system relies on short-term radiometric (power) stability of the LD radiation, which is largely related to temperature and drive current, both of which can be readily achieved for the <1-minute timescales required. Wavelength stability or knowledge to 0.1 nm is required for the life of the mission. The calibration system, with the exception of the CSAR and the IS are in an enclosed environment and never exposed to direct sunlight. Although in this baseline design only LDs, diffuser plate and cavities of the CSAR are fully redundant, this is likely to change in the flight version.

11.2.3.2.6 Payload Performance

Table 11.6 shows the uncertainty budget for the calibration system, comparing the traditional NMI laboratory-based performance, with the TRUTHS calibration system breadboard to the expected flight model performance. This table presents the principal sources of uncertainty in the calibration process of the HIS but does not account for any potential residual stray-light, or non-linearity of the HIS. The latter will be evaluated by varying calibration radiance levels (laser diode power) and stray light will be evaluated as part of the calibration using the monochromatic wavelengths on-board to monitor the more detailed pre-flight characterisation using a full spectral calibration with a tuneable laser facility. The calibration system itself will be non-polarised- the LDs themselves, the optical fibres and scatter from the walls of the IS and diffusers ensuring that this is the case and so no component has been included for this in the uncertainty budget.

Table 11.6: Calibration system & HIS radiometric uncertainty (k=2)

Uncertainty Source	Lab-based uncertainty	Breadboard-based Uncertainty	Space-based Uncertainty	Notes
Laser (diodes) Radiometric stability (60 sec)	0.01%	0.07-0.3%	<0.07%	Space qualified, stabilized DFB lasers. Note for the breadboard testing not all lasers were of DFB quality resulting in poor stability
CSAR / primary std	0.02%	0.06 %	<0.06 %	Worst-case scenario for laser diode power levels
Prism arm	<0.01%	< 0.01 %	< 0.01 %	Negligible
Transfer radiometer	0.02%	0.03 %	<0.03 %	Voltage measurement uncertainty
External aperture	0.02%	0.02%	0.02%	Calibrated pre-flight
Traceability	0.01%	0.08%	<0.08%	Worst-case scenario
HIS thermal control (1K)			0.01-0.20%	<0.05% at all wavelengths, except at extremes (<350 nm & >2200 nm)
HIS SNR			0.03%	Required laser source integration times from 7-60 sec, and some spatial binning for solar spectral irradiance
TOTAL	0.04%	0.16-0.32%	0.16-0.26%	Uncertainties added in quadrature

| CSAR (On-board SI Traceability primary standard) | → | HIS (On board calibration system) | → | SNO inter-calibration between 2 satellites | → | L2+ application product |

Element	Uc (%)
Measurement of electrical power	0.010
Cavity absorptance	0.010
Scattered light	0.004
Random noise	0.06
TOTAL	0.02-0.07

Element	Uc (%)
CSAR	<0.06
Prism arm	< 0.01
Transfer radiometer	0.03
External aperture	0.02
Traceability	0.08
HIS thermal control (1K)	0.01-0.20
HIS SNR	0.03
TOTAL	0.16-0.26

Element	Uc (%)
TRUTHS HIS	0.16-0.26
Spectral mismatch	0.1-0.2
Spatial mismatch	0.1
View Angle	0.1-0.2
Atmos. corr.	0.1-0.3
BRDF	0.1
TOTAL	0.4-0.7

Element	Uc (%)
GHG retrievals	1% = 0.1ppm
Ocean Colour	0.5% = 5% WLR
Cloud Radiative Forcing	0.3%

Figure 11.16: Shows the progression of uncertainty propagation, with typical uncertainty budgets from the SI-traceable CSAR instrument, through to the HIS on-board calibration, sensor-to-sensor SNO cross calibration (see Table 20) and final example L2 product upgrade for the TRUTHS mission. Uncertainty (k=2) propagation to inter-calibration & L2+ products

11.2.3.3   Operational Modes

Table 11.7 provides an outline of the observational plan for TRUTHS. The full calibration mode indicated to nominally take place bi-monthly will vary from beginning to end of life as a degradation profile is established. This full calibration mode includes all wavelengths traceable back to the CSAR and will be carried out in a continuous cyclic

> SITSats like TRUTHS will provide an in-orbit standard for reference intercalibration for other EO satellite instruments

manner. However, calibrations of the imager can take place daily using coefficients of the calibration system established on an ongoing basis. Not all spectral channels need to be calibrated each cycle unless significant degradation is found, and similarly at least one wavelength can be done per orbit on the

Earth shadow side of the orbit. On occasions, particularly during commissioning phase, some HIS calibrations at some wavelengths are likely to be carried out to assess any intra-orbital and or pointing effects.

Table 11.7: TRUTHS operational modes

Operational Mode	View	Frequency	Length of operation	Notes
Solar measurements	Solar	Every orbit	5-10 mins per orbit	Probably polar views
Calibration of the calibration system to CSAR	Internal satellite diffuser	Potentially every orbit. Frequency to be defined based on observed ageing	30 minutes, one or two wavelengths per orbit	Carried out during dark side, builds a calibration of the TR so that it can be used with diffuser on a daily basis
Full calibration of HIS Earth Shadow	Internal Satellite diffuser	Nominally achieved Bi-monthly (timed defined following in-orbit degradation monitoring). Can be carried out on as needs basis	1 day accumulated (over several orbits)	Performed during shadow phase wavelength by wavelength
Calibration monitoring of HIS	Laser/lamp illuminated diffuser	Daily using ongoing updates of Cal-system coefficients	Few minutes	Generally Performed in shadow but can be carried out at any part of orbit
Climate benchmarking	Earth (nadir view)	Bulk of operations – most of the orbit	~35% duty cycle	
Cross–calibration of sensors using angular movement	Earth – test sites (non-nadir)	~1- per day (but could be orbital)	~ 5 minutes	Only when required

11.2.4   Conclusions on TRUTHS

Climate change is the most critical issue facing mankind today. The enormous cost implications of policy decisions based on forecasted impacts resulting from the predictions of a warming Earth demand that the science community finds and delivers the necessary information with the highest possible confidence in the shortest possible time. The challenge to the metrology community is equally severe.

The IPCC [107] concludes that the mix of natural variability and anthropogenic effects on decadal timescales is far from fully understood or measured, requiring significant improvements in accuracy. Unequivocal attribution and quantification of subtle fingerprint indicators from this noisy background are fundamental to our ability to predict climate reliably and use appropriate mitigation/adaptation strategies. The uncertainty in climate prediction lies in the complexity of the models, our inadequate understanding of the Earth system and its feedback mechanisms, and the relatively poor quality of available data against which to test predictions on the necessary decadal timescales.

Establishing rigorous SI traceability to the key measurands underpinning the ECVs, with sufficient accuracy, is a central pillar to achieving this goal. The satellite community has over the years developed a number of strategies to support this objective, but as yet all fall dramatically short of the required accuracy, forcing the adoption of high-risk philosophies seeking to monitor 'change' through normalization of overlapping datasets. While pre-flight calibrations can be made traceable, the harsh environment of space following the shock of launch means that few, if any, of the radiometric ground calibrations can be relied upon in space. Efforts to recover some of the information can be carried out using a variety of post-launch methods, but none have sufficient accuracy to meet the needs of climate [89].

This sub-section has described an example of the only real solution available to the EO community, i.e., to establish high-accuracy SI traceability in flight, on-board the spacecraft. One mission, TRUTHS, which is designed to achieve this for the solar-reflective domain, has been described in some detail. Its sister CLARREO and its pathfinder demonstrator complements this in the solar-reflective domain and extends the capability into the IR spectral region, and a similar Chinese mission is also under-development.

TRUTHS would become 'a standards laboratory in space' providing directly traceable measurements of unprecedented accuracy (factor of 10 improvement) in SI units, in orbit, through the deployment of a primary radiometric standard and associated calibration methodology. This unprecedented accuracy will establish benchmark measurements for the detection of decadal change in the most sensitive (but least understood) climate radiative forcings, responses and feedbacks in the solar reflective domain.

With spectrometer resolution sensors of unprecedented accuracy, TRUTHS can observe climate-relevant processes related to the atmosphere, the oceans and the land surface. TRUTHS' observations will test and advance the development of climate models, allowing more accurate climate change hindcasting and forecasting. In addition, TRUTHS' measurements of ground-based reference sites (and the Moon) will allow retrospective improvements to the calibration of existing satellites and their data.

SITSats, like TRUTHS and CLARREO, will provide an in-orbit standard for reference intercalibration for other EO satellite instruments (with benefits for both science applications and operational services). The TRUTHS and CLARREO missions are planned to fly in an orbit that allows frequent 'cross-overs' with other in-flight sensors. Together with their own pointing capabilities, and ability to match spectral and spatial resolution, the high calibration accuracy and SI-traceability will transfer to other sensors through simultaneous observations of a target.

SI-traceable observations at climate change accuracy from different instruments can then be objectively linked to a common baseline time-series even if no sensor-to-sensor overlaps are available. Had an in-orbit calibration observatory similar to TRUTHS/CLARREO already flown, this benefit would exist now. Delaying the installation of such a system reduces the value of the climate records and creates the constant risk of data records being lost completely should an overlap be lost. The full value of SITSats will be gained in the future, when a series of small platform in-orbit calibration instruments anchor EO time series, providing the highest possible confidence in any observed trends and at relatively low cost.

The realization of SI-traceable measurements in orbit is achievable now and time critical. This 'grand challenge' project between the metrology and Earth/climate science community must become a priority if society is to reap the commercial benefits of EO, but more fundamentally, without it, policy-makers will be acting blindly in their efforts to ensure long-term sustainability and growth within an ever-changing climate.

11.3 Chinese Radiometric Benchmark of Reflected-Solar Band Based on Space Cryogenic Absolute Radiometer

Calibration is important for the development of optical remote sensors for the quality of remote sensing data. The remote sensors can be calibrated with high accuracy before launch. The radiometric scale is often traced to ground-based calibrations. But this traceability chain can be affected by the launch process, space environment, and instrument calibration drift. So, it is necessary to calibrate the optical remote sensor in-orbit. The in-orbit calibrations often adopt a solar diffuser, standard lamp, or standard blackbody at present, the foremost of which only tracks relative changes after launch. The EOS/MODIS uses a solar diffuser to realize the highest accuracy in-orbit calibration in the field of spectral imaging, achieving a measurement accuracy of 2%. The on-satellite radiometric scale cannot be verified beyond

this due to degradations of the calibration system, such as the diffuser, the standard lamp, etc. The remote sensing data of different satellites are thus difficult to compare. Such remote sensors cannot satisfy the urgent need of climate-change research due to the limited accuracies of in-orbit radiometric calibration.

A Chinese expert group on Earth observation proposed the concept of a radiometric benchmark satellite in 2006. The Chinese Space-based Radiometric Benchmark (CSRB) project has been under development since 2014. The goal of the CSRB project is to launch a radiometric benchmark satellite that adopts a new in-obit calibration system principle similar to that of the Traceable Radiometry Underpinning Terrestrial-and Helio-Studies (TRUTHS) as well as the Climate Absolute Radiance and Refractivity Observatory (CLARREO). The radiometric benchmark satellite has ultra-high accuracy via self-calibration in orbit. The radiometric scale of the radiometric benchmark satellite is transferred to other satellites by synchronous observations during orbit-track crossings. The radiometric benchmark satellite will improve the measurement accuracy and long-term stability of measurements of emitted Earth spectrum, the incident solar spectrum, and the reflected solar spectrum.

The development of the CSRB for the reflected solar band is introduced here. The development is supported by the National High-tech Research and Development Plan (863 Plan) and the National key R&D program of China, and includes the following key technologies:

- A space-based cryogenic absolute radiation measurement
- Establishing a high-precision and high-stability thermal environment
- Space-based mechanical refrigeration with low temperature and large cooling capacity
- A depolarizing telescope system
- A large dynamic range imaging spectrometer
- High-precision power-to-radiance benchmark conversion

The Space Cryogenic Absolute Radiometer (SCAR) is used to realize the super-high accuracy radiometry on-satellite referencing the ground-based optical standard. The reflected solar spectral radiance is measured by the Earth-Moon Imaging Spectrometer (EMIS). The EMIS is regularly calibrated by SCAR and the

CSRB project aims to launch a radiometric benchmark satellite

Benchmark Transfer Chain (BTC) in order to improve the measurement accuracy and long-term stability. The Total Solar Irradiance Monitor (see §6.1.9) is used to acquire long-term measurements of the total solar irradiance, which is calibrated by the SCAR using direct solar observations.

11.3.1 Principle of the CSRB

The radiometric benchmark in the reflected-solar band uses the SCAR to establish the instrument's calibrations instead of the traditional approaches of solar diffusers, use of standard lamps, vicarious calibration methods, and ground-based calibration techniques, as shown in Figure 11.17. The calibration system consists of the SCAR and the BTC.

11.3.1.1 Space Cryogenic Absolute Radiometer (SCAR)

At present, the primary standard for laboratory radiometric calibrations is the cryogenic radiometer, allowing direct traceability to the international system of units (SI). The Spectral Irradiance and Radiance Responsivity Calibrations using Uniform Sources (SIRCUS) developed by NIST is one of the best ground-based spectral radiometric calibration devices currently. The uncertainty of this cryogenic-radiometer-based calibration is 0.1%. However, due to the impact of the launch process, the space environment, and subsequent instrument changes, the traceability link may be broken, and the remote-sensing data after launch cannot be unambiguously traced back to SI. Standard lamps, blackbodies, and

solar-diffusing reflectors are often used in on-orbit radiometric calibrations. The spectral imaging instruments MODIS and VIIRS utilize on-orbit calibration systems consisting of solar-diffuse reflectors (SD) and solar-diffuse reflectance stability monitors (SDSM) to maintain their solar reflection spectrum calibrations. The reflectivity of the SD decreases significantly, however, during long-term on-orbit use, and the calibration accuracy of on-orbit absolute radiation is thus 2 % rather than the desired 0.3 %.

> **SCAR is used to realize high accuracy radiometry on-satellite, referencing the ground-based optical standard**

While pre-flight radiometric calibrations are based on the development of standard blackbodies and absolute detectors, further development is needed to apply these on-orbit. Cryogenic radiometers are generally based on electrical substitution radiometers operating at cryogenic temperatures. Based on the equivalence of electric heating and incident light radiation heating the low-temperature radiometer in a superconducting state, the unknown optical power can be calibrated against the equivalent electric power, which can be accurately measured using the working principle of electric substitution. A space-based cryogenic radiometer could be used to realize ultra-high accuracy absolute radiometric measurements on a spacecraft instrument.

In order to realize on-orbit traceability, absolute measurement accuracy, and long-term radiometric-and spectral-calibration stability of optical remote-sensing payloads in the reflected-solar spectral region, a space-based cryogenic radiometer is proposed to establish a radiometric benchmark on orbit with an intended measurement accuracy of 0.02 %. Several different measurements are then tied to this cryogenic radiometer.

The SCAR is an electrical substitution radiometer operating at 20 K, based on a blackbody cavity with super high absorptance. Incident light induces a temperature increase of the blackbody cavity by absorption. The power of the incident light can be obtained by precisely measuring the electrical power applied in order to maintain constant temperature as the incident light is duty cycled and its power replaced by electrical heater power. The heating effectiveness of the incident light and electrical heater are nearly equivalent at 20K, reducing non-equivalence corrections.
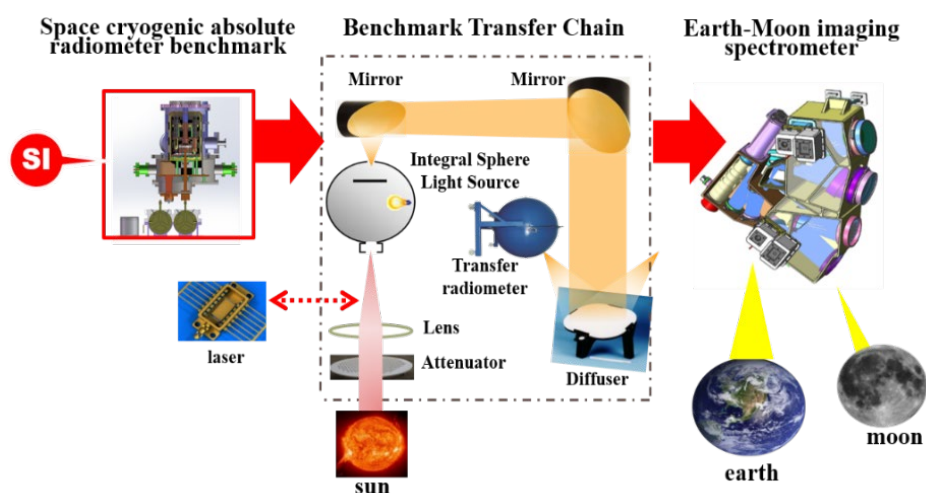

Figure 11.17 The principle of the radiometric benchmark in the reflected-solar band

Table 11.8 The goals of radiometric benchmark in the reflected-solar band

Instrument	Observation target	Parameter	Technical indicator
SCAR	Sun	Uncertainty	0.03% (k=2)
		Working temperature	20K
		Dynamic range	1 mW-30 mW
		Spectral range	380 nm-2350 nm
EMIS	Earth	Radiance uncertainty	1% (k=2)
		Spatial resolution	100m-500m
		Spectral range	380nm-2350nm
		Spectral calibration uncertainty	0.5nm
	Moon	Irradiance uncertainty	2% (k=2)

11.3.1.2 Earth-Moon Imaging Spectrometer (EMIS)

The EMIS is used to measure the radiance of the Earth and Moon. The optical design of the EMIS consists of the telescope and the hyperspectral imaging spectrometer as shown in Figure 11.18. The telescope utilizes a four-mirror anastigmat (4MA) to eliminate aberration. The hyperspectral imaging spectrometer is based on an Offner design. A prism is used as the dispersion element with VNIR and SWIR channels covering a spectral range of 380-2350 nm. The telescope uses the image space telecentric structure to achieve matching conditions with the pupil of the spectrometer. By setting baffles at the intermediate image plane, the influence of stray light is reduced. The EMIS makes a trade-off between the spectral and spatial resolution, with spectral and spatial sampling better than 10 nm and 100 m, respectively. The swath width is about 50 km at nadir from a 600-km orbit. The EMIS selects lens parameters, such as thickness, curvature, etc., to achieve lower dispersion non-linearities and better spectral performance.
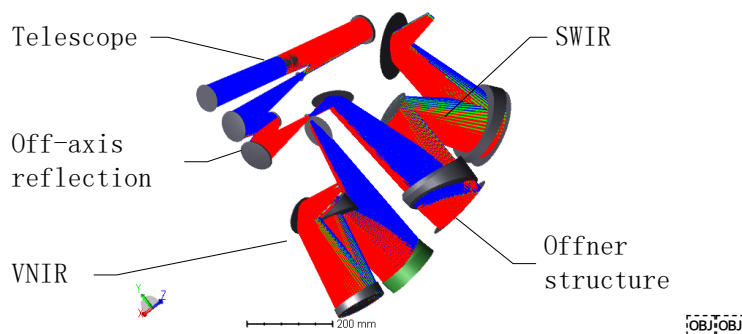
Figure 11.18 Optical design of EMIS

The radiances of the Earth and Moon are measured by the Earth-Moon Imaging Spectrometer (EMIS), requiring a high signal-to-noise ratio and large dynamic range. The power scale of the SCAR is converted to radiance by the BTC. Based on multi-wavelength laser diodes and a halogen tungsten lamp, the EMIS can be radiance calibrated by the transfer radiometer. The linearity of the EMIS can be calibrated by the Sun attenuator. The goal of the radiometric benchmark of the reflected-solar band is shown in Table 11.8. The radiance uncertainty is expected to reach 1% (*k*=2).

11.3.1.3 Benchmark Transfer Chain (BTC)

While the radiometric scale of the EMIS can be traced to the SCAR, the measurement accuracy and long-term stability of the EMIS can be improved by on-board hyperspectral calibration from both the SCAR and the BTC. The SCAR is the on-board primary benchmark and realizes highly accurate radiation measurements with long-term stability. The Transfer

> **The EMIS is regularly calibrated by SCAR and the Benchmark Transfer Chain**

Radiometer (TR) is calibrated and used as the working benchmark by the laser power measurement and comparison. The multi-spectral radiance of the tungsten halogen lamp is calibrated by the TR. The spectral radiance of the tungsten halogen lamp in the reflected solar band is reconstructed by a fitting algorithm. Then the hyperspectral calibration of the EMIS can be realized by the tungsten halogen lamp. The response linearity of the EMIS is ascertained by the solar attenuator.

11.3.1.4 On-Orbit CSRB Measurement Requirements

The high precision and high stability observations are intended to achieve the following measurement requirements:

Total solar irradiance: Uncertainty 0.02% (k=2), long-term stability 0.005%/10 years; spectral range 0.2 μm to 35 μm.

Earth radiance: Uncertainty 0.3%-1% (k=2); spatial resolution 100 m to 500 m; spectral range 380 nm to 2350 nm; spectral calibration accuracy 0.5 nm.

Lunar radiance (Whole): Uncertainty 2%.

The key technologies of the CSBR for the reflected-solar band are being developed. The prototype of SCAR has been in development since 2015, supported by the National High-tech Research and Development Plan (863 Plan). The prototype of the radiometric benchmark payload, as shown in Figure 11.19, has been in development since 2018 and is supported by the National key R&D program of China.
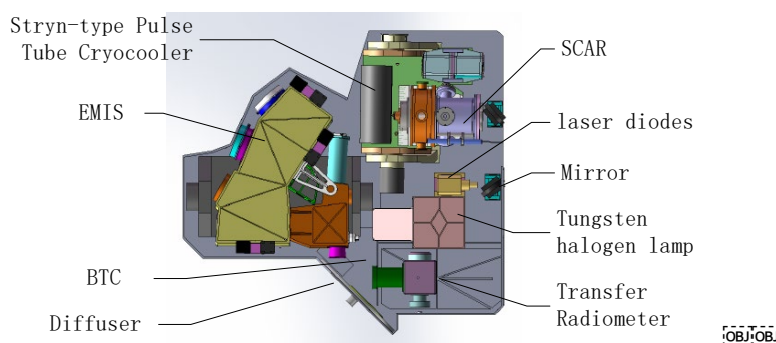
Figure 11.19 The design of the reflected-solar spectrum observation instrument

11.3.1.5 Cryogenic Absolute Measurement

The prototype of SCAR consists of the absolute radiation receiver, a Stryn-type Pulse Tube Cryocooler (SPTC), the measurement system, and the vacuum pump, as shown in Figure 11.20. We have solved the problems of radiation heat leakage, the needed high thermal-resistance connection, and cryogenic refrigeration. The sensitivity of the blackbody cavity successfully achieved 3.95 K/mW. The blackbody cavity is designed according to the effective emissivity simulation results of Dr. Fang, adopting a cylindrical cavity with a conical bottom in order to increase the number of reflections of incident light.

The internal surface of the blackbody cavity is spray painted black. Experimental measurement results show the blackbody cavity absorption is 0.999928±0.000006 (1σ) at a wavelength of 632 nm.
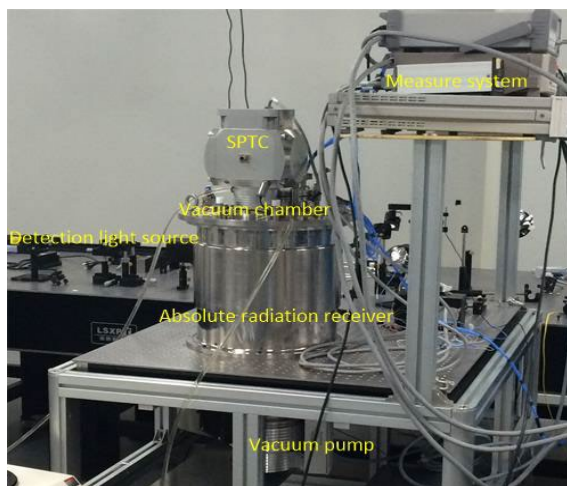
Figure 11.20 The SCAR prototype

11.3.1.6   Calibration Lamp for the Reflected-Solar Band

The calibration light source for the reflected-solar band is a tungsten halogen lamp, which has a smooth spectrum, as shown in Figure 11.21, that can be precisely obtained by an inversion algorithm using multispectral calibration data. The long-term variation of the spectral distribution curve has been experimentally measured. The experimental results show a redshift with time.
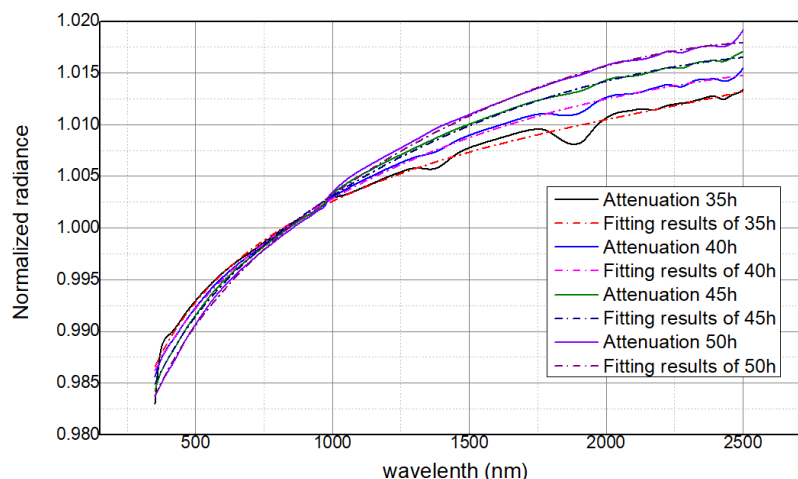
Figure 11.21 The spectral radiance attenuation of tungsten halogen lamp

A dual Babinet depolarizer is used in the telescope to reduce the polarization sensitivity of the optical system. This depolarizer consists of two series H-V depolarization devices. The Müller matrix of the first H-V depolarization device is expressed as

$$M = \begin{bmatrix} 1 & 0 & 0 & 0 \\ 0 & 1 & 0 & 0 \\ 0 & 0 & \cos\delta_1 x & \sin\delta_1 x \\ 0 & 0 & -\sin\delta_1 x & \cos\delta_1 x \end{bmatrix}$$

Equation 29

and $\delta_1 x$ is depicted by

$$\delta_1 x = \frac{2\pi}{\lambda}[n_0(\lambda) - n_e(\lambda)][(t_1 - rx\tan\beta) - (t_2 + rx\tan\beta)]$$
$$= k\Delta n(\lambda)[2rx\tan\beta + (t_1 - t_2)]$$

<div align="right">*Equation 30*</div>

where λ is the wavelength, x is the normalized position coordinates, n_o is the refractive index of O light, n_e is the refractive index of X light, r is the radius of the depolarizer, and β is the angle between the two wedge plates. The second H-V depolarization device is placed behind the first H-V depolarization device. The angle between the two depolarizers is 45°.

11.3.2   Uncertainty Decomposition

The uncertainty of the CSBR is shown in Table 11.9. The radiometric uncertainty of SCAR is 0.03%. The radiance uncertainty of EMIS is 0.3%. Thus, the uncertainty of the radiance calibration is expected to reach 0.5%, which achieves the less than 1% uncertainty of the hyperspectral radiance measurement requirement.

<div align="center">Table 11.9 Reflected solar spectrum observation uncertainty</div>

Component	Impact factor		Uncertainty (k=2)
SCAR	radiometric uncertainty		0.03%
Radiance Calibration			0.5%
	Laser diode	power stability	0.1%
	Transfer radiometer	optical power measurement	0.1%
		optical-radiance conversion	0.08%
		radiance measurement	0.1%
		photodiode detector	0.14%
	Full spectral light	spectral radiance stability	0.2%
		spectral radiance reconstruction	0.3%
	diffuser	reflection uniformity	0.15%
		stray light	0.2%
EMIS	radiance uncertainty		0.3%
Total			0.6%

In summary, the application of the new space absolute radiation system is intended to realize ultra-high absolute-accuracy radiometric measurements on orbit, establishing an on-orbit traceable radiometric benchmark for the reflected-solar spectrum. The uncertainty and long-term stability of the total solar irradiance as well as lunar- and terrestrial-spectral radiation measurements will be improved by on-board calibrations. The radiation scale on orbit can be verified by cross-calibrations with other benchmark instruments, such as SITSATs.

11.3.3   Infrared Spectrometer (IRS) for Chinese LIBRA Mission

The following description of the Infrared Spectrometer (IRS) instrument to be flown on the Chinese LIBRA mission was provided by Peng Zhang, and is taken with kind permission directly from the following paper which appeared in the Special Issue of the Remote Sensing dedicated to this workshop:

Zhang, P.; Lu, N.; Li, C.; Ding, L.; Zheng, X.; Zhang, X.; Hu, X.; Ye, X.; Ma, L.; Xu, N.; Chen, L.; Schmetz, J. Development of the Chinese Space-Based Radiometric Benchmark Mission LIBRA. Remote Sens. 2020, 12, 2179.

The CSRB includes infrared measurements as well [39], [99]. This instrument acquires a 17-km nadir field of view (similar to FORUM, AIRS, IASI, and CrIS) and covers the contiguous 600 to 2700 cm^{-1} wavelength region with spectral resolution of 0.5 cm^{-1}. The instrument design achieves its accuracy by following the concepts developed by the University of Wisconsin prototype described in Revercomb et al (§8.4). The first CSRB instrument's SI-traceable accuracy goal is less than 0.07 K (k=1), or about a factor of 2 worse than that of FORUM, although later flights of CSRB are planned to reach the 0.03 K (k=1) climate goal [39].

> **The LIBRA Infrared Spectrometer aims to provide high-precision IR spectra traceable to SI**

Aiming at high-precision measurements as a space-based reference for the infrared spectrum, a hyperspectral infrared sounder is being designed traceable to international units. Fourier infrared spectrum detection technology and miniature phase-change cells as temperature standard technology are adopted for the IRS. Schematic diagram of the optical system for the IRS is drawn in Figure 11.22. Accurate blackbody temperatures (fixed points) are based on 'phase-change cells' technology.
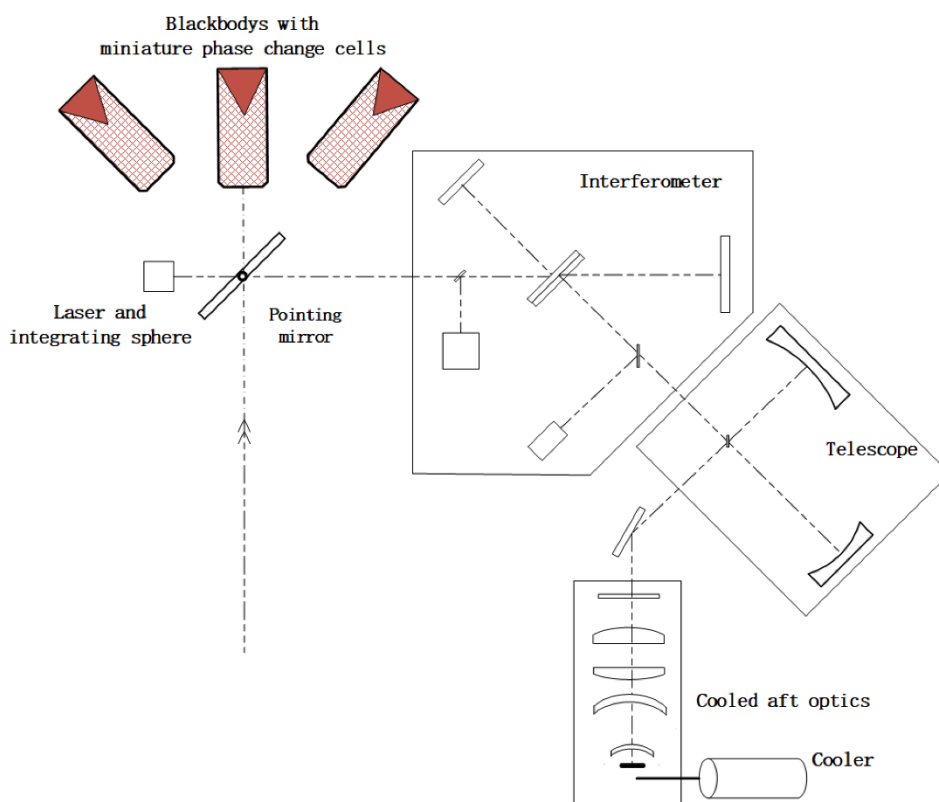
Figure 11.22 Schematic diagram of the optical system for the Infrared Spectrometer (IRS). Accurate blackbody temperatures (fixed points) are based on 'phase-change cells' technology.

Traceability chain of the IRS is shown in Figure 11.23. Three on-orbit absolute radiance IR calibrators realize on-orbit self-calibration of the cavity blackbody. An on-orbit temperature scale from 270 to 350 K is established using ITS-90 miniature phase-change cells traceable to ITS-90 with an uncertainty of better than 10 mK (k = 2) [388]. Based on high precision temperature control and a transfer method, the blackbody temperature is traceable to the SI standard. The blackbody emissivity is measured based on the controlled environment radiation method and is transferred to another blackbody using the laser.
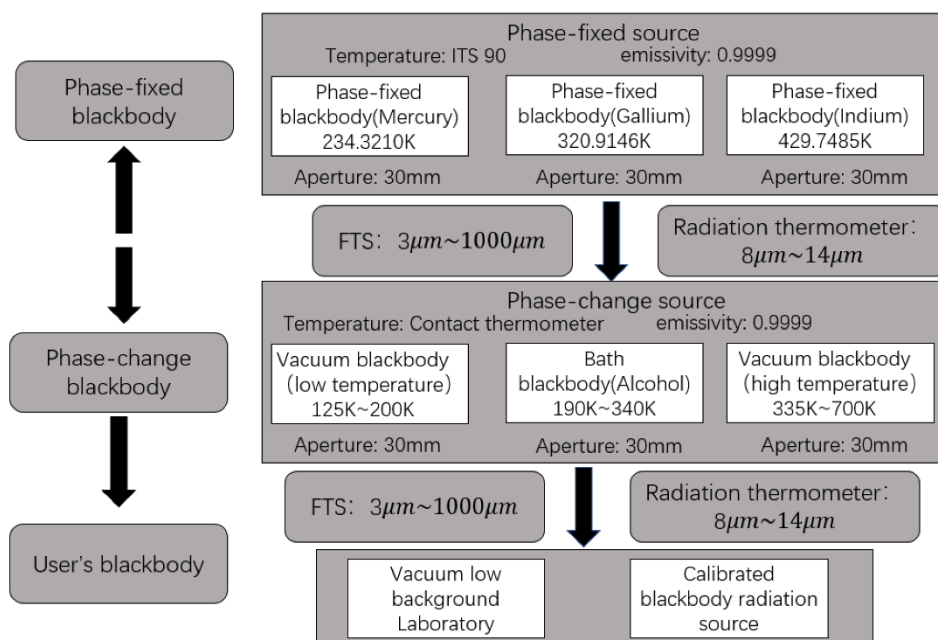
Figure 11.23 Traceability chain of the Infrared Spectrometer (IRS).

The infrared interferometer realizes the high spectral resolution measurement over the thermal infrared spectrum. The high sensitivity response over the wide spectral band is achieved by using a small-array detector. The high stability performance is realized by system temperature control technology using multiple temperature zones. High accuracy spectral calibration is achieved by referring to a standard spectral line source (high frequency infrared laser and gas absorption line).

11.4 FORUM

11.4.1 Motivation

The far infrared (far-ir: defined here as wavenumbers < 667 cm^{-1}) plays a pivotal role in determining our planet's energy balance [389]. Under all-sky conditions model simulations imply that in the global mean, approximately half of the Earth's emission to

> **Emissions in the far infrared dominate radiative cooling in clear skies from the mid and upper troposphere**

space occurs within the far-ir [390]. The dominant role of the far-ir in determining the Earth's Outgoing Longwave Radiation (OLR) is in part due to the strong water vapour rotation band at wavenumbers < 600 cm^{-1}. This in turn means that radiative emission in the far-ir is particularly sensitive to water vapour in the climatologically important upper troposphere/lower stratosphere region [391]. Similarly, clear-sky longwave radiative cooling through the mid and upper troposphere is dominated by the contribution from the far-ir [392].

For much of the globe this water vapour absorption means that far-ir surface emission cannot be sensed from space. However, in very dry, clear conditions the OLR becomes sensitive to surface emission within the far-ir as the region becomes progressively more transmissive as water vapour concentration reduces [393]. Studies show that this relatively unexplored phenomenon may play a critical role in both reducing persistent climate model biases and determining the pace of Arctic and Antarctic climate change [394], [395].

Outgoing longwave radiation is critically dependent on ice cloud properties

Moreover, recent observations from active sensors have highlighted the prevalence of ice clouds, particularly optically thin ice clouds, in the climate system [396]. Our ability to correctly simulate the interaction of the radiation spectrum with these clouds relies on the capability of optical models to adequately represent their scattering and absorption properties. These are critically dependent on the complex ice-crystal shapes and their size distribution within the clouds. Recent advances in ice cloud optical modelling have attempted to capture their bulk microphysical properties spanning the entire electromagnetic spectrum [397], [398]. However, while there are many satellite observations of visible, near, and mid-infrared radiation in the presence of ice clouds that can be exploited to test these developments, there are no such observations that span the far-ir. This represents a major barrier to improving our confidence in our ability to understand and monitor ice cloud properties and, crucially, their influence on the Earth's outgoing longwave energy. Indeed, the spectral behaviour of the refractive index of ice implies that unique information relating to cloud phase and microphysics can be leveraged from measurements of the far-ir spectrum [399]–[401].

Despite the sensitivity of far-ir radiation to these key climate drivers, to date there has been no dedicated satellite mission to observe the complete, radiatively important far-ir spectrum. Those space-based data which do extend into the far-ir, from the InfraRed Interferometer Spectrometer (IRIS-D) mission [402] and the Spectrometer Interferometer-1 [403] only reach 400 cm^{-1}, have relatively coarse spectral and spatial resolution, and are limited in temporal extent to less than a year's worth of data throughout the 1970s. Moreover, there are questions regarding their suitability for quantitative climate related studies [404]. This is a major motivation for FORUM's high absolute accuracy requirements.

From a purely energetics viewpoint the absence of a dedicated far-ir mission constitutes the major missing element of our global climate observing system. Recognising this shortcoming, the Far infrared Outgoing Radiation Understanding and Monitoring (FORUM) mission has recently been selected as the European Space Agency's 9th Earth Explorer. In the following sections the underlying mission objectives and design of the instrumental suite will be described as it currently stands after completion of Phase A studies.

11.4.2 Mission Objectives

FORUM addresses the absence of far-IR elements of our global climate observing system

FORUM will provide the first spectral observations necessary to test our understanding of key physical processes operating in the energetically significant far-ir. These measurements will enable us to understand exactly how the Earth currently cools to space, and, critically, how it responds to both natural and anthropogenic change. Therefore, the overarching research goal of the FORUM mission is "to evaluate the role of the far infrared in shaping our current climate and thus reduce uncertainty in predictions of future climate change"

This goal will be accomplished by

- building, for the first time, a highly accurate global dataset of far-IR radiances for validation of the present-day climate state as captured by Earth system models;
- using these measurements to understand and constrain the processes that control far-IR radiative transfer and hence the Earth's greenhouse effect;
- updating the parametrisations of these processes for implementation in radiative transfer codes, and ultimately in Earth system models;
- characterising critical feedback mechanisms.

Because the OLR far-IR spectrum has never been measured in its entirety from space, predicting exactly what can be additionally leveraged from the observations depends on a number of assumptions. Nonetheless, our current understanding, based on a combination of theoretical calculations, field measurements and campaigns, suggests that highly accurate space-based far-IR observations will provide:

- an improved characterisation of mid-upper tropospheric/lower stratospheric water vapour – critical for climate sensitivity and trends, and with potential benefit for NWP forecasting;
- the ability to detect optically thin ice clouds from passive observations. Better detection may also benefit NWP forecasting by enabling improved discrimination between clear and cloudy radiances;
- a direct measurement of the far-IR radiative forcing of ice clouds – it is currently estimated only from theoretical computations;
- enhanced sensitivity to ice cloud particle size and shape;
- enhanced capability for cloud phase discrimination;
- the ability to retrieve and monitor far-IR land surface emissivity in polar regions, high altitude regions and over deserts.
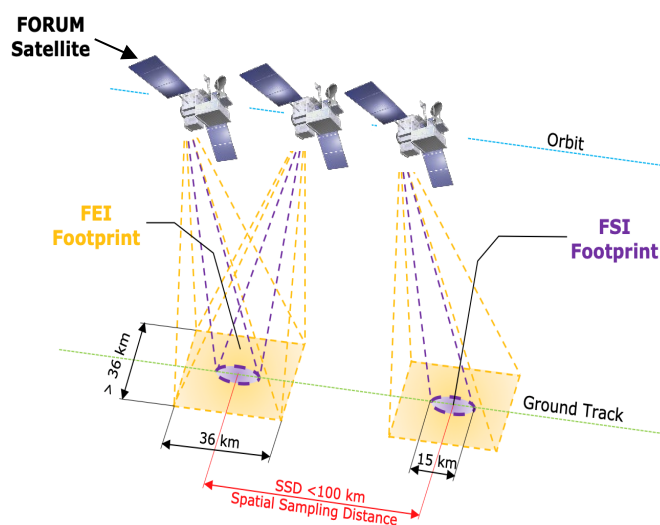
Figure 11.24 FORUM sampling concept: To enable sufficient signal to reach the Forum Sounding Instrument (FSI) a stop-and-stare technique will be used, freezing the FSI field of view (FOV). The FEI views the same scene and its surroundings with much greater spatial resolution to characterise its homogeneity (B. Carnicero-Dominguez, pers. comm. 2019)

11.4.3   Mission Design

To meet the mission requirements, the FORUM payload will consist of two instruments, the FORUM Sounding Instrument (FSI) and the FORUM Embedded Imager (FEI). Table 11.10 gives key requirements for both instruments while Figure 11.24 provides a schematic of the anticipated sampling, with the FEI providing the

> FORUM includes a far IR Sounding Instrument and an Embedded Imager

spatial context for the FSI spectral measurements. At present, two industrial consortia are competing to build the instrumentation, so exact instrument details are yet to be finalised and can vary between the competing bids. Nevertheless, in both cases the envisaged FSI is a four-port double pendulum type interferometer.

FORUM will fly for at least 4 years, in loose formation with MetOp-SG-A1, with the intent to exploit observations from the Infrared Atmospheric Sounding Instrument – Next Generation (IASI-NG) to enable coverage of the complete infrared spectrum. This enforces a 29-day repeat cycle, Sun-synchronous orbit with a 9:30 local equator crossing time, with the FORUM satellite at ~830 km altitude. Co-registration will be less than 1 minute and less than 100km from the MetOp-SG-A1 orbit track.

> **Far IR sounding places strong demands on absolute accuracy**

As shown by Table 11.10 a key requirement of the FORUM mission is high absolute accuracy across the far-IR, needed to discern the subtle fingerprints of climate forcings and feedbacks with confidence, and to provide a legacy dataset for future climate research. The absolute accuracy required for the FORUM FSI instrument is very demanding, particularly in the spectral region between 300 cm^{-1} and 1100 cm^{-1} and at the low end of the dynamic range (i.e. 190 K), where a goal accuracy of 0.1 K is specified (Table 11.10). This requirement drives the calibration strategy, the maximum tolerable noise in the calibration measurements, the blackbody emissivity, the frequency bandwidth to avoid aliasing of the out-of-band signal, the thermal stability and thermal design of the instrument and the blackbody design.

The anticipated calibration strategy varies according to consortia, but in both cases the FSI acquisitions will be split between science observations and radiometric calibration. When in calibration mode the FSI will look into either a hot onboard blackbody (traceable to SI units) or deep space. The loss of science acquisitions owing to radiometric calibrations will be less than 20% of the total number of observations, taking care that there is no systematic loss of science acquisitions at any particular Earth location, while meeting the demanding absolute radiometric accuracy requirements. Further details of the two instrument designs and calibration approaches, correct as of the end of Phase A studies, can be found in [405].

Table 11.10 Key requirements for the FSI and FEI instruments. G: Goal; T: Threshold.

	FSI	FEI
Spectral Range	100-1600 cm^{-1}	Single channel at 10.5 μm
Spectral Resolution (FWHM)	0.36 cm^{-1} (G); 0.5 cm^{-1} (T)	1.5 μm
Radiometric Accuracy	200-300 cm^{-1}: 0.2 K (G); 0.25 (T) 300-1100 cm^{-1}: 0.1 K (G); 0.25 K (T) 1100-1300 cm^{-1}: 0.2 K (G); 0.25 (T) Elsewhere: 1 K (values given as 3-sigma margins)	1 K (G); 3 K (T)
Radiometric Precision	200-800 cm^{-1}: 0.4 (G) mW m^{-2} sr^{-1} (cm^{-1})$^{-1}$ 0.6 (T) mW m^{-2} sr^{-1} (cm^{-1})$^{-1}$ Elsewhere: 1.0 (G) mW m^{-2} sr^{-1} (cm^{-1})$^{-1}$ 2.0 (T) mW m^{-2} sr^{-1} (cm^{-1})$^{-1}$ (1-sigma margins)	NEdT (at 210 K): 0.3 K (G); 0.8 K (T)
Spatial resolution	12 km (G); 15 km (T)	0.6 km (over 36 x 36 km)

11.4.4 Outlook

The mission is currently in Phase B1, progressing to an anticipated launch in the 2025 timeframe. Between now and then the industrial teams will work on the mission implementation while the science

teams will be working to refine the mission exploitation and design in collaboration with the scientific community to ensure that the observational products have maximum utility and impact.

§11.1 Authors: **Greg Kopp[1], Peter Pilewskie[1], Paul Smith[1], Bruce Wielicki[2], C. Lukashin[2], G. Fleming[2], C. Currey[2], D. Goldin[3], C.M. Roithmayr[2], Y. Shea[2], W. Sun[3], K. Thome[4], A. Wu[3],** and **X. Xiong[4],**
[1]LASP, Univ. of Colorado, [2]NASA-LARC, [3]SSAI, [4]NASA-GSFC

§11.2 Authors: **Nigel Fox, Paul Green**, NPL, UK

§11.3 Authors: **Xin Ye, Xuejun Zhang, Xiaolong Yi, Chao Lin, Long Wang,**
Changchun Institute of Optics, Chinese Academy of Sciences

§11.4 Authors: **H. Brindley[1], R. Bantges[1], L. Palchetti[2], S. Buehler[3], B. M. Dinelli[4], L. Labonnote[5], Q. Libois[6], M. Mlynczak[7], H. Oetjen[8], M. Ridolfi[2], M. Riese[9], R. Saunders[10],**
[1]Imperial College London, [2]CNR, Florence, [3]Universität Hamburg, [4]CNR, Bologna, [5]Université de Lille, [6]CNRM, Université de Toulouse, Météo-France, CNRS, Toulouse, [7]NASA-Langley, [8]ESTEC, ESA, [9]IEK-7, Forschungszentrum Jülich, [10]Met Office, UK,

§11 Editor: **Tim Hewison**, EUMETSAT

12 Conclusions

Climate change is one of the most critical issues facing mankind today. The enormous cost implications of policy decisions based on forecasted impacts resulting from the predictions of a warming Earth demand that the science community finds and delivers the necessary information with the highest possible confidence in the shortest possible time. The challenge to the metrology community is equally severe.

The IPCC AR4 Report [107] concludes that the mix of natural variability and anthropogenic effects on decadal timescales is far from fully understood or measured, requiring significant improvements in accuracy. Unequivocal attribution and quantification of subtle fingerprint indicators from this noisy background are fundamental to our ability to predict climate reliably and institute appropriate mitigation/adaptation strategies. This is especially true should society decide to use geo-engineering methods to reduce warming. The uncertainty in climate prediction lies in the complexity of the models, our inadequate understanding of the Earth system and its feedback mechanisms, and the current quality of available data against which to test predictions on the necessary decadal timescales.

> **Major advances have been made in the last 10 to 20 years to enable climate accuracy SI traceability in orbiting reference sensors across the reflected-solar and thermal-infrared spectrum**

Establishing rigorous SI traceability to the key observations underpinning the ECVs with sufficient accuracy is a central pillar to achieving this goal. The satellite community has developed a number of strategies to support this objective over the years, including the creation of FRM quality measurements to help validate in an SI-traceable manner, but as yet most fall dramatically short of the required accuracy, forcing the adoption of high-risk approaches, such as attempting to monitor climate change through the normalization of overlapping continuous datasets. While pre-flight calibrations can be made traceable, the harsh environment of space following the shock of launch can limit the reliability of – or confidence in maintaining – radiometric ground calibrations. Efforts to recover some of the information can be carried out using a variety of post-launch methods, but none have sufficient accuracy to meet the needs of climate [89] and §7.4 .

This workshop report has summarized a wide range of advances since the ASIC[3] satellite calibration report in 2007 [2]. These include advances in ground-based metrology standards, space-borne instrument calibration methods, determination of more rigorous requirements for satellite-based climate change observations and estimates of the very large economic return on investment to society of a more rigorous and accurate climate observing system.

As shown in this workshop report, technologies and analysis capabilities have now reached the SI-traceable uncertainties required for application to future climate change observations throughout the thermal infrared and reflected solar spectrum. Reaching this goal requires SI Traceable Satellites (SITSats) that can provide in-orbit calibration reference instruments. These are typically spectrometers that can cover the entire reflected solar and thermal infrared spectrum. These SITSats can then be used to inter-calibrate dozens to hundreds of operational and research satellite sensors during orbit crossings. Several SITSats are currently in development for planned launch between 2023 and 2026. The table below summarizes the SITSats currently in development.

SITsat Spectrometer	Spectral Range	SI Traceable Accuracy in Orbit	Estimated Launch Date
CLARREO Pathfinder (NASA)	350 - 2350 nm	0.3%, *k=1*	2023
TRUTHS (ESA)	320 - 2450 nm	0.15%, *k=1*	2026
CSRB (China)	380 - 2350 nm	0.5%, *k=1*	2025
FORUM (ESA)	100 - 1600 cm^{-1}	0.03 - 0.06K, *k=1*	2026
LIBRA (China)	600 - 2700 cm^{-1}	0.05K, *k=1*	2025

The mid 2020's will see 5 new SI-traceable satellites (SITSats) provide reference inter-calibration in orbit for a wide range of satellite sensors

Determination of the uncertainty of ground-based SI standards is verified by inter-comparisons of independently-developed standards at multiple metrology laboratories. This inter-comparison is required to reach the high confidence that society requires to rely on these standards in a wide range of applications. SITSats will require a similar verification of their on-orbit uncertainty analysis by inter-comparisons at orbit crossings to independently-developed SITSat sensors in orbit. The table above suggests that this can be achieved in the reflected solar if the CLARREO Pathfinder mission is extended beyond a nominal 1-year mission life on the ISS to a 5-year life to achieve multi-year overlap with the TRUTHS and CSRB SITSats. The current limit on that lifetime is controlled by the time allotment on the ISS platform (currently 1 year nominal with 3 years tentatively planned). The FORUM and LIBRA will provide the first inter-comparisons in the thermal infrared, but development and launch of the U.S. CLARREO infrared spectrometer would allow an equivalent 3-way verification and high confidence in reference calibration for the thermal infrared. Since the new accuracy capabilities are a factor of 5 to 10 beyond current satellite sensors, independent verification is critical for high confidence in the SITSats' abilities to serve as the inter-calibration references for other sensors on orbit, especially for climate change observations.

While the currently planned SITSat reflected-solar and infrared spectrometers represent a great advance, the following further efforts are needed across the climate observing system to achieve the required accuracies and increase confidence in climate change observations:

Based on climate requirements and new SITSat capabilities, a set of recommendations for next steps has been developed

- *The reflected-solar SITSat teams should consider use of the Moon as a stability verification over long time periods independently of their existing SI-traceability approaches. This may allow reaching stability verification at the < 0.1%/decade level at relatively low cost via options such as the ARCSTONE (see §7.4). Further improvements in the accuracy of lunar irradiance models, particularly the ROLO model also described in §7.4, are also required.*

- *Current NASA plans for the CLARREO Pathfinder mission include demonstration of intercalibration for VIIRS and CERES instruments on JPSS, but should be extended to include geostationary imagers and chemistry sensors, PACE ocean color, Landsat, Sentinel 2, SmallSat land-imaging constellations and international surfac. These plans should also extend the mission operations plan from the current one year to five years to enable overlap with the TRUTHS and CSRB SITSats.*

- *Improvements need to be made in the thermal infrared to reach the required SI-traceability goals from independent sensors through at least 200 to 2000 cm^{-1}. FORUM will not meet this accuracy through the entire infrared spectrum, and its accuracy goals are still in development. The Chinese LIBRA mission is meant to achieve those goals through improvement over multiple missions. The developed*

infrared SITSat spectrometer intended for the full CLARREO mission is intended to meet these goals but has not yet been manifested for flight. An infrared CLARREO Pathfinder mission should be developed and launched as soon as practical.

- The world's space agencies should initiate plans to strategically sustain on an operational basis an SI traceable climate observing system into the long-term in readiness to continue and reap full benefit from the current planned SITSats. While one of the benefits of high accuracy SI traceability means that gaps in observations between missions can exist without necessarily compromising the longer-term data record, overlapping continuity reduces sensitivities in monitoring climate change resulting from natural events like ENSO and volcanoes.- Passive microwave instruments require further work on laboratory calibration references, SI traceability at climate change accuracies, and flight of demonstration reference calibration sensors in orbit.

- Active sensing by radar, lidar, and gravity missions are newer satellite capabilities and have recently begun to consider climate change requirements and SI-traceability requirements on orbit. These sensors were not considered in the current report. Extensive additional research on SI traceability is needed in the area of active sensors.

- Continued efforts to increase the number and nature of FRM-quality surface measurements to provide complementarity to the SITSats and the need to build confidence in the complete network of EO observations in-situ and in space, as well as their integration to further improve models and understanding of processes and Earth cycles.

- A follow-on SITSCOS workshop should be planned for 2026 to consider early results and status of the SITSat missions, as well as to extend the scope of the next workshop to include progress and plans for SI traceability of microwave and active satellite sensors including lidar, radar, gravity, and radio occultation sensors, which are an increasingly critical part of climate observing system monitoring as well as studies of climate processes.

The realization of SI-traceable measurements in orbit is achievable in the very near future and is time critical. This 'grand challenge' project involving both the metrology and Earth/climate science communities must become a priority if society is to reap the full benefits of EO. Without it *policy-makers will be acting blindly in their efforts to ensure long-term sustainability and growth within an ever-changing climate.*

§12   Authors: **B. A. Wielicki[1], T. Hewison[2], N. Fox[3], G. Kopp[4]**, [1]NASA / LaRC, [2]EUMETSAT, [3]NPL, [4]Univ. of Colorado / LASP

References

[1]   G. Ohring, B. Wielicki, R. Spencer, B. Emery, and R. Datla, "Satellite instrument calibration for measuring global climate change: Report of a workshop," *Bull. Am. Meteorol. Soc.*, vol. 86, no. 9, pp. 1303–1313, Sep. 2005, doi: 10.1175/BAMS-86-9-1303.

[2]   G. Ohring *et al.*, "Achieving Satellite Instrument Calibration for Climate Change," *Eos, Trans. Am. Geophys. Union*, vol. 88, no. 11, p. 136, Mar. 2007, doi: 10.1029/2007EO110015.

[3]   NASEM, *Earth science and applications from space: National imperatives for the next decade and beyond*. National Academies Press, 2007.

[4]   R. Goody and R. Haskins, "Calibration of radiances from space," *J. Clim.*, vol. 11, no. 4, pp. 754–767, Apr. 1998, doi: 10.1175/1520-0442(1998)011<0754:corfs>2.0.co;2.

[5]   J. G. Anderson, J. A. Dykema, R. M. Goody, H. Hu, and D. B. Kirk-Davidoff, "Absolute, spectrally-resolved, thermal radiance: A benchmark for climate monitoring from space," *J. Quant. Spectrosc. Radiat. Transf.*, vol. 85, no. 3–4, pp. 367–383, May 2004, doi: 10.1016/S0022-4073(03)00232-2.

[6]   B. A. Wielicki *et al.*, "Achieving Climate Change Absolute Accuracy in Orbit," *Bull. Am. Meteorol. Soc.*, vol. 94, no. 10, pp. 1519–1539, Oct. 2013, doi: 10.1175/BAMS-D-12-00149.1.

[7]   N. Fox *et al.*, "Traceable Radiometry Underpinning Terrestrial - and Helio- Studies (TRUTHS)," *Adv. Sp. Res.*, vol. 32, no. 11, pp. 2253–2261, Dec. 2003, doi: 10.1016/S0273-1177(03)90551-5.

[8]   N. Fox *et al.*, "Accurate radiometry from space: an essential tool for climate studies," *Philos. Trans. R. Soc. A Math. Phys. Eng. Sci.*, vol. 369, no. 1953, pp. 4028–4063, Oct. 2011, doi: 10.1098/rsta.2011.0246.

[9]   M. Dowell *et al.*, "Strategy Towards an Architecture for Climate Monitoring from Space," 2013. Accessed: Jun. 09, 2020. [Online]. Available: www.ceos.org;www.wmo.int/sat;http://www.cgms-info.org/.

[10]   NASEM, *Continuity of NASA earth observations from space: A value framework*. National Academies Press, 2015.

[11]   World Meteorological Organization, "THE GLOBAL OBSERVING SYSTEM FOR CLIMATE: IMPLEMENTATION NEEDS GCOS-200 (GOOS-214)."

[12]   NASEM, *Thriving on Our Changing Planet: A Decadal Strategy for Earth Observation from Space*. Washington, DC: National Academies Press, 2017.

[13]   E. C. Weatherhead *et al.*, "Designing the Climate Observing System of the Future," *Earth's Futur.*, vol. 6, no. 1, pp. 80–102, Jan. 2018, doi: 10.1002/2017EF000627.

[14]   N. Fox and P. Green, "Traceable Radiometry Underpinning Terrestrial- and Helio-Studies (TRUTHS): An Element of a Space-Based Climate and Calibration Observatory," *Remote Sens.*, vol. 12, no. 15, p. 2400, Jul. 2020, doi: 10.3390/rs12152400.

[15]   K. E. Trenberth *et al.*, "Challenges of a Sustained Climate Observing System," in *Climate Science for Serving Society*, Springer Netherlands, 2013, pp. 13–50.

[16]   NASEM, *Abrupt Impacts of Climate Change*. National Academies Press, 2013.

[17]   R. Cooke, B. A. Wielicki, D. F. Young, and M. G. Mlynczak, "Value of information for climate observing systems," *Environ. Syst. Decis.*, vol. 34, no. 1, pp. 98–109, Mar. 2014, doi:

10.1007/s10669-013-9451-8.

[18]   R. Cooke, A. Golub, B. A. Wielicki, D. F. Young, M. G. Mlynczak, and R. R. Baize, "Using the social cost of carbon to value earth observing systems," *Clim. Policy*, vol. 17, no. 3, pp. 330–345, Apr. 2017, doi: 10.1080/14693062.2015.1110109.

[19]   R. M. Cooke, A. Golub, B. Wielicki, M. Mlynczak, D. Young, and R. R. Baize, "Monetizing the Value of Measurements of Equilibrium Climate Sensitivity Using the Social Cost of Carbon," *Environ. Model. Assess.*, vol. 25, no. 1, pp. 59–72, Feb. 2020, doi: 10.1007/s10666-019-09662-0.

[20]   S. S. Leroy, J. G. Anderson, and G. Ohring, "Climate Signal Detection Times and Constraints on Climate Benchmark Accuracy Requirements," *J. Clim.*, vol. 21, no. 4, pp. 841–846, Feb. 2008, doi: 10.1175/2007JCLI1946.1.

[21]   Y. L. Shea, B. A. Wielicki, S. Sun-Mack, and P. Minnis, "Quantifying the Dependence of Satellite Cloud Retrievals on Instrument Uncertainty," *J. Clim.*, vol. 30, no. 17, pp. 6959–6976, Sep. 2017, doi: 10.1175/JCLI-D-16-0429.1.

[22]   C. Y. Liu, J. Li, S. P. Ho, G. R. Liu, T. H. Lin, and C. C. Young, "Retrieval of Atmospheric Thermodynamic State from Synergistic Use of Radio Occultation and Hyperspectral Infrared Radiances Observations," *IEEE J. Sel. Top. Appl. Earth Obs. Remote Sens.*, vol. 9, no. 2, pp. 744–756, Feb. 2016, doi: 10.1109/JSTARS.2015.2444274.

[23]   C. Liu *et al.*, "Evaluation of satellite and reanalysis-based global net surface energy flux and uncertainty estimates," *J. Geophys. Res. Atmos.*, vol. 122, no. 12, pp. 6250–6272, Jun. 2017, doi: 10.1002/2017JD026616.

[24]   G. Kopp, "An assessment of the solar irradiance record for climate studies," *J. Sp. Weather Sp. Clim.*, vol. 4, p. A14, 2014, doi: 10.1051/SWSC/2014012.

[25]   E. Richard *et al.*, "Future Long-term Measurements of Solar Spectral Irradiance by the TSIS Spectral Irradiance Monitor: Improvements in Measurement Accuracy and Stability."

[26]   K. J. Priestley *et al.*, "Radiometric Performance of the CERES Earth Radiation Budget Climate Record Sensors on the EOS Aqua and Terra Spacecraft through Clouds and the Earth's Radiant Energy System (CERES) View project Radiometric Performance of the CERES Earth Radiation Budget Climate Record Sensors on the EOS Aqua and Terra Spacecraft through April 2007," *Artic. J. Atmos. Ocean. Technol.*, 2011, doi: 10.1175/2010JTECHA1521.1.

[27]   N. Loeb, N. Manalo-Smith, W. Su, M. Shankar, and S. Thomas, "CERES Top-of-Atmosphere Earth Radiation Budget Climate Data Record: Accounting for in-Orbit Changes in Instrument Calibration," *Remote Sens.*, vol. 8, no. 3, p. 182, Feb. 2016, doi: 10.3390/rs8030182.

[28]   X. Xiong *et al.*, "Updates of Moderate Resolution Imaging Spectroradiometer on-orbit calibration uncertainty assessments," *J. Appl. Remote Sens.*, vol. 12, no. 03, p. 1, Jul. 2018, doi: 10.1117/1.jrs.12.034001.

[29]   X. Xiong *et al.*, "Global space-based inter-calibration system reflective solar calibration reference: from Aqua MODIS to S-NPP VIIRS," in *Earth Observing Missions and Sensors: Development, Implementation, and Characterization IV*, May 2016, vol. 9881, p. 98811D, doi: 10.1117/12.2224320.

[30]   J. F. Meirink, R. A. Roebeling, and P. Stammes, "Inter-calibration of polar imager solar channels using SEVIRI," *Atmos. Meas. Tech.*, vol. 6, no. 9, pp. 2495–2508, Sep. 2013, doi: 10.5194/amt-6-2495-2013.

[31]   EUMETSAT, "Typical Radiometric Noise, Calibration Bias and Stability for Meteosat-8, -9, -

10 and -11 SEVIRI," 2019. [Online]. Available: https://www.eumetsat.int/seviri-instrument-status-calibration.

[32] F. Yu, X. Wu, H. Yoo, Z. Wang, H. Qian, and X. Shao, "Radiometric calibration performance of GOES-17 Advanced Baseline Imager (ABI)," in *Earth Observing Systems XXIV*, Sep. 2019, vol. 11127, p. 48, doi: 10.1117/12.2531407.

[33] B. Markham *et al.*, "Landsat-8 operational land imager radiometric calibration and stability," *Remote Sens.*, vol. 6, no. 12, pp. 12275–12308, 2014, doi: 10.3390/rs61212275.

[34] C. Bouzinac *et al.*, "Sentinel-2 level-1 calibration and validation status from the mission performance centre," in *International Geoscience and Remote Sensing Symposium (IGARSS)*, Oct. 2018, vol. 2018-July, pp. 4347–4350, doi: 10.1109/IGARSS.2018.8518033.

[35] G. Kopp and J. L. Lean, "A new, lower value of total solar irradiance: Evidence and climate significance," *Geophys. Res. Lett.*, vol. 38, no. 1, Jan. 2011, doi: 10.1029/2010GL045777.

[36] H. H. Kieffer and T. C. Stone, "The Spectral Irradiance of the Moon," *Astron. J.*, vol. 129, no. 6, pp. 2887–2901, Jun. 2005, doi: 10.1086/430185.

[37] T. C. Stone, H. Kieffer, C. Lukashin, and K. Turpie, "The Moon as a Climate-Quality Radiometric Calibration Reference," *Remote Sens.*, vol. 12, no. 11, p. 1837, Jun. 2020, doi: 10.3390/rs12111837.

[38] G. Kopp *et al.*, "Radiometric flight results from the HyperSpectral Imager for Climate Science (HySICS)," *Geosci. Instrumentation, Methods Data Syst. Discuss.*, pp. 1–35, Dec. 2017, doi: 10.5194/gi-2016-37.

[39] P. Zhang *et al.*, "Development of the Chinese Space-Based Radiometric Benchmark Mission LIBRA," *Remote Sens.*, vol. 12, no. 14, p. 2179, Jul. 2020, doi: 10.3390/rs12142179.

[40] Y. Xie, A. Wu, and X. Xiong, "Tracking long-term stability of Aqua MODIS and AIRS at different scan angles," in *Earth Observing Systems XV*, Aug. 2010, vol. 7807, p. 780718, doi: 10.1117/12.858616.

[41] T. S. Pagano, E. M. Manning, S. Broberg, H. H. Aumann, L. Strow, and M. Weiler, "Reducing uncertainty in the AIRS radiometric calibration," Sep. 2018, p. 23, doi: 10.1117/12.2320906.

[42] L. Larrabee Strow and S. Desouza-Machado, "Establishment of AIRS climate-level radiometric stability using radiance anomaly retrievals of minor gases and sea surface temperature," *Atmos. Meas. Tech.*, vol. 13, no. 9, pp. 4619–4644, Aug. 2020, doi: 10.5194/amt-13-4619-2020.

[43] D. Tobin *et al.*, "Suomi-NPP CrIS radiometric calibration uncertainty," *J. Geophys. Res. Atmos.*, vol. 118, no. 18, pp. 10,589-10,600, Sep. 2013, doi: 10.1002/jgrd.50809.

[44] L. Le Barbier and C. Pierangelo, "Performance status of GSICS Reference IASI A/B/C," *GSICS Q. Newsl.*, vol. 14, no. 4, 2021.

[45] L. Palchetti *et al.*, "Forum: Unique far-infrared satellite observations to better understand how earth radiates energy to space," *Bulletin of the American Meteorological Society*, vol. 101, no. 12. American Meteorological Society, pp. E2030–E2046, Dec. 08, 2021, doi: 10.1175/BAMS-D-19-0322.1.

[46] P. Rosenkranz, W. Blackwell, and R. Leslie, "Climate-Quality Calibration for Low Earth-Orbit Microwave Radiometry," *Remote Sens.*, vol. 12, no. 2, p. 241, Jan. 2020, doi: 10.3390/rs12020241.

[47] M. J. Burgdorf, T. G. Müller, S. A. Buehler, M. Prange, and M. Brath, "Characterization of the High-Resolution Infrared Radiation Sounder Using Lunar Observations," *Remote Sens.*, vol. 12,

no. 9, p. 1488, May 2020, doi: 10.3390/rs12091488.

[48] S. A. Buehler, "A simple method to relate microwave radiances to upper tropospheric humidity," *J. Geophys. Res.*, vol. 110, no. D2, p. D02110, Jan. 2005, doi: 10.1029/2004JD005111.

[49] F. J. Wentz and D. Draper, "On-orbit absolute calibration of the global precipitation measurement microwave imager," *J. Atmos. Ocean. Technol.*, vol. 33, no. 7, pp. 1393–1412, Jul. 2016, doi: 10.1175/JTECH-D-15-0212.1.

[50] R. Chen, A. Santos-Garcia, S. Farrar, and W. L. Jones, "Assessment of the long-term radiometric calibration stability of the TRMM microwave imager and the WindSat Satellite Radiometers," in *13th Specialist Meeting on Microwave Radiometry and Remote Sensing of the Environment, MicroRad 2014 - Proceedings*, 2014, pp. 187–191, doi: 10.1109/MicroRad.2014.6878936.

[51] M. A. Martin-Delgado, "The New SI and the Fundamental Constants of Nature," *Eur. J. Phys.*, vol. 41, no. 6, Apr. 2020, doi: 10.1088/1361-6404/abab5e.

[52] T. J. Quinn and J. E. Martin, "A radiometric determination of the Stefan-Boltzmann constant and thermodynamic temperatures between -40 °C and +100 °C," *Philos. Trans. R. Soc.*, vol. 316, pp. 85–189, 1985.

[53] J. E. Martin, N. P. Fox, and P. J. Key, "A Cryogenic Radiometer for Absolute Radiometric Measurements," *Metrologia*, vol. 21, no. 3, p. 147, 1985, doi: 10.1088/0026-1394/21/3/007.

[54] N. P. Fox, "Radiometry with cryogenic radiometers and semiconductor photodiodes," in *Metrologia*, Dec. 1995, vol. 32, no. 6, pp. 535–543, doi: 10.1088/0026-1394/32/6/28.

[55] "Mise en Pratique for the definition of the candela and associated derived units for photometric and radiometric quantities in the SI." https://www.bipm.org/utils/en/pdf/si-mep/SI-App2-candela.pdf (accessed Aug. 05, 2020).

[56] E. F. Zalewski and C. R. Duda, "Silicon photodiode device with 100% external quantum efficiency," *Appl. Opt.*, vol. 22, no. 18, p. 2867, Sep. 1983, doi: 10.1364/ao.22.002867.

[57] N. P. Fox, "Trap detectors and their properties," *Metrologia*, vol. 28, no. 3, pp. 197–202, Jan. 1991, doi: 10.1088/0026-1394/28/3/018.

[58] V. E. Anderson, N. P. Fox, and D. H. Nettleton, "Highly stable, monochromatic and tunable optical radiation source and its application to high accuracy spectrophotometry," *Appl. Opt.*, vol. 31, no. 4, p. 536, Feb. 1992, doi: 10.1364/ao.31.000536.

[59] E. R. Woolliams, N. P. Fox, M. G. Cox, P. M. Harris, and N. J. Harrison, "The CCPR K1-a key comparison of spectral irradiance from 250 nm to 2500 nm: Measurements, analysis and results," in *Metrologia*, Apr. 2006, vol. 43, no. 2, p. S98, doi: 10.1088/0026-1394/43/2/S20.

[60] H. W. Yoon, C. E. Gibson, and P. Y. Barnes, "Realization of the National Institute of Standards and Technology detector-based spectral irradiance scale," 2002.

[61] N. P. Fox, J. E. Martin, and D. H. Nettleton, "Absolute spectral radiometric determination of the thermodynamic temperatures of the melting/freezing points of gold, silver and aluminium," *Metrologia*, vol. 28, no. 5, pp. 357–374, Jan. 1991, doi: 10.1088/0026-1394/28/5/001.

[62] S. W. Brown, G. P. Eppeldauer, and K. R. Lykke, "Facility for spectral irradiance and radiance responsivity calibrations using uniform sources," *Metrologia*, vol. 37, pp. 579–582, 2000.

[63] M. Schuster, S. Nevas, A. Sperling, and S. Völker, "Spectral calibration of radiometric detectors using Tunable Laser sources," *Appl. Opt.*, vol. 51, no. 12, pp. 1950–1961, Apr. 2012, doi: 10.1364/AO.51.001950.

[64]   "GLAMR." https://glamr.gsfc.nasa.gov/ (accessed Apr. 19, 2021).

[65]   M. Goldberg *et al.*, "The global space-based inter-calibration system," *Bull. Am. Meteorol. Soc.*, vol. 92, no. 4, pp. 467–475, Apr. 2011, doi: 10.1175/2010BAMS2967.1.

[66]   A. C. Kren, P. Pilewskie, and O. Coddington, "Where does Earth's atmosphere get its energy?," *J. Sp. Weather Sp. Clim.*, vol. 7, p. A10, 2017, doi: 10.1051/SWSC/2017007.

[67]   J. L. Lean, "Cycles and trends in solar irradiance and climate," *Wiley Interdiscip. Rev. Clim. Chang.*, vol. 1, no. 1, pp. 111–122, Jan. 2010, doi: 10.1002/wcc.18.

[68]   N. G. Loeb *et al.*, "Toward optimal closure of the Earth's top-of-atmosphere radiation budget," *J. Clim.*, vol. 22, no. 3, pp. 748–766, Feb. 2009, doi: 10.1175/2008JCLI2637.1.

[69]   L. J. Gray *et al.*, "Solar influences on climate," *Rev. Geophys.*, vol. 48, no. 4, Dec. 2010, doi: 10.1029/2009RG000282.

[70]   T. Dudok de Wit, G. Kopp, C. Fröhlich, and M. Schöll, "Methodology to create a new total solar irradiance record: Making a composite out of multiple data records," *Geophys. Res. Lett.*, vol. 44, no. 3, pp. 1196–1203, Feb. 2017, doi: 10.1002/2016GL071866.

[71]   J. L. Lean, "Estimating Solar Irradiance Since 850 CE," *Earth Sp. Sci.*, vol. 5, no. 4, pp. 133–149, Apr. 2018, doi: 10.1002/2017EA000357.

[72]   S. Dewitte and N. Clerbaux, "Measurement of the Earth Radiation Budget at the Top of the Atmosphere—A Review," *Remote Sens.*, vol. 9, no. 11, p. 1143, Nov. 2017, doi: 10.3390/rs9111143.

[73]   K. Von Schuckmann *et al.*, "An imperative to monitor Earth's energy imbalance," *Nature Climate Change*, vol. 6, no. 2. Nature Publishing Group, pp. 138–144, Jan. 27, 2016, doi: 10.1038/nclimate2876.

[74]   N. Loeb, T. Thorsen, J. Norris, H. Wang, and W. Su, "Changes in Earth's Energy Budget during and after the 'Pause' in Global Warming: An Observational Perspective," *Climate*, vol. 6, no. 3, p. 62, Jul. 2018, doi: 10.3390/cli6030062.

[75]   C. Zhou, M. D. Zelinka, A. E. Dessler, and S. A. Klein, "The relationship between interannual and long-term cloud feedbacks," *Geophys. Res. Lett.*, vol. 42, no. 23, pp. 10463–10469, Dec. 2015, doi: 10.1002/2015GL066698.

[76]   B. A. Wielicki *et al.*, "Clouds and the Earth's Radiant Energy System (CERES): An Earth Observing System Experiment," *https://doi.org/10.1175/1520-0477(1996)077<0853:CATERE>2.0.CO;2*, May 1996, doi: 10.1175/1520-0477(1996)077<0853:CATERE>2.0.CO;2.

[77]   H. E. Brindley and J. E. Russell, "Top of atmosphere broadband radiative fluxes from geostationary satellite observations," in *Comprehensive Remote Sensing*, vol. 1–9, Elsevier, 2017, pp. 85–113.

[78]   N. G. Loeb, B. A. Wielicki, T. Wong, and P. A. Parker, "Impact of data gaps on satellite broadband radiation records," *J. Geophys. Res.*, vol. 114, no. D11, p. D11109, Jun. 2009, doi: 10.1029/2008JD011183.

[79]   C. Lukashin, B. A. Wielicki, D. F. Young, K. Thome, Z. Jin, and W. Sun, "Uncertainty estimates for imager reference inter-calibration with CLARREO reflected solar spectrometer," *IEEE Trans. Geosci. Remote Sens.*, vol. 51, no. 3, pp. 1425–1436, 2013, doi: 10.1109/TGRS.2012.2233480.

[80]   C. M. Roithmayr *et al.*, "CLARREO approach for reference intercalibration of reflected solar

sensors: On-orbit data matching and sampling," *IEEE Trans. Geosci. Remote Sens.*, vol. 52, no. 10, pp. 6762–6774, 2014, doi: 10.1109/TGRS.2014.2302397.

[81] D. Tobin, R. Holz, F. Nagle, and H. Revercomb, "Characterization of the Climate Absolute Radiance and Refractivity Observatory (CLARREO) ability to serve as an infrared satellite intercalibration reference," *J. Geophys. Res. Atmos.*, vol. 121, no. 8, pp. 4258–4271, Apr. 2016, doi: 10.1002/2016JD024770.

[82] N. Mishra, D. Helder, J. Barsi, and B. Markham, "Continuous calibration improvement in solar reflective bands: Landsat 5 through Landsat 8," *Remote Sens. Environ.*, vol. 185, pp. 7–15, Nov. 2016, doi: 10.1016/j.rse.2016.07.032.

[83] "Sentinel-2 Mission Requirements Document."

[84] C. Revel *et al.*, "Sentinel-2A and 2B absolute calibration monitoring," *Eur. J. Remote Sens.*, vol. 52, no. 1, pp. 122–137, Jan. 2019, doi: 10.1080/22797254.2018.1562311.

[85] B. A. Franz, S. W. Bailey, P. J. Werdell, and C. R. McClain, "Sensor-independent approach to the vicarious calibration of satellite ocean color radiometry," *Appl. Opt.*, vol. 46, no. 22, pp. 5068–5082, Aug. 2007, doi: 10.1364/AO.46.005068.

[86] R. E. Eplee, Jr., R. A. Barnes, F. S. Patt, G. Meister, and C. R. McClain, "SeaWiFS lunar calibration methodology after six years on orbit," in *Earth Observing Systems IX*, Oct. 2004, vol. 5542, p. 1, doi: 10.1117/12.556408.

[87] A. Richter, "Satellite remote sensing of tropospheric composition – principles, results, and challenges," *EPJ Web Conf.*, vol. 9, pp. 181–189, Dec. 2010, doi: 10.1051/epjconf/201009014.

[88] M. Bouvet *et al.*, "RadCalNet: A Radiometric Calibration Network for Earth Observing Imagers Operating in the Visible to Shortwave Infrared Spectral Range," *Remote Sens.*, vol. 11, no. 20, p. 2401, Oct. 2019, doi: 10.3390/rs11202401.

[89] G. Chander, T. J. Hewison, N. Fox, X. Wu, X. Xiong, and W. J. Blackwell, "Overview of Intercalibration of Satellite Instruments," *IEEE Trans. Geosci. Remote Sens.*, vol. 51, no. 3, pp. 1056–1080, Mar. 2013, doi: 10.1109/TGRS.2012.2228654.

[90] S. Sterckx *et al.*, "Towards a European Cal/Val service for earth observation," *Int. J. Remote Sens.*, vol. 41, no. 12, pp. 4496–4511, Jun. 2020, doi: 10.1080/01431161.2020.1718240.

[91] J. Gorroño, A. C. Banks, N. P. Fox, and C. Underwood, "Radiometric inter-sensor cross-calibration uncertainty using a traceable high accuracy reference hyperspectral imager," *ISPRS J. Photogramm. Remote Sens.*, vol. 130, pp. 393–417, Aug. 2017, doi: 10.1016/j.isprsjprs.2017.07.002.

[92] C. M. Roithmayr *et al.*, "CLARREO Approach for Reference Intercalibration of Reflected Solar Sensors: On-Orbit Data Matching and Sampling," *IEEE Trans. Geosci. Remote Sens.*, vol. 52, no. 10, 2014, doi: 10.1109/TGRS.2014.2302397.

[93] BIPM, "Evaluation of measurement data: Guide to the expression of uncertainty in measurement," 2008. Accessed: Jun. 09, 2020. [Online]. Available: www.bipm.org.

[94] Woolliams; Emma, Taylor; Sarah, Toledano; Carlos, Adriaensen; Stefan, Barreto; Africa, and Berjón; Alberto, "Lunar spectral irradiance measurement and modelling for absolute calibration of EO optical sensors - Final Report," 2019. Accessed: Apr. 19, 2021. [Online]. Available: http://calvalportal.ceos.org/documents/10136/703678/ESA+Lunar+Final+Report_reviewed_FINAL.pdf/671b88ba-d75f-4a93-947d-075793d30c06.

[95] R. Swanson *et al.*, "The ARCSTONE Project to Calibrate Lunar Reflectance," *IEEE Aerosp.*

Conf. Proc., Mar. 2020, doi: 10.1109/AERO47225.2020.9172629.

[96] C.-Y. Liu et al., "Optimal Use of Space-Borne Advanced Infrared and Microwave Soundings for Regional Numerical Weather Prediction," *Remote Sens.*, vol. 8, no. 10, p. 816, Sep. 2016, doi: 10.3390/rs8100816.

[97] W. P. Menzel, T. J. Schmit, P. Zhang, and J. Li, "Satellite-based atmospheric infrared sounder development and applications," *Bull. Am. Meteorol. Soc.*, vol. 99, no. 3, pp. 583–603, Mar. 2018, doi: 10.1175/BAMS-D-16-0293.1.

[98] F. Hilton et al., "Hyperspectral earth observation from IASI: four years of accomplishments," *Bull. Am. Meteorol. Soc.*, vol. 93, no. 3, pp. 347–370, Mar. 2012, doi: 10.1175/BAMS-D-11-00027.1.

[99] X. Ye et al., "Instrument Development: Chinese Radiometric Benchmark of Reflected Solar Band Based on Space Cryogenic Absolute Radiometer," *Remote Sens.*, vol. 12, no. 17, p. 2856, Sep. 2020, doi: 10.3390/rs12172856.

[100] Y. Li, X. Xiong, J. McIntire, and A. Wu, "Comparison of the MODIS and VIIRS thermal emissive band radiometric calibration," *IEEE Trans. Geosci. Remote Sens.*, vol. 58, no. 7, pp. 4852–4859, Jul. 2020, doi: 10.1109/TGRS.2020.2968037.

[101] R. Datla, X. Shao, C. Cao, and X. Wu, "Comparison of the Calibration Algorithms and SI Traceability of MODIS, VIIRS, GOES, and GOES-R ABI Sensors," *Remote Sens.*, vol. 8, no. 2, p. 126, Feb. 2016, doi: 10.3390/rs8020126.

[102] D. C. Tobin, H. E. Revercomb, C. C. Moeller, and T. S. Pagano, "Use of Atmospheric Infrared Sounder high–spectral resolution spectra to assess the calibration of Moderate resolution Imaging Spectroradiometer on EOS Aqua," *J. Geophys. Res.*, vol. 111, no. D9, p. D09S05, May 2006, doi: 10.1029/2005JD006095.

[103] A. K. Steiner, B. C. Lackner, F. Ladstdter, B. Scherllin-Pirscher, U. Foelsche, and G. Kirchengast, "GPS radio occultation for climate monitoring and change detection," *Radio Sci.*, vol. 46, no. 6, 2011, doi: 10.1029/2010RS004614.

[104] S. P. Ho et al., "The COSMIC/FORMOSAT-3 radio occultation mission after 12 years: Accomplishments, remaining challenges, and potential impacts of COSMIC-2," *Bull. Am. Meteorol. Soc.*, vol. 101, no. 7, pp. E1107–E1136, Jul. 2020, doi: 10.1175/BAMS-D-18-0290.1.

[105] D. Winker, H. Chepfer, V. Noel, and X. Cai, "Observational Constraints on Cloud Feedbacks: The Role of Active Satellite Sensors," *Surv. Geophys.*, vol. 38, no. 6, pp. 1483–1508, Nov. 2017, doi: 10.1007/s10712-017-9452-0.

[106] H. Chepfer et al., "The Potential of a Multidecade Spaceborne Lidar Record to Constrain Cloud Feedback," *J. Geophys. Res. Atmos.*, vol. 123, no. 10, pp. 5433–5454, May 2018, doi: 10.1002/2017JD027742.

[107] Intergovernmental Panel on Climate Change, *Climate Change 2013: The Physical Science Basis*. Geneva, Switzerland, 2013.

[108] National Research Council, *Assessing the reliability of complex models: Mathematical and statistical foundations of verification, validation, and uncertainty quantification*. National Academies Press, 2012.

[109] C. Hope, "The $10 trillion value of better information about the transient climate response," *Philos. Trans. R. Soc. A Math. Phys. Eng. Sci.*, vol. 373, no. 2054, Nov. 2015, doi: 10.1098/rsta.2014.0429.

[110] U. S. G. (IWG S. Interagency Working Group on Social Cost of Carbon, "SOCIAL COST OF CARBON FOR REGULATORY IMPACT ANALYSIS UNDER EXECUTIVE ORDER 12866, APPENDIX 15A," 2010.

[111] N. Stern, "The economics of climate change," in *American Economic Review*, May 2008, vol. 98, no. 2, pp. 1–37, doi: 10.1257/aer.98.2.1.

[112] J. K. Lazo and D. M. Waldman, "Valuing improved hurricane forecasts," *Econ. Lett.*, vol. 111, no. 1, pp. 43–46, Apr. 2011, doi: 10.1016/j.econlet.2010.12.012.

[113] C. J. Merchant *et al.*, "Uncertainty information in climate data records from Earth observation," *Earth Syst. Sci. Data*, vol. 9, no. 2, pp. 511–527, Jul. 2017, doi: 10.5194/essd-9-511-2017.

[114] QA4EO Task Team, "A Quality Assurance Framework for Earth Observation," 2010.

[115] J. Mittaz, C. J. Merchant, and E. R. Woolliams, "Applying principles of metrology to historical Earth observations from satellites," *Metrologia*, 2019, doi: 10.1088/1681-7575/ab1705.

[116] J. P. Rice and B. C. Johnson, "The NIST EOS thermal-infrared transfer radiometer," *Metrologia*, vol. 35, no. 4, p. 505, 1998, doi: 10.1088/0026-1394/35/4/51.

[117] E. Theocharous, N. P. Fox, V. I. Sapritsky, S. N. Mekhontsev, and S. P. Morozova, "Absolute measurements of black-body emitted radiance," *Metrologia*, vol. 35, no. 4, pp. 549–554, Aug. 1998, doi: 10.1088/0026-1394/35/4/58.

[118] E. Theocharous, R. Deshpande, A. C. Dillon, and J. Lehman, "Evaluation of a pyroelectric detector with a carbon multiwalled nanotube black coating in the infrared," *Appl. Opt.*, vol. 45, no. 6, pp. 1093–1097, Feb. 2006, doi: 10.1364/AO.45.001093.

[119] "ESA - A new satellite to understand how Earth is losing its cool." https://www.esa.int/Applications/Observing_the_Earth/A_new_satellite_to_understand_how_ Earth_is_losing_its_cool (accessed Apr. 20, 2021).

[120] P. J. Gero *et al.*, "The heated halo for space-based blackbody emissivity measurement," in *Multispectral, Hyperspectral, and Ultraspectral Remote Sensing Technology, Techniques and Applications IV*, Nov. 2012, vol. 8527, p. 85270O, doi: 10.1117/12.977548.

[121] "Spectralon® Diffuse Reflectance Material - Labsphere | Internationally Recognized Photonics Company." https://www.labsphere.com/labsphere-products-solutions/materials-coatings-2/coatings-materials/spectralon/ (accessed Apr. 20, 2021).

[122] F. Riehle and B. Wende, "Electron storage ring BESSY as a radiometric source of calculable spectral radiant power between 05 and 1000 nm," *Opt. Lett.*, vol. 10, no. 7, p. 365, Jul. 1985, doi: 10.1364/ol.10.000365.

[123] CCPR, "Definition of the Candela and associated derived units for photometric and radiometric quantities in the SI Consultative Committee for Photometry and Radiometry."

[124] J. Geist, W. K. Gladden, and E. F. Zalewski, "PHYSICS OF PHOTON-FLUX MEASUREMENTS WITH SILICON PHOTODIODES.," in *Journal of the Optical Society of America*, Aug. 1982, vol. 72, no. 8, pp. 1068–1075, doi: 10.1364/JOSA.72.001068.

[125] B. Walter *et al.*, "Direct Solar Irradiance measurements with a Cryogenic Solar Absolute Radiometer," in *AIP Conference Proceedings*, Feb. 2017, vol. 1810, no. 1, p. 080007, doi: 10.1063/1.4975538.

[126] B. Walter, A. Fehlmann, W. Finsterle, M. Suter, R. Soder, and W. Schmutz, "Spectrally integrated window transmittance measurements for a cryogenic solar absolute radiometer," *Metrologia*, vol. 51, no. 6, pp. S344–S349, Dec. 2014, doi: 10.1088/0026-1394/51/6/S344.

[127] I. Tomazic *et al.*, "Initial comparison between Sentinel-3A SLSTR and IASI aboard MetOp-A and MetOp-B," *GSICS Q.*, vol. 10, no. 3, 2016.

[128] J. T. Woodward, P. S. Shaw, H. W. Yoon, Y. Zong, S. W. Brown, and K. R. Lykke, "Invited Article: Advances in tunable laser-based radiometric calibration applications at the National Institute of Standards and Technology, USA," *Rev. Sci. Instrum.*, vol. 89, no. 9, p. 091301, Sep. 2018, doi: 10.1063/1.5004810.

[129] S. Devlin *et al.*, "The STAR-CC-OGSE system for pre-flight sensor calibration," vol. 11852, no. 11, p. 118526J, Jun. 2021, doi: 10.1117/12.2600300.

[130] T. J. Hewison *et al.*, "GSICS inter-calibration of infrared channels of geostationary imagers using metop/IASI," *IEEE Trans. Geosci. Remote Sens.*, 2013, doi: 10.1109/TGRS.2013.2238544.

[131] C. Cao and A. K. Heidinger, "Inter-comparison of the longwave infrared channels of MODIS and AVHRR/NOAA-16 using simultaneous nadir observations at orbit intersections," in *Earth Observing Systems VII*, Sep. 2002, vol. 4814, p. 306, doi: 10.1117/12.451690.

[132] H. Xu, Y. Chen, and L. Wang, "Cross-Track Infrared Sounder Spectral Gap Filling Toward Improving Intercalibration Uncertainties," *IEEE Trans. Geosci. Remote Sens.*, vol. 57, no. 1, pp. 509–519, Jan. 2019, doi: 10.1109/TGRS.2018.2857833.

[133] D. Doelling, C. Haney, R. Bhatt, B. Scarino, and A. Gopalan, "Geostationary Visible Imager Calibration for the CERES SYN1deg Edition 4 Product," *Remote Sens.*, vol. 10, no. 2, p. 288, Feb. 2018, doi: 10.3390/rs10020288.

[134] S. C. Wagner, T. Hewison, T. Stone, S. Lachérade, B. Fougnie, and X. Xiong, "A summary of the joint GSICS – CEOS/IVOS lunar calibration workshop: moving towards intercalibration using the Moon as a transfer target," in *Sensors, Systems, and Next-Generation Satellites XIX*, Oct. 2015, vol. 9639, p. 96390Z, doi: 10.1117/12.2193161.

[135] B. R. Scarino *et al.*, "A Web-Based Tool for Calculating Spectral Band Difference Adjustment Factors Derived from SCIAMACHY Hyperspectral Data," *IEEE Trans. Geosci. Remote Sens.*, vol. 54, no. 5, pp. 2529–2542, May 2016, doi: 10.1109/TGRS.2015.2502904.

[136] F. Chen and M. Niu, "Research on the Moon as an exoatmospheric longwave infrared reference," Feb. 2018, p. 305, doi: 10.1117/12.2315585.

[137] T. J. Hewison, "An evaluation of the uncertainty of the GSICS SEVIRI-IASI intercalibration products," *IEEE Trans. Geosci. Remote Sens.*, vol. 51, no. 3, pp. 1171–1181, 2013, doi: 10.1109/TGRS.2012.2236330.

[138] EUMETSAT, "ATBD for EUMETSAT Demonstration Prime GSICS Corrections for Meteosat-SEVIRI," pp. 1–28, 2016.

[139] T. Tabata, V. O. John, R. A. Roebeling, T. Hewison, and J. Schulz, "Recalibration of over 35 Years of Infrared and Water Vapor Channel Radiances of the JMA Geostationary Satellites," *Remote Sens.*, vol. 11, no. 10, p. 1189, May 2019, doi: 10.3390/rs11101189.

[140] EUMETSAT, "GSICS Traceability Statement for IASI and AIRS," pp. 1–11, 2014, [Online]. Available: http://www.eumetsat.int.

[141] S.-H. Ham and B. J. Sohn, "Assessment of the calibration performance of satellite visible channels using cloud targets: application to Meteosat-8/9 and MTSAT-1R," *Atmos. Chem. Phys. Discuss.*, vol. 10, no. 5, pp. 12629–12664, May 2010, doi: 10.5194/acpd-10-12629-2010.

[142] A. Okuyama, "Outlined Algorithm Theoretical Basis for MTSAT visible Calibration for GSICS

(Liquid cloud method),” 2011.

[143]   “GSICS   calibration   monitoring   page   for   MTSAT-2.”
        http://www.data.jma.go.jp/mscweb/data/monitoring/gsics/ir/gsir_mt2.html (accessed Jul. 30,
        2020).

[144]   “JMA   AHI-8   Performance   Test   Results.”
        https://www.data.jma.go.jp/mscweb/en/himawari89/space_segment/doc/AHI8_performance_te
        st_en.pdf (accessed Jul. 30, 2020).

[145]   K. Bessho *et al.*, “An Introduction to Himawari-8/9 - Japan’s new-generation geostationary
        meteorological satellites,” *J. Meteorol. Soc. Japan*, vol. 94, no. 2, pp. 151–183, 2016, doi:
        10.2151/jmsj.2016-009.

[146]   NASA, “GOES-R Series Data Book.”

[147]   R. Bhatt, D. R. Doelling, C. O. Haney, B. R. Scarino, and A. Gopalan, “Radiometric inter-
        comparison between GOES-16 ABI and NOAA-20 VIIRS reflective solar bands,” *J. Appl.
        Remote Sens.*, 2019.

[148]   X. Xiong *et al.*, “MODIS reflective solar bands on-orbit calibration and performance,” *IEEE
        Trans. Geosci. Remote Sens.*, vol. 57, no. 9, pp. 6355–6371, Sep. 2019, doi:
        10.1109/TGRS.2019.2905792.

[149]   L. Zajiczek, R. Winkler, T. Hobson, P. Green, and N. Fox, “Prototype of Cryogenic Solar
        Absolute Radiometer and Transfer Radiometer for On-Board Calibration of Spectral Earth
        Imager Related content Cryogenic Solar Absolute Radiometer (CSAR)-Spectrally integrated
        window transmittance measurements for a cryogenic solar absolute radiometer-The 12th
        international conference on new developments and applications in optical radiometry Prototype
        of Cryogenic Solar Absolute Radiometer and Transfer Radiometer for On-Board Calibration of
        Spectral Earth Imager,” *IOP Conf. Ser. J. Phys. Conf. Ser.*, vol. 972, p. 12005, 2018, doi:
        10.1088/1742-6596/972/1/012005.

[150]   V. O. John *et al.*, “On the Methods for Recalibrating Geostationary Longwave Channels Using
        Polar Orbiting Infrared Sounders,” *Remote Sens.*, vol. 11, no. 10, p. 1171, May 2019, doi:
        10.3390/rs11101171.

[151]   C. Lukashin, Y. Shea, K. Thome, and B. A. Wielicki, “CLARREO Pathfinder Inter-calibration:
        Requirements and Objectives,” 2019.

[152]   G. Kopp, “Magnitudes and Timescales of Total Solar Irradiance Variability,” *J. Sp. Weather Sp.
        Clim.*, Jun. 2016, doi: 10.1051/swsc/2016025.

[153]   G. Kopp, “Earth’s incoming energy: The total solar irradiance,” in *Comprehensive Remote
        Sensing*, vol. 1–9, Elsevier, 2017, pp. 32–66.

[154]   N. R. Council, *Review of NOAA working group report on maintaining the continuation of long-
        term satellite total solar irradiance observation*. National Academies Press, 2013.

[155]   G. Kopp and G. Lawrence, “The Total Irradiance Monitor (TIM): Instrument design,” in *The
        Solar Radiation and Climate Experiment (SORCE): Mission Description and Early Results*,
        Springer New York, 2005, pp. 91–109.

[156]   C. Fröhlich, “Solar irradiance variability since 1978: Revision of the PMOD composite during
        solar cycle 21,” *Space Sci. Rev.*, vol. 125, no. 1–4, pp. 53–65, Apr. 2006, doi: 10.1007/s11214-
        006-9046-5.

[157]   R. C. Willson and A. V. Mordvinov, “Secular total solar irradiance trend during solar cycles 21-

23," *Geophys. Res. Lett.*, vol. 30, no. 5, p. n/a-n/a, Mar. 2003, doi: 10.1029/2002gl016038.

[158] S. Dewitte, D. Crommelynck, S. Mekaoui, and A. Joukoff, "Measurement and uncertainty of the long-term total solar irradiance trend," in *Solar Physics*, Oct. 2004, vol. 224, no. 1–2, pp. 209–216, doi: 10.1007/s11207-005-5698-7.

[159] O. Coddington, J. L. Lean, P. Pilewskie, M. Snow, and D. Lindholm, "A solar irradiance climate data record," *Bull. Am. Meteorol. Soc.*, vol. 97, no. 7, pp. 1265–1282, Jul. 2016, doi: 10.1175/BAMS-D-14-00265.1.

[160] N. A. Krivova, L. E. A. Vieira, and S. K. Solanki, "Reconstruction of solar spectral irradiance since the Maunder minimum," *J. Geophys. Res. Sp. Phys.*, vol. 115, no. 12, Dec. 2010, doi: 10.1029/2010JA015431.

[161] C.-J. Wu, N. A. Krivova, S. K. Solanki, and I. G. Usoskin, "Solar total and spectral irradiance reconstruction over the last 9000 years," Nov. 2018, doi: 10.1051/0004-6361/201832956.

[162] G. Kopp, K. Heuerman, D. Harber, and G. Drake, "The TSI Radiometer Facility: absolute calibrations for total solar irradiance instruments," in *Earth Observing Systems XII*, Sep. 2007, vol. 6677, p. 667709, doi: 10.1117/12.734553.

[163] B. Walter *et al.*, "First TSI results and status report of the CLARA/NorSat-1 solar absolute radiometer," *Proc. Int. Astron. Union*, vol. 14, no. A30, pp. 358–360, 2018, doi: 10.1017/S1743921319004617.

[164] J. D. Haigh, "The impact of solar variability on climate," *Science (80-.).*, vol. 272, no. 5264, pp. 981–984, May 1996, doi: 10.1126/science.272.5264.981.

[165] P. Pilewskie, G. Rottman, and E. Richard, "An overview of the disposition of solar radiation in the lower atmosphere: Connections to the SORCE mission and climate change," in *The Solar Radiation and Climate Experiment (SORCE): Mission Description and Early Results*, Springer New York, 2005, pp. 55–69.

[166] J. Lean, G. Rottman, J. Harder, and G. Kopp, "SORCE contributions to new understanding of global change and solar variability," in *The Solar Radiation and Climate Experiment (SORCE): Mission Description and Early Results*, Springer New York, 2005, pp. 27–53.

[167] H. Brindley and J. Russell, "Monitoring the Climate system from space: progress, pitfalls and possibilities," 2013. Accessed: Jun. 11, 2020. [Online]. Available: www.imperial.

[168] J. L. Lean and M. T. DeLand, "How does the Sun's spectrum vary?," *J. Clim.*, vol. 25, no. 7, pp. 2555–2560, Apr. 2012, doi: 10.1175/JCLI-D-11-00571.1.

[169] NPOESS, "Technical Requirements Document." NPOESS-Integrated Program Office (IPO), 2007.

[170] NOAA, "Total and Spectral Solar Irradiance Sensor (TSIS) Requirements Document." 2010.

[171] B. Guenther James Butler and P. Ardanuy, "Workshop on Strategies for Calibration and Validation of Global Change Measurements," 1997. Accessed: Jun. 11, 2020. [Online]. Available: https://ntrs.nasa.gov/search.jsp?R=19970014648.

[172] N. R. Council, *Issues in the Integration of Research and Operational Satellite Systems for Climate Research*. National Academies Press, 2000.

[173] BIPM, *The International System of Units (SI)*, 7th ed. Paris, 1998.

[174] NIST, "Guide for the Use of the International System of Units (SI), NIST Special Publication 811," 1995.

[175] S. W. Brown, G. P. Eppeldauer, J. P. Rice, J. Zhang, and K. R. Lykke, "Spectral Irradiance and Radiance Responsivity Calibrations Using Uniform Sources (SIRCUS) Facility at NIST," in *SPIE Proceedings*, vol. 5542, pp. 363–374.

[176] B. C. Johnson, S. W. Brown, and J. P. Rice, "Metrology for Remote Sensing Radiometry." .

[177] J. M. Houston and J. P. Rice, "NIST Reference Cryogenic Radiometer Designed for Versatile Performance," *Metrologia*, vol. 43, 2006.

[178] G. Thuillier *et al.*, "The solar spectral irradiance from 200 to 2400 nm as measured by the SOLSPEC spectrometer from the ATLAS and EURECA missions," *Sol. Phys.*, vol. 214, no. 1, pp. 1–22, May 2003, doi: 10.1023/A:1024048429145.

[179] M. Haberreiter *et al.*, "A new observational solar irradiance composite," *J. Geophys. Res. Sp. Phys.*, vol. 122, no. 6, pp. 5910–5930, Jun. 2017, doi: 10.1002/2016JA023492.

[180] K. Chance and R. L. Kurucz, "An improved high-resolution solar reference spectrum for earth's atmosphere measurements in the ultraviolet, visible, and near infrared," *J. Quant. Spectrosc. Radiat. Transf.*, vol. 111, no. 9, pp. 1289–1295, Jun. 2010, doi: 10.1016/j.jqsrt.2010.01.036.

[181] M. Meftah *et al.*, "SOLAR-ISS: A new reference spectrum based on SOLAR/SOLSPEC observations," *A&A*, vol. 611, 2018, doi: 10.1051/0004-6361/201731316.

[182] O. Coddington *et al.*, "Solar Irradiance Variability: Comparisons of Models and Measurements," *Earth Sp. Sci.*, vol. 6, no. 12, pp. 2525–2555, Dec. 2019, doi: 10.1029/2019EA000693.

[183] E. C. Richard *et al.*, "The compact spectral irradiance monitor flight demonstration mission," in *CubeSats and SmallSats for Remote Sensing III*, Aug. 2019, vol. 11131, p. 4, doi: 10.1117/12.2531268.

[184] Graeme Stephens *et al.*, "The emerging technological revolution in earth observations," *Bull. Am. Meteorol. Soc.*, vol. 101, no. 3, pp. E274–E285, Mar. 2020, doi: 10.1175/BAMS-D-19-0146.1.

[185] F. B. House, A. Gruber, G. E. Hunt, and A. T. Mecherikunnel, "History of satellite missions and measurements of the Earth Radiation Budget (1957–1984)," *Rev. Geophys.*, vol. 24, no. 2, p. 357, May 1986, doi: 10.1029/RG024i002p00357.

[186] J. E. Harries *et al.*, "The Geostationary Earth Radiation Budget project," *Bulletin of the American Meteorological Society*, vol. 86, no. 7. American Meteorological Society, pp. 945–960, Jul. 01, 2005, doi: 10.1175/BAMS-86-7-945.

[187] M. E. Caldwell, D. A. V. Spilling, J. Delderfield, K. Ward, and M. Whalley, "Radiometric characteristics of the Broadband Radiometer (BBR) instrument for the EarthCARE mission," *J. Atmos. Ocean. Technol.*, vol. 34, no. 8, pp. 1783–1794, Aug. 2017, doi: 10.1175/JTECH-D-16-0168.1.

[188] A. J. Illingworth *et al.*, "The EarthCARE satellite : The next step forward in global measurements of clouds, aerosols, precipitation, and radiation," *Bull. Am. Meteorol. Soc.*, vol. 96, no. 8, pp. 1311–1332, Aug. 2015, doi: 10.1175/BAMS-D-12-00227.1.

[189] W. L. Barnes and V. V. Salomonson, "MODIS: A Global Image Spectroradiometer for the Earth Observing System," in *Proc. of SPIE 10269 - Optical Technologies for Aerospace Sensing: A Critical Review*, 1993, pp. 285–307, Accessed: Jun. 11, 2020. [Online]. Available: https://mcst.gsfc.nasa.gov/content/modis-global-image-spectroradiometer-earth-observing-system.

[190] X. Xiong *et al.*, "Terra and aqua MODIS design, radiometry, and geometry in support of land

remote sensing," in *Remote Sensing and Digital Image Processing*, vol. 11, Springer International Publishing, 2011, pp. 133–164.

[191] C. F. Schueler, J. E. Clement, P. E. Ardanuy, C. Welsch, F. DeLuccia, and H. Swenson, "NPOESS VIIRS sensor design overview," in *Earth Observing Systems VI*, Jan. 2002, vol. 4483, pp. 11–23, doi: 10.1117/12.453451.

[192] C. Cao, F. J. De Luccia, X. Xiong, R. Wolfe, and F. Weng, "Early on-orbit performance of the visible infrared imaging radiometer suite onboard the suomi national polar-orbiting partnership (S-NPP) satellite," *IEEE Trans. Geosci. Remote Sens.*, vol. 52, no. 2, pp. 1142–1156, Feb. 2014, doi: 10.1109/TGRS.2013.2247768.

[193] X. Xiong *et al.*, "VIIRS on-orbit calibration methodology and performance," *J. Geophys. Res.*, vol. 119, no. 9, pp. 5065–5078, May 2014, doi: 10.1002/2013JD020423.

[194] V. V. Salomonson, W. L. Barnes, P. W. Maymon, H. E. Montgomery, and H. Ostrow, "MODIS: Advanced Facility Instrument for Studies of the Earth as a System," *IEEE Trans. Geosci. Remote Sens.*, vol. 27, no. 2, pp. 145–153, 1989, doi: 10.1109/36.20292.

[195] P. E. Ardanuy *et al.*, "NPOESS VIIRS Design Process," in *Earth Observing Systems VI*, Jan. 2002, vol. 4483, pp. 24–34, doi: 10.1117/12.453461.

[196] T. F. Lee, S. D. Miller, C. Schueler, and S. Miller, "NASA MODIS previews NPOESS VIIRS capabilities," *Weather Forecast.*, vol. 21, no. 4, pp. 649–655, Aug. 2006, doi: 10.1175/WAF935.1.

[197] W. L. Barnes, T. S. Pagano, and V. V. Salomonson, "Prelaunch characteristics of the moderate resolution imaging spectroradiometer (MODIS) on EOS-AMI," *IEEE Trans. Geosci. Remote Sens.*, vol. 36, no. 4, pp. 1088–1100, 1998, doi: 10.1109/36.700993.

[198] H. Oudrari *et al.*, "Prelaunch radiometric characterization and calibration of the S-NPP VIIRS sensor," *IEEE Trans. Geosci. Remote Sens.*, vol. 53, no. 4, pp. 2195–2210, Apr. 2015, doi: 10.1109/TGRS.2014.2357678.

[199] J. J. Butler *et al.*, "Radiometric measurement comparison on the integrating sphere source used to calibrate the Moderate Resolution Imaging Spectroradiometer (MODIS) and the Landsat 7 Enhanced Thematic Mapper Plus (ETM+)," *J. Res. Natl. Inst. Stand. Technol.*, vol. 108, no. 3, pp. 199–228, 2003, doi: 10.6028/jres.108.020.

[200] R. A. Barnes *et al.*, "Comparison of two methodologies for calibrating satellite instruments in the visible and near-infrared," *Appl. Opt.*, vol. 54, no. 35, p. 10376, Dec. 2015, doi: 10.1364/ao.54.010376.

[201] A. P. Levick *et al.*, "Spectral radiance source based on supercontinuum laser and wavelength tunable bandpass filter: the spectrally tunable absolute irradiance and radiance source," *Appl. Opt.*, vol. 53, no. 16, p. 3508, Jun. 2014, doi: 10.1364/ao.53.003508.

[202] J. T. Woodward, A. W. Smith, C. A. Jenkins, C. Lin, S. W. Brown, and K. R. Lykke, "Supercontinuum sources for metrology," *Metrologia*, vol. 46, no. 4, p. S277, Jun. 2009, doi: 10.1088/0026-1394/46/4/S27.

[203] S. W. Brown, "Private Communication."

[204] X. Xiong, N. Che, and W. Barnes, "Terra MODIS on-orbit spatial characterization and performance," *IEEE Trans. Geosci. Remote Sens.*, vol. 43, no. 2, pp. 355–364, Feb. 2005, doi: 10.1109/TGRS.2004.840643.

[205] X. Xiong, N. Che, and W. L. Barnes, "Terra MODIS on-orbit spectral characterization and

performance," *IEEE Trans. Geosci. Remote Sens.*, vol. 44, no. 8, pp. 2198–2206, Aug. 2006, doi: 10.1109/TGRS.2006.872083.

[206] Z. Wang and X. Xiong, "VIIRS on-orbit spatial characterization using the moon," *IEEE Geosci. Remote Sens. Lett.*, vol. 11, no. 6, pp. 1116–1120, Jun. 2014, doi: 10.1109/LGRS.2013.2287791.

[207] Z. Wang, X. Xiong, and Y. Li, "Improved Band-to-Band Registration Characterization for VIIRS Reflective Solar Bands Based on Lunar Observations," *Remote Sens.*, vol. 8, no. 1, p. 27, Dec. 2015, doi: 10.3390/rs8010027.

[208] J. Sun, X. Xiong, A. Angal, H. Chen, A. Wu, and X. Geng, "Time-dependent response versus scan angle for MODIS reflective solar bands," *IEEE Trans. Geosci. Remote Sens.*, vol. 52, no. 6, pp. 3159–3174, 2014, doi: 10.1109/TGRS.2013.2271448.

[209] E. J. Kwiatkowska, B. A. Franz, G. Meister, C. R. McClain, and X. Xiong, "Cross calibration of ocean-color bands from Moderate Resolution Imaging Spectroradiometer on Terra platform," *Appl. Opt.*, vol. 47, no. 36, pp. 6796–6810, Dec. 2008, doi: 10.1364/AO.47.006796.

[210] G. Meister, R. E. Eplee, and B. A. Franz, "Corrections to MODIS Terra calibration and polarization trending derived from ocean color products," in *Earth Observing Systems XIX*, Oct. 2014, vol. 9218, p. 92180V, doi: 10.1117/12.2062714.

[211] A. Wu, X. Geng, A. Wald, A. Angal, and X. Xiong, "Assessment of terra MODIS on-orbit polarization sensitivity using pseudoinvariant desert sites," *IEEE Trans. Geosci. Remote Sens.*, vol. 55, no. 7, pp. 4168–4176, Jul. 2017, doi: 10.1109/TGRS.2017.2689719.

[212] D. Goldin, X. Xiong, Y. Shea, and C. Lukashin, "CLARREO Pathfinder/VIIRS Intercalibration: Quantifying the Polarization Effects on Reflectance and the Intercalibration Uncertainty," *Remote Sens.*, vol. 11, no. 16, p. 1914, Aug. 2019, doi: 10.3390/rs11161914.

[213] H. H. Kieffer, "Photometric Stability of the Lunar Surface," *Icarus*, vol. 130, no. 2, pp. 323–327, Dec. 1997, doi: 10.1006/icar.1997.5822.

[214] C. M. Pieters and J. F. Mustard, "Exploration of crustal/mantle material for the earth and moon using reflectance spectroscopy," *Remote Sens. Environ.*, vol. 24, no. 1, pp. 151–178, Feb. 1988, doi: 10.1016/0034-4257(88)90010-7.

[215] T. B. McCord, "Moon: near-infrared spectral reflectance, a first good look.," *J. Geophys. Res.*, vol. 86, no. B11, pp. 10883–10892, Nov. 1981, doi: 10.1029/JB086iB11p10883.

[216] C. E. Cramer, K. R. Lykke, J. T. Woodward, and A. W. Smith, "Precise Measurement of Lunar Spectral Irradiance at Visible Wavelengths," *J. Res. Natl. Inst. Stand. Technol.*, vol. 118, p. 396, Oct. 2013, doi: 10.6028/jres.118.020.

[217] K. J. Thome, B. G. Crowther, and S. F. Biggar, "Reflectance- and irradiance-based calibration of landsat-5 thematic mapper," *Can. J. Remote Sens.*, vol. 23, no. 4, pp. 309–317, 1997, doi: 10.1080/07038992.1997.10855217.

[218] H. Cosnefroy, M. Leroy, and X. Briottet, "Selection and characterization of Saharan and Arabian desert sites forthe calibration of optical satellite sensors," *Remote Sens. Environ.*, vol. 58, no. 1, pp. 101–114, Oct. 1996, doi: 10.1016/0034-4257(95)00211-1.

[219] K. J. Thome, "Absolute radiometric calibration of Landsat 7 ETM+ using the reflectance-based method," *Remote Sens. Environ.*, vol. 78, no. 1–2, pp. 27–38, Oct. 2001, doi: 10.1016/S0034-4257(01)00247-4.

[220] K. J. Thome, S. F. Biggar, and H. J. Choi, "Vicarious calibration of Terra ASTER, MISR, and MODIS," in *Earth Observing Systems IX*, Oct. 2004, vol. 5542, p. 290, doi: 10.1117/12.559942.

[221] S. F. Biggar, K. J. Thome, and W. Wisniewski, "Vicarious radiometric calibration of EO-1 sensors by reference to high-reflectance ground targets," *IEEE Trans. Geosci. Remote Sens.*, vol. 41, no. 6 PART I, pp. 1174–1179, Jun. 2003, doi: 10.1109/TGRS.2003.813211.

[222] K. P. Scott, K. J. Thome, and M. R. Brownlee, "Evaluation of Railroad Valley playa for use in vicarious calibration," in *Multispectral Imaging for Terrestrial Applications*, Nov. 1996, vol. 2818, p. 158, doi: 10.1117/12.256090.

[223] X. Jing, L. Leigh, C. Teixeira Pinto, and D. Helder, "Evaluation of RadCalNet Output Data Using Landsat 7, Landsat 8, Sentinel 2A, and Sentinel 2B Sensors," *Remote Sens.*, vol. 11, no. 5, p. 541, Mar. 2019, doi: 10.3390/rs11050541.

[224] D. Doelling, D. Helder, J. Schott, T. Stone, and C. T. Pinto, "Vicarious calibration and validation," in *Comprehensive Remote Sensing*, vol. 1–9, Elsevier, 2017, pp. 475–518.

[225] D. Helder *et al.*, "Recent surface reflectance measurement campaigns with emphasis on best practices, SI traceability and uncertainty estimation," *Metrologia*, vol. 49, no. 2, p. S21, Mar. 2012, doi: 10.1088/0026-1394/49/2/S21.

[226] D. L. Helder, B. Basnet, and D. L. Morstad, "Optimized identification of worldwide radiometric pseudo-invariant calibration sites," *Can. J. Remote Sens.*, vol. 36, no. 5, pp. 527–539, Oct. 2010, doi: 10.5589/m10-085.

[227] D. Helder, H. Vuppula, L. Ervin, R. Tabassum, and M. Kaewmanee, "PICS Normalization: Improved Temporal Trending Using PICS," Logan, Utah, 2016.

[228] T. Chang, X. Xiong, A. Angal, A. Wu, and X. Geng, "Aqua and Terra MODIS RSB Calibration Comparison Using BRDF Modeled Reflectance," *IEEE Trans. Geosci. Remote Sens.*, vol. 55, no. 4, pp. 2288–2298, Apr. 2017, doi: 10.1109/TGRS.2016.2641258.

[229] D. Helder *et al.*, "Absolute radiometric calibration of landsat using a pseudo invariant calibration site," *IEEE Trans. Geosci. Remote Sens.*, vol. 51, no. 3, pp. 1360–1369, 2013, doi: 10.1109/TGRS.2013.2243738.

[230] N. Mishra, D. Helder, A. Angal, J. Choi, and X. Xiong, "Absolute Calibration of Optical Satellite Sensors Using Libya 4 Pseudo Invariant Calibration Site," *Remote Sens.*, vol. 6, no. 2, pp. 1327–1346, Feb. 2014, doi: 10.3390/rs6021327.

[231] "Landsat Calibration Technical Interchange Meeting, USGS EROS." Sep. 2019, Accessed: Jun. 10, 2020. [Online]. Available: https://www.usgs.gov/land-resources/nli/landsat/sept-17-2019-landsat-calibration-and-validation-meeting-south-dakota.

[232] M. D. King, Y. J. Kaufman, W. P. Menzel, and D. Tanré, "Remote Sensing of Cloud, Aerosol, and Water Vapor Properties from the Moderate Resolution Imaging Spectrometer (MODIS)," *IEEE Transactions on Geoscience and Remote Sensing*, vol. 30, no. 1. pp. 2–27, 1992, doi: 10.1109/36.124212.

[233] F.-M. Breon and F. Nadal, "Parameterization of Surface Polarized Reflectance Derived from POLDER Spaceborne Measurements ," *IEEE Trans. Geosci. Remote Sens.*, vol. 37, no. 3, 1999, doi: 10.1109/36.763292.

[234] F. Maignan, F. M. Bréon, E. Fédèle, and M. Bouvier, "Polarized reflectances of natural surfaces: Spaceborne measurements and analytical modeling," *Remote Sens. Environ.*, vol. 113, no. 12, pp. 2642–2650, Dec. 2009, doi: 10.1016/j.rse.2009.07.022.

[235] P. Y. Deschamps *et al.*, "The POLDER Mission: Instrument Characteristics and Scientific Objectives," *IEEE Trans. Geosci. Remote Sens.*, vol. 32, no. 3, pp. 598–615, 1994, doi: 10.1109/36.297978.

[236] "CPF-02-011 Rev. D – Science and Mission Requirements Document."

[237] J. Q. Sun and X. Xiong, "MODIS polarization-sensitivity analysis," *IEEE Trans. Geosci. Remote Sens.*, vol. 45, no. 9, pp. 2875–2885, Sep. 2007, doi: 10.1109/TGRS.2007.900672.

[238] C. Cox and W. Munk, "Measurement of the Roughness of the Sea Surface from Photographs of the Sun's Glitter," *J. Opt. Soc. Am.*, vol. 44, no. 11, p. 838, Nov. 1954, doi: 10.1364/josa.44.000838.

[239] C. Cox and W. Munk, " Slopes of the sea surface deduced from photographs of sun glitter," Sep. 1956.

[240] "Executive Summary for CEOI-10 Pathfinder HHRTII (Hyperspectral High-Resolution Thermal Infrared Imager)."

[241] "WMO OSCAR | Observing Systems Capability Analysis and Review Tool - Home." https://www.wmo-sat.info/oscar/ (accessed Jul. 30, 2020).

[242] M. Drinkwater and H. Rebhan, "Sentinel-3 Mission Requirements Document."

[243] I. M. Mason, P. H. Sheather, J. A. Bowles, and G. Davies, "Blackbody calibration sources of high accuracy for a spaceborne infrared instrument: the Along Track Scanning Radiometer," *Appl. Opt.*, vol. 35, no. 4, p. 629, Feb. 1996, doi: 10.1364/ao.35.000629.

[244] K. Ostojic, D. M. Peters, and D. Smith, "The Challenges of Thermal Testing and Correlation of Blackbody Cavities," 2019.

[245] D. L. Smith *et al.*, "Calibration approach and plan for the sea and land surface temperature radiometer," *J. Appl. Remote Sens.*, vol. 8, no. 1, p. 084980, Jun. 2014, doi: 10.1117/1.jrs.8.084980.

[246] D. Smith *et al.*, "Pre-Launch Calibration of the Sea and Land Surface Temperature Radiometer," 2018.

[247] S. Lacherade, B. Fougnie, P. Henry, and P. Gamet, "Cross calibration over desert sites: Description, methodology, and operational implementation," *IEEE Trans. Geosci. Remote Sens.*, vol. 51, no. 3, pp. 1098–1113, 2013, doi: 10.1109/TGRS.2012.2227061.

[248] D. L. Smith and C. V. Cox, "(A)ATSR solar channel on-orbit radiometric calibration," *IEEE Trans. Geosci. Remote Sens.*, vol. 51, no. 3, pp. 1370–1382, 2013, doi: 10.1109/TGRS.2012.2230333.

[249] F. A. Best, D. P. Adler, C. Pettersen, H. E. Revercomb, and J. H. Perepezko, "On-orbit absolute temperature calibration using multiple phase change materials: overview of recent technology advancements," in *Multispectral, Hyperspectral, and Ultraspectral Remote Sensing Technology, Techniques, and Applications III*, Oct. 2010, vol. 7857, p. 78570J, doi: 10.1117/12.869564.

[250] RAL SPACE, "CEOI-11, NGenIRS Final Report."

[251] J. V Pearce, R. I. Veltcheva, D. M. Peters, D. Smith, and T. Nightingale, "Miniature gallium phase-change cells for in situ thermometry calibrations in space," *Meas. Sci. Technol.*, vol. 30, no. 12, p. 124003, Sep. 2019, doi: 10.1088/1361-6501/AB38E4.

[252] H. Preston-Thomas, "The International Temperature Scale of 1990 (ITS-90)," *Metrologia*, vol. 27, no. 1, p. 3, 1990, doi: 10.1088/0026-1394/27/1/002.

[253] S. N. Mekhontsev, V. B. Khromchenko, and L. M. Hanssen, "NIST radiance temperature and infrared spectral radiance scales at near-ambient temperatures," *Int. J. Thermophys.*, vol. 29, no.

3, pp. 1026–1040, Jun. 2008, doi: 10.1007/s10765-008-0384-2.

[254] J. B. Fowler, "A Third Generation Water Bath Based Blackbody Source," *J. Res. Natl. Inst. Stand. Technol.*, vol. 100, no. 5, p. 591, Sep. 1995, doi: 10.6028/jres.100.044.

[255] J. B. Fowler, B. C. Johnson, J. P. Rice, and S. R. Lorentz, "The new cryogenic vacuum chamber and black-body source for infrared calibrations at the NIST's FARCAL facility," *Metrologia*, vol. 35, no. 4, p. 323, 1998, doi: 10.1088/0026-1394/35/4/18.

[256] X. Xiong, K. F. Chiang, A. Wu, W. L. Barnes, B. Guenther, and V. V. Salomonson, "Multiyear on-orbit calibration and performance of terra MODIS thermal emissive bands," *IEEE Trans. Geosci. Remote Sens.*, vol. 46, no. 6, pp. 1790–1803, Jun. 2008, doi: 10.1109/TGRS.2008.916217.

[257] X. Xiong, B. N. Wenny, A. Wu, W. L. Barnes, and V. V. Salomonson, "Aqua MODIS thermal emissive band on-Orbit calibration, characterization, and performance," *IEEE Trans. Geosci. Remote Sens.*, vol. 47, no. 3, pp. 803–814, Mar. 2009, doi: 10.1109/TGRS.2008.2005109.

[258] B. Efremova, J. McIntire, D. Moyer, A. Wu, and X. Xiong, "S-NPP VIIRS thermal emissive bands on-orbit calibration and performance," *J. Geophys. Res. Atmos.*, vol. 119, no. 18, pp. 10,859-10,875, Sep. 2014, doi: 10.1002/2014JD022078.

[259] T. S. Pagano *et al.*, "Standard and research products from the AIRS and AMSU on the EOS aqua spacecraft," in *Atmospheric and Environmental Remote Sensing Data Processing and Utilization: Numerical Atmospheric Prediction and Environmental Monitoring*, Aug. 2005, vol. 5890, p. 58900R, doi: 10.1117/12.616245.

[260] J. Le Marshall *et al.*, "Impact of atmospheric infrared sounder observations on weather forecasts," *Eos, Trans. Am. Geophys. Union*, vol. 86, no. 11, pp. 109–116, Mar. 2005, doi: 10.1029/2005EO110002.

[261] "Meteorological Satellite Center (MSC) | GSICS Infrared Inter-calibration." https://www.data.jma.go.jp/mscweb/data/monitoring/gsics/ir/monit_geoleoir.html (accessed Mar. 11, 2021).

[262] "(No Title)." http://nmsc.kma.go.kr/html/homepage/en/gsics/Infrared/gsicsIrTimeSequence.do (accessed Mar. 11, 2021).

[263] "GSICS Coordination Center - Product Data." https://www.star.nesdis.noaa.gov/smcd/GCC/ProductCatalog.php (accessed Mar. 11, 2021).

[264] T. S. Pagano, H. H. Aumann, D. E. Hagan, and K. Overoye, "Prelaunch and in-flight radiometric calibration of the Atmospheric Infrared Sounder (AIRS)," *IEEE Trans. Geosci. Remote Sens.*, vol. 41, no. 2 PART 1, pp. 265–273, Jul. 2003, doi: 10.1109/TGRS.2002.808324.

[265] S. Broberg, H. H. Aumann, and E. M. Manning, "Radiometric stability in 16 years of AIRS hyperspectral infrared data," in *Earth Observing Systems XXIII*, Sep. 2018, vol. 10764, p. 24, doi: 10.1117/12.2320727.

[266] L. L. Strow, S. E. Hannon, S. De-Souza Machado, H. E. Motteler, and D. C. Tobin, "Validation of the Atmospheric Infrared Sounder radiative transfer algorithm," *J. Geophys. Res.*, vol. 111, no. D9, p. D09S06, May 2006, doi: 10.1029/2005JD006146.

[267] "(No Title)." https://docserver.gesdisc.eosdis.nasa.gov/repository/Mission/AIRS/3.3_ScienceDataProductDocumentation/ 3.3.4_ProductGenerationAlgorithms/V5_L1B_QA_QuickStart.pdf (accessed Mar. 11, 2021).

[268] H. E. Revercomb *et al.*, "Infrared calibration for climate: a perspective on present and future high-spectral resolution instruments," in *Multispectral, Hyperspectral, and Ultraspectral Remote Sensing Technology, Techniques, and Applications*, Dec. 2006, vol. 6405, p. 640501, doi: 10.1117/12.694084.

[269] J. K. Taylor *et al.*, "The University of Wisconsin Space Science and Engineering Center Absolute Radiance Interferometer (ARI): instrument overview and radiometric performance," in *Optics InfoBase Conference Papers*, Nov. 2012, vol. 8527, p. 85270P, doi: 10.1117/12.977533.

[270] J. K. Taylor *et al.*, "The University of Wisconsin Space Science and Engineering Center Absolute Radiance Interferometer (ARI): instrument overview and radiometric performance," Nov. 2014, vol. 9263, p. 926313, doi: 10.1117/12.2069318.

[271] P. Howarth and F. Redgrave, *Metrology - In Short*, 3rd ed. 2008.

[272] F. A. Best, D. P. Adler, S. D. Ellington, D. J. Thielman, and H. E. Revercomb, "On-orbit absolute calibration of temperature with application to the CLARREO mission," in *Earth Observing Systems XIII*, Aug. 2008, vol. 7081, p. 70810O, doi: 10.1117/12.795457.

[273] F. A. Best *et al.*, "Results from recent vacuum testing of an on-orbit absolute radiance standard (OARS) intended for the next generation of infrared remote sensing instruments," in *Multispectral, Hyperspectral, and Ultraspectral Remote Sensing Technology, Techniques and Applications V*, Nov. 2014, vol. 9263, p. 926314, doi: 10.1117/12.2069338.

[274] P. J. Gero, J. K. Taylor, F. A. Best, R. K. Garcia, and H. E. Revercomb, "On-orbit absolute blackbody emissivity determination using the heated halo method," *Metrologia*, vol. 49, no. 2, p. S1, Mar. 2012, doi: 10.1088/0026-1394/49/2/S1.

[275] H. Revercomb *et al.*, "Monitoring climate from space: a metrology perspective," in *Earth Observing Missions and Sensors: Development, Implementation, and Characterization IV*, May 2016, vol. 9881, p. 98810F, doi: 10.1117/12.2223978.

[276] D. Gu, D. Houtz, J. Randa, and D. K. Walker, "Reflectivity study of microwave blackbody target," in *IEEE Transactions on Geoscience and Remote Sensing*, Sep. 2011, vol. 49, no. 9, pp. 3443–3451, doi: 10.1109/TGRS.2011.2125975.

[277] J. Randa, D. K. Walker, A. E. Cox, and R. L. Billinger, "Errors resulting from the reflectivity of calibration targets," *IEEE Trans. Geosci. Remote Sens.*, vol. 43, no. 1, pp. 50–58, Jan. 2005, doi: 10.1109/TGRS.2004.839809.

[278] D. A. Houtz *et al.*, "Electromagnetic Design and Performance of a Conical Microwave Blackbody Target for Radiometer Calibration," *IEEE Trans. Geosci. Remote Sens.*, vol. 55, no. 8, pp. 4586–4596, Aug. 2017, doi: 10.1109/TGRS.2017.2694319.

[279] A. Schroder, A. Murk, R. Wylde, D. Schobert, and M. Winser, "Brightness Temperature Computation of Microwave Calibration Targets," *IEEE Trans. Geosci. Remote Sens.*, vol. 55, no. 12, pp. 7104–7112, Dec. 2017, doi: 10.1109/TGRS.2017.2740559.

[280] D. M. Jackson and A. J. Gasiewski, "Electromagnetic and thermal analyses of radiometer calibration targets," in *International Geoscience and Remote Sensing Symposium (IGARSS)*, 2000, vol. 7, pp. 2827–2829, doi: 10.1109/igarss.2000.860261.

[281] A. Schröder *et al.*, "Electromagnetic Design of Calibration Targets for MetOp-SG Microwave Instruments," *IEEE Trans. Terahertz Sci. Technol.*, vol. 7, no. 6, pp. 677–685, Nov. 2017, doi: 10.1109/TTHZ.2017.2757442.

[282] P. Yagoubov, A. Murk, R. Wylde, G. Bell, and G. H. Tan, "Calibration loads for ALMA," in

IRMMW-THz 2011 - 36th International Conference on Infrared, Millimeter, and Terahertz Waves, 2011, doi: 10.1109/irmmw-THz.2011.6105120.

[283] A. Murk *et al.*, "Development of microwave calibration targets for upcoming ESA missions," in *International Geoscience and Remote Sensing Symposium (IGARSS)*, 2012, pp. 2949–2952, doi: 10.1109/IGARSS.2012.6350707.

[284] D. A. Houtz, W. Emery, D. Gu, and D. K. Walker, "Brightness temperature calculation and uncertainty propagation for conical microwave blackbody targets," *IEEE Trans. Geosci. Remote Sens.*, vol. 56, no. 12, pp. 7246–7256, Dec. 2018, doi: 10.1109/TGRS.2018.2849647.

[285] D. W. Draper, D. A. Newell, D. A. Teusch, and P. K. Yoho, "Global precipitation measurement microwave imager prelaunch hot load calibration," *IEEE Trans. Geosci. Remote Sens.*, vol. 51, no. 9, pp. 4731–4742, Feb. 2013, doi: 10.1109/TGRS.2013.2239300.

[286] E. M. Twarog, W. E. Purdy, P. W. Gaiser, K. H. Cheung, and B. E. Keim, "WindSat on-orbit warm load calibration," *IEEE Trans. Geosci. Remote Sens.*, vol. 44, no. 3, pp. 516–529, Mar. 2006, doi: 10.1109/TGRS.2005.863300.

[287] D. A. Houtz and D. K. Walker, "A finite element thermal simulation of a microwave blackbody calibration target," in *International Geoscience and Remote Sensing Symposium (IGARSS)*, 2013, pp. 394–397, doi: 10.1109/IGARSS.2013.6721175.

[288] S. Fernandez, A. Murk, and N. Kämpfer, "Design and characterization of a peltier-cold calibration target for a 110-GHz radiometer," *IEEE Trans. Geosci. Remote Sens.*, vol. 53, no. 1, pp. 344–351, 2015, doi: 10.1109/TGRS.2014.2322336.

[289] D. Gu, D. Houtz, J. Randa, and D. K. Walker, "Extraction of illumination efficiency by solely radiometric measurements for improved brightness-temperature characterization of microwave blackbody target," *IEEE Trans. Geosci. Remote Sens.*, vol. 50, no. 11 PART2, pp. 4575–4583, 2012, doi: 10.1109/TGRS.2012.2193890.

[290] J. Randa, "Uncertainties in NIST noises-temperature measurements," 1998. doi: 10.6028/NIST.TN.1502.

[291] D. Gu, D. Houtz, J. Randa, and D. K. Walker, "Realization of a standard radiometer for microwave brightness-temperature measurements traceable to fundamental noise standards," in *International Geoscience and Remote Sensing Symposium (IGARSS)*, 2012, pp. 2941–2944, doi: 10.1109/IGARSS.2012.6350709.

[292] D. A. Houtz and W. J. Emery, *NIST Microwave Blackbody: The Design, Testing, and Verification of a Conical Brightness Temperature Source*. 2017.

[293] P. W. Thorne, J. R. Lanzante, T. C. Peterson, D. J. Seidel, and K. P. Shine, "Tropospheric temperature trends: history of an ongoing controversy," *Wiley Interdiscip. Rev. Clim. Chang.*, vol. 2, no. 1, pp. 66–88, Jan. 2011, doi: 10.1002/wcc.80.

[294] N. C. Grody, K. Y. Vinnikov, M. D. Goldberg, J. T. Sullivan, and J. D. Tarpley, "Calibration of multisatellite observations for climatic studies: Microwave Sounding Unit (MSU)," *J. Geophys. Res. D Atmos.*, vol. 109, no. 24, pp. 1–12, Dec. 2004, doi: 10.1029/2004JD005079.

[295] W. J. Blackwell *et al.*, "Radiometer calibration using colocated GPS radio occultation measurements," *IEEE Trans. Geosci. Remote Sens.*, vol. 52, no. 10, pp. 6423–6433, 2014, doi: 10.1109/TGRS.2013.2296558.

[296] P. W. Rosenkranz *et al.*, "Designing a Climate-Monitoring Microwave Radiometer," in *2017 United States National Committee of URSI National Radio Science Meeting, USNC-URSI NRSM 2017*, Mar. 2017, doi: 10.1109/USNC-URSI-NRSM.2017.7878313.

[297] D. W. Draper, D. A. Newell, D. S. McKague, and J. R. Piepmeier, "Assessing Calibration Stability Using the Global Precipitation Measurement (GPM) Microwave Imager (GMI) Noise Diodes," in *IEEE Journal of Selected Topics in Applied Earth Observations and Remote Sensing*, Sep. 2015, vol. 8, no. 9, pp. 4239–4247, doi: 10.1109/JSTARS.2015.2406661.

[298] C. A. Mears, F. J. Wentz, P. Thorne, and D. Bernie, "Assessing uncertainty in estimates of atmospheric temperature changes from MSU and AMSU using a Monte-Carlo estimation technique," *J. Geophys. Res. Atmos.*, vol. 116, no. 8, 2011, doi: 10.1029/2010JD014954.

[299] S. S. Leroy, C. O. Ao, and O. P. Verkhoglyadova, "Temperature Trends and Anomalies in Modern Satellite Data: Infrared Sounding and GPS Radio Occultation," *J. Geophys. Res. Atmos.*, vol. 123, no. 20, pp. 11,431-11,444, Oct. 2018, doi: 10.1029/2018JD028990.

[300] E. R. Kursinski, G. A. Hajj, S. S. Leroy, and B. Herman, "The GPS Radio Occultation Technique," *Terr. Atmos. Ocean. Sci.*, vol. 11, no. 1, p. 053, 2000, doi: 10.3319/TAO.2000.11.1.53(COSMIC).

[301] E. R. Kursinski, G. A. Hajj, J. T. Schofield, R. P. Linfield, and K. R. Hardy, "Observing Earth's atmosphere with radio occultation measurements using the global positioning system," *J. Geophys. Res. Atmos.*, vol. 102, no. 19, pp. 23429–23465, Oct. 1997, doi: 10.1029/97jd01569.

[302] A. Crews, K. Cahoy, W. Blackwell, R. V. Leslie, and M. Grant, "Solar and Lunar Calibration for Miniaturized Microwave Radiometers," in *IEEE Aerospace Conference Proceedings*, Mar. 2019, vol. 2019-March, doi: 10.1109/AERO.2019.8741641.

[303] V. D. Krotikov and V. S. Troitskiĭ, "RADIO EMISSION AND NATURE OF THE MOON," *Sov. Phys. Uspekhi*, vol. 6, no. 6, pp. 841–871, Jun. 1964, doi: 10.1070/pu1964v006n06abeh003615.

[304] H. Yang and F. Weng, "On-orbit ATMS lunar contamination corrections ," *IEEE Transactions on Geoscience and Remote Sensing*, vol. 54, no. 4. Institute of Electrical and Electronics Engineers Inc., pp. 1918–1924, Apr. 01, 2016, doi: 10.1109/TGRS.2015.2490198.

[305] H. Yang *et al.*, "Developing vicarious calibration for microwave sounding instruments using lunar radiation," *IEEE Trans. Geosci. Remote Sens.*, vol. 56, no. 11, pp. 6723–6733, Nov. 2018, doi: 10.1109/TGRS.2018.2841997.

[306] M. Burgdorf, S. A. Buehler, T. Lang, S. Michel, and I. Hans, "The Moon as a photometric calibration standard for microwave sensors," *Atmos. Meas. Tech.*, vol. 9, no. 8, pp. 3467–3475, Aug. 2016, doi: 10.5194/amt-9-3467-2016.

[307] M. J. Burgdorf, S. A. Buehler, I. Hans, and M. Prange, "Disk-Integrated Lunar Brightness Temperatures between 89 and 190 GHz," *Adv. Astron.*, pp. 1–8, 2019, doi: 10.1155/2019/2350476.

[308] H. Yang *et al.*, "2-D Lunar Microwave Radiance Observations From the NOAA-20 ATMS," *IEEE Geosci. Remote Sens. Lett.*, pp. 1–4, Aug. 2020, doi: 10.1109/LGRS.2020.3012518.

[309] S. J. Keihm, "Interpretation of the lunar microwave brightness temperature spectrum: Feasibility of orbital heat flow mapping," *Icarus*, vol. 60, no. 3, pp. 568–589, Dec. 1984, doi: 10.1016/0019-1035(84)90165-9.

[310] N. Liu and Y. Q. Jin, "Average Brightness Temperature of Lunar Surface for Calibration of Multichannel Millimeter-Wave Radiometer from 89 to 183 GHz and Data Validation," *IEEE Trans. Geosci. Remote Sens.*, vol. 59, no. 2, pp. 1345–1354, Feb. 2021, doi: 10.1109/TGRS.2020.3000230.

[311] H. Yang, "Millimeter Lunar Microwave Radiance: Model simulation and satellite observations,"

in *IGARSS*, 2021.

[312] T. Auligné, A. P. McNally, and D. P. Dee, "Adaptive bias correction for satellite data in a numerical weather prediction system," *Q. J. R. Meteorol. Soc.*, vol. 133, no. 624 PART A, pp. 631–642, Apr. 2007, doi: 10.1002/qj.56.

[313] J. R. Eyre, "Observation bias correction schemes in data assimilation systems: a theoretical study of some of their properties," *Q. J. R. Meteorol. Soc.*, vol. 142, no. 699, pp. 2284–2291, Jul. 2016, doi: 10.1002/qj.2819.

[314] F. Carminati *et al.*, "Using reference radiosondes to characterise NWP model uncertainty for improved satellite calibration and validation," *Atmos. Meas. Tech.*, vol. 12, no. 1, pp. 83–106, Jan. 2019, doi: 10.5194/amt-12-83-2019.

[315] F. J. Immler, J. Dykema, T. Gardiner, D. N. Whiteman, P. W. Thorne, and H. Vömel, "Reference Quality Upper-Air Measurements: guidance for developing GRUAN data products," *Atmos. Meas. Tech.*, vol. 3, no. 5, pp. 1217–1231, Sep. 2010, doi: 10.5194/amt-3-1217-2010.

[316] S. Newman, F. Carminati, H. Lawrence, N. Bormann, K. Salonen, and W. Bell, "Assessment of New Satellite Missions within the Framework of Numerical Weather Prediction," *Remote Sens.*, vol. 12, no. 10, p. 1580, May 2020, doi: 10.3390/rs12101580.

[317] W. Han and N. Bormann, "Constrained adaptive bias correction for satellite radiance assimilation in the ECMWF 4D-Var system," 2016. Accessed: Jun. 09, 2020. [Online]. Available: https://www.nwpsaf.eu/vs_reports/nwpsaf-ec-vs-028.pdf.

[318] N. Bormann, W. Bell, P. Laloyaux, and K. Clarke, "ECMWF/NWP-SAF Workshop on the Treatment of Random and Systematic Errors in Satellite Data Assimilation Characterisation of uncertainties in observations and models." Accessed: Mar. 11, 2021. [Online]. Available: https://events.ecmwf.int/event/170/.

[319] National Research Council, *Carbon Dioxide and Climate*. Washington, D.C.: National Academies Press, 1979.

[320] J. Vial, J. L. Dufresne, and S. Bony, "On the interpretation of inter-model spread in CMIP5 climate sensitivity estimates," *Clim. Dyn.*, vol. 41, no. 11–12, pp. 3339–3362, Dec. 2013, doi: 10.1007/s00382-013-1725-9.

[321] N. G. Loeb *et al.*, "Advances in Understanding Top-of-Atmosphere Radiation Variability from Satellite Observations," *Surv. Geophys.*, vol. 33, no. 3–4, pp. 359–385, Jul. 2012, doi: 10.1007/s10712-012-9175-1.

[322] B. J. Soden, I. M. Held, R. Colman, K. M. Shell, J. T. Kiehl, and C. A. Shields, "Quantifying Climate Feedbacks Using Radiative Kernels," *J. Clim.*, vol. 21, no. 14, pp. 3504–3520, Jul. 2008, doi: 10.1175/2007JCLI2110.1.

[323] M. D. Zelinka *et al.*, "Contributions of Different Cloud Types to Feedbacks and Rapid Adjustments in CMIP5," *J. Clim.*, vol. 26, no. 14, pp. 5007–5027, Jul. 2013, doi: 10.1175/JCLI-D-12-00555.1.

[324] P. Ceppi, D. T. McCoy, and D. L. Hartmann, "Observational evidence for a negative shortwave cloud feedback in middle to high latitudes," *Geophys. Res. Lett.*, vol. 43, no. 3, pp. 1331–1339, Feb. 2016, doi: 10.1002/2015GL067499.

[325] E. C. Weatherhead *et al.*, "Factors affecting the detection of trends: Statistical considerations and applications to environmental data," *J. Geophys. Res. Atmos.*, vol. 103, no. D14, pp. 17149–17161, Jul. 1998, doi: 10.1029/98JD00995.

[326] "Landsat Satellite Missions." https://landsat.usgs.gov.

[327] "Sentinel-2 Missions ." https://sentinel.esa.int/web/sentinel/missions/sentinel-2 (accessed Jun. 09, 2020).

[328] V. V. Salomonson, W. Barnes, and E. J. Masuoka, "Introduction to MODIS and an overview of associated activities," in *Earth Science Satellite Remote Sensing: Science and Instruments*, 2006, vol. 1, pp. 12–32, doi: 10.1007/978-3-540-37293-6_2.

[329] "Planet Monitoring." https://www.planet.com/products/monitoring/ (accessed Jun. 09, 2020).

[330] X. Xiong and W. Barnes, "An overview of MODIS radiometric calibration and characterization," *Advances in Atmospheric Sciences*, vol. 23, no. 1. Springer, pp. 69–79, Jan. 2006, doi: 10.1007/s00376-006-0008-3.

[331] F. Gascon *et al.*, "Copernicus Sentinel-2A Calibration and Products Validation Status," *Remote Sens.*, vol. 9, no. 6, p. 584, Jun. 2017, doi: 10.3390/rs9060584.

[332] E. Knight and G. Kvaran, "Landsat-8 Operational Land Imager Design, Characterization and Performance," *Remote Sens.*, vol. 6, no. 11, pp. 10286–10305, Oct. 2014, doi: 10.3390/rs61110286.

[333] A. Angal, J. McCorkel, and K. Thome, "Evaluation of GLAMR-based calibration for SI-traceable field reflectance retrievals," in *Earth Observing Systems XXI*, Sep. 2016, vol. 9972, p. 99721U, doi: 10.1117/12.2238630.

[334] J. Barsi *et al.*, "Landsat-8 on-orbit and Landsat-9 pre-launch sensor radiometric characterization," in *Earth Observing Missions and Sensors: Development, Implementation, and Characterization V*, Oct. 2018, vol. 10781, p. 3, doi: 10.1117/12.2324715.

[335] C. Ong, K. Thome, and A. Kuze, "Role of CEOS Working Group on Calibration and Validation in Analysis Ready Data Products," in *International Geoscience and Remote Sensing Symposium (IGARSS)*, Jul. 2019, pp. 5538–5540, doi: 10.1109/IGARSS.2019.8899301.

[336] D. Helder *et al.*, "Observations and Recommendations for the Calibration of Landsat 8 OLI and Sentinel 2 MSI for Improved Data Interoperability," *Remote Sens.*, vol. 10, no. 9, p. 1340, Aug. 2018, doi: 10.3390/rs10091340.

[337] X. Xiong *et al.*, "Terra MODIS: 20 years of on-orbit calibration and performance," in *Earth Observing Systems XXIV*, Sep. 2019, vol. 11127, p. 40, doi: 10.1117/12.2531933.

[338] N. Pahlevan, S. Balasubramanian, S. Sarkar, and B. Franz, "Toward Long-Term Aquatic Science Products from Heritage Landsat Missions," *Remote Sens.*, vol. 10, no. 9, p. 1337, Aug. 2018, doi: 10.3390/rs10091337.

[339] M. Claverie *et al.*, "The Harmonized Landsat and Sentinel-2 surface reflectance data set," *Remote Sens. Environ.*, vol. 219, pp. 145–161, Dec. 2018, doi: 10.1016/j.rse.2018.09.002.

[340] IOCCG, "Minimum Requirements for an Operational, Ocean-Colour Sensor for the Open Ocean," Accessed: Jun. 09, 2020. [Online]. Available: www.ioccg.org.

[341] IOCCG, "Why Ocean Colour? The Societal Benefits of Ocean-Colour Technology," in *Reports of the International Ocean-Colour Coordinating Group*, 2008.

[342] World Meteorological Organization, *Systematic Observation Requirements for Satellite-based Products for Climate Supplemental details to the satellite-based component of the Implementation Plan for the Global Observing System for Climate in Support of the UNFCCC*. Geneva: WMO, 2011.

[343] J. J. Butler, B. C. Johnson, J. P. Rice, S. W. Brown, and R. Barnes, "Validation of Radiometric Standards for the Laboratory Calibration of Reflected-Solar Earth Observing Satellite Instruments."

[344] R. E. Eplee, J. Q. Sun, G. Meister, F. S. Patt, X. Xiong, and C. R. McClain, "Cross calibration of SeaWiFS and MODIS using on-orbit observations of the Moon," *Appl. Opt.*, vol. 50, no. 2, pp. 120–133, Jan. 2011, doi: 10.1364/AO.50.000120.

[345] J. A. Esposito, X. Xiong, A. Wu, J. Sun, and W. L. Barnes, "MODIS reflective solar bands uncertainty analysis," in *Earth Observing Systems IX*, Oct. 2004, vol. 5542, p. 448, doi: 10.1117/12.558106.

[346] IOCCG, "Atmospheric Correction for Remotely-Sensed Ocean-Colour Products," in *Reports of the International Ocean-Colour Coordinating Group*, M. Wang, Ed. 2010.

[347] G. Zibordi *et al.*, "System vicarious calibration for ocean color climate change applications: Requirements for in situ data," *Remote Sens. Environ.*, vol. 159, pp. 361–369, Mar. 2015, doi: 10.1016/j.rse.2014.12.015.

[348] G. Zibordi, M. Talone, K. J. Voss, and B. C. Johnson, "Impact of spectral resolution of in situ ocean color radiometric data in satellite matchups analyses," *Opt. Express*, vol. 25, no. 16, p. A798, Aug. 2017, doi: 10.1364/oe.25.00a798.

[349] G. Zibordi and K. J. Voss, "In situ optical radiometry in the visible and near infrared," in *Experimental Methods in the Physical Sciences*, vol. 47, Academic Press, 2014, pp. 247–304.

[350] GCOS and WMO, "Essential Climate Variables." https://gcos.wmo.int/en/essential-climate-variables (accessed Jun. 09, 2020).

[351] P. Friedlingstein *et al.*, "Global carbon budget 2019," *Earth Syst. Sci. Data*, vol. 11, no. 4, pp. 1783–1838, Dec. 2019, doi: 10.5194/essd-11-1783-2019.

[352] M. Bevis, S. Businger, T. A. Herring, C. Rocken, R. A. Anthes, and R. H. Ware, "GPS meteorology: Remote sensing of atmospheric water vapor using the global positioning system," *J. Geophys. Res.*, vol. 97, no. D14, p. 15787, Oct. 1992, doi: 10.1029/92JD01517.

[353] A. E. Dessler, Z. Zhang, and P. Yang, "Water-vapor climate feedback inferred from climate fluctuations, 2003–2008," *Geophys. Res. Lett.*, vol. 35, no. 20, p. L20704, Oct. 2008, doi: 10.1029/2008GL035333.

[354] E. S. Chung, B. Soden, B. J. Sohn, and L. Shi, "Upper-tropospheric moistening in response to anthropogenic warming," *Proc. Natl. Acad. Sci. U. S. A.*, vol. 111, no. 32, pp. 11636–11641, Aug. 2014, doi: 10.1073/pnas.1409659111.

[355] S. C. Sherwood, R. Roca, T. M. Weckwerth, and N. G. Andronova, "Tropospheric water vapor, convection, and climate," *Rev. Geophys.*, vol. 48, no. 2, p. RG2001, Apr. 2010, doi: 10.1029/2009RG000301.

[356] I. M. Held and B. J. Soden, "Water vapor feedback and global warming," *Annu. Rev. Energy Environ.*, vol. 25, no. 1, pp. 441–475, Nov. 2000, doi: 10.1146/annurev.energy.25.1.441.

[357] K. E. Trenberth, J. Fasullo, and L. Smith, "Trends and variability in column-integrated atmospheric water vapor," *Clim. Dyn.*, vol. 24, no. 7–8, pp. 741–758, May 2005, doi: 10.1007/s00382-005-0017-4.

[358] A. J. Cogan *et al.*, "Atmospheric carbon dioxide retrieved from the Greenhouse gases Observing SATellite (GOSAT): Comparison with ground-based TCCON observations and GEOS-Chem model calculations," *J. Geophys. Res. Atmos.*, vol. 117, no. D21, p. n/a-n/a, Nov. 2012, doi:

10.1029/2012JD018087.

[359] L. Feng, P. I. Palmer, H. Bösch, and S. Dance, "Estimating surface CO2 fluxes from space-borne CO2 dry air mole fraction observations using an ensemble Kalman Filter," *Atmos. Chem. Phys.*, vol. 9, no. 8, pp. 2619–2633, 2009, doi: 10.5194/acp-9-2619-2009.

[360] P. I. Palmer, L. Feng, D. Baker, F. Chevallier, H. Bösch, and P. Somkuti, "Net carbon emissions from African biosphere dominate pan-tropical atmospheric CO2 signal," *Nat. Commun.*, vol. 10, no. 1, pp. 1–9, Dec. 2019, doi: 10.1038/s41467-019-11097-w.

[361] M. Buchwitz *et al.*, "Global satellite observations of column-averaged carbon dioxide and methane: The GHG-CCI XCO2 and XCH4 CRDP3 data set," *Remote Sens. Environ.*, vol. 203, pp. 276–295, Dec. 2017, doi: 10.1016/j.rse.2016.12.027.

[362] M. Reuter *et al.*, "Ensemble-based satellite-derived carbon dioxide and methane column-averaged dry-air mole fraction data sets (2003-2018) for carbon and climate applications," *Atmos. Meas. Tech.*, vol. 13, no. 2, pp. 789–819, Feb. 2020, doi: 10.5194/amt-13-789-2020.

[363] G. Janssens-Maenhout *et al.*, "Toward an operational anthropogenic CO2 emissions monitoring and verification support capacity," *Bull. Am. Meteorol. Soc.*, vol. 101, no. 8, pp. E1439–E1451, Sep. 2021, doi: 10.1175/BAMS-D-19-0017.1.

[364] "A CONSTELLATION ARCHITECTURE FOR MONITORING CARBON DIOXIDE AND METHANE FROM SPACE Prepared by the CEOS Atmospheric Composition Virtual Constellation Greenhouse Gas Team."

[365] F. J. Wentz and M. Schabel, "Precise climate monitoring using complementary satellite data sets," *Nature*, vol. 403, no. 6768, pp. 414–416, Jan. 2000, doi: 10.1038/35000184.

[366] M. Schröder *et al.*, "The GEWEX Water Vapor Assessment: Overview and Introduction to Results and Recommendations," *Remote Sens.*, vol. 11, no. 3, p. 251, Jan. 2019, doi: 10.3390/rs11030251.

[367] F. Chevallier, P. I. Palmer, L. Feng, H. Boesch, C. W. O'Dell, and P. Bousquet, "Toward robust and consistent regional CO2 flux estimates from in situ and spaceborne measurements of atmospheric CO2," *Geophys. Res. Lett.*, vol. 41, no. 3, pp. 1065–1070, Feb. 2014, doi: 10.1002/2013GL058772.

[368] "ESA Climate Change Initiative (CCI) User Requirements Document Version 3.0 (URDv3.0)." Accessed: Mar. 11, 2021. [Online]. Available: http://cci.esa.int/ghg/.

[369] "Copernicus CO 2 Monitoring Mission Requirements Document."

[370] D. Crisp *et al.*, "The on-orbit performance of the Orbiting Carbon Observatory-2 (OCO-2) instrument and its radiometrically calibrated products," *Atmos. Meas. Tech.*, vol. 10, no. 1, pp. 59–81, Jan. 2017, doi: 10.5194/amt-10-59-2017.

[371] M. Schröder, M. Lockhoff, J. M. Forsythe, H. Q. Cronk, T. H. V. Haar, and R. Bennartz, "The GEWEX water vapor assessment: Results from intercomparison, trend, and homogeneity analysis of total column water vapor," *J. Appl. Meteorol. Climatol.*, vol. 55, no. 7, pp. 1633–1649, Jul. 2016, doi: 10.1175/jamc-d-15-0304.1.

[372] M. Hegglin, M. Schröder, H. Brogniez, and D. Hubert, "Water Vapour Climate Change Initiative-CCI+ Phase 1 User Requirements Document (URD)," 2019.

[373] "SIM - Spectral Irradiance Monitor." https://lasp.colorado.edu/home/tsis/instruments/sim-spectral-irradiance-monitor/ (accessed Aug. 26, 2020).

[374] C. M. Roithmayr *et al.*, "Opportunities to intercalibrate radiometric sensors from international

space station," *J. Atmos. Ocean. Technol.*, vol. 31, no. 4, pp. 890–902, Apr. 2014, doi: 10.1175/JTECH-D-13-00163.1.

[375] B. A. Wielicki, D. R. Doelling, D. F. Young, N. G. Loeb, D. P. Garber, and D. G. MacDonnell, "Climate quality broadband and narrowband solar reflected radiance calibration between sensors in orbit," in *International Geoscience and Remote Sensing Symposium (IGARSS)*, 2008, vol. 1, no. 1, doi: 10.1109/IGARSS.2008.4778842.

[376] J. Sun, X. Xiong, E. Waluschka, and M. Wang, "Suomi National Polar-Orbiting Partnership Visible Infrared Imaging Radiometer Suite polarization sensitivity analysis," *Appl. Opt.*, vol. 55, no. 27, p. 7645, Sep. 2016, doi: 10.1364/ao.55.007645.

[377] W. Sun, C. Lukashin, R. R. Baize, and D. Goldin, "Modeling polarized solar radiation for CLARREO inter-calibration applications: Validation with PARASOL data," *J. Quant. Spectrosc. Radiat. Transf.*, vol. 150, pp. 121–133, Jan. 2015, doi: 10.1016/j.jqsrt.2014.05.013.

[378] D. Goldin and C. Lukashin, "Empirical polarization distribution models for CLARREO-imager intercalibration," *J. Atmos. Ocean. Technol.*, vol. 33, no. 3, pp. 439–451, Mar. 2016, doi: 10.1175/JTECH-D-15-0165.1.

[379] A. Wu, X. Xiong, Z. Jin, C. Lukashin, B. N. Wenny, and J. J. Butler, "Sensitivity of Intercalibration Uncertainty of the CLARREO Reflected Solar Spectrometer Features," *IEEE Trans. Geosci. Remote Sens.*, vol. 53, no. 9, pp. 4741–4751, Sep. 2015, doi: 10.1109/TGRS.2015.2409030.

[380] C. Currey, A. Bartle, C. Lukashin, C. Roithmayr, and J. Gallagher, "Multi-Instrument Inter-Calibration (MIIC) System," *Remote Sens.*, vol. 8, no. 11, p. 902, Nov. 2016, doi: 10.3390/rs8110902.

[381] N. P. Fox, P. R. Haycocks, J. E. Martin, and I. Ul-Haq, "A mechanically cooled portable cryogenic radiometer," *Metrologia*, vol. 32, no. 6, p. 581, 1995, doi: 10.1088/0026-1394/32/6/36.

[382] T. R. Gentile, J. M. Houston, J. E. Hardis, C. L. Cromer, and A. C. Parr, "National Institute of Standards and Technology high-accuracy cryogenic radiometer," *Appl. Opt.*, vol. 35, no. 7, p. 1056, Mar. 1996, doi: 10.1364/ao.35.001056.

[383] R. Goebel, M. Stock, and R. Köhler, "BIPM Report on the International Comparison of Cryogenic Radiometers."

[384] K. Ångström, "Eine electrische Kompensationsmethode zur quantitativen Bestimmung strahlender Wärme," *Nov. Acta Soc. Sci. Upsal. Ser. 3*, 1893.

[385] F. Kurlbaum, "Notiz über eine Methode zur quantitativen Bestimmung strahlender Wärme," *Ann. Phys.*, vol. 287, no. 3, pp. 591–592, Jan. 1894, doi: 10.1002/andp.18942870314.

[386] T. J. Quinnf and J. E. Martin, "A radiometric determination of the Stefan-Boltzmann constant and thermodynamic temperatures between -40 °C and +100 °C," *Philos. Trans. R. Soc. London. Ser. A, Math. Phys. Sci.*, vol. 316, no. 1536, pp. 85–189, Nov. 1985, doi: 10.1098/rsta.1985.0058.

[387] "TRUTHS, Traceable Radiometry Underpinning Terrestrial- and Helio- Studies." https://www.youtube.com/watch?v=-_BznE1Ckgc&feature=youtu.be (accessed Aug. 05, 2020).

[388] X. P. Hao *et al.*, "Miniature Fixed Points as Temperature Standards for In Situ Calibration of Temperature Sensors," *Int. J. Thermophys.*, vol. 38, no. 6, pp. 1–13, Jun. 2017, doi: 10.1007/s10765-017-2223-9.

[389] J. Harries *et al.*, "The far-infrared earth," *Rev. Geophys.*, vol. 46, no. 4, Dec. 2008, doi: 10.1029/2007RG000233.

[390] M. G. Mlynczak, D. G. Johnson, and D. P. Kratz, "The Far-Infrared Spectrum: Exploring a New Frontier in the Remote Sensing of the Earth's Climate," in *Fourier Transform Spectroscopy/ Hyperspectral Imaging and Sounding of the Environment*, Feb. 2007, p. HMA1, doi: 10.1364/HISE.2007.HMA1.

[391] H. E. Brindley and J. E. Harries, "The impact of far i.r. absorption on clear sky greenhouse forcing: Sensitivity studies at high spectral resolution," *J. Quant. Spectrosc. Radiat. Transf.*, vol. 60, no. 2, pp. 151–180, Aug. 1998, doi: 10.1016/S0022-4073(97)00152-0.

[392] S. A. Clough, M. J. Iacono, and J. L. Moncet, "Line-by-line calculations of atmospheric fluxes and cooling rates: application to water vapor," *J. Geophys. Res.*, vol. 97, no. D14, pp. 15761–15785, Oct. 1992, doi: 10.1029/92jd01419.

[393] D. R. Feldman, W. D. Collins, R. Pincus, X. Huang, and X. Chen, "Far-infrared surface emissivity and climate," *Proc. Natl. Acad. Sci. U. S. A.*, vol. 111, no. 46, pp. 16297–162302, Nov. 2014, doi: 10.1073/pnas.1413640111.

[394] C. Kuo, D. R. Feldman, X. Huang, M. Flanner, P. Yang, and X. Chen, "Time-Dependent Cryospheric Longwave Surface Emissivity Feedback in the Community Earth System Model," *J. Geophys. Res. Atmos.*, vol. 123, no. 2, pp. 789–813, Jan. 2018, doi: 10.1002/2017JD027595.

[395] X. Huang, X. Chen, M. Flanner, P. Yang, D. Feldman, and C. Kuo, "Improved representation of surface spectral emissivity in a global climate model and its impact on simulated climate," *J. Clim.*, vol. 31, no. 9, pp. 3711–3727, May 2018, doi: 10.1175/JCLI-D-17-0125.1.

[396] Y. Hong and G. Liu, "The characteristics of ice cloud properties derived from CloudSat and CALIPSO measurements," *J. Clim.*, vol. 28, no. 9, pp. 3880–3901, May 2015, doi: 10.1175/JCLI-D-14-00666.1.

[397] P. Yang *et al.*, "Spectrally consistent scattering, absorption, and polarization properties of atmospheric ice crystals at wavelengths from 0.2 to 100 μm," *J. Atmos. Sci.*, vol. 70, no. 1, pp. 330–347, Jan. 2013, doi: 10.1175/JAS-D-12-039.1.

[398] B. A. Baum *et al.*, "Ice cloud single-scattering property models with the full phase matrix at wavelengths from 0.2 to 100μm," *J. Quant. Spectrosc. Radiat. Transf.*, vol. 146, pp. 123–139, Oct. 2014, doi: 10.1016/j.jqsrt.2014.02.029.

[399] P. Yang *et al.*, "Spectral signature of ice clouds in the far-infrared region: Single-scattering calculations and radiative sensitivity study," *J. Geophys. Res. D Atmos.*, vol. 108, no. 18, Sep. 2003, doi: 10.1029/2002jd003291.

[400] L. Palchetti, G. Di Natale, and G. Bianchini, "Remote sensing of cirrus cloud microphysical properties using spectral measurements over the full range of their thermal emission," *J. Geophys. Res. Atmos.*, vol. 121, no. 18, pp. 10,804-10,819, Sep. 2016, doi: 10.1002/2016JD025162.

[401] T. Maestri, W. Cossich, and I. Sbrolli, "Cloud identification and classification from high spectral resolution data in the far infrared and mid-infrared," *Atmos. Meas. Tech.*, vol. 12, no. 7, pp. 3521–3540, Jul. 2019, doi: 10.5194/amt-12-3521-2019.

[402] R. A. Hanel *et al.*, "The Nimbus 4 infrared spectroscopy experiment: 1. Calibrated thermal emission spectra," *J. Geophys. Res.*, vol. 77, no. 15, pp. 2629–2641, May 1972, doi: 10.1029/jc077i015p02629.

[403] D. Spänkuch, "Arbeiten des Meteorologischen Dienstes der DDR auf dem Gebiet der indirekten

Sondierung.," *Zeitschrift für Meteorol.*, vol. 30, pp. 205–214, 1980.

[404] R. J. Bantges, H. E. Brindley, X. H. Chen, X. L. Huang, J. E. Harries, and J. E. Murray, "On the detection of robust multidecadal changes in Earth's outgoing longwave radiation spectrum," *J. Clim.*, vol. 29, no. 13, pp. 4939–4947, Jul. 2016, doi: 10.1175/JCLI-D-15-0713.1.

[405] "Report for Mission selection: Earth Explorer 9 Candidate Mission FORUM — Report for Mission Selection," 2019.